Open Research Online

The Open University's repository of research publications
and other research outputs

Permeation studies of hydrogen in nickel, molybdenum and M316 stainless steel: the influence of phase boundary processes

Thesis

How to cite:

Reuben, Robert L (1981). Permeation studies of hydrogen in nickel, molybdenum and M316 stainless steel: the influence of phase boundary processes. PhD thesis The Open University.

For guidance on citations see FAQs.

© 1981 The Author

https://creativecommons.org/licenses/by-nc-nd/4.0/

Version: Version of Record

Link(s) to article on publisher's website:
http://dx.doi.org/doi:10.21954/ou.ro.0000f819

Copyright and Moral Rights for the articles on this site are retained by the individual authors and/or other copyright owners. For more information on Open Research Online's data policy on reuse of materials please consult the policies page.

oro.open.ac.uk

D 38662/81

UNRESTRICTED

PERMEATION STUDIES OF HYDROGEN IN NICKEL, MOLYBDENUM AND M316 STAINLESS STEEL : THE INFLUENCE OF PHASE BOUNDARY PROCESSES

A Thesis submitted for the degree of

Doctor of Philosophy of

The Open University

By

ROBERT L. REUBEN, B.Sc.

Oxford Research Unit,

The Open University

March, 1981

Date of submission: 3.4.81
Date of award: 24.6.81

ProQuest Number: 27777218

All rights reserved

INFORMATION TO ALL USERS
The quality of this reproduction is dependent on the quality of the copy submitted.

In the unlikely event that the author did not send a complete manuscript
and there are missing pages, these will be noted. Also, if material had to be removed,
a note will indicate the deletion.

ProQuest 27777218

Published by ProQuest LLC (2020). Copyright of the Dissertation is held by the Author.

All Rights Reserved.
This work is protected against unauthorized copying under Title 17, United States Code
Microform Edition © ProQuest LLC.

ProQuest LLC
789 East Eisenhower Parkway
P.O. Box 1346
Ann Arbor, MI 48106 - 1346

CONTENTS

Page

APPENDIX

LIST OF FIGURES

Page

Page

ACKNOWLEDGEMENTS

Thanks are due to:

The Science Research Council and The Open University for providing finance to keep both myself and my equipment in running order.

My colleagues at the O.R.U., especially:

Derek Cummings who kept the computers running and who made a significant contribution to the surface analysis model.

Eser Faraj who shared the traumas.

Sue Whitburn who was going to write the graph-plotting routine - but wrote her thesis instead.

The Technical Staff: Peter Finnimore, Ted Beaver and Alan Knight for techs, mechs, ceps, sparks (and the occasional explosion).

The Secretarial Staff: Jill Uttley and Rosemary Loving without whose stationery this thesis would never have been written.

David Blackburn: Mentor, fund-raiser and slave driver.

without all of whom this project would have been all work and no fun.

ABSTRACT

The permeation of hydrogen through nickel, molybdenum and M316 stainless steel has been studied by both time-dependent and time-independent methods. Both of these types of measurement have been made simultaneously by the application of Fourier Analysis and Signal Averaging to a modulated experiment.

Measurements consisted of the phases amplitudes and mean values of two modulating pressures one on either side of the experimental metal. The upstream pressure was driven by a gas pressure control system designed specially for the purpose. The downstream vacuum chamber was continuously pumped.

The relationship between the phase-lag of the downstream pressure relative to the upstream pressure yielded the diffusion coefficient; the relative mean values of the two modulated pressures yielded the permeability, and the relationship between the amplitudes of the two waves was dependent on both the diffusivity and the permeability.

The relationships between the phases, amplitudes and mean values were modified when account was taken of the possibility that hydrogen enters and leaves the metal at a finite rate. These modified relationships have been used to derive some of the parameters characterising such finite solubilisation processes.

CHAPTER 1

INTRODUCTION

1.1 Background

Diffusion is a process where a material moves in such a way as to reduce gradients of chemical potential. More specifically, a solid solution which has an inhomogeneity in the concentration of one or more of its components will tend to homogenise and reach an equilibrium where there are no concentration (or, more accurately, chemical potential) gradients. The particular case upon which attention is focussed here is on the diffusion of hydrogen in metal lattices.

Hydrogen dissolves in metals to an extent governed by the temperature, ambient hydrogen pressure and the host lattice. In the hydrogen/metal systems considered here hydrogen does not form compounds or have any other such strong interactions with the host lattice atoms. Thus, provided that concentrations are low enough that hydrogen-hydrogen interactions can be neglected, it can be considered to behave as an ideal solute. The system to be described here, therefore, is a relatively immobile metal lattice with a highly mobile ideal interstitial solute.

The diffusion of hydrogen in metals is a subject of long-standing interest. Hydrogen distributes very rapidly in most metals and can have deleterious effects on mechanical properties particularly in welded metals where very high temperatures and rapid cooling rates can lead to very large hydrogen concentrations. It is not expected that this work will be of any direct relevance to the prevention of such problems but a more modern interest in hydrogen diffusion, or more appropriately, hydrogen permeation has developed over the past few years.

This is, of course, the problem of hydrogen isotope permeation of the various containment walls of fusion reactors designed to operate on the D-T fuel cycle. The prevention of tritium loss is of particular importance because of the scarcity, and, therefore, cost, of the material and also because of its rather dangerous nature.

Two of the materials investigated in this study are candidate materials for such a fusion reactor(1) and it is believed that the state of knowledge of at least some aspects of the rather complex permeation processes which occur in these materials has been in some way improved.

Tritium permeation is also important in light water reactors where fission product tritium may diffuse through fuel element cladding into the coolant(2). As has been pointed out by numerous authors, permeation experiments can give rise to more problems than they solve since the rate-limiting process occurring in a given experiment is by no means necessarily the diffusion of hydrogen in the host lattice. Such effects as surface holdup (whether due to surface films or to non-infinite solubilisation processes) and non-Fickian diffusion (whether due to trapping, concentration-dependent diffusion, hydride precipitation, etc.) can, and often do, affect the rate at which gas passes through a metal membrane.

It will be shown that the experimental techniques used in this work are sensitive to such 'non-classical' effects. Often, these effects only exhibit partial control so that the complete permeation process can be described in terms of the diffusion coefficient, the solubility and some additional parameter(s) However, if the non-classical process is very much slower than

than the diffusion process, total dominance may occur so that the diffusion coefficient and solubility have no effect on permeation.

1.2 The Basic Phenomenology of Diffusion

The fundamental law governing transport of matter down a concentration gradient was first formulated by Fick in 1855 and with the advent of the Thermodynamics of Irreversible Processes in about 1930 was seen to be one of a family of physical laws relating thermodynamic 'forces' and 'fluxes'.

Fick's Law states that a flux of diffusing species is linearly related to the gradient of the concentration of that species (in the absence of other thermodynamic forces).

This law is empirical and recent literature on irreversible processes contains some argument as to whether such a relationship is valid throughout the known domain of fluxes and forces(3). Such a failure would, of course, be reflected by a concentration-dependent diffusion coefficient.

It is well-known that hydrogen dissolves and diffuses in metals as interstitial atoms. This fact along with the small size and mass of hydrogen atoms combine to make hydrogen the most mobile solute in metal lattices.

This work is only concerned with diffusion in one direction. Furthermore, interstitial diffusion in a metal matrix occurs at a much faster rate than does substitutional- or self-diffusion in the same matrix so that cross-effects resulting from matrix diffusion 'past' the solute do not arise. Finally, for the case of hydrogen in the metals and at the temperatures used in this study, solute concentrations are low enough that the

solution can be considered to be ideal so that Fick's First Law can be adequately stated by:

$$J_I = -D_I \frac{\partial C_I}{\partial x}$$

where J_I is the flux of interstitial atoms / unit area / unit time

D_I is the interstitial diffusion coefficient / unit area / unit time

$\frac{\partial C_I}{\partial x}$ is the 1-D concentration gradient of interstitial atoms / unit length / unit volume

A useful extension of Fick's First Law is obtained by considering two parallel unit planes a distance, dx, apart.

In one dimension, the flux through the first plane is:

$$J = -D \frac{\partial C}{\partial x}$$

and the flux through the second plane is:

$$J + \frac{\partial J}{\partial x} dx = -D \frac{\partial C}{\partial x} - \frac{\partial}{\partial x} \left(D \frac{\partial C}{\partial x}\right) dx$$

Subtracting

$$\frac{\partial J}{\partial x} = - \frac{\partial}{\partial x} \left(D \frac{\partial C}{\partial x}\right)$$

But $\partial J/\partial x$ equals the negative rate of concentration change in the element bounded by the two parallel planes so that

$$\frac{\partial C}{\partial t} = \frac{\partial}{\partial x} D \frac{\partial C}{\partial x}$$

$$= D \frac{\partial^2 C}{\partial x^2} \quad \text{(if D is invariant with concentration)}$$

1.3 The Measurement of Diffusion Coefficient

Methods of obtaining the diffusion coefficient can be broadly categorised as those in which a flux is measured and those in which a concentration distribution is measured.

In contrast, there are the 'microscopic' techniques including quasi-elastic scattering of thermal neutrons, nuclear magnetic resonance, etc. Such techniques look directly at the jump process in a way not even approached by macroscopic methods. However, from a technological point of view it is not the detail of the jump process which requires to be known but rather the effect of a very large number of such processes in an imperfect crystal in a macroscopic system. Returning to the macroscopic methods, it can be seen that a solution of Fick's Second Law for a given set of boundary conditions will be a concentration distribution (with x), which is some function of time, and the diffusion coefficient. One example of such a distribution is the semi-infinite solution obtained when the surface of a very thick slab of material has a concentration maintained at a value say, C_o, with an initial distribution in the solid of zero concentration (say) giving the boundary conditions:

$$C = C_o \quad \text{at} \quad x = o \qquad t \geq o$$

$$C = o \qquad x = o \rightarrow \infty \qquad t = o$$

The solution of Fick's Second Law is well known:

$$C(x,t) = C_o \left[1 - \text{erf} \left\{ \frac{x}{2\sqrt{Dt}} \right\} \right]$$

Such experiments have the advantage that, since concentrations are being measured in the solid there is no question of the results being misinterpreted because of rate-limiting processes during the entry of the diffusant into the host (provided that the surface concentration does stay truly constant).

The principal disadvantage is that, in order to make a measurement, the experiment must be halted and this normally requires cooling of the specimen during which additional diffusion may occur. Furthermore, the measurement of the concentration distribution is normally destructive, involving either auto-radiography of sections parallel to the diffusion direction or chemical analysis/radiography of the sections perpendicular to the diffusion direction. Thus, although distance can be treated as a continuous variable, time can only be treated discontinuously. Radioactive isotopes of the diffusant are often used in this type of technique since their concentrations can be particularly easily measured but a number of other methods can be used, most of which are unsuitable if hydrogen is the diffusant. Such methods have been used for the measurement of tritium diffusivities in stainless steels(4).

In contrast to the experiments involving measurement of the concentration distribution at a given time, we can also measure fluxes. This type of measurement is less direct since fluxes are measured outside the solid and the fluxes within the solid are only deduced by implication. This usually requires that some assumption is made regarding the way in which material is transferred across the phase boundary between the solid and its environment.

Limiting the discussion to a single interstitial solute diffusing in one dimension through a relatively immobile isothermal metal lattice with no abnormal diffusion effects, Fick's Second Law can be used to describe the interstitial transport behaviour while it is in the bulk of the solid.

$$\frac{\partial C}{\partial t} = D \frac{\partial^2 C}{\partial x^2} \qquad (1.1)$$

If a concentration of the solute, C, is induced and held at the surface $x = o$, the solute will flow in the positive x-direction so as to reduce the concentration gradient. If sufficient time is allowed, appreciable amounts of solute will reach the 'downstream' face of the specimen. If this surface is blocked in any way so that solute cannot escape from it, diffusion will continue to occur until the concentration gradient is totally neutralised and equilibrium is established throughout the specimen.

However, in a permeation experiment diffusant does emerge from the downstream surface of the specimen and the flux leaving this surface can be measured. Flux measurement need not be confined to permeation experiments and other techniques can be used such as the rate of intake of gas by a hot metal or the rate of evolution of gas from a metal which has previously been saturated at a known temperature.

If the concentration at the downstream side of the specimen is also held at a time invariant value, say C', at $x = l$ the flowing gas will never attain equilibrium but after some time the concentration in the solid will stop changing with time and the system will have reached a steady-state.

Since $\frac{\partial C}{\partial t}$ is now zero

$$D \frac{\partial^2 C}{\partial x^2} = 0 \qquad (1.2)$$

and hence $C(x) = A + Bx$

Applying the already specified boundary conditions

$$C(o,t) = C$$

$$C(1,t) = C'$$

$$\text{Gives } C(x) = C + \frac{(C - C')x}{1} \qquad (1.3)$$

This same concentration gradient will be set up whatever the value of the diffusion coefficient and therefore measurements of the concentration gradient at steady-state cannot of themselves furnish values of the diffusion coefficient.

However, if the flux passing through the specimen is measured, the diffusion coefficient can be calculated since:

$$J = -D \frac{\partial C}{\partial x} \qquad (1.4)$$

$$\text{i.e.} \quad J = \frac{D(C - C')}{1} \qquad (1.5)$$

provided that both C and C' are known. This type of method has been used to calculate diffusion coefficients by, for example, Smith(5) for carbon in iron, except that he used the corresponding cylindrical solution of the diffusion equation.

It can be seen from (1.3) and (1.5) that the equilibrium state of zero concentration gradient and hence zero flux through the specimen is merely a special case of the stationary state where J = O and hence C = C' (or vice versa).

In this connection a quantity called permeability can

be defined. The permeability P_m is the product of the diffusivity and the Sieverts constant K_{sm} defined as the equilibrium constant for the reaction:

$$\tfrac{1}{2}H_2(g) \rightleftharpoons \underline{H} \qquad K_{sm} = \frac{C_H}{\sqrt{P_{H_2}}} \tag{1.6}$$

The quantity, P_m, is generally used to characterise steady-state experiments instead of the diffusion coefficient, and it takes cognizance of the fact that the solubility of the gas in the metal is also involved.

Permeation experiments for hydrogen are normally carried out using two gas spaces separated by a barrier of the experimental metal. The pressures of the diffusant gas in the two gas spaces are the quantities which are measured and these pressures are linked to the concentrations at the two metal surfaces.

In the simplest case, the time taken for the solubilisation process is assumed to be rapid compared with the diffusion time. Concentrations at the input and output surfaces are then given by:

$$C = K_{sm}\sqrt{p}$$

$$C' = K_{sm}\sqrt{p'}$$

Applying these to (1.5) gives:

$$J = DK_{sm}\,\frac{\sqrt{p} - \sqrt{p'}}{l} \tag{1.7}$$

where $DK_{sm} = P_m$, the permeability.

This equation is sometimes known as the Richardson equation(6). Under normal conditions of temperature, input pressure,

diffusion coefficient, and thickness $p' \ll p$ and according to (1.7) the permeation flux is proportional to the square root of input pressure. Deviations from this behaviour are not necessarily always obvious from steady-state experiments(7), particularly if p is not used as an experimental variable.

1.4 Genesis of the Technique

Whereas steady-state experiments can only provide values for the permeability the diffusion coefficient can be obtained more directly by making use of measurements during the transient conditions leading up to steady-state. In this case the Sieverts constant need not be known and the measurement is made over a range of one of the diffusion equation variables (namely time), and checks of consistency can be made.

The so-called time lag technique makes direct use of this effect. Quite simply, some steady-state condition is perturbed by a very rapid step change in one of the pressures and the response of the other pressure is noted as a function of time.

One example of this type of situation might be a system with an initial concentration in the specimen

$$C = f(x) \qquad o < x < l \quad \text{at } t = o$$

If this system is then perturbed according to the boundary condition:

$$C = C \; ; \quad x = o \qquad t \geq o$$

$$C = C' \; ; \quad x = l \qquad t \geq o$$

The solution can be obtained by separation of variables(8) and is given by:

$$C(x,t)=C+(C'-C)\frac{x}{l} + \frac{2}{\pi}\sum_{1}^{\infty}\frac{C'\cos n\pi - C}{n} \sin\frac{n\pi x}{l} \exp(-Dn^2\pi^2 t/l^2)$$

$$+ \frac{2}{l}\sum_{1}^{\infty}\sin\frac{n\pi x}{l} \exp(-Dn^2\pi^2 t/l^2)\int_{o}^{l} f(x') \sin\frac{n\pi x'}{l}dx'$$

Time-lag analysis is normally applied to experiments by measuring the total amount of gas which has passed through the membrane up to a time, t. The rate of emergence of gas from x=l is taken to be given by $-D\left[\frac{\partial C}{\partial x}\right]_l$ and integrating this with respect to time gives the required quantity of gas, Q_t. The analysis can be carried out to fairly large times where steady-state eventually prevails and Q_t/lC becomes linear in $\frac{Dt}{l^2}$. If C = C' = o

$$Q_t \rightarrow \frac{DC}{l}\left[t - \frac{l^2}{6D}\right]$$

If Q_t is plotted against time(8), extrapolation to Q_t=O gives the time-lag $L = \frac{l^2}{6D}$.

There are many variations on this method but all depend on the measurement of a time, characteristic of the rate of approach to the steady-state.

One such variation has been used by Chung(9) in an experiment where the output gas space was pumped. When the input pressure was stepped from zero to a finite value, the output pressure responded with a rather slower rise to its final steady-state value p'_s. At any time, the ratio of the output pressure to p'_s was given by:

$$R = \frac{p'}{p'_s} = 1-e^{-K't}\ 2\sum_{1}^{\infty}(-1)^n \frac{\exp\left[-\left\{\frac{m\pi}{l}\right\}^2 Dt\right]-\exp(-K't)}{1-\left\{\frac{m\pi}{l}\right\}^2 \frac{D}{K'}}$$

where K' was the quotient of output chamber pumping speed to output chamber volume.

The current work is a natural extension of this type of technique. Those methods which employ a step-function input pressure are obviously useful since they are both dynamic and provide internal checks in that the system must behave in a certain way with time and must eventually settle to a steady-state. Some experimenters have carried such work a little further, e.g. Caskey *et al.*(10), by removing the gas from the input chamber in a step fashion once steady-state has been reached and measuring evolution rates as a function of time. However, it is not necessarily desirable to have large changes in the input or output surface concentrations from the point of view of defining the boundary conditions necessary for the solution of the diffusion equation.

Such an input pressure function may now be envisaged as a train of low amplitude pulses of low frequency. Since it is difficult to produce a true step function in pressure one might as well use a continuous function of time for the input pressure, say a sine wave. Since a square wave can be regarded as the sum of a series of sine waves of varying amplitudes and frequencies and the diffusion equation is a linear differential equation, an experiment carried out with sinusoidal input pressure over a range of frequencies must furnish the same information as would the corresponding experiment with a single frequency square wave. The mean value of each sine wave will, of course, carry the steady-state information which is lost by using a continuous input pressure function.

The solution to the diffusion equation relevant to such a boundary condition will be discussed in more detail in Chapter 3, but for the purposes of comparison with other techniques its form will be indicated here.

From the point of view of algebraic manipulation it is convenient to describe harmonic quantities in complex form so that a quantity $Ae^{i(\omega t+\phi)}$ represents a cosine wave of phase ϕ and amplitude A.

An input pressure wave of arbitrary phase of the form:

$$p_t = p + p_H e^{i\omega t}$$

will give rise to an output wave:

$$p'_t = p' + p'_H e^{i(\omega t - \phi')}$$

The phase lag, ϕ', is a function of the diffusion coefficient and the input pressure wave frequency. The phase lag decreases as the frequency decreases eventually becoming zero for infinitely low frequencies. ϕ' is also decreased by increasing diffusion coefficient becoming zero for infinitely rapid diffusion.

The output pressure amplitude, p'_H, is a function of the diffusion coefficient, the solubility and the frequency. p'_H increases with increasing D and K_{sm} and decreases with increasing ω.

The output pressure mean value, p', is essentially the same as the steady-state pressure produced by an input pressure, p, and is therefore dependent on D and K_{sm} but not on ω.

Phase boundary processes occurring at the input or output surfaces will modify these conclusions but for the purposes of comparison with the foregoing techniques those are adequate.

This method of performing permeation experiments has several advantages over the rate-of-rise technique.

(i) It is truly continuous and the output and input waves can be signal averaged over as many periods as are required

to filter out random noise. This produces 'clean' input and output functions so that their relationship is less likely to be obscured by poor experimental control or measurement.

(ii) Information is carried in three measured quantities, namely the phase lag between the input and output waves, the amplitude ratio between the input and output waves and the offset (average value) of input to output waves. This means that a larger number of internal consistency checks can be made.

(iii) The input wave is measured as well as the output wave and the difficulties associated with producing a true square wave or step increase or decrease in pressure are avoided.

(iv) Only minor perturbations from the steady-state are used and therefore no concentration in the solid or pressure is varying widely enough to seriously affect any rate processes which are occurring at the surfaces of the specimens. Problems which may be associated with filling of voidage in the specimen are also avoided.

With these advantages in mind an input pressure modulation has been used in this work to investigate both classical and non-classical permeation of hydrogen through nickel, molybdenum and stainless steel.

1.5 More Complex Permeation Processes

'Classical' permeation experiments are interpreted in terms of the Richardson equation and, as such, are based on the assumptions:

(i) That diffusion is the only rate-limiting process.

(ii) That the input pressure (or surface concentration) is so much larger than the output that the latter can be neglected.

(iii) That no processes occur in the solid which interfere with classical (Fickian) diffusion.

and these assumptions are often sufficient to adequately describe the permeation process. The first two conditions are normally fulfilled when the specimen is thick, the diffusion coefficient is small or the input pressure is high. Thus, phase boundary processes are unlikely to be seen unless they are slowed down (by using low pressures) or the diffusion process is speeded up.

Also, the growing interest in transport properties in industrial alloys may also require some knowledge of the effects of such processes as trapping, precipitation, radiation damage, porosity, etc., and of course those processes need not be confined to alloys but may be present in, for example, polycrystals or metals which form hydrides.

The foregoing description of the relationship between oscillatory input and output pressures has indicated that, in principle, the diffusion coefficient and solubility can be derived from a single frequency experiment. The use of a range of frequencies, aside from providing a check of internal consistency, can detect behaviour which is not consistent with the assumptions of classical permeation. On this basis the pressure modulation approach may be useful not only for measuring D and K_{sm} but may also provide information about non-classical processes.

Analysis of a permeation experiment, as opposed to a measurement of concentration distribution, relies on the fact that the experimenter is aware of all the processes which may be undergone by gas atoms after the pressure is measured at the input side of the specimen and before the pressure is measured at the output side.

The processes can be sub-divided into three categories:

(i) Processes occurring in the bulk of the solid

(ii) Processes occurring on the surfaces of the specimen

(iii) Processes occurring remote from the specimen.

The last category is largely a function of the experiment itself and will, therefore, be discussed in Chapter 2.

1.5.1 Processes occurring in the bulk of the solid

Bulk processes are those which modify the diffusion effect as stated by Fick's Laws.

A macroscopic flow proportional to concentration gradient occurs when atoms follow a random path. However, atoms may meet regions within the solid which modify this random motion. Such regions may be short circuit paths (highly disordered regions such as dislocation cores, grain boundaries, interphase boundaries, etc.) or traps which do not allow motion but delay atoms for a longer mean time than they would be held in normal structural interstices.

It is obvious that only a perfect single crystal can be free of such 'faults' and, therefore, we might expect effective diffusion coefficients to vary rather markedly with such factors as grain size, degree of cold work, composition, impurity content, etc. Such correlations do not appear to be very striking from the literature for the materials used in this investigation (e.g. Robertson (11)).

No dual phase alloys are used in this investigation so that extended regions of the solid where the diffusion coefficient is different from the matrix are not encountered.

There is evidence to suggest that grain boundary diffusion, if important at all in such materials only becomes apparent at very

low temperatures(11, 12).

Trapping is a complicated process to describe in terms of differential equations of diffusion. These equations can only be applied effectively in relatively few simple limiting cases.

The model most often quoted is that of McNabb and Foster(13). This model considers that there are three types of trap: those which cause negligible delay, those which cause permanent delay, and reversible traps whose delay times are of the same order as the delay which an atom would normally suffer in its transit through a trap-free solid. The parameters of the model are the concentration of traps per unit volume, N, the probability of atom release, p, and a parameter related to the probability of atom capture, k.

It is assumed that the release rate from traps is proportional to p, N and the fraction, n, of occupied traps and that the capture rate is proportional to k, the local concentration of diffusant, C, and the fraction of unoccupied traps, (1 - n).

By considering the kinetics of the total trapped and dissolved H and applying Fick's Law to the dissolved part of the total concentration McNabb and Foster arrive at:

$$\frac{\partial C}{\partial t} + N \frac{\partial n}{\partial t} = \text{div } (D \text{ grad } C)$$

and

$$\frac{\partial n}{\partial t} = kC\,(1 - n) - pn$$

These equations may be solved to give a non-linear equation for C and n. However, McNabb and Foster recognise an approximation for small concentrations where the cross-term $Cn \ll C$ or n giving for one dimension:

$$\left.\begin{aligned} \frac{\partial n}{\partial t} &= kC - pn \\ \frac{\partial C}{\partial t} + N\frac{\partial n}{\partial t} &= D\frac{\partial^2 C}{\partial x^2} \end{aligned}\right\} \qquad (1.9)$$

The solution of this pair of equations for the oscillatory conditions is dealt with in the Appendix (A.3).

The trapping phenomenon seems to be particularly prevalent in cold-worked mild steels(14,15).

A further 'internal' phenomenon related to trapping is that due to 'microvoids'. In this case the hydrogen is trapped as a gas in micropores in the metal.

According to the analysis of Ellerbrock et al.(16) the pressure inside these pores is proportional to the square of the local concentration. Two concentrations, in pore, C_2, and dissolved, C_1, are considered and f is the volume fraction of pores

$$\frac{\partial(C_1 + C_2)}{\partial t} = \text{div } D \text{ grad } C_1$$

$$\text{i.e. } \frac{\partial C_1}{\partial t} = D^* \text{grad } C_1$$

$$D^* = \frac{D}{1 + K(T)fC_1}$$

i.e. this appears as an apparently concentration-dependent diffusivity, and K(T) is a function of temperature.

One final 'anomalous' internal effect was suggested by Darken(17) and questions the traditional statistical interpretation of the diffusion coefficient since it implies that diffusion occurs down a chemical potential gradient as opposed to a concentration gradient. Darken writes the diffusion velocity as a product of

the thermodynamic force $-\frac{1}{N}\frac{d\overline{Gi}}{dx}$ (N = Avogadro's number and $\overline{Gi}$ = p.m.f.e. of diffusant) and the velocity/unit force (mobility), B_i,

$$\text{i.e. } J_i = C_i v_i = -\frac{1}{N}\frac{d\overline{Gi}}{dx} B_i C_i = -D_i \frac{dC_i}{dx}$$

$$\text{Since } G_i = RT\ln(a_i) \text{ we obtain } D_i = kTB_i\left(1 + \frac{d\ln\gamma_i}{d\ln C_i}\right)$$

This treatment has two implications, one interpretative which will be dealt with later in this chapter and the other which is phenomenological and suggests that the diffusion coefficient is less simple than implied by Fick's Law if the diffusant solution is non-ideal.

However, for the cases considered here one can suppose that γ_i is invariant with concentration and hence $D_i = kTB_i$.

1.5.2 Processes occurring on the specimen surfaces

Many permeation experiments are analysed supposing that the specimen surfaces are at thermodynamic equilibrium with the gas with which they are in contact. Such an assumption simplifies the boundary problem greatly since, at one or both surfaces

$$C = K_{sm}\sqrt{p}$$

and

$$J = -D\left[\frac{\partial C}{\partial x}\right]_{x = \text{surface}}$$

There is, however, growing evidence that permeation is not quite as simple a phenomenon. Phase boundary processes on the solid surface can account for a measurable fraction of the average time it takes for an atom to traverse a membrane. As pointed out by Le Claire(18) it is unreasonable to expect no delay in crossing a surface since this would imply zero gradient in chemical potential between the gas and the solid and hence no

driving force for solution of gas into the metal.

The implication of the Richardson equation is, of course, not that equilibrium actually prevails at the gas solid interfaces but rather that the process of solution is so rapid compared with that of diffusion through the solid that it is not detectable using normal experimental procedures.

The basis for the description of permeation by multi-atomic gases through metals was laid down by Richardson(6) who considered that, in the general case four equilibria pertain to a system of an n-atomic gas in contact with a dissolving matrix

$$\frac{c_o^n}{C_o} = k_o \qquad \frac{c_i^n}{C_i} = k_i$$

$c_{o,i}$ = concentration of dissociated species in gas(o) and solid(i)

$C_{o,i}$ = concentration of undissociated species in gas(o) and solid(i)

n = atomicity

and

$$C_o = AC_i \qquad c_o = ac_i$$

He then calculated the steady-state concentrations through a diaphragm which had an external pressure P_o on one side and zero on the other and a small degree of dissociation outside the solution.

$$\frac{1}{n} c + \frac{\mu}{\mu_n} C = \left\{ \frac{1}{n} \left[\frac{k_i}{A} \right]^{1/n} P_o^{1/n} + \frac{\mu}{\mu_n} \frac{P_o}{A} \right\} \left\{ 1 - \frac{x}{l} \right\}$$

where μ, μ_n are the diffusion coefficients (in the solid) of the undissociated and dissociated species so that flow was proportional to $P_o^{1/n}$ or P_o depending on the relative diffusion coefficients and the degree of dissociation in the solid.

If the gas in the solid was completely dissociated (Sieverts Law) then C = o and $\mu_n \gg \mu$ and k_i is very large

$$\text{i.e.} \qquad c = \left(\frac{k_i}{A}\right)^{1/n} P_o^{1/n}\left\{1 - \frac{x}{l}\right\}$$

this gave the flow rate

$$n = \frac{k}{l} p^{\frac{1}{2}} T^{\frac{1}{2}} e^{-b/t} \qquad \text{(Richardson equation)}$$

Smithells and Ransley (7) used this equation in their experimental investigations of permeation. They found that the $p^{\frac{1}{2}}$ relationship was not always followed, rates at low pressures being somewhat less than predicted by a linear extrapolation. Smithells and Ransley proposed that this effect was due to the fact that at low pressures the specimen surface would not be sufficiently covered by gas atoms to replenish all the material diffusing away from the surface region. They supposed that this effect could be treated as an effective decrease in the geometrical area of the specimen to a fraction θ of its high pressure value. They supposed the Langmuir isotherm to be valid so that $\theta = \frac{ap}{1 + ap}$. Wang(19) carried the model a few stages further.

He considered a series of processes to occur in the permeation system. With a pressure, p, at the input and a pressure of 0 at the output he supposed that:

(i) Gas molecules are simultaneously adsorbed and dissolved

$$\underrightarrow{J} = A(1 - \theta_1^2)p$$

(ii) Reverse of (i)

$$\underleftarrow{J} = B\theta_1^2$$

$$\left.\begin{array}{l} \\ \\ \end{array}\right\} J = A(1 - \theta_1)^2 p - B\theta_1^2$$

(iii) Adsorbed atoms go into solution

(iv) Reverse of (iii)

$$\left.\begin{array}{l} \\ \\ \end{array}\right\} J = C\theta_1 - D\nu_1(1 - \theta_1)$$

where θ_1 is the fraction of the surface covered by adsorbed atoms and ν_1 is the surface concentration.

The same set of equations (except in the reverse sense) described the output surface but in this case $p = o$.

Employing Fick's first law ($n = -E \frac{\partial \nu}{\partial x}$) and considering the steady-state permeation rate where $J \neq f(x,t)$ he obtained:

$$\frac{A}{B} p = \frac{n}{B + n} \left\{ 1 + \left[1 + \frac{B + n}{C - n} \left\{ \frac{1D}{E\sqrt{B}} + \frac{2(B + C)}{(\sqrt{B} - \sqrt{n})(B + n)} \right\} n^{\frac{1}{2}} \right]^2 \right\}$$

Such multi-parametric non-linear equations for the permeation rate are typical when surface processes are taken into account and the best that can be done to render these of practical use is to consider approximations which may be valid under certain conditions of temperature, pressure, concentration, diffusion coefficient, etc.

This approximation process is perhaps the most difficult aspect of this type of analysis since the number of possible limiting cases is large and their functional relationships to the experimental variables can differ widely.

Wang's approximations were made in the hope of explaining the results of Smithells and Ransley's experiments and were concerned with surface coverage. It is interesting to note that Wang in his surface coverage approximations took no cognizance of the fact that the coverage on the output surface may be much less than on the input surface but considered both to be in the same regime, i.e. if e.g. $n \rightarrow B$, corresponding to surface saturation this was considered to occur on the output surface as well.

At any rate, he produced the normal limiting cases where permeation rate may be proportional to p or $\sqrt{p}$ as is quite standard in such analyses.

A further complication to the surface processes was also introduced to account for the possibility that some atoms may by-pass part of the process of solution by moving from the bulk to a site occupied by an adsorbed atom and immediately moving into the gas phase (and vice versa). This was introduced to avoid the implication that at very large pressures the permeation rate would become proportional to p again.

Fast(20, 21) discussed the problem and has performed some qualitative experiments to support his hypotheses regarding the solution process. He examined surface roughness effects and the effect of pre-dissociating the H_2 gas using a hot tungsten spiral. His approach was to consider that smooth surfaces are more likely to be adsorption limited than are rough surfaces. The effects are summarised in the Table:

Permeability	Input Surface		Output Surface	
	Rougher	Smoother	Rougher	Smoother
H	decrease	increase	increase	decrease
H_2	increase	decrease	increase	decrease

As expected, pre-dissociation only affected the role of the input surface. Rough surfaces had a tendency to increase the adsorption rate (probably by increasing the effective surface area) but would 'trap' hydrogen atoms possibly on 'points' on the surface so that the solution step becomes more difficult. It is not clear why roughing of the output surface should increase the permeability since one might expect that the recombination rate would be lowered by the increased surface area.

Ash and Barrer (22) have considered a similar model

to that of Wang and examined a number of limiting cases where the permeability can vary with thickness from l^0 to l^{-1} and with pressure from p^0 to p^1.

Further analyses by, for example Ali-Khan *et al.*(23), Shupe(24) and Perkins and Noda(25) are little different in essence except that some of the steps are removed in some cases for simplicity.

The problems encountered by Ash and Barrer in the solution of even the steady-state flux equation can be simplified by disregarding surface coverage effects. This is tantamount to assuming that when a hydrogen atom arrives at an adsorption site it is unlikely that another hydrogen atom will already be occupying that site. This means that θ can be disregarded in comparison with unity in Wang's flux equations.

A rather different surface process is one where the permeatio rate is reduced by a film on the metal surface (e.g. oxides on stainless steel). This problem has been considered by Strehlow and Savage(26) who suppose that the principal diffusion path is through defects in the oxide film. They use an electrical analogue for the constriction resistance of a set of circular pores. They arrived at:

$$J = \frac{DK_{sm}}{\left[x + \frac{l^2}{a} - 1\right]}\left[p_2^{\frac{1}{2}} - p_1^{\frac{1}{2}}\right]$$

where x is the thickness and a and 2l are the average radius and separation of the pores.

Another possible treatment of this problem, e.g. Le Claire(18 is to consider that the gas dissolves molecularly in the film and to treat the problem as one of permeation through a composite medium.

1.6 Diffusion as an Activated Process

A vast amount has been written on the atomistic interpretation of the diffusion coefficient. Since none of this work is fully quantitative (i.e. the diffusion coefficient of hydrogen in a specified metal cannot be calculated from other, more fundamental, properties) it is of little value for present purposes to go deeply into the statistical or quantum mechanics employed by such models. It is intended here only to give justification for the experimentally observable property of the diffusion coefficient - that it follows on Arrhenius relationship with temperature $D = D_o \exp \frac{-E}{RT}$. For this purpose it is sufficient to consider a very simple statistical model for diffusion.

Firstly, we might expect that the source of the thermal activation for the diffusion coefficient lies in the fact that the lattice can be seen as a 3-D space with a periodically varying potential. The constituent atoms of this lattice are in vibrational (and sometimes translational) motion and thus the potential is periodic in time as well as space. If an interstitial solute is introduced into this lattice (it is a point of detail whether or not the interstitial is considered to disturb the potential field) at a well in potential, the probability of a diffusion event will be a function of the height of the potential energy barrier between the occupied site and the next stable interstitial site.

In order that an atom, however small, can move between the sites of the host lattice, the lattice must make some accommodating movement, i.e. the host lattice atoms must move apart (through thermal vibration) and, therefore, it might be

expected that the diffusion coefficient will be in some way related to the interstitial size, the site size, the lattice type, temperature and the vibrational frequency and amplitude of the lattice. Since hydrogen is the smallest of the interstitials it might be expected that it will show a relatively rapid rate of diffusions in metals as is the case.

If the flux of atoms from one atomic plane to the next is defined as a jump frequency, Γ , times the atomic concentration/unit area difference across two adjacent atomic planes, the well known relationship between the lattice parameter a , jump frequency and diffusion coefficient can be obtained:

$$D = f \Gamma a^2$$

where f is a geometrical factor.

However, Γ is a hardly more fundamental quantity than is D and further investigation is required to render this approach useful. Broadly speaking, this jump frequency can be seen as the product of some frequency of vibration and a probability that can be seen as a concentration of activated complexes or as a probability that an interstitial atom will have the requisite activation energy to move though the saddle point created by the lattice vibrations and this latter is the source of the activation energy.

1.7 Choice of Materials

It has already been stated that hydrogen moves very quickly through metals compared with substitutional and other interstitial solutes.

This property ensures that the output signal produced by a relatively small input modulation will be large enough to

be detected in the temperature and thickness range used in this work.

For this reason hydrogen has been chosen as the diffusant. Other isotopes of hydrogen have not been used but Faraj(27) has studied the permeation of hydrogen and deuterium through metal foils in a very similar oscillatory experiment.

Three specimen materials have been used in this study: nickel, molybdenum and stainless steel.

Of the two pure metals, nickel was chosen because of the remarkable reproducibility of the classical permeation quantities P_M, D obtained by other investigators with a wide variety of techniques(11). This material was, therefore, included as a trial of the technique under relatively well known conditions.

Molybdenum was chosen for the opposite reason. Classical permeation quantities measured in this material vary quite considerably(1). This suggests that some measurable non-classical processes may be occurring in the H-Mo system.

Stainless steel is a complex material for two reasons. Firstly, it is an alloy containing a large fraction of substitutional solutes (principally Cr, Ni) which may produce local distortions in the lattice capable of trapping hydrogen atoms. Secondly it forms a very stable and relatively impermeable oxide layer which, although thin, can produce large reductions in the permeation rate, (e.g(28)).

It was hoped that these materials would provide a range of behavioural responses in order to test the usefulness of the oscillatory technique.

1.8 Summary

In the foregoing chapter measurements of the diffusion process *via* concentration and flux measurements have been reviewed and compared. It has been concluded that fluxes allow *in situ* measurement but that this may be complicated by the effects of phase-boundary processes. Such complications may, of themselves, be interesting technologically especially where permeation from very low pressures is involved, as is the case for tritium in fusion reactors.

Methods of studying permeation through metals have been considered and the importance of time-dependent techniques in obtaining the diffusion coefficient as opposed to the permeability has been stressed.

The various possible sources of 'non-classical' behaviour have been categorised and reviewed with particular emphasis on those applicable to the present work.

It has been suggested that the oscillatory technique may be useful not only for obtaining D, K_{sm} but, by using a variety of modulatory frequencies, non-classical behaviour may, if present, be detected.

Chapter 2 describes an experiment which was devised to measure the pressure at the output surface of a metal diaphragm produced by a modulated input pressure preparatory to examining the relationship between these two oscillatory quantities produced by a diaphragm of a specified material.

CHAPTER 2.

APPARATUS AND EXPERIMENTAL PROCEDURE

2.1 General Specification

The aim of this experiment was to measure the parameters determining the permeation of hydrogen through the three specimen materials using a modulated driving pressure.

It was necessary, in order to deduce the permeation parameters, to measure phase and amplitude relationships between the input and output waves. To this end, both input and output pressures were measured as a function of time. Furthermore, it was necessary to devise a control system for the input pressure so that it could be caused to follow a specified function of time. The useful frequency range could be estimated by the requirement that the diffusion time ($\sim\frac{l^2}{D}$) be an appreciable fraction of the period of oscillation.

With these requirements in mind a double vacuum system was constructed with two chambers being separated by a diaphragm of the specimen material.

The input pressure was modulated by around 10% over a mean value of 10^{0} to 10^{-2} torr. The detectable flux modulation in the output chamber was about 10^{-3} of its mean value but this could be enhanced by signal averaging.

Some of the stringency in input pressure control could be relieved by Fourier analysis and signal averaging of both the input and output signals.

2.2 Schematic Diagram

In the interests of clarity the experimental system is presented in Figure 2.1 in a schematic form.

Vacuum pipework is shown as parallel thick lines except for the bakeable region which is shown in block form. Valves are represented by circles enclosing crosses and ancillary vacuum components by oblong boxes connected to the tubing.

The bakeable region terminates at valves V6 and V7 and these and other valves within the bakeable region are copper/knife-edge sealed U.H.V. valves. All control units and mains supply are omitted for clarity. Other electronic components are represented by oblong boxes.

The region below the horizontal dotted line represents the experimental system and that above the dotted line the measurement and control system.

All components are numbered and valve numbers are prefixed by the letter 'V'. Data communication is represented by thin lines and each unique line has a letter associated with it. Transfers through, and processing by electronics units are represented by dotted lines within the appropriate box.

The circle in the centre of the upper portion of the diagram represents the experimenter and the thick lines radiating from this circle represent the experimenter-controlled inputs. Detailed operation is described later.

The key to the components is as follows:

1: Experimenter

2: Triton Trivector Minicomputer

3: Floppy Disc Data Storage

4: Newbury Visual Display Unit for experimental input and output interrogation

5: West Viscount Room-Temperature Compensated Temperature Controller

6: Solartron 3510 Integrated Measurement System

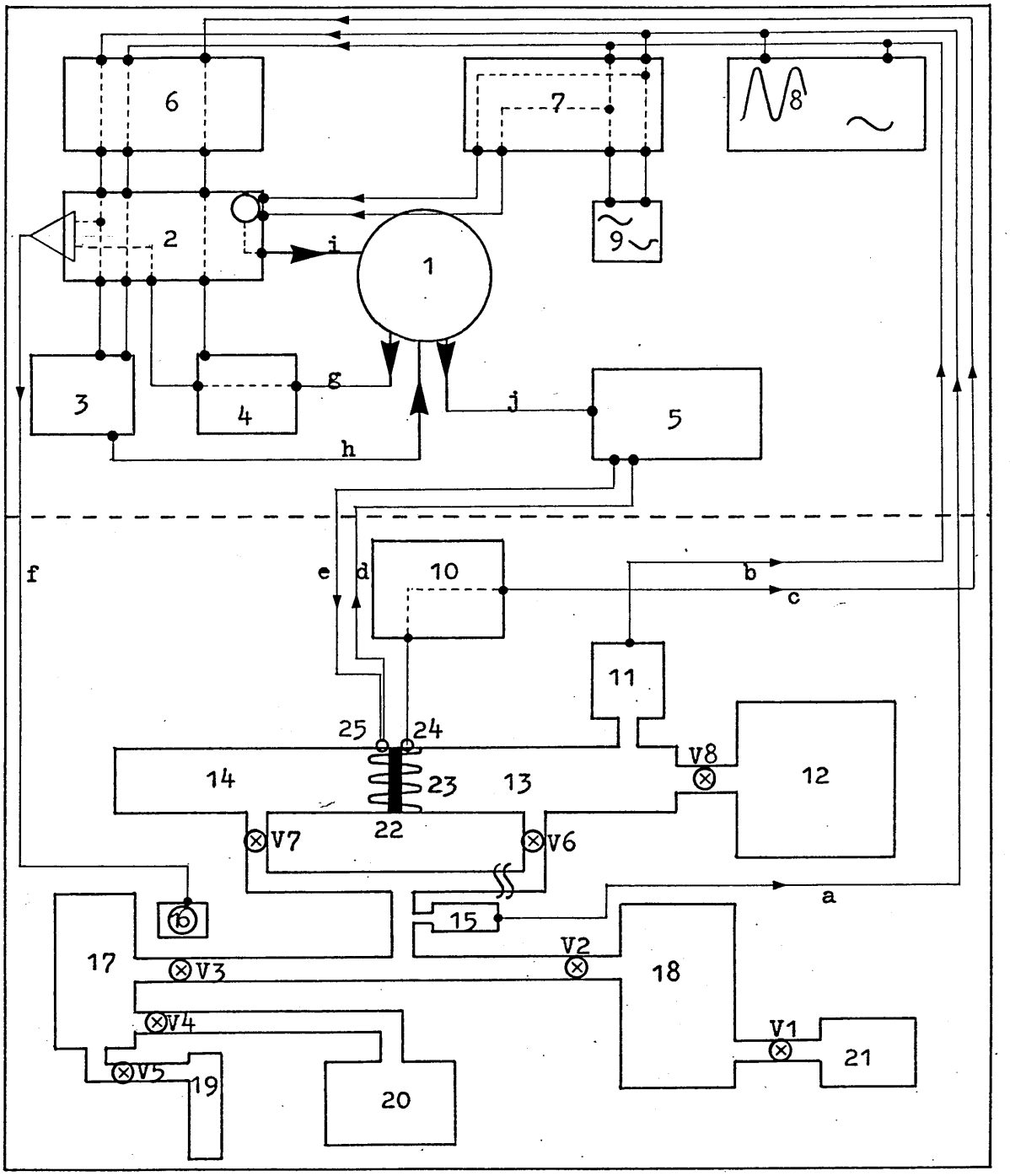

Figure 2.1 Schematic Diagram of the Experimental System

7: Datalab DL4000 Signal Averager

8: Twin Pen Chart Recorder

9: Advance Oscilloscope

10: Delristor Icell (Thermocouple Cold Junction)

11: V.G. Micromass M/M1 Residual Gas Analyser

12: A.E.I. P60 Triode Ion Pump

13: Output U.H.V. Chamber

14: Input U.H.V. Chamber

15: Edwards Pirani 9 Vacuum Gauge calibrated for hydrogen

16: Parvalux 24V D.C. Motor for leak valve control

17: Stainless Steel Ballast Volume (1 liter)

18: Leybold (DIFF170) Diffusion Pump fitted with low vapour pressure fluid (Santovac 5)

19: Hydrogen cylinder (Research Grade)

20: } Leybold Trivac D4A Rotary Pump
21: }

22: Specimen

23: Mineral insulated coaxial cable wound furnace for specimen heating

24: Measuring Chromel/Alumel Thermocouple

25: Control Pt/Pt 13% Rh Thermocouple

The key to information transfer is as follows:

a: Input pressure

b: Output pressure

c: Specimen temperature (Measurement)

d: Specimen temperature (Controller)

e: Furnace Power (this is exceptional in that it is not information)

f: Error signal between reference and measured input pressure

g: Reference input pressure wave

h: Summarised results (from floppy disc/computer)

i: Summarised results (from Datalab/computer)

j: Required specimen temperature

The specimen material in the form of a foil of thickness between .5 and .1 mm separated two high vacuum chambers. A modulated pressure of hydrogen was supplied to the input chamber and the pressure in the output chamber followed.

Analysis of the results was in terms of the response of the output pressure to the time variation of the input pressure. In the particular case of a sinusoidal input pressure the measured parameters are the input mean value and amplitude p, p_H, the output mean value and amplitude p', p'_H and the phase lag between the input and output waves, ϕ.

In addition to the pressures other experimental variables are angular frequency of modulation, ω, specimen temperature, T, specimen thickness, l, and specimen material.

2.3 Vacuum

The vacuum system included a bakeable and a non-bakeable region. The bakeable region consisted of the input and output chambers and was of all stainless steel construction sealed with vacuum generators FC38 copper/knife-edge flanges.

The specimen chamber consisted of two copper/knife-edge seal to gold wire compression seal adaptors, the gold seal flanges being used to seal the specimen disc in a flange/gold wire/specimen/gold wire/flange sandwich. This assembly could be demounted from

the system to allow careful positioning of the specimen and gold seals.

The output chamber included a U.H.V. valve (V6)to the roughing line and two back-to-back U.H.V. valves (V8) separated the Ion Pump from the output chamber. This latter configuration ensured a high conductance between the output chamber and its high vacuum pump and therefore reduced the pumping speed in the output chamber to give higher output pressure amplitude for a given input pressure amplitude.

The analyser head of the mass spectrometer was mounted at right angles to the specimen-pump flow direction. This ensured that gas molecules coming from the specimen had at least one cold wall collision before pressure measurement. Before operation of the experiment the pipework below valve V6 was disconnected to ensure that no leakage occurred from the input chamber to the output chamber by this route.

The bakeable region of the input chamber contained only the input side of the specimen assembly and a U.H.V. valve, V7, to isolate it from the roughing line.

The non-bakeable region of the system consisted of the pressure modulating valve, V3, the ballast volume, the rough pumping system, and input pressure measurement.

The roughing system consisted of a Leybold Diffusion Pump with water-cooled trap backed by a rotary pump. No by-pass facility was fitted around the diffusion pump and rotary pumping was achieved through the body of the diffusion pump incidentally providing the reduction in pumping speed required for efficient operation of the modulator. Further choking of the rotary pumping speed could be obtained by adjusting valves V1 and V2 and a foreline

trap was fitted between V1 and the diffusion pump to avoid rotary pump oil contamination of the U.H.V. region of the input chamber. The fluid used in the diffusion pump was of a special low vapour pressure type (Santovac 5). The ballast tank assembly was locally baked and flushed several times using the hydrogen cylinder (19) and rotary pump (20). After this treatment contact between atmosphere and the ballast volume was avoided.

The pipework in the non-bakeable region was Viton 'O' ring sealed with Edwards 'Speedivac' couplings and valves were of SC25 Viton sealed type with the exception of the valve V3 to be described later.

After mounting a new specimen the bakeable section was enclosed in an aluminium box and heated to 250-300°C with valves V6 and V7 open to the roughing line and with the ion pump switched off and also heated to dump all the hydrogen accumulated during the previous run and to eliminate memory effect as much as possible.

During this operation the specimen furnace was switched on and the specimen heated to its maximum temperature, usually 600-700°C. The outgassing period lasted for several hours and afterwards, with the system still hot, valve V6 was shut and the ion pump started. As soon as possible the mass-spectrometer filament was switched on. The system was left to cool (with the specimen still hot) in this condition while hydrogen was trickled through the modulator leak valve (V3).

The system was then usually left overnight to equilibrate and to 'condition' the specimen.

After such treatment the ultimate pressure in the input chamber was $\sim 5 \times 10^{-6}$ torr and that in the output $\sim 5 \times 10^{-9}$ torr.

The hydrogen leakage rate to the input chamber was then

stepped up and the diffusion pump switched off so that the input system was only being pumped by the rotary pump. The valve V6 was then disconnected from the input system and the whole system was leak-checked. The specimen was checked for leakage from the input direction by substituting He for H_2 in the ballast tank and raising the input chamber to 1 atmosphere of He. No increase in the He partial pressure in the output chamber was ever seen under this test to a detection limit of 10^{-11} torr.

The experiment was then ready to run.

2.4 Pressure Control

The elements of the pressure modulation system were as follows:

The ballast volume containing the experimental gas was separated by a Vacuum Generators MD6 leak valve from the input chamber which was continuously pumped (choked, if necessary, by valves V1 and V2) by the rotary pump (21). The input pressure as measured by the Pirani gauge was fed *via* the gauge control unit as a voltage to the Solartron 3510 Integrated Measurement System and the value of pressure was deciphered from this voltage by the computer which had previously been provided with the calibration information.

Simultaneously, the computer had generated a reference input pressure wave from parameters fed to it *via* the V.D.U. (4) and a D.L.O. facility in the machine sent a pulse to hold one of the datalines high for a time proportional to the deviation of the measured signal from the reference signal. (This constant of proportionality could be altered quite easily by changing one line of the control program.) One of the datalines would hold

the motor on in a direction which closed the valve V3 while the other opened the valve, the choice being made by the computer according to whether the error signal was positive or negative. The D.L.O. facility requires that only one dataline can be held high at any time so that a third (null) line was employed which was sent high to end the 'on time' of the motor after the required time.

The control program was also employed to dump pressure-time data onto the floppy disc. This aspect will be dealt with later.

The resolution of the computer internal clock and the time of execution of the solartron reading statements in the computer program limited the minimum time between control actions to about two seconds. In practice, this made control of the modulation difficult for angular frequencies greater than about .15 radians sec^{-1}. Higher frequencies than this are not desirable anyway for reasons described later. The low frequency limit was determined only by the experimenter's patience.

The range of input pressure mean value was determined by a multiplicity of factors. The maximum value of p was approximately 1 torr. At pressures above this the fine control valve appeared to lose sensitivity and the ballast volume was very quickly emptied. Alternatively, if the valves V1 and V2 were choked back too far the response of the system became very sluggish and only suitable for low frequencies which were precisely those which could not be used because of the limitations of the ballast tank capacity.

The low pressure limit was .01 torr which, aside from being the pressure at which the Pirani Gauge ceased to function

well, was also the point at which pumping had to be undertaken by the diffusion pump. It was found that the pumping speed of the diffusion pump was far too rapid and erratic for the control valve to cope even with severe choking.

Within those limits pressure control was automated to a high degree. At lower frequencies when the system was entirely operated by the computer it was possible to feed the control program with a set of ω, p, p_H and leave the system to complete the experiment provided that p was kept low enough to avoid running out of gas.

2.5 Specimen Temperature Control

The specimen was heated by means of a thermocoax wound pyrophorite furnace rated at about 500 Watt. The power supply to this furnace was fed through a temperature controller and the set-point temperature was dialled on this controller and measured by means of a Pt/Pt 13% Rh thermocouple for which the unit was room-temperature compensated. A second Chromel/Alumel thermocouple wired through a $0^{\circ}C$ cold junction (Delristor I cell) and then through the Solartron 3510 was used for actual measurement of the specimen temperature. The Solartron 3510, although lacking a display could be interrogated at any time via the computer and V.D.U. and the temperature during a run was periodically checked in this way.

The dialled set point on the controller and the measured temperature normally agreed to less than 1° and variation in the measured temperature was sub-degree.

Stabilisation of the specimen temperature after a change

usually took about $\frac{1}{2}$ hr per 50^{o}, but a much longer time (usually overnight) was normally allowed between runs which involved a change in temperature.

The thermocouple probes were placed as close to the specimen as conditions would allow.

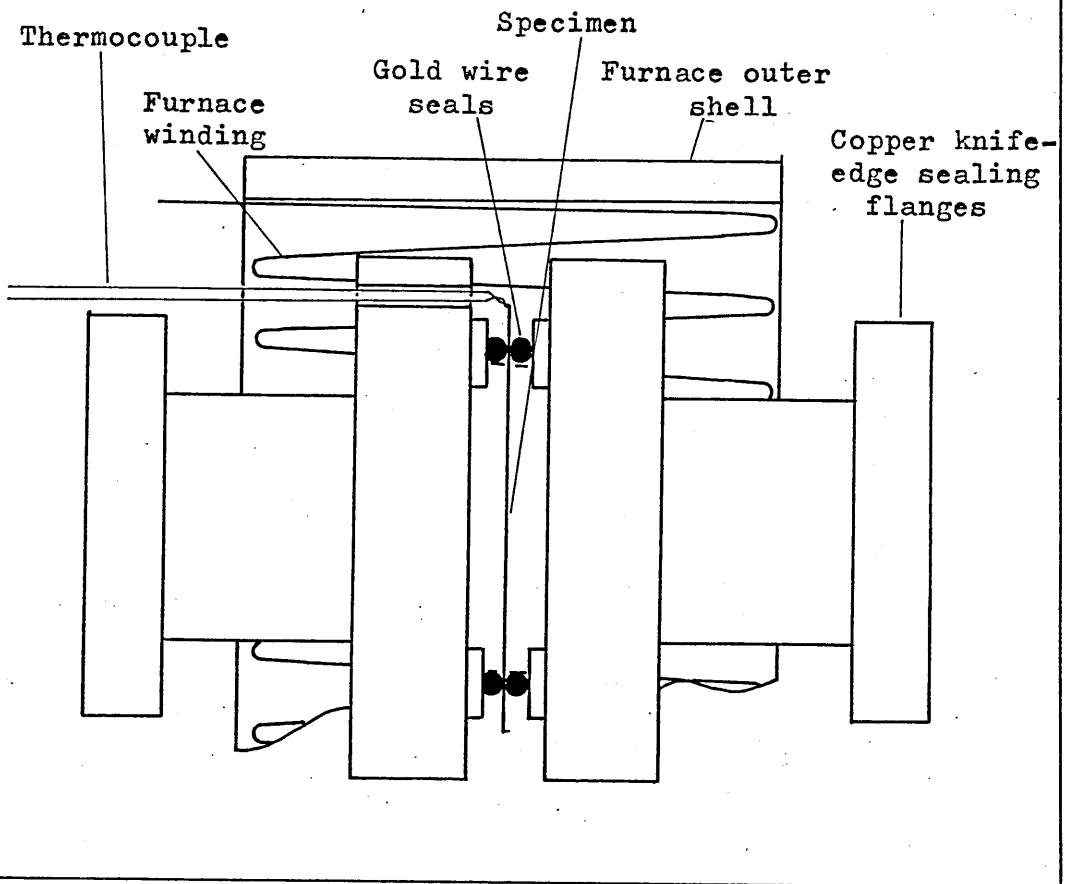

Figure 2.2 Specimen chamber, furnace and thermocouple placement

The most obvious place, i.e. inside the vacuum, against the specimen surface was discarded because of the danger of damaging the specimen if the couple was spot-welded to it or, of not, the danger of the thermocouple not making proper thermal contact with the specimen surface. It was considered that gradients between the specimen temperature outside the vacuum and that inside the vacuum would

be much less than a possible gradient across low pressure gas which may arise if an attempt were made to measure the specimen temperature inside the vacuum. For this reason the thermocouple probes were pressed into specially drilled holes through the faces of the flanges which gripped the specimen so that contact was made with the specimen material itself (Figure 2.2).

The maximum attainable temperature was limited by the nature of the specimen and of the sealing mechanism including the flanges. The dangers were as follows:

1. Melting of gold (at $\sim 1000^{\circ}C$)
2. Softening of the stainless steel faces ($800 - 1400^{\circ}C$)
3. Oxidation damage to the stainless steel
4. Melting of the specimen
5. Differential thermal expansion between stainless steel, gold and the specimen material.

In practice a safe compromise of $750^{\circ}C$ was accepted for the maximum operating temperature but specimens were not often taken above $650^{\circ}C$ except for outgassing. Also, to minimise the possibility of loss of the seal due to differential thermal expansion specimens were not heated or cooled at a rate exceeding 20° per minute.

Temperature changes were carried out in a piecewise fashion in that no specific order was followed for the temperatures investigated. The order of temperatures was never detectable from the results indicating that specimen degradation was not a problem over the times taken to conduct the experiment on a given material.

2.6 Materials and Preparation

Three different specimen materials were investigated. These materials were Molybdenum at thicknesses .25 and .5 mm, Nickel at .5 mm and M316 Stainless Steel at .1 and .25 mm. All materials were supplied by Goodfellow Metals, Ltd and typical analyses are as follows:

Stainless Steel A1S1 316: Annealed:

Cr 16.5-20%; Mn 2%; Ni 8-14%; C 1200 ppm; Mo 2.5-3.5%, Fe bal.

Nickel: High Purity: 99.99+%: Annealed:

Ag 1ppm, Al 1ppm, Ca 1ppm, Cr 1ppm, Cu 3ppm, Fe 15ppm, Mg 1ppm, Mn 1ppm, Si 2ppm, Sn 1ppm.

Molybdenum: 99.9%: Annealed:

Al 20ppm, Ca 20ppm, Cr 50ppm, Cu 20ppm, Fe 50ppm, K 2ppm, Mg 20ppm, Pb 30ppm, Si 50ppm, Ti 30ppm, W 10ppm, C 40ppm, H 5ppm, N 10ppm, O 30ppm.

Thicknesses were checked with a micrometer screw gauge and found not to vary significantly from the quoted values. The specimen area varied slightly with the diameter of the gold seal and this was measured (by measuring the diameter inside the seal) for each specimen. The value was always around $10cm^2$.

All materials were polished to a mirror surface with 0.3 micron γ - Alumina on a Selvyt cloth, washed thoroughly in detergent, ultrasonically shaken in acetone and finally rinsed in hot distilled water and blown dry. The flange sealing faces were re-cut by lathe after every specimen removal and the chamber scrubbed on the outside to remove any scale, and cleaned on the inside in a similar fashion to the specimen material (without

the γ-Alumina polish).

Neither the specimen nor the inside of the specimen chamber was again touched except with lint-free gloves or clean tweezers.

The specimen was mounted as quickly as possible after cleaning without loss of care in sealing the specimen. The chamber was then bolted between the input and output chambers on the copper/knife-edge seals and quickly pumped out with the roughing system. Failures in sealing either of the specimen or of the specimen chamber to main system seals were normally detected at this stage and were always detected before outgassing was undertaken. Failures rarely occurred in the specimen seals and were much more likely in the specimen chamber to main system seals. The success rate for the whole operation was about 70%.

The time from final washing of the specimen to 10^{-5} torr vacuum is estimated to be of the order of 2 hrs. The specimens were all degassed and treated with hydrogen as described in Section 2.2 with the exception of molybdenum which merits some special treatment by virtue of the physical properties and thermodynamic stability of its oxide.

Although the oxide of molybdenum is stable to very low partial pressures of oxygen it has the useful property of subliming at around 700°C(29). For this reason the molybdenum specimens were taken to about 750°C during the outgassing treatment.

All specimens were left for at least 24 hours at their maximum temperature under flowing (and permeating) hydrogen before any measurements were made.

Research grade hydrogen was used and all lines were thoroughly flushed and baked where possible.

2.7 Method of Measurement

The measurement of temperature has already been dealt with and this section is concerned with the means by which the six pressure parameters were measured.

As indicated earlier the experimental technique consisted of examining the response of an output wave

$$p' + p'_H e^{i(\omega t + \phi_2)}$$

to a controlled input wave

$$p + p_H e^{i(\omega t + \phi_1)}$$

Information gathered included the D.C. or steady-state levels p' and p, the amplitude p_H and p'_H and the phases ϕ_1, and ϕ_2.

Two parallel methods were used to obtain these pieces of information, each being stronger in a given frequency range.

2.7.1 Computer analysis via the Solartron 3510

In the process of controlling the input pressure to the specimen chamber the Triton Microcomputer generated a reference wave using its own internal clock.

Every time the computer required information to prompt the motor to make a control action it read the time according to its internal clock and the input pressure via the Solartron 3510. This opportunity was also used to read the output pressure so that a complete set of input pressure, output pressure and time was dumped onto the floppy disc at every control action. This data could then be recalled at any time for analysis. The integration time of the Solartron 3510 was variable in the range 1-1000 ms but 100 ms was used throughout the experiment. In

the range of frequencies in which this method was used for time-dependent measurements the 100 ms represented a phase-lag increase of only 1×10^{-3} radians at most and was not an important source of error.

The dumped data was recalled in the form of input pressure and output pressure as a function of time. These data were handled by simultaneous Fourier Analysis and signal averaging. This process was carried out in two equivalent, but distinct, ways:

(i) Each period was analysed separately for its D.C. level and the Fourier sine and cosine coefficients of the fundamental wave. This method was applied to the output wave only.

Since the Fourier coefficients were available for each period of the output wave, the consistency from period to period could easily be determined. The Fourier coefficients for the individual periods were averaged and the standard deviations calculated. The D.C. level, phase and amplitude of the output wave was then calculated from the average Fourier coefficients and the standard deviations on these quantities calculated from the standard deviations on the Fourier coefficients using the appropriate transformation equations. The source of the deviations in the output wave could, of course, have arisen from deviations on the input wave.

(ii) The waves were signal averaged, each pressure reading being added to the corresponding value at a time $2\pi/\omega$ later. The final averaged wave was analysed for the Fourier coefficients which were then divided by the number of periods. This process was applied to both input and output waves.

The phase lag was calculated after the averaging procedure had been completed on the input wave.

The deviation on the D.C. level was generally less than 1% of its value and those on the phase and amplitude varied with the frequency of the wave. Deviations in the averaged phase and amplitude rarely exceeded 10% at the higher frequency end of the spectrum with deviations becoming less as the frequency was decreased. This method of measurement was deemed questionable when either of the Fourier coefficients of the fundamental wave became doubtful in sign.

Under normal conditions, acceptable measurements could be made for frequencies up to 1.2×10^{-2} radians/sec. Above this point, the number of measurements which could be made in a cycle was too low to give an acceptable deviation after a reasonable number of cycles.

There were two possible reasons for loss of sensitivity in the output pressure in this operating mode. The first was when too few points were taken in each period to allow accurate Fourier integration as described in the previous paragraph. The second was loss of signal in the output chamber because permeation was slow and the only solution in this case was to increase the input pressure and its modulation.

Below 1.2×10^{-2} radians/sec the second parallel method of measurement was used but this method was always used to obtain the D.C. levels.

2.7.2 Signal Averaging in the Datalab DL4000

The Datalab DL4000 is a device which performs signal averaging in much the same way as the analysis program described in the previous section. It took two inputs (input and output pressure) and divided each into 256 channels. An internal clock

was set to scan the channels at the same frequency as that which was fed to the control program. The number of sweeps (periods) to be performed by the Datalab was set on the machine and it added pressures which were separated by a time $= 2\pi/\omega$.

The inputs were amplified by up to 1000x to give a signal of amplitude around $\pm 1V$ to make maximum use of the sensitivity of the machine. For this reason, a quite considerable offset was required on the amplifiers which rendered the D.C. value difficult to obtain.

Datalab operations were in real-time in that averaging took place as the experiment was run. The averaged waves were displayed on an oscilloscope during the run and provided a qualitative check that an acceptable signal/noise ratio was being obtained.

On completion of a run, the data pertaining to an averaged wave were transferred to disc. They were then available for Fourier Analysis by the computer. The input and output waves were treated separately. An additional check on the strength of the fundamental (i.e. signal/noise ratio) could be made by examining the amplitude of the first harmonic of each wave and this was always less (usually considerably so) than 10% of the fundamental.

The high frequency limit of this technique was higher than the maximum attainable frequency of the modulator. Very low frequencies were not undertaken because of the requirement that the machine be supervised whereas the other route was capable of performing a set of low frequencies without supervision.

The number of periods required for a 'clean' averaged signal was a function of both frequency and of the permeation rate of hydrogen through the material under investigation.

Typically about 16 periods were used at the high frequency end of each method. This value changed little for the Datalab method but at very low frequencies using the Solartron method remarkable reproducibility could be obtained with as few as three cycles.

2.8 Calibration

Since the Solartron 3510 IMS, as well as being a voltmeter, has analogue to digital conversion this makes it suitable for reading by computer. Calibration of all quantities which were to be treated by the computer could then be fed to the computer as arrays of digital information (e.g. pressure - voltage matrices) providing results in particularly useful (digital) form.

2.8.1 Pressure measurement

The input pressure Pirani gauge was calibrated for hydrogen against both a Bourdon and a McLeod Gauge over the range 10^{-2} - 10 torr on a small vacuum rig specially designed for the purpose. The voltages recorded on the output from the Pirani control unit and the corresponding pressure measurements were shown on disc as an array which could be accessed by the pressure control and Fourier Analysis/signal averaging programmes, so that control inputs at the V.D.U. and the results of analysis could be made in terms of pressure (rather than voltage) avoiding the necessity for manual reading of calibration curves.

The computer performed a simple linear interpolation between the calibration data points. At pressures below 10^{-2} torr the Pirani 9 became relatively insensitive to pressure changes and at pressures above about 1 torr the slope of voltage vs. pressure became extremely high and these formed an additional

but acceptable, restriction on the operating pressure range.

The mass spectrometer had a chart recorder output of 0 - 100 mV which was linear in pressure, 100 mV corresponding to the full scale deflection of the meter reading. Full scale sensitivity could be dialled in factors of ~3 over the range 3×10^{-4} torr to 3×10^{-10} torr. Conversion of this voltage to a pressure by the computer was a simple matter the only input required being the F.S.D. of the spectrometer.

In practice, pressures above about 5×10^{-5} torr in the output chamber were inadvisable because they severely restricted filament life and outgassing would take place to such a level that the ion pump would be overloaded.

There are also difficulties of operation at very low pressures (low permeation rates). As the experimental pressure approaches that of the hydrogen background in the system, any fluctuations of the background contribute significant noise to the readings of the D.C. hydrogen signal. In addition, the net pumping rate becomes small so that the phase-lag due to pumping (see Section 2.8.3) becomes larger.

2.8.2 Temperature measurement

Temperature control and measurement were handled by separate thermocouples.

The measurement couple was calibrated against an N.P.L. Calibrated Pt-Pt - 13% Rh couple in a tube furnace whose temperature was held constant by the control unit. This incidentally provided a check on the operation of the control unit and the accuracy of its set point which were found to be acceptable to 1°.

2.8.3. Flux calibration

When a vacuum system is pumped, the ultimately attainable pressure is never zero but is given by a balance between the gas entering the system (by outgassing, leakage, etc.) and the gas being evacuated from the system by the pump. Thus, measurement of pressure in a pumped U.H.V. system gives a direct indication of the flux of gas entering the system, provided that the evacuatory flux is known. The specification of the P60 Ion Pump indicates that the pumping speed is constant over the range 10^{-4} to 10^{-8} torr. The pumping equation is:

$$\frac{dp}{dt} = J' - \beta(p - p_u)$$

where J' is the modified flux into the system, β is the pump characteristic and p_u is the pressure obtained in the output chamber when J' = 0.

The modified flux J' must be expressed as torr/sec., whereas fluxes calculated from the diffusion equation are normally expressed as J = moles $H_2/cm^2 sec$. Thus the relationship between J and J' is:-

$$J' = J \frac{ART}{V}$$

where A is specimen area in cm^2

R is gas constant as liter torr $mole^{-1}$ $^oK^{-1}$

V is system volume in liters

T is ambient temperature, ^oK

To obtain values for fluxes through the specimens it is necessary to make a measurement of β.

A leak experiment, similar in nature to the real experiment,

was performed in order to make a direct measurement of the parameter β.

The specimen was replaced by an Edwards reference leak calibrated for dry air.

The mass flow rate through a leak is given by (30)

$$Q = \sqrt{\frac{kT}{2\pi m}} \; (p_t - p_t') \; A$$

For a constant area and known leak rate.

$$Q = L' \; \frac{1}{\sqrt{m}} \; (p_t - p_t') \text{ torr liter sec}^{-1}$$

The quoted rate Q_R for the standard leak is in torr liter sec^{-1} from 1 Atmosphere to negligible pressure for dry air

$$Q_R = L' \; \frac{1}{\sqrt{m_{air}}} \; 760 \text{ torr liter sec}^{-1}$$

So that the leak rate from a pressure p_t to a pressure p_t' for hydrogen:

$$Q = \frac{Q_R \sqrt{m_{air}}}{760\sqrt{m_{H_2}}} \; (p_t - p_t') \text{ torr liter sec}^{-1}$$

The pumping rate in the output chamber can be represented by:

$$\left[\frac{\partial p_t'}{\partial t}\right]_p = -\beta \; (p_t - p_t') \text{ torr/sec}$$

and the leak rate in comparable units:

$$\left[\frac{\partial p_t'}{\partial t}\right]_1 = \frac{Q}{V} = \frac{Q_R \sqrt{m_{air}}}{V.760\sqrt{m_{H_2}}} \; (p_t - p_t') \text{ torr/sec}$$

Thus, the net change in p

$$\frac{\partial p_t'}{\partial t} = \left[\frac{\partial p_t'}{\partial t}\right]_p + \left[\frac{\partial p_t'}{\partial t}\right]_l = \frac{Q_l \sqrt{m_{air}}}{V.760\sqrt{m_{H_2}}} (p_t - p_t') - \beta(p_t' - p_u')$$

$$= Ap_t - (A + \beta)p_t' + \beta p_u'$$

where $A = \frac{Q_R \sqrt{m_{air}}}{V.760\sqrt{m_{H_2}}}$

If the input pressure is modulated we can write:

$$p_t = p + p_H e^{i\omega t}$$

$$p_t' = p' + p_H' e^{i(\omega t + \xi)}$$

Substituting and equating the time dependent and non time-dependent parts:

$$\tan \xi = \frac{\omega}{A + \beta}$$

$$p_H' = \frac{A\, p_H}{\sqrt{\omega^2 + (A+\beta)^2}}$$

$$p' = \frac{Ap + \beta p_u'}{(A + \beta)}$$

In practice, the reference leak which was made from compound metal powder, was not entirely free from phase effects. It was found that a better measurement of β resulted from a simple D.C. experiment where the pressure was held at a controlled level on the input side and the pressure on the output side was measured. This D.C. experiment was carried out in the range 0 - 20 torr of input pressure but, because of the steepness of the calibration of the input Pirani gauge for hydrogen at pressures above about 10 torr the scatter of the straight line of p vs. p' was unacceptable. Measurements in the range of input pressure from 0 - 10 torr are

shown in Figure 2.3 along with the best fit regression line:

$$p' = 4.8868 \times 10^{-9}(6.9 \times 10^{-11})\ p + 2.2081 \times 10^{-8}(3.09 \times 10^{-10})$$

$$= mp + c$$

The volume of the output chamber was measured by pressure dropping from a known volume and also by calculation from the dimensions of the components and its value found to be 4.35 l (±.06 l). The value of A was found using the reference leak rate and the other parameters in the defining equation and hence

$$\beta V = \frac{AV}{m} = 7.56 \text{ liters sec}^{-1} \ (\pm .08)$$

Although the full range of input pressure was investigated with this experiment, the leak rate was too small to allow large output pressures to be investigated. In order to ensure that β did not change appreciably with output pressures a further series of experiments were carried out with the valve V6 deliberately poorly sealed in order that a fairly large leakage into the output chamber could be investigated. Although the value of A was not known in this case, the p' vs. p curves remained linear right up to output pressures of 5×10^{-5} torr indicating that β did not change appreciably over the full experimental range.

2.8.4 Equipment response times

Since the experimental technique relies on the response of the output pressure to modulation of the input pressure it is of importance to ensure that equipment response times are not so slow as to cause serious modifications of the measured amplitude ratios and phase-lags. In general, the measurement of a simple harmonic pressure wave will be attenuated and phase-lagged with respect to the wave itself.

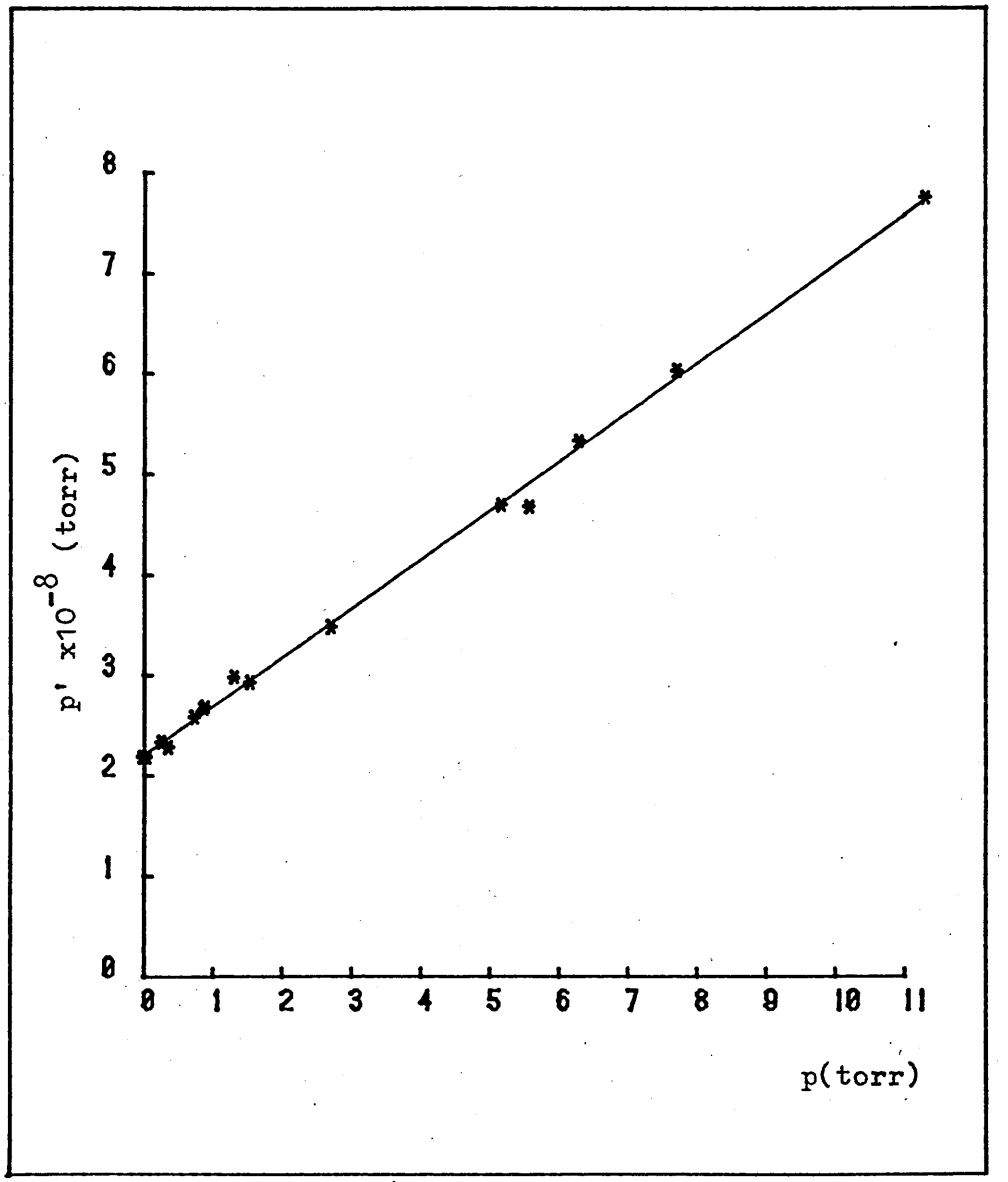

Figure 2.3 Output pressure as a function of input pressure through the calibrated leak

A simple electrical analogue can be used to examine the effect of equipment response. (Not really an analogue since the origin of the effect is probably electrical anyway.)

The true pressure is seen as passing through an R-C circuit as shown and the measured pressure is represented as the voltage across the capacitor:

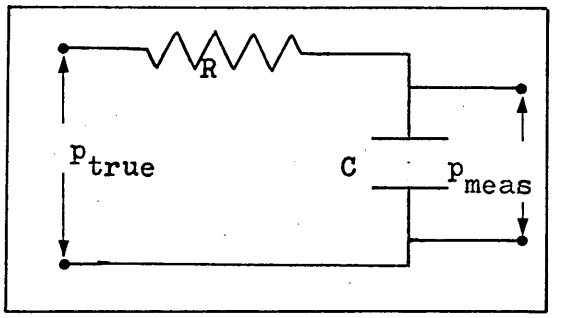

From simple a.c. circuit theory it can be seen that

$$p_{meas} = \exp\frac{-t}{\tau} \int \frac{1}{\tau} p_{true} \exp\frac{-t}{\tau}\, dt$$

A sudden change in the true pressure to a value p_{true} will cause a response in the measured pressure given by:

$$p_{meas} = p^{o}_{true} + (p^{o}_{meas} - p^{o}_{true})\exp\frac{-t}{\tau}$$

where p^{o}_{meas} is the measured value at $t = 0$

This means that changes which occur in times of the order τ cannot be effectively measured.

More specifically if the true pressure is a wave of the form:

$$p_{true} = p^{o}_{true} + p'_{true}\, e^{i\omega t}$$

then $$p_{meas} = p^{o}_{meas} + p'_{meas}\, e^{i(\omega t + \delta)}$$

where $p^{o}_{meas} = p^{o}_{true}$ after a time $\gg \tau$

and $$\tan \delta = \omega\tau$$

$$p'_{meas} = \frac{p'_{true}}{\sqrt{1+\omega^2\tau^2}}$$

The response times, τ , for the mass spectrometer and the Pirani gauge were measured by their responses to an electronic step change simulating the pressure. The value was about .1 sec for the mass spectrometer and rather less than this for the Pirani gauge. Since the range of angular frequencies used experimentally do not exceed .1 sec^{-1} it can be seen that this effect is negligible. It should, however, be noted that this effect places a severe restriction on the possibility of measuring the pump characteristic, β , by measuring pumpdown rates in the output chamber with zero specimen flux. If this is attempted, most of the pressure change occurs in a time much less than 1 sec. and the response time of the instrument, in this case the mass spectrometer, is too slow to resolve this curve with any degree of accuracy.

2.9 Summary

In this chapter an experiment has been devised to the general specification suggested by the brief description of the modulatory technique.

With this apparatus it was possible to produce input pressures modulated about D.C. levels of 10^{0} to 10^{-2} torr. Angular frequency was variable in the range .15 to 10^{-3} radians per second. Phase lags down to .1 radians were measurable over this full range corresponding to time lags as small as .5 sec., although normally this was not necessary. D.C. levels of down to 10^{-8} torr could easily be measured corresponding to fluxes of around 4×10^{-12} moles/sec. Variations in the D.C. flux during an experiment were less than 1%.

Chapter III will go on to develop the solution of the

diffusion equation for the oscillatory boundary condition as a prelude to discussing the methods of interpretation of the experimental results.

CHAPTER 3

GENERAL SCHEME AND SOLUTIONS OF THE SURFACE REACTION MODEL

3.1 Requirements of the Model

As mentioned in Chapter I, a relationship is sought between the pressure measured in the output chamber and the controlled, modulated pressure in the input chamber.

This relationship will be split into three parts linking the steady-state levels, the amplitudes and the phases of the input and output pressures.

In this chapter these relationships are found by solving Fick's Laws for diffusion in the solid (i.e. assuming no 'internal' effects as described in Chapter I) for boundary conditions which depend on the model adopted for the solution process. Much of the discussion is concerned with the effect that finite solution rates have on the steady-state, amplitude and phase relations.

This development is not concerned with solutions which are due to a superposition of the rate-of-rise to steady-state and oscillatory experiments, i.e. the system is assumed to have been in a modulatory state for long enough that such transient effects have died out.

3.2 Definitions and Terminology

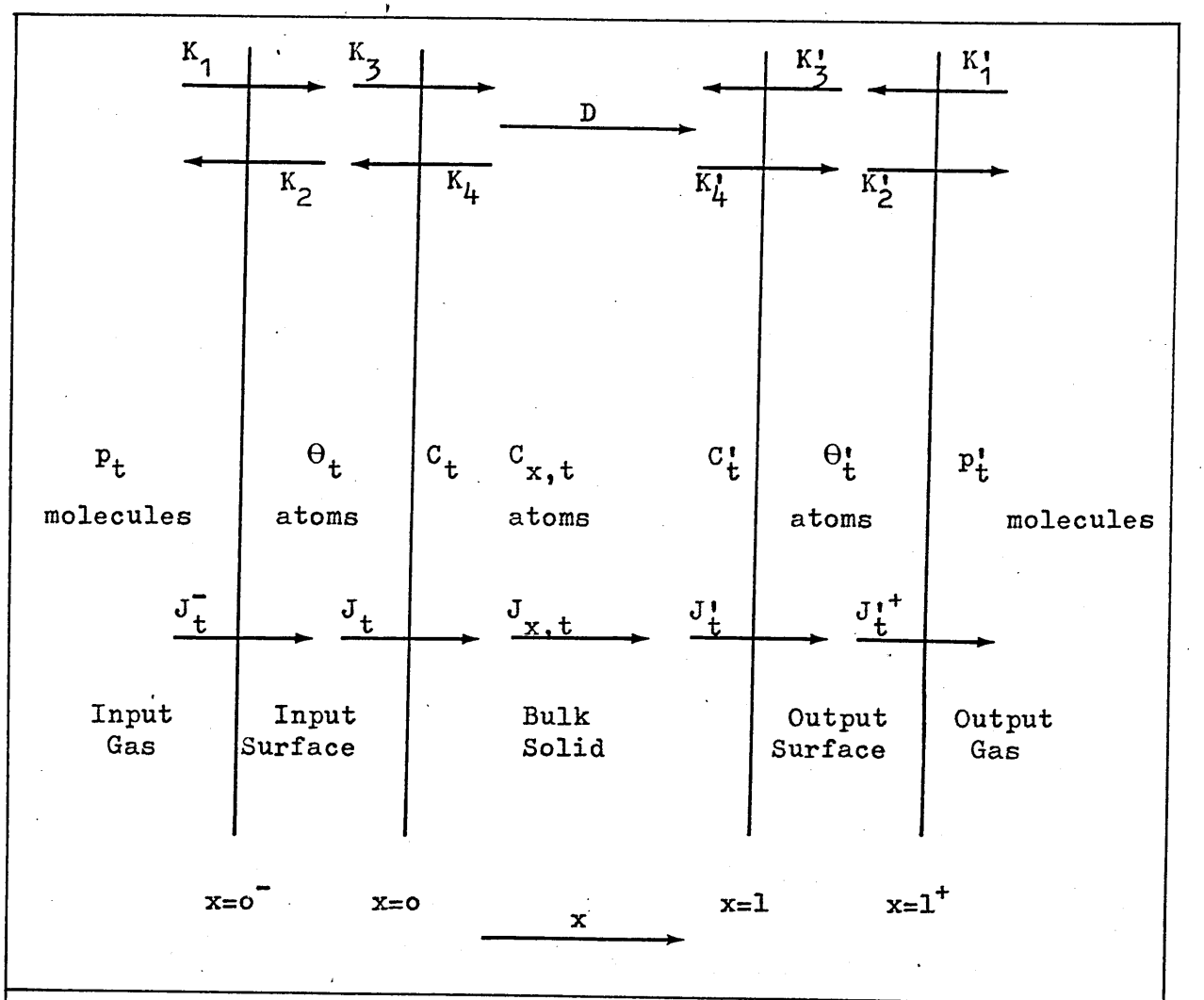

Figure 3.1 Definitions of the various quantities used in the model

Figure 3.1 shows the transport parameters and concentration and flux variables involved in the model. The transport parameters D, K_i, K'_i operate on the concentration parameters p_t, θ_t, C_t, C'_t, θ'_t, p'_t to produce the fluxes according to the scheme:

$$J_t^- = K_1 p_t - K_2 \theta_t^2$$

$$J_t = K_3 \theta_t - K_4 C_t$$

$$J_{x,t} = -D \left(\frac{\partial C}{\partial x} x,t \right)_x$$

$$J'_t = K'_4 C'_t - K'_3 \theta'_t$$

$$J'^{+}_t = K'_2 \theta'^{2}_t - K'_1 p'_t$$

where θ is a surface density of atoms

C is a concentration

p is a pressure

J is a flux.

Fluxes in the positive x-direction (defined in Figure 3.1) are positive.

Each of the fluxes, pressures, surface densities and concentrations is split into two components: a harmonic part and a steady-state part. Also, each quantity has a corresponding input and output value.

The convention applied throughout this work is to represent total (harmonic plus steady-state) quantities by a symbol with the suffix, t. For input quantities the symbol will be displayed only with its suffix: it will be primed for the output quantity. The rate parameters (K_i, K'_i) are not harmonic and the numeric suffixes correspond to their functions as indicated in Figure 3.1. Again, a prime is used to distinguish the output quantity. The steady-state part of each of the modulatory quantities is unsuffixed and the harmonic part has the suffix, H.

Thus:

$$p_t = p + p_H e^{i\omega t} \quad \text{(Input chamber pressure)}$$

$$C_t = C + C_H e^{i(\omega t + \psi)} \quad \text{(Input surface concentration)}$$

$$J'_t = J' + J'_H e^{i(\omega t - \psi - \phi)} \quad \text{(Flux crossing surface } x = 1\text{)}$$

$$J'^{+}_t = J'^{+} + J'^{+}_H e^{i(\omega t - \psi - \phi - \zeta)} \quad \text{(Emergent flux at } x = 1^{+}\text{)}$$

$$p'_t = p' + p'_H e^{i(\omega t - \psi - \phi - \zeta - \xi)} \quad \text{(Output chamber pressure)}$$

As can be seen from the above, the total phase lag between the input and output pressures can be seen as the sum of phase lags between each of the above quantities and these lags occur between the surfaces $x = 0^{-}$, $x = 0$, $x = 1$, $x = 1^{+}$. The final phase lag ξ between the emergent flux J'^{*}_t and the output chamber pressure p'_t is to do with the pumping term, β, and will also be dealt with in this chapter.

Of course, all the fluxes, pressures, surface densities and concentrations can be represented in this form with their associated phase lags. However, the quantities displayed above are those of the most significance in the development of the solutions.

Further quantities of which use is made are the Sieverts constant, K_{sm}, the concentration within the bulk of the solid $C_{x,t} = C_x + C_{H,x} e^{i(\omega t + \delta)}$, the specimen thickness, l, the output chamber pump characteristic, β, the permeability, P_M, and a useful quantity derived from the diffusion coefficient, D, and the angular frequency of modulation, ω, called k where $k = \sqrt{\frac{\omega}{2D}}$.

Other parameters of transitory use will be defined as required.

Complex quantities are written with a subaccent thus: $\underset{\sim}{A}$

3.3 Steady-State Solution

The simplest analysis of the problem suggested by the boundary effects of Figure 3.1 is based on a solution where the harmonic parts are zero (e.g. $p_t = p$).

When the system does not change with time continuity requires that:

$$K_{1p}-K_2\theta^2 = K_3\theta-K_4C = K_4'C'-K_3'\theta' = K_2'\theta'^2-K_1'p' = \frac{-D(C'-C)}{l} = J \quad (3.1)$$

(Note that in the steady-state case J is independent of x,t and does not require a suffix.)

Combining equations (3.1) and rearranging gives:

$$J = \frac{-D}{l}\left[\frac{J}{K_4'} + \frac{K_3'}{K_4'}\sqrt{\frac{J + K_1'p'}{K_2'}} + \frac{J}{K_4} - \frac{K_3}{K_4}\sqrt{\frac{K_1p-J}{K_2}}\right] \quad (3.2)$$

Also:

(i) J = 0: The system is in thermodynamic equilibrium; i.e. p' = p and C' = C.

From (3.1):

$$\frac{C}{\sqrt{p}} = \frac{K_3}{K_4}\left(\frac{K_1}{K_2}\right)^{\frac{1}{2}}$$

$$\frac{C'}{\sqrt{p'}} = \frac{K_3'}{K_4'}\left(\frac{K_1'}{K_2'}\right)^{\frac{1}{2}}$$

Hence:
$$\frac{K_3}{K_4}\left(\frac{K_1}{K_2}\right)^{\frac{1}{2}} = \frac{K_3'}{K_4'}\left(\frac{K_1'}{K_2'}\right)^{\frac{1}{2}} = K_{sm} \quad (3.3)$$

(ii) Diffusion-limited flow

When the flux through the specimen is totally diffusion-limited this means that all the surface fluxes are very rapid compared to the diffusion

flux $D(C-C')/l$.

The system of simultaneous equations (3.1) no longer holds since each surface can be considered to be in thermodynamic equilibrium, i.e. $K_1p-K_2\theta^2$ etc. = 0, and therefore:

$$J = \frac{D(C-C')}{l}$$

$$\theta^2 = \frac{K_1p}{K_2}$$

$$\theta = \frac{K_4C}{K_3} \quad \text{etc.}$$

Hence:

$$J = DK_{sm}\frac{(\sqrt{p} - \sqrt{p'})}{l}$$

i.e.
$$J = P_M\frac{(\sqrt{p} - \sqrt{p'})}{l} \tag{3.4}$$

which is Richardson's classical permeation equation.

Equation (3.2) identifies two distinct types of modification which surface effects can exert on the system. Using equation (3.3), (3.2) can be rewritten:

$$J\left[1 + \frac{D}{lK_4} + \frac{D}{lK_4'}\right] = \frac{DK_{sm}}{l}\left[\sqrt{p}\sqrt{1 - \frac{J}{K_1p}} - \sqrt{p}\sqrt{\frac{J}{K_1'p} + \frac{p'}{p}}\right] \tag{3.5}$$

Comparison of (3.5) with (3.4) shows that the steady-state flux through the specimen can be modified by quantities of the type $\frac{D}{lK_4}$ or $\frac{J}{K_1p}$. It is important to recognise that the first of these quantities is liable to be more significant when the specimen is thin or when the diffusion coefficient is large. The second is dependent on pressure. The partitioning

of the surface effect in terms of these two types of control will also become apparent in the oscillatory solutions.

3.4 The General Oscillatory Solution

For the purposes of this analysis the 'concentration' variables have been separated into oscillatory and steady-state parts. This is legitimate since Fick's second law is a linear differential equation so that the problem can be solved separately for each of the steady-state and oscillatory parts of the input concentration and the solutions added together. The remaining analysis is concerned with the oscillatory part of this solution.

It can be shown by separation of variables on the time-dependent diffusion equation in one dimension

$$\frac{\partial C}{\partial t} = -D \frac{\partial^2 C}{\partial x^2} \tag{3.6}$$

that the oscillatory solution (for the principal harmonic only) can be given by (Appendix A.2):

$$\underset{\sim}{C}_{H,x} = \left[\underset{\sim}{A}\, e^{\underset{\sim}{a}(x-1)} + \underset{\sim}{B}\, e^{\underset{\sim}{a}(1-x)} \right] e^{i\omega t} \tag{3.7}$$

where $\underset{\sim}{a} = (1 + i)k$

The harmonic quantities in this development are all written in complex form $(x + iy)$ for convenience of manipulation. The real quantity associated with this form has an amplitude $A = \sqrt{(x+iy)(x-iy)}$ and a phase $\Phi = \arctan\left(\frac{Y}{X}\right)$.

Equation (3.7) is valid whatever the surface process since it describes only movement of matter within the bulk of the solid. The effect of surface processes can be isolated from the problem and examined by means of the boundary values which

will fix the arbitrary constants $\underset{\sim}{A}$ and $\underset{\sim}{B}$ in equation (3.7).

The boundary conditions can be written in a quite general form and made more specific for each actual surface process or combination thereof.

The general boundary condition is therefore a non-specific phase-amplitude relationship between $\underset{\sim}{A}$ and $\underset{\sim}{B}$ expressible as:

$$\underset{\sim}{A}(x + iy) = \underset{\sim}{B}(r + is) \qquad (3.8)$$

where x, y, r, s are real constants which describe the phase/amplitude relationship between the complex constants $\underset{\sim}{A}$ and $\underset{\sim}{B}$. In the latter parts of this development one rarely starts with a knowledge of either of the surface concentrations. It is therefore necessary that they be written in some general form so that the interfacial flux equations (i.e. those involving the K_i) can be used to define the values of x, y, r, s. Sections 3.5 and 3.6 use simple boundary conditions and do not make use of this facility.

3.5 The Classical Oscillatory Solution

The simplest boundary condition for the solution (3.7) is that which supposes equilibrium at the input surface so that:

$$C_H = \frac{K_{sm}\ p_H}{2\sqrt{p}} \quad \text{(See A.1) and} \quad \psi = 0$$

where ψ is the phase-lag between the input pressure and the input surface concentration.

The other boundary condition supposes that the output surface concentration is very small and that the flux leaving this surface is given by Fick's First Law applied to the concentration

gradient at the point $x = 1$ so that $C'_H = 0$ and $\zeta = 0$.

Also,

$$J'_H = J'^{+}_H = -D \left(\frac{\partial \underset{\sim}{C}_H, x}{\partial x} \right)_{x=1}$$

Applying these two conditions to (3.7) gives

$$\underset{\sim}{A} = -\underset{\sim}{B}$$

$$\text{and} \quad \underset{\sim}{A} = \frac{K_{sm}\, p_H}{2\sqrt{p}} \Bigg/ \left(e^{-\underset{\sim}{a}l} - e^{\underset{\sim}{a}l} \right)$$

Back-substituting the values for $\underset{\sim}{A}$ and $\underset{\sim}{B}$ into equation (3.7) and differentiating with respect to x, evaluating the result at $x = 1$ and writing the resulting complex quantity in phase/amplitude form gives:

$$J'_H = J'^{+}_H = C_H . B^{clas} = \frac{K_{sm}\, p_H}{2\sqrt{p}} \cdot \frac{\sqrt{2\ kD}}{\sqrt{\sinh^2 kl + \sin^2 kl}} \qquad (3.9)$$

and

$$\phi = \arctan \left[\frac{\tan kl - \tanh kl}{\tan kl + \tanh kl} \right] \qquad (3.10)$$

where the factor B^{clas} is introduced for later convenience.

It is worth noting at this point that the condition $\underset{\sim}{A} = -\underset{\sim}{B}$ encountered in this treatment demands that $x = -r$ and $y = -s$ in the general boundary condition (3.8).

3.6 Pumping Modification

When the output chamber is pumped the output pressure responds in a specific way to the emergent flux. This modification is not included as a boundary condition since it is independent of any effects due to the specimen.

In the presence of pumping the rate of change of pressure in the output chamber can be given by

$$\frac{dp'_t}{dt} = \frac{ART_c}{V} J'^{+}_t - \beta(p'_t - p'_u)$$

i.e. the emergent flux tends to increase the output pressure whereas pumping tends to decrease it, the net time rate of change of the output pressure being given by the sum of these two components.

where

A = specimen area

R = gas constant

T_c = output chamber temperature

V = output chamber volume

β = pump characteristic defined in Section 2.8.3

p'_u = ultimate pressure which would be obtained in output chamber if J'^{+}_t were zero

Solving the above differential equation for a harmonic emergent flux of arbitrary phase and amplitude J'^{+}_H to produce a harmonic output pressure gives:

$$p'_H = J'^{+}_H \frac{ART}{V(\omega^2 + \beta^2)} \qquad (3.11)$$

for the amplitude of the output pressure referred to the emergent flux amplitude, and

$$\xi = \arctan \frac{\omega}{\beta} \qquad (3.12)$$

for the phase-lag of the output pressure with respect to the emergent flux.

3.7 Surface Modifications

Having considered the classical and pumping effects the modifications to the classical equations (3.9) and (3.10) which arise due to surface effects can now be investigated.

It is convenient first to divide the system up into three regions. This division is suggested by Figure 3.1 and the equations following it. Processes occurring at the input surface due to non-equilibrium can be represented by a modification of the input concentration amplitude, C_H, from its equilibrium value $\frac{K_{sm} p_H}{2\sqrt{p}}$ and by phase-lag of the surface concentration relative to the input pressure, ψ.

Processes occurring at the surface $x = 1$ due to non-zero values of C' affecting the bulk concentration gradients and hence affecting the diffusion flux can be represented by a modification of the amplitude of the flux crossing the plane $x = 1$, (J_H'), by a factor B from the input concentration amplitude. A phase lag, ϕ, between the input concentration and the flux J_H' is also required. The quantities B, ϕ include the 'classical' contributions, equations (3.9) and (3.10), for the modifications due to diffusion in the solid.

The effect of a finite evaporation rate from the surface $x = 1^+$ can be represented by a modification to account for the fact that $J_t^{+'}$ is lagged and attenuated relative to J_t'. This modification is again represented by an amplitude factor, C, and a phase-lag, ζ.

The full solutions for each of these effects will be discussed separately. It should be noted that, since modulations are, in general, small relative to the steady-state levels of the quantities the surface rates have been assumed to be functions only of the steady-state levels of the surface concentrations.

The detailed dependence of the solutions on the experimental variables is treated in Chapter 4.

3.8 Bulk Diffusion Modification (B, ϕ)

When the boundary conditions applied in Section 3.5 are not used a rather different answer is obtained for the quantities B and ϕ in equations (3.9) and (3.10). These two quantities represent the attenuation and phase-lag of the flux across the surface $x = 1$ referred to the input surface concentration. In contrast to the 'classical' situation of Section 3.5, the surface concentrations are not known and the boundary conditions become a set of simultaneous equations. Considering only the oscillatory part:

$$\underset{\sim}{J}'_H = K'_4 \underset{\sim}{C}'_H - K'_3 \underset{\sim}{\Theta}'_H = -D \left(\frac{\partial \underset{\sim}{C}_H, x}{\partial x} \right)_1$$

$$\underset{\sim}{J}'^{+}_H = 2K'_2 \underset{\sim}{\Theta}'_H \theta' - K'_1 \underset{\sim}{p}'_H$$

$$\frac{\partial \underset{\sim}{\Theta}'_H}{\partial t} = \underset{\sim}{J}'_H - \underset{\sim}{J}'^{+}_H$$

$$\frac{\partial \underset{\sim}{p}'_H}{\partial t} = \frac{ART}{V} \underset{\sim}{J}'^{+}_H - \beta \underset{\sim}{p}'_H$$

[The first term in the second of these equations is the oscillatory part of $\theta'^2_t = (\theta' + \underset{\sim}{\theta}'_H)^2 \simeq \theta'^2 + 2\underset{\sim}{\theta}'_H \theta'$ if $\underset{\sim}{\theta}'_H \ll \theta'$]

The above four equations can be combined to eliminate $\underset{\sim}{p}'_H$ and $\underset{\sim}{\Theta}'_H$ to give an expression for the concentration only at $x = 1$.

$$\left[\left(\frac{\partial}{\partial t} + \beta \right) \left(\frac{\partial}{\partial t} + 2K'_2 \theta' \right) - K'_1 \frac{ART}{V} \frac{\partial}{\partial t} \right] K'_4 \underset{\sim}{C}'_H +$$

$$\left[\left(\frac{\partial}{\partial t} + \beta \right) \left(\frac{\partial}{\partial t} + K'_a \right) - K'_1 \frac{ART}{V} \left(\frac{\partial}{\partial t} + K'_3 \right) \right] D \left(\frac{\partial \underset{\sim}{C}_H, x}{\partial x} \right)_1 = 0$$

Using equation (3.7) and its derivative with respect to x both evaluated at $x = 1$, i.e.

$$\underset{\sim}{C}'_H = (\underset{\sim}{A} + \underset{\sim}{B})\, e^{i\omega t}$$

and $$\left(\frac{\partial \underset{\sim}{C}_H, x}{\partial x}\right)_1 = \underset{\sim}{a}(\underset{\sim}{A} - \underset{\sim}{B})_e i\omega t$$

and substituting these into the concentration expression above yields a complex expression for $\underset{\sim}{A}$ in terms of $\underset{\sim}{B}$. It is at this point that the general boundary condition (3.8) becomes useful since this expression is of the form (See Appendix A.5)

$$\underset{\sim}{A}(x + iy) = \underset{\sim}{B}(r + is)$$

where x, y, r, s are power series in the square root of frequency of the form

$$x = \sum_{n=o}^{5} x_n\, \omega^{n/2}$$

and the x_n, y_n, r_n, s_n are given in the table:

n	x_n	y_n	r_n	s_n
0	$2\beta K'_2 K'_4 \theta'$	0	$-x_o$	0
1	$\left(\beta K'_a + K'_1 K'_3 \frac{ART}{V}\right)\frac{D^{\frac{1}{2}}}{\sqrt{2}}$	x_1	x_1	x_1
2	0	$K'_4\left(2K'_2\theta' + \beta - K'_1 \frac{ART}{V}\right)$	0	$-y_2$
3	$-\left(\beta + K'_a - K'_1 \frac{ART}{V}\right)\frac{D^{\frac{1}{2}}}{\sqrt{2}}$	$-x_3$	x_3	$-x_3$
4	$-K'_4$	0	$-x_4$	0
5	$-\frac{D^{\frac{1}{2}}}{\sqrt{2}}$	x_5	x_5	x_5

and $$K'_a = K'_3 + 2K'_2\theta'$$

Now, using the equations (derived from the general solution (3.7)) at x = 0 and x = 1 respectively:

$$\underset{\sim}{C}_H = \left[\underset{\sim}{A}e^{-\underset{\sim}{a}l} + \underset{\sim}{B}e^{\underset{\sim}{a}l}\right]e^{i\omega t}$$

and

$$-D\left(\frac{\partial \underset{\sim}{C}_H, x}{\partial x}\right)_1 = (\underset{\sim}{A} - \underset{\sim}{B})e^{i\omega t} = \underset{\sim}{J}'_H$$

along with the general boundary condition linking $\underset{\sim}{A}$ and $\underset{\sim}{B}$, the attenuation and phase-lag of the flux crossing the surface x = 1 ($\underset{\sim}{J}'_H$) referred to the input concentration, $\underset{\sim}{C}_H$, can now be evaluated in terms of the x, y, r, s:

$$J'_H = C_H B = C_H \frac{\sqrt{2}\, kD\sqrt{\gamma}}{\sqrt{\delta\cosh 2kl + \alpha\sinh 2kl + \epsilon\cos 2kl - \beta\sin 2kl}} \qquad (3.13)$$

$$\phi = \arctan\left[\frac{\gamma(\tan kl - \tanh kl) - (\alpha+\beta) + (\alpha-\beta)\tan kl \tanh kl}{\gamma(\tan kl + \tanh kl) + (\alpha-\beta) + (\alpha+\beta)\tan kl \tanh kl}\right] \qquad (3.14)$$

where $$\alpha = x^2 + y^2 - r^2 - s^2$$

$$\beta = 2(yr - sx)$$

$$\gamma = (x - r)^2 + (y - s)^2$$

$$\delta = x^2 + y^2 + r^2 + s^2$$

$$\epsilon = 2(xr + ys)$$

As mentioned in Section 3.5, the classical boundary conditions lead to values of the x, y, r, s given by x = -r, y = -s so that:

$$\alpha = 0$$

$$\beta = 0$$

$$\gamma = (2x)^2 + (2y)^2$$

$$\delta = 2x^2 + 2y^2$$

$$\epsilon = -2x^2 - 2y^2$$

Applying these values to equations (3.13) and (3.14) reproduces the classical results (3.9) and (3.10). Thus, the extent of the deviation of the bulk phase-lag, ϕ, and amplitude attenuation, B, can be given by the quantities $(x + r)$ and $(y + s)$ which are both zero in the classical case. A more practicable reduction to classical behaviour can also be obtained by truncating the series for x, y, r, s to neglect terms higher than ω^0 and such truncations will be dealt with again in Section 3.11.

3.9 Input Surface Modification (A, ψ)

Having found the attenuation and phase-lag between the flux across the surface $x = 1$ and the input surface concentration it is now necessary to find a similar relationship between the input surface concentration and the input pressure. In contrast to the case for the bulk phase-lag and attenuation, this modification introduces a further set of parameters which are linked to the input rate-constants, K_i, rather than the output rate-constants, K_i', as was the case in Section 3.8. However, since the defining equations also involve the general solution, the x, y, r, s are again involved in this solution.

Proceeding as in Section (3.8), a set of simultaneous equations containing the required oscillatory quantities can again be written, this time governing the input surface:

$$\underset{\sim}{J}_H^- = K_1 \underset{\sim}{p}_H - K_2 \underset{\sim}{\Theta}_H \qquad (\underset{\sim}{\Theta}_H \ll \Theta)$$

$$\underset{\sim}{J}_H = K_3 \underset{\sim}{\Theta}_H - K_4 \underset{\sim}{C}_H = -D \left(\frac{\partial \underset{\sim}{C}_H, x}{\partial x} \right)_{x=o}$$

$$\frac{\partial \underset{\sim}{\Theta}_H}{\partial t} = \underset{\sim}{J}_H^- - \underset{\sim}{J}_H$$

These equations can be combined as before to eliminate $\underset{\sim}{\Theta}_H$ yielding an equation for $\underset{\sim}{p}_H$ and $\underset{\sim}{C}_H$ only at $x = o$:

$$\frac{K_2^{\frac{1}{2}}\Theta}{(K_1 p)^{\frac{1}{2}}} \underset{\sim}{C}_H - \left[\frac{K_{sm}}{2K_1 p^{\frac{1}{2}}} + \frac{K_2^{\frac{1}{2}}\Theta}{(K_1 p)^{\frac{1}{2}}} \frac{1}{K_4} \right] D \left(\frac{\partial \underset{\sim}{C}_H, x}{\partial x} \right)_{x=o} +$$

$$+ \frac{1}{2(K_1 K_2 p)^{\frac{1}{2}}} \left[\frac{\partial \underset{\sim}{C}_H, x}{\partial t} - \frac{D}{K_4} \frac{\partial^2 \underset{\sim}{C}_H, x}{\partial x \partial t} \right]_{x=o} = \frac{K_{sm} \underset{\sim}{p}_H}{2\sqrt{p}}$$

Where the left hand side represents the equilibrium value of $\underset{\sim}{C}_H$ as evaluated in Section A.1 and use has been made of the identity $K_{sm} = \sqrt{\frac{K_1}{K_2}} \frac{K_3}{K_4}$.

Using the general solution (3.7) at $x = o$:

$$\underset{\sim}{C}_H = \left(\underset{\sim}{A} e^{-\underset{\sim}{a}l} + \underset{\sim}{B} e^{\underset{\sim}{a}l} \right) e^{i\omega t}$$

and

$$\left(\frac{\partial \underset{\sim}{C}_H, x}{\partial x} \right)_{x=o} = \underset{\sim}{a} \left[\underset{\sim}{A} e^{-\underset{\sim}{a}l} + \underset{\sim}{B} e^{\underset{\sim}{a}l} \right] e^{i\omega t}$$

and the required time derivatives of these.

Also, assigning zero relative phase to the input pressure

$$\underset{\sim}{p}_H = p_H e^{i\omega t}$$

and substituting these into the expression for $\underset{\sim}{p}_H$ and $\underset{\sim}{C}_H$ another complex equation is obtained for $\underset{\sim}{A}$ and $\underset{\sim}{B}$ in terms of $\underset{\sim}{p}_H$ of the form:

$$\frac{K_{sm}}{2\sqrt{p}}\,\underset{\sim}{p}_H = \underset{\sim}{A}\, e^{-\underset{\sim}{a}l}(m \mp in) \mp \underset{\sim}{B}\, e^{\underset{\sim}{a}l}(u \mp iv)$$

where m, n, u, v are power series in $\omega^{\frac{1}{2}}$ of the form:

$$m = \sum_{n=o}^{3} m_n \omega^{n/2}$$

and the m_n, n_n, u_n, v_n are given by the table:

n	m_n	n_n	u_n	v_n
0	e_o	0	e_o	0
1	$-e_1$	$-e_1$	e_1	e_1
2	0	e_2	0	e_2
3	e_3	$-e_3$	$-e_3$	e_3

and $$e_o = \frac{K_2^{\frac{1}{2}}\theta}{(K_1 p)^{\frac{1}{2}}}$$

$$e_1 = \frac{D^{\frac{1}{2}}}{\sqrt{2}}\left[\frac{K_{sm}}{2K_1 p^{\frac{1}{2}}} + \frac{e_o}{K_4}\right]$$

$$e_2 = 1 \Big/ 2(K_1 K_2 p)^{\frac{1}{2}}$$

$$e_3 = D^{\frac{1}{2}} \Big/ 2\sqrt{2}\; K_4 (K_1 K_2 p)^{\frac{1}{2}}$$

However, it has already been established that

$$\underset{\sim}{A}(x + iy) = \underset{\sim}{B}(r + is)$$

and the x, y, r, s have been evaluated.

Thus, solution of the two simultaneous equations

$$\begin{bmatrix} \frac{K_{sm}p_H}{2\sqrt{p}} \\ \\ 0 \end{bmatrix} = \begin{bmatrix} e^{-\underset{\sim}{a}l}(m + in) & e^{\underset{\sim}{a}l}(u + iv) \\ \\ (x + iy) & (r + is) \end{bmatrix} \begin{bmatrix} \underset{\sim}{A} \\ \\ \underset{\sim}{B} \end{bmatrix}$$

gives the values of $\underset{\sim}{A}$ and $\underset{\sim}{B}$ and hence the phase/amplitude relationship between the input pressure and the input concentration:

$$C_H = PA = \frac{K_{sm}p_H}{2\sqrt{p}} \sqrt{\frac{\left[\delta \cosh 2kl + \alpha \sinh 2kl \mp \epsilon \cos 2kl - \beta \sin 2kl\right]}{\left[\left(\frac{\delta-\alpha}{2}\right)(m^2 + n^2) \mp \left(\frac{\delta+\alpha}{2}\right)(u^2 \mp v^2)\right] \cosh 2kl}} \quad (3.15)$$

$$+ \left[\left(\frac{\alpha-\delta}{2}\right)(m^2 \mp n^2) \mp \left(\frac{\delta+\alpha}{2}\right)(u^2 \mp v^2)\right] \sinh 2kl$$

$$+ \left[\epsilon(um + vn) \mp \beta(un - vm)\right] \cos 2kl$$

$$+ \left[\epsilon(un - vm) - \beta(um \mp vn)\right] \sin 2kl$$

and

$$= \arctan \left[\frac{\left[(\alpha+\delta)v \mp (\delta-\alpha)n\right]\cosh 2kl \mp \left[(\alpha+\delta)v - (\delta-\alpha)n\right] \sinh 2kl}{\mp\left[\epsilon(u-m) - \beta(n+v)\right]\sin 2kl \mp \left[\epsilon(v+n) \mp \beta(u-m)\right]\cos 2kl} \right] \quad (3.16)$$

$$\left[\frac{\left[(\alpha+\delta)u \mp (\delta-\alpha)m\right]\cosh 2kl \mp \left[(\alpha+\delta)u - (\delta-\alpha)m\right]\sinh 2kl}{+\left[\epsilon(n-v) - \beta(u+m)\right]\sin 2kl \mp \left[\epsilon(u+m) - \beta(v-n)\right]\cos 2kl} \right]$$

where α, β, δ, ϵ are as before.

$$P = \frac{K_{sm}\, p_H}{2\sqrt{p}}$$

and A is an amplitude modification factor similar to B in Section 3.8 this time operating on the equilibrium surface concentration

amplitude to produce the non-equilibrium surface concentration amplitude, i.e. when the input surface is at equilibrium, the factor A becomes unity.

3.10 Output Surface Modification (C, ζ)

It now only remains to find the phase/amplitude relationship between the flux across the surface x = 1, i.e. $\underset{\sim}{J}'_H$ and the emergent flux $\underset{\sim}{J}'^{+}_H$ across the surface $x = 1^+$

Again writing flux equations at x = 1:

$$\underset{\sim}{J}'^{+}_H = 2K'_2 \underset{\sim}{\theta}'_H \theta' - K'_1 \underset{\sim}{p}'_H$$

$$\frac{\partial \underset{\sim}{\theta}'_H}{\partial t} = \underset{\sim}{J}'_H - \underset{\sim}{J}'^{+}_H$$

$$\frac{\partial \underset{\sim}{p}'_H}{\partial t} = \frac{ART}{V} \underset{\sim}{J}'^{+}_H - \beta \underset{\sim}{p}'_H$$

Combining these and eliminating $\underset{\sim}{\theta}'_H$ yields a direct relationship between $\underset{\sim}{J}'^{+}_H$ and $\underset{\sim}{J}'_H$:

$$2K'_2 \theta' \left[\frac{\partial}{\partial t} + \beta\right] \underset{\sim}{J}'_H = \left[\frac{\partial^2}{\partial t^2} + (\beta + K'_1 \frac{ART}{V} + 2K'_2 \theta')\frac{\partial}{\partial t} + 2K'_2 \theta' \beta\right] \underset{\sim}{J}'^{+}_H$$

which can be solved to yield the desired phase and amplitude expressions:

$$J'^{+}_H = J'_H C = J'_H \sqrt{\frac{4K'_2 \theta'^2 (\omega^2 + \beta^2)}{(2K'_2 \theta' \beta - \omega^2)^2 + \omega^2 (\beta + K'_1 \frac{ART}{V} + 2K'_2 \theta')^2}}$$

and

$$\zeta = \arctan\left[\frac{(\omega^2 + \beta^2) + \beta K'_1 \frac{ART}{V}}{(\omega^2 + \beta^2) 2K'_2 \theta' + \omega^2 K'_1 \frac{ART}{V}}\right]$$

For small ω/β these equations can be simplified to:

$$J_H'^{\ddagger} = J_H'C = J_H' \sqrt{\frac{1}{1+\left(\frac{\omega}{2K_2'\Theta'}\right)^2}} \qquad (3.17)$$

and

$$\zeta = \arctan\left(\frac{\omega}{2K_2'\Theta'}\right) \qquad (3.18)$$

and these represent the final correction terms to be applied to account for finite phase-boundary processes at the $x = 1 \longrightarrow 1^{\ddagger}$ layer. It can be seen that when these processes are rapid (i.e. large K_2') that $\zeta \rightarrow 0$ and $C \rightarrow 1$, i.e. $J_H'^{\ddagger} \rightarrow J_H'$ and the output surface modification disappears.

3.11 Low Order Approximations

It is plainly of importance, in the interests of simplicity and clarity, to consider approximations which may be applied to the various modifications. This is particularly important for the input and bulk modifications in order that the practical significance of these results can be seen. It is necessary to ensure that the simplifications are not so severe as to impair the applicability of these results, and in particular to ensure that sensible limiting cases can be obtained.

From the form of the results in Sections 3.8 and 3.9 the most obvious method of reduction is to truncate the series for the (m, n, u, v), x, y, r, s at an appropriate power of $\omega^{\frac{1}{2}}$. Truncation at ω^{0} is evidently too severe since this merely leads to the classical approximation.

The order of allowable approximation can be gauged by the expressions for the final amplitude and phase due to pumping

equations (3.11) and (3.12) where neglect of terms lower than the first power of ω would imply that this correction should be neglected. Thus the second power of $\omega^{\frac{1}{2}}$ has been chosen as a compromise between simplicity and applicability.

A further approximation, or rather restriction, which must be applied to the model to retain a sensible level of simplicity is to consider that only one surface of the specimen will be rate-determining at any time.

This means that the expressions for ψ and C_H can be further simplified by neglecting terms containing the output parameters x, y, r, s.

A final check on the applicability of these approximations can then be made by ensuring that all the expressions can be reduced to the classical limit by suitable choice of the rate parameters and this will be done in the next chapter.

Applying the above restrictions to equations (3.13) and (3.14) gives:

$$\phi = \arctan \left[\frac{\tan kl - \tanh kl \mp \frac{2x_1}{x_o} \omega^{\frac{1}{2}} \tan kl \tanh kl}{\tan kl \mp \tanh kl \mp \frac{2x_1}{x_o} \omega^{\frac{1}{2}}} \right] \qquad (3.19)$$

$$J_H' = C_H \frac{2kD}{\sqrt{(\cosh 2kl - \cos 2kl) \mp \frac{2x_1}{x_o} \omega^{\frac{1}{2}} (\sinh 2kl \mp \sin 2kl) + 2\left(\frac{x_1}{x_o}\right)^2 \omega (\cosh 2kl + \cos 2kl)}} \qquad (3.20)$$

and to equations (3.15) and (3.16)

$$\psi = \arctan\left[\frac{(e_2+\frac{2x_1}{x_o}e_1)\omega(\cosh 2kl-\cos 2kl)+e_1\omega^{\frac{1}{2}}(\sinh 2kl-\sin 2kl)}{\left\{e_o(\cosh 2kl-\cos 2kl)+(e_1+\frac{2x_1}{x_o}e_o)\,\omega^{\frac{1}{2}}(\sinh 2kl+\sin 2kl)\right.}\right.$$
$$\left.\left.+2\left[\left(\frac{x_1}{x_o}\right)^2 e_o+\frac{x_1}{x_o}e_1\right]\omega(\cosh 2kl+\cos 2kl)\right\}\right] \quad (3.21)$$

$$C_H=\frac{K_{sm}p_H}{2\sqrt{p}}\sqrt{\frac{\left\{(\cosh 2kl-\cos 2kl)+\frac{2x_1}{x_o}\omega^{\frac{1}{2}}(\sinh 2kl+\sin 2kl)+\frac{2x_1}{x_o}^2\omega(\cosh 2kl+\cos 2kl)\right\}}{\left\{e_o^2(\cosh 2kl-\cos 2kl)+2(e_oe_1+\frac{x_1}{x_o}e_o^2)\,\omega^{\frac{1}{2}}(\sinh 2kl+\sin 2kl)\right.}} \quad (3.22)$$
$$\left.+2\left[e_1^2+\frac{2x_1}{x_o}e_oe_1+\left(\frac{x_1}{x_o}\right)^2e_o^2\right]\omega(\cosh 2kl+\cos 2kl)\right\}$$

Although these equations do not look a great deal simpler, they contain less adjustable parameters than the fuller forms. In addition (3.21) and (3.22) can be further simplified by removing the terms containing $\frac{x_1}{x_o}$ for single (input) surface control. Further approximations will be dealt with in Chapter 4.

3.12 Summary

This chapter has dealt with the general solution of the diffusion equation for a modulated input pressure leading to modulating concentrations in the solid. The general solution has been made particular first for 'classical' boundary conditions corresponding to the steady-state Richardson equation and then for more complicated boundary conditions which allow for finite surface rate processes.

In this latter case it was found useful to split the

problem into several parts so that first the steady-state solution could be dealt with and the phase/amplitude expressions could be developed between key quantities in the system (input pressure, input concentration, flux across surface $x = 1$, flux across surface $x = 1^+$, output pressure).

In particular the output pressure can be obtained from the input pressure via these quantities by a chain of phase/amplitude relations of the form

$$|\underset{\sim}{X}| = A|\underset{\sim}{Y}|$$

and

$$/\underset{\sim}{Y} - /\underset{\sim}{X} = \Phi$$

The chain commences with the input pressure, $\underset{\sim}{p}_H$ of known amplitude and zero relative phase and proceeds through the input surface concentration $\underset{\sim}{C}_H$ to the flux across the bulk-subsurface interface ($x = 1$), $\underset{\sim}{J}'_H$ to the emergent flux across the subsurface - gas interface ($x = 1^+$), $\underset{\sim}{J}'^{+}_H$ and finally to the output pressure $\underset{\sim}{p}'_H$.

Discussion of the solutions has been minimal. Chapter 4 goes on to consider the form of these solutions, how they are affected by the various rate parameters and what information they may yield in an experiment such as that described in Chapter 2.

CHAPTER 4

APPLICATION OF THE SURFACE MODEL TO THE EXPERIMENT

4.1 Interpretation of the Surface Reaction Model in terms of the Measured Quantities

The algebraic solutions of the diffusion equation for boundary conditions which allow the possibility of finite rate processes at the surfaces of the specimen are set out in Chapter 3 and it was seen there that the phase lag can be written as a series of terms representing possible rate-limiting processes:

$$\phi' = (\psi + \phi + \zeta + \xi) \qquad (4.1)$$

Throughout the analysis, the pumping phase-lag $\tan \xi = \frac{\omega}{\beta}$ will be understood to be automatically subtracted from all measurements and is therefore not considered further.

The amplitude of the output pressure can be written as a product of terms corresponding to the above phase processes:

$$\left.\begin{aligned} P' &= \frac{ART}{V\beta} \\ p'_H &= J'^{+}_H P' \\ J'^{+}_H &= J'_H C \\ J'_H &= C_H B \\ C_H &= PA \\ P &= \frac{K_{sm} p_H}{2\sqrt{p}} \end{aligned}\right\} \quad \text{i.e.} \quad p'_H = PABCP' \qquad (4.2)$$

The factors P and P' are independent of the boundary conditions and discussion of the oscillatory solutions is therefore centred round the values of ψ, ϕ and ζ for the phase-lag and A, B, C for the amplitude.

The steady-state flux, J, is a fairly complicated function of the various rate-processes and approximations to the full equation set out in Section 3.3 will be considered for the various following cases.

4.2 The Classical Approximation

The solution for the boundary condition $C_H = \frac{K_{sm} p_H}{2\sqrt{p}}$ and $C'_H = 0$ corresponds to Richardson's equation for the steady permeation rate

$$J = \frac{D K_{sm} \sqrt{p}}{l} \qquad (4.3)$$

which is the same as equation (3.4) with $\sqrt{p'}$ negligible with respect to $\sqrt{p}$. Since this value of J is independent of x and t it can also describe the emergent flux from the specimen (at steady-state). Thus, the pumping equation in Section 3.6 can be used to determine the steady-state output pressure for such a flux ($\partial p'/\partial t = 0$)

$$p' = \frac{ART_c}{V\beta} \frac{D K_{sm}}{l} \sqrt{p} \qquad (4.4)$$

(for small p'_u, i.e. low background compared with signal)

The multiplier $\frac{ART_c}{V\beta} = P'$ operates on all steady-state fluxes and emergent flux amplitudes to give the corresponding steady-state pressure or oscillatory pressure amplitude. This means that fluxes and flux amplitudes can be discussed in terms of the measured pressure quantities provided that the factor P' is understood. P' is a totally system-dependent parameter and is constant throughout the experiment.

The classical oscillatory solution (Section 3.5) is

characterised by the following values of the phase and amplitude parameters of equations (4.1) and (4.2)

$$\psi = \zeta = 0$$

$$A = C = 1$$

$$B = \frac{\sqrt{2}kD}{\sqrt{\sinh^2 kl + \sin^2 kl}} = \frac{2kD}{\sqrt{\cosh 2kl - \cos 2kl}} = \sqrt{2}DF(\omega) \qquad (4.5)$$

$$\tan \phi = \left[\frac{\tan kl - \tanh kl}{\tan kl + \tanh kl}\right]$$

The two functions, $F(\omega)$ and ϕ, are shown in Figures 4.1 and 4.2. There are a few features of each of these functions which can be used as indicators of 'classical behaviour':

$F(\omega)$: as $\omega \to 0$

$$F(\omega) \approx \frac{\sqrt{2}}{1} \frac{kl}{\left[\left(1+\frac{(2kl)^2}{2}+\frac{(2kl)^4}{4}\right) - \left(1-\frac{(2kl)^2}{2}+\frac{(2kl)^4}{4}\right)\right]^{\frac{1}{2}}}$$

$$\simeq \frac{1}{\sqrt{2}\,1}$$

and as $\omega \to \infty$

$$F(\omega) \to 0$$

Thus, as modulation becomes very slow the bulk diffusion amplitude attenuation factor tends towards the maximum value $\hat{B} = D/l$. The maximum output pressure amplitude can therefore be written in terms of the steady-state output pressure as

$$\frac{\hat{p}'_H}{p_H}\frac{\sqrt{p}}{} = \frac{p'}{2\sqrt{p}} \qquad (4.6)$$

Thus, a plot of the 'normalised' output pressure amplitude, $p'_H \frac{\sqrt{p}}{p_H}$, against $F(\omega)$ should be a straight line extrapolating through zero at $F(\omega) = 0$ and through $\frac{p'}{2\sqrt{p}}$ when $F(\omega) = \frac{1}{\sqrt{2}\ l}$ (i.e. $\omega \to 0$).

This condition is used here as a yardstick to illustrate the effect that the various surface processes have on the output pressure amplitude. The subsequent amplitude curves are standardised in that $\frac{p'}{2\sqrt{p}}$ has been taken as $10\sqrt{\text{torr}}$, l as .05 cm and $D = 5 \times 10^{-5}$ $cm^2 sec^{-1}$ throughout. Since amplitude effects are relative, i.e. the surface effects can be seen as multipliers on the classical amplitude, it does not matter what value is taken for the reference $\frac{p'}{2\sqrt{p}}$. All amplitude graphs are shown with dotted lines to indicate the value $F(\omega) = \frac{1}{\sqrt{2}\ l}$ and to indicate the classical values to which they are referred.

Phase lag: as $\omega \longrightarrow 0$

$\phi \longrightarrow 0$

as ω becomes large $(kl \gtrsim \frac{\pi}{2})$

$\tanh kl \longrightarrow 1$

and $\tan \phi \longrightarrow \frac{\tan kl - 1}{\tan kl + 1}$

i.e. $\tan \phi = \tan (kl - \pi/4)$

Thus, a plot of ϕ vs. $\sqrt{\omega}$ should become linear as ω becomes large and the linear portion should extrapolate through a value of $-\pi/4$ at $\omega = 0$ and should have a slope of $l/\sqrt{2D}$. This is taken to be the yardstick of classical phase-lag behaviour and all subsequent plots are referred to the classical phase-lags given by $D = 5 \times 10^{-5}$ cm^2/sec and $l = .05$ cm.

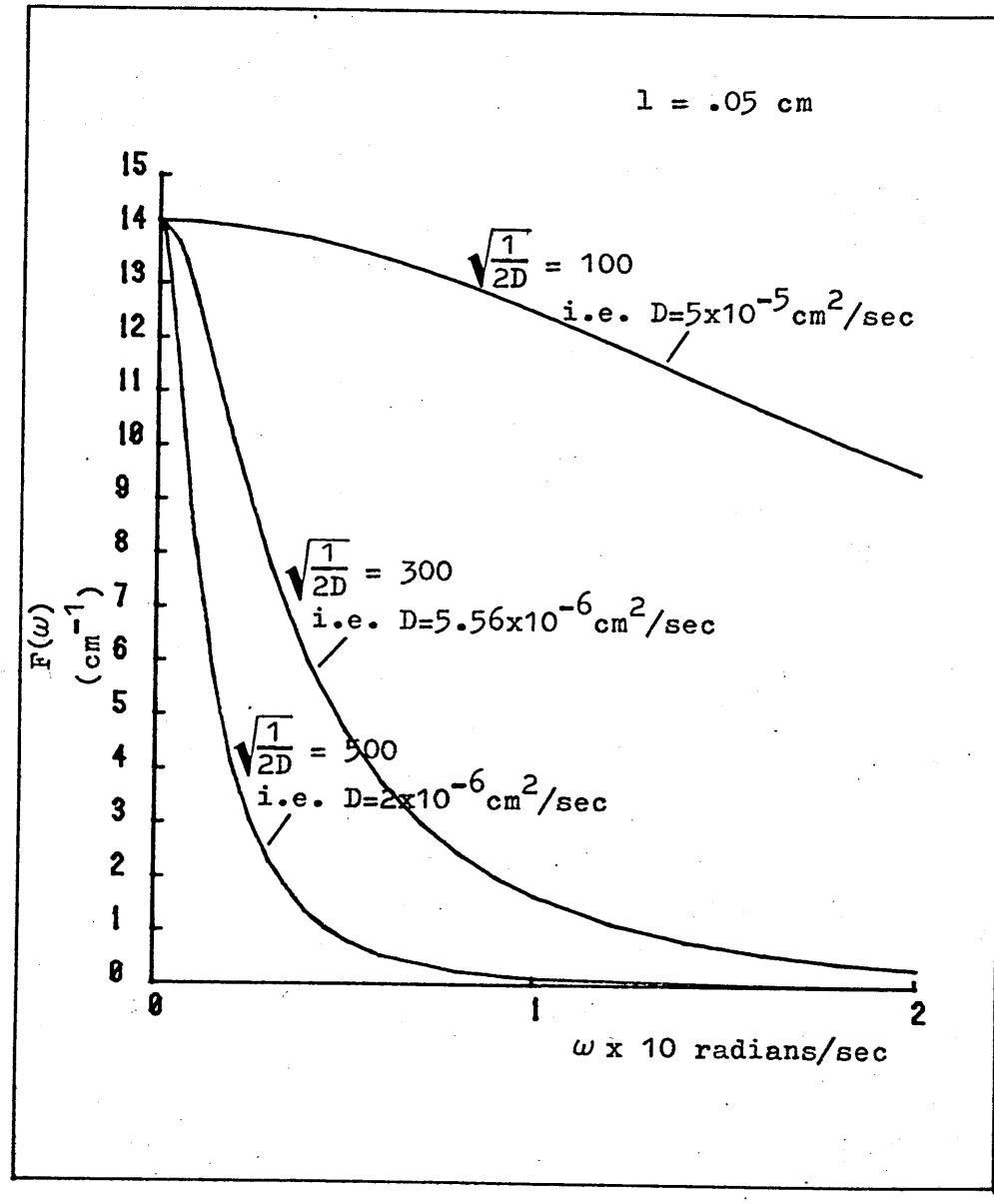

Figure 4.1 The function $F(\omega)$ vs. ω for a variety of diffusion coefficients

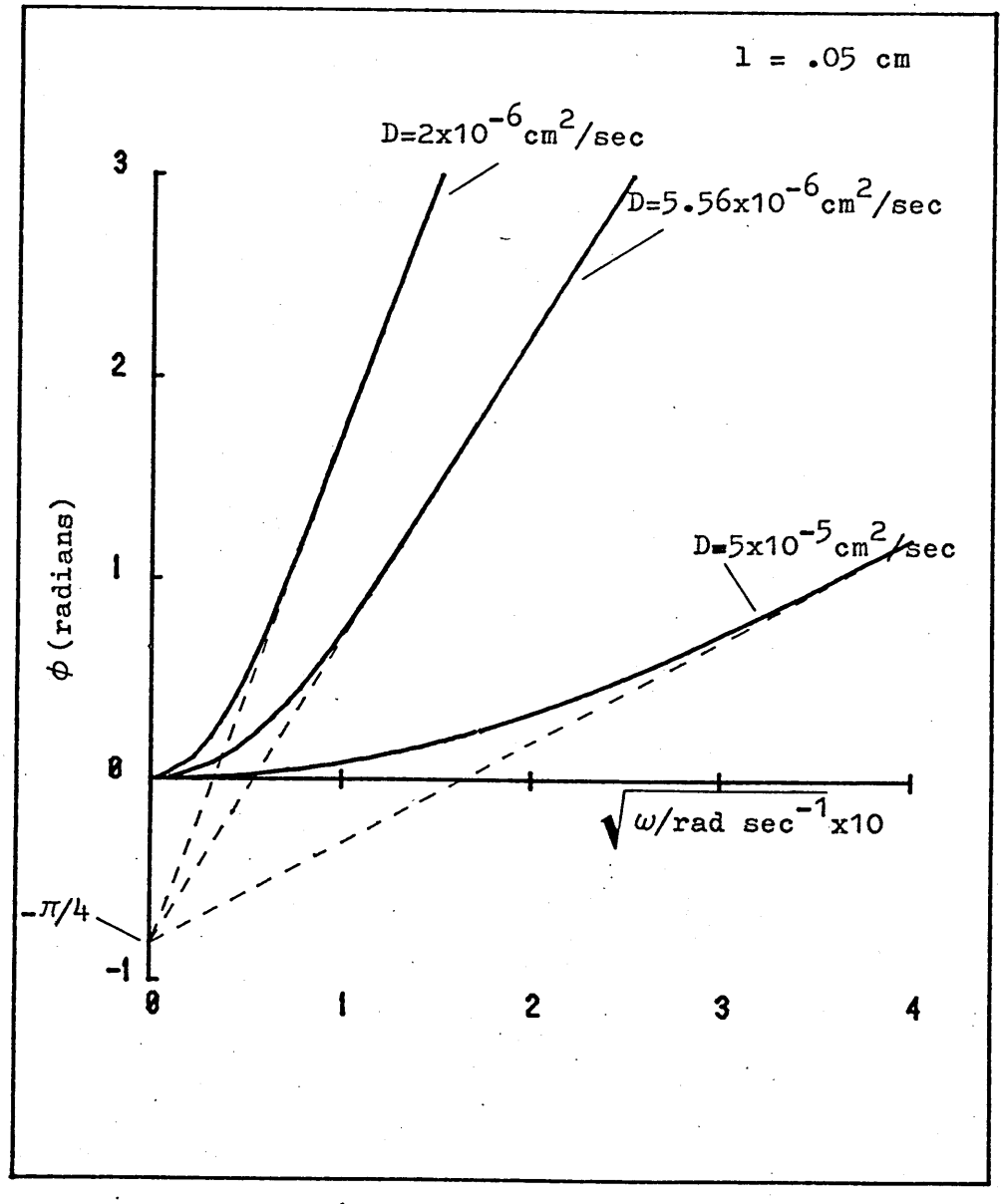

Figure 4.2 The function $=\text{atn}\,\frac{\tan kl-\tanh kl}{\tan kl+\tanh kl}$ vs. $\sqrt{\omega}$ for a variety of diffusion coefficients

4.3 The Input Condition

Consider now the situation where the input surface produces an appreciable holdup but the output surface provides no appreciable modification. In this case, the output surface is considered to have negligible values for its surface concentration and pressure and the emergent flux is given by the application of Fick's First Law to the concentration gradient at x = 1.

The steady-state flux equations (3.1) become:

$$J = K_1 p - K_2 \theta^2 = K_3 \theta - K_4 C = \frac{DC}{l}$$

Rearranging:

$$J(1 + K_4 \frac{l}{D}) = K_3 \sqrt{\frac{K_1 p - J}{K_2}}$$

Using

$$J_{CLAS} = \frac{DK_{sm}\sqrt{p}}{l} \quad \text{and} \quad K_{sm} = \left(\frac{K_1}{K_2}\right)^{\frac{1}{2}} \frac{K_3}{K_4}$$

one obtains the steady-state flux, J, in terms of the classical steady-state flux, J_{CLAS}:

$$J = J_{CLAS} \frac{\sqrt{1 - \frac{J}{K_1 p}}}{\left(\frac{D}{lK_4} + 1\right)} \tag{4.7}$$

From this, two limiting cases (aside from the classical case) can be identified according as whether the rate-constant K_1 is large, that is $\frac{J}{K_1 p} \ll 1$ or the rate-constant K_4 is large, that is $\frac{D}{lK_4} \ll 1$.

Case (i): $\frac{D}{lK_4} \ll 1$ gives

$$J = J_{CLAS} \sqrt{1 - \frac{J}{K_1 p}} \tag{4.8}$$

This implies that the surface x = o (see Figure 3.1) produces an insignificant delay and that the modification is confined to the surface $x = o^-$. The indicator of this delay is the ratio of the flux passing through the surface $x = o^-$ (i.e. J) to the flux impinging on that surface due to the fugacity of the input gas (i.e. $K_1 p$).

The corresponding oscillatory effect can be obtained from the simplified solutions (neglecting output terms containing x_1/x_o) (3.21) and (3.22). First, the terms e_o, e_1, e_2 (Section 3.9) can be reduced for large K_3 and K_4 giving:

$$\left.\begin{aligned} e_o &= \left(1 - \frac{J}{K_1 p}\right)^{\frac{1}{2}} = \frac{J}{J_{CLAS}} \\ e_1 &= \frac{D^{\frac{1}{2}}}{\sqrt{2}} \frac{K_{sm}}{2K_1 p^{\frac{1}{2}}} = \frac{J_{CLAS}}{K_1 p} \frac{1}{2\sqrt{2D}} \end{aligned}\right\} e_1 e_o = \frac{-1}{2\sqrt{2D}} \left[\left(\frac{J}{J_{CLAS}}\right)^2 - 1\right]$$

$$e_2 = \frac{1}{2(K_1 K_2 p)^{\frac{1}{2}}}$$

The amplitude modification factor, A, can be written from equation (3.22):

$$A = \frac{1}{\sqrt{e_o^2 + 2e_o e_1 \omega^{\frac{1}{2}} \left(\frac{\sinh 2kl + \sin 2kl}{\cosh 2kl - \cos 2kl}\right) + 2e_1^2 \omega \left(\frac{\cosh 2kl + \cos 2kl}{\cosh 2kl - \cos 2kl}\right)}} \tag{4.9}$$

Using power series expansion for low ω's it can be seen that, as $\omega \longrightarrow o$:

$$2e_o e_1 \omega^{\frac{1}{2}} \left(\frac{\sinh 2kl+\sin 2kl}{\cosh 2kl-\cos 2kl}\right) \longrightarrow \frac{2e_o e_1 \sqrt{2D}}{l} = \frac{e_o J_{CLAS}}{K_1 p} = \frac{J}{K_1 p}$$

$$2e_1^2 \omega \left(\frac{\cosh 2kl+\cos 2kl}{\cosh 2kl-\cos 2kl}\right) \longrightarrow \frac{2e_1^2 D}{l^2} = \frac{1}{4}\left(\frac{J_{CLAS}}{K_1 p}\right)^2$$

So that, as $\omega \longrightarrow o$

$$\hat{A} = \left[1 + \left(\frac{J_{CLAS}}{2K_1 p}\right)^2\right]^{-\frac{1}{2}} = \left[1 + \frac{(J/K_1 p)^2}{4(1-J/K_1 p)}\right]^{-\frac{1}{2}} \qquad (4.10)$$

Figure 4.3 shows the functions $\hat{A}$ and J from equations (4.10) and (4.8) normalised to an arbitrary value of 20. It can be seen that the maximum amplitude is less sensitive to $J/K_1 p$ than is the flux but that both decrease to zero as $J/K_1 p$ tends towards its maximum value of unity. (J cannot exceed $K_1 p$ since this would imply a net flux across $x = o^-$ which is greater than the incident flux on the surface from the gas.)

Figure 4.4 illustrates the effect of A (equation (4.9)) on the output pressure amplitude. As shown in Section 4.2 a plot of normalised output pressure $p'_H \frac{\sqrt{p}}{p_H}$ against the function $F(\omega) = k[\sin^2 kl + \sinh^2 kl]^{-\frac{1}{2}}$ will, for the classical case be linear passing through the origin and through $p'/2\sqrt{p}$ at $F(\omega) = 1/\sqrt{2}l$ (= 14.14 for the 'standard' value of $l = .05$).

Figure 4.4 shows the deviations from this 'classical' behaviour caused by the factor A, equation (4.9) as $J/K_1 p$ varies. It can be seen that finite values of $J/K_1 p$ cause a curvature of the classical plot and also a downward shift of the extrapolated amplitude at $\omega \longrightarrow o$ ($F(\omega) \longrightarrow 1/\sqrt{2}l$) according to the curve for $\hat{A}$ in Figure 4.3. It should also be noted that the value 10 in Figure 4.4 refers only to the classical value of $p'/2\sqrt{p}$ (modified steady-state output pressure) and that for values of $J/K_1 p$

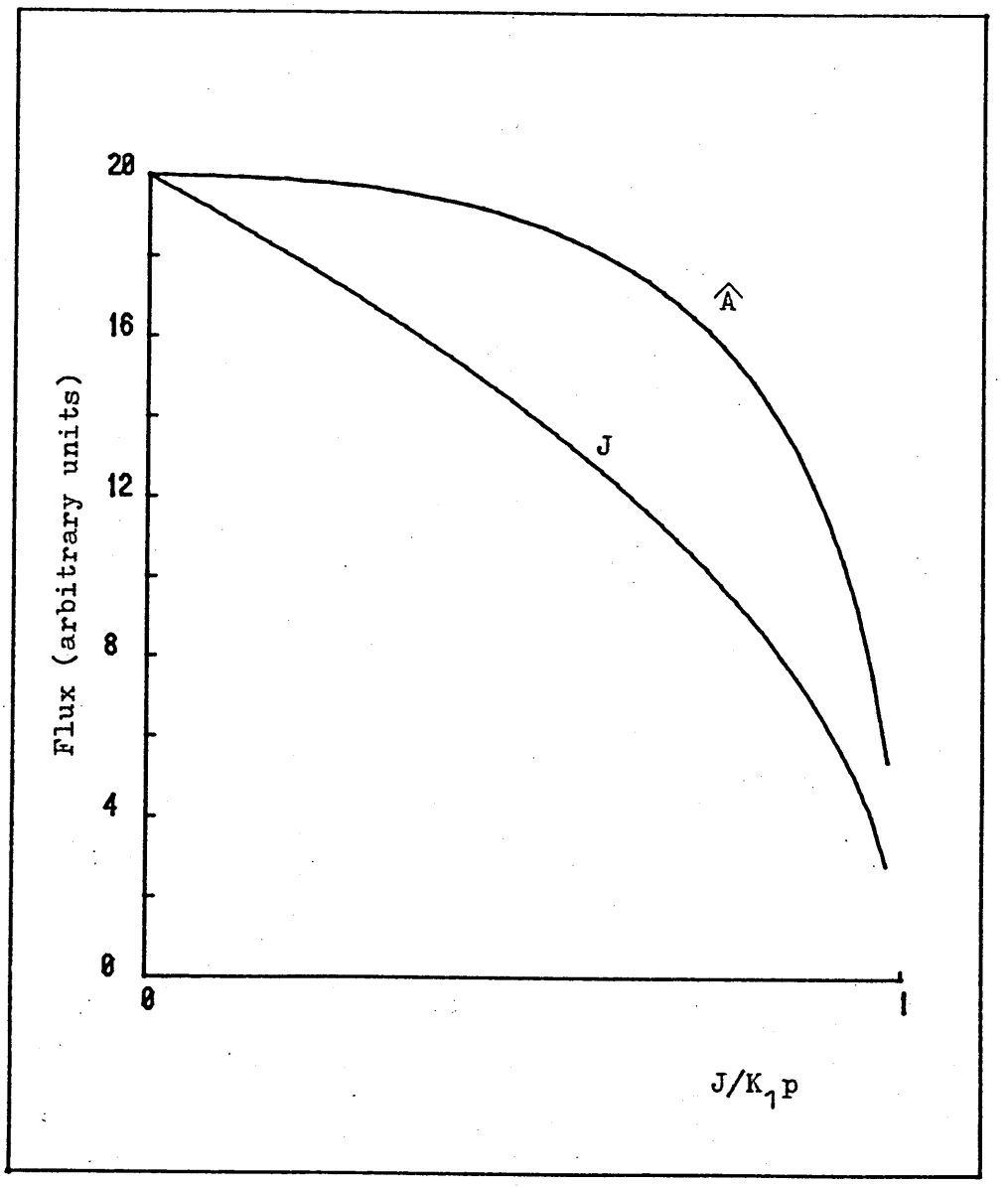

Figure 4.3 The maximum amplitude modification, $\hat{A}$, and the steady-state flux, J, both as a function of J/K_1p, both normalised to a maximum value of 20 for comparison

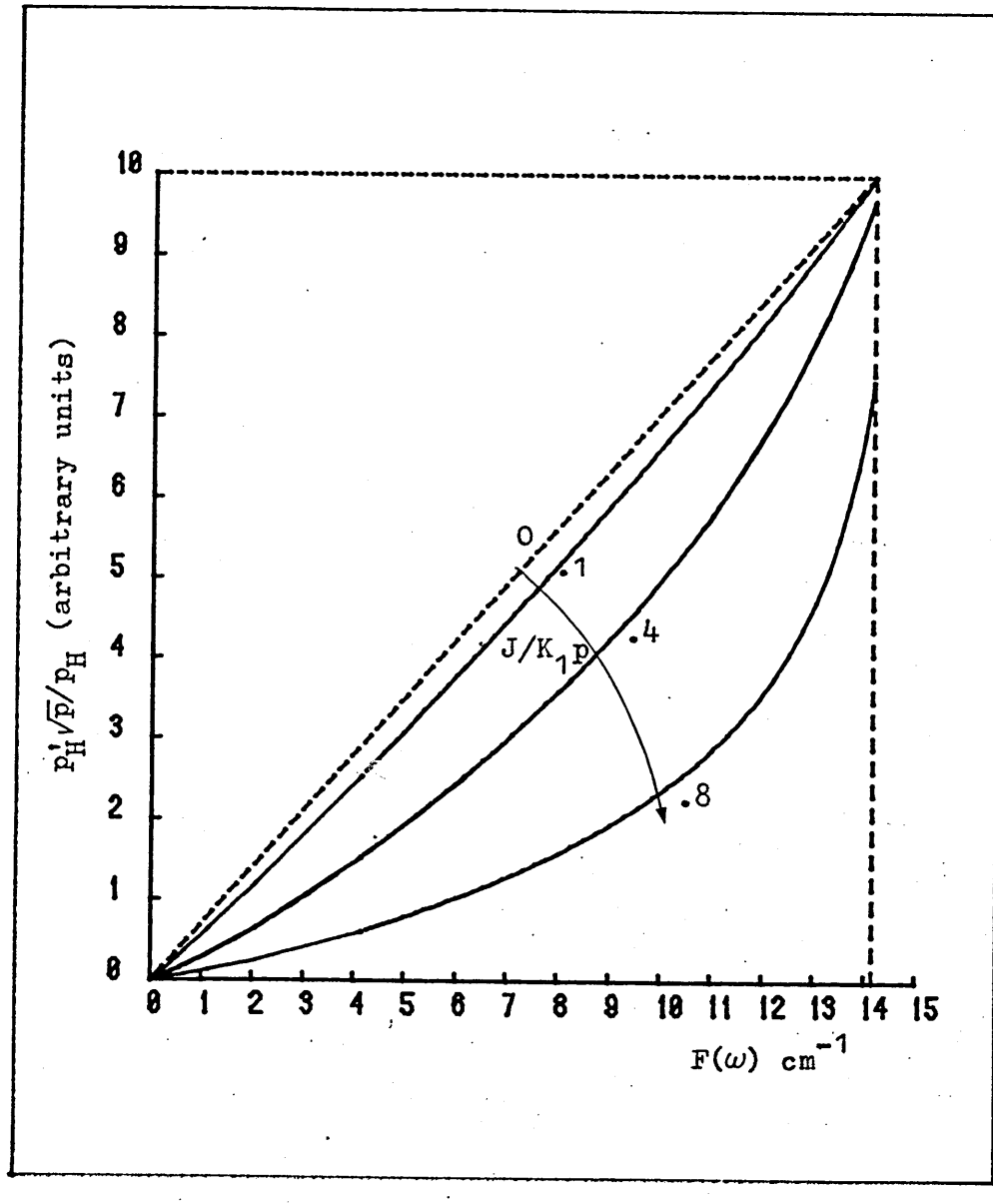

Figure 4.4 The effect of the input parameter J/K_1p on the amplitude attenuation for output pressure

appreciably different from zero the measured values of $p'/2\sqrt{p}$ will be shifted downwards according to the curve for J in Figure 4.3. Thus, an attempt to construct a plot such as Figure 4.4 in the non-classical case would produce a curved, normalised amplitude which extrapolates above the measured value of $p'/2\sqrt{p}$. The difference between $p'_H\sqrt{p}/p_H$ and $p'/2\sqrt{p}$ will at first increase and then decrease with increasing J/K_1p according to Figure 4.3.

The phase lag due to the input surface is given by equation (3.21) again neglecting terms in x_1/x_o:

$$\tan\psi = \frac{\omega + \frac{e_1}{e_2}\omega^{\frac{1}{2}}\left(\frac{\sinh 2kl-\sin 2kl}{\cosh 2kl-\cos 2kl}\right)}{\frac{e_o}{e_2} + \frac{e_1}{e_2}\omega^{\frac{1}{2}}\left(\frac{\sinh 2kl+\sin 2kl}{\cosh 2kl-\cos 2kl}\right)} \qquad (4.11)$$

where $\frac{e_1}{e_2} = \frac{D^{\frac{1}{2}}}{\sqrt{2}} K_{sm}\sqrt{\frac{K_2}{K_1}}$

[an alternative form for small e_2, i.e.

$$\tan\psi = \frac{\frac{e_1}{e_o}\omega^{\frac{1}{2}}\left(\frac{\sinh 2kl-\sin 2kl}{\cosh 2kl-\cos 2kl}\right)}{1 + \frac{e_1}{e_o}\omega^{\frac{1}{2}}\left(\frac{\sinh 2kl+\sin 2kl}{\cosh 2kl-\cos 2kl}\right)}$$

is discussed under D/lK_4 control (Figure 4.7)]

Figure 4.5 shows the phase-lag $\psi + \phi$ (where ϕ is given by equation (4.5)) for a variety of values of e_1/e_2 and e_o/e_2. The standard values of D, l (i.e. 5×10^{-5} and .05) were used in this calculation and the corresponding classical plot is shown for comparison. It is not possible to relate the phase effects in this case directly to J/K_1p because of the form of the parameter e_2

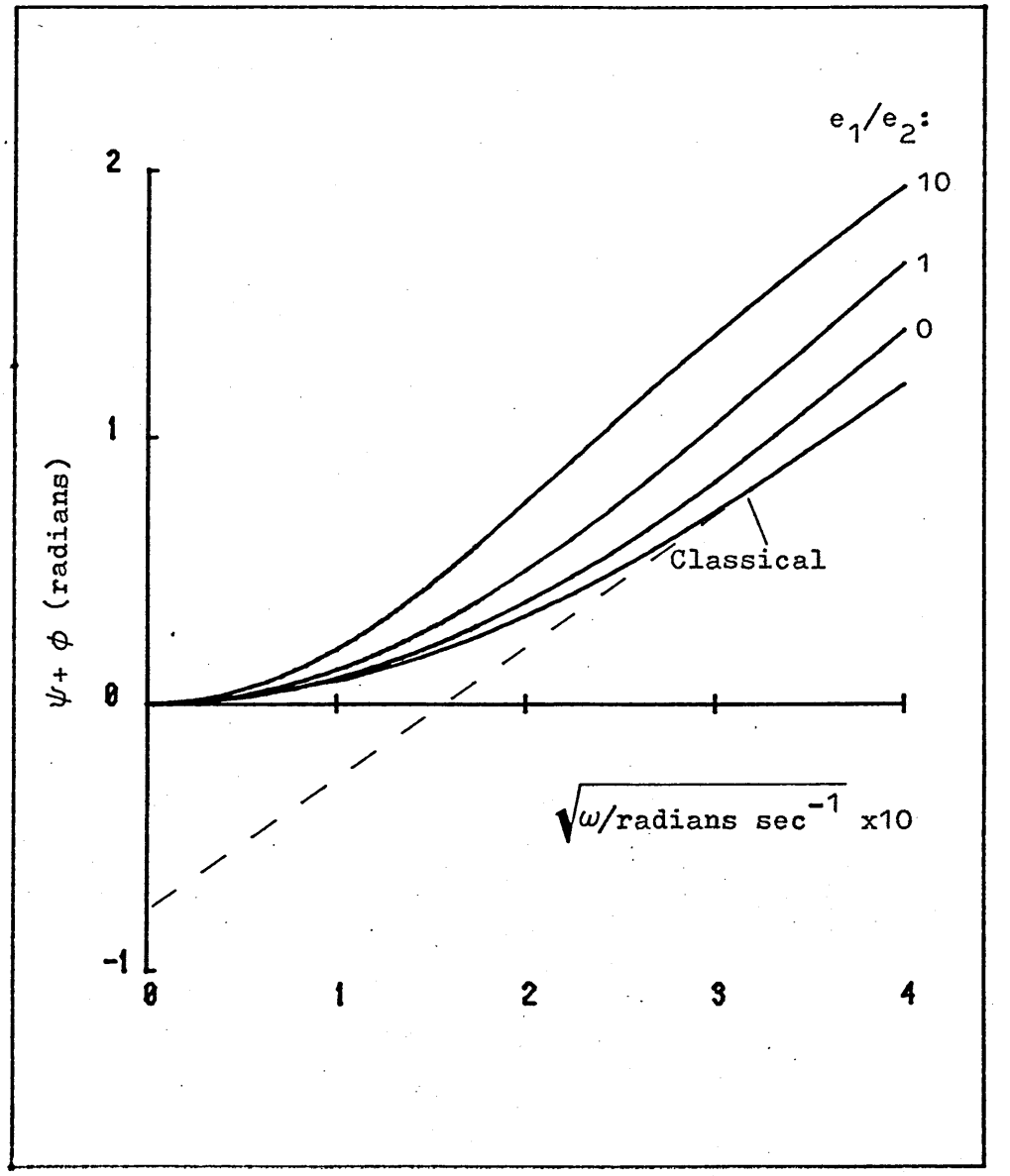

Figure 4.5 The effect of the input parameter e_1/e_2 on the phase lag with the input parameter $e_o/e_2 = 0.8$

Case (ii): $J/K_1 p << 1$ gives:

$$J = \frac{J_{CLAS}}{\left(\frac{D}{lK_4} + 1\right)} \tag{4.12}$$

This case is complementary to case (i) and covers the situation where there is insignificant delay at the surface $x = o^-$ and holdup is confined to the surface $x = o$. The indicator of this delay is D/lK_4 which is a comparison of the flux through the specimen DC/l to the de-solution flux at the input surface, $-K_4C$.

For large K_1, K_2 the terms e_o, e_1, e_2 in Section 3.9 can be approximated:

$$e_o = 1$$

$$e_1 = D^{\frac{1}{2}}/\sqrt{2}\ K_4$$

$$e_2 = o$$

The amplitude modification factor is the same as for case (i), equation (4.9), (except that $e_o = 1$) and can be expanded as before for low ω to yield its maximum value

$$\hat{A} = 1/(1 + e_1\sqrt{2D}/l) = 1/(1+D/lK_4) \tag{4.13}$$

Figure 4.6 shows the variation of the modified output pressure amplitude, $p'_H\sqrt{p}/p_H$, caused by various values of the factor D/lK_4. The major difference between this case and case (i) is that here $\hat{A}$ and J go down in the same proportion on increasing D/lK_4 (equations (4.12) and (4.13)). This is in direct contrast to the case for $J/K_1 p$ control as shown by equations (4.8) and (4.10) and Figure 4.3. Thus, for D/lK_4 control the curve for

measured $p'_H\sqrt{p}/p_H$ versus $F(\omega)$ will always extrapolate to $p'/2\sqrt{p}$ when $\omega \longrightarrow o$. The only indication of non-classical behaviour will be in a curvature of the plots. The equation for tan ψ is the same as for the low e_2 version of equation (4.11) except that here $e_o = 1$ and thus:

$$\tan \psi = \frac{e_1 \omega^{\frac{1}{2}} \left(\frac{\sinh 2kl - \sin 2kl}{\cosh 2kl - \cos 2kl}\right)}{1 + e_1 \omega^{\frac{1}{2}} \left(\frac{\sinh 2kl + \sin 2kl}{\cosh 2kl - \cos 2kl}\right)} \qquad (4.14)$$

Figure 4.7 compares $\psi + \phi$ with the corresponding classical equation (i.e. $\psi = o$). One important point about equation (4.14) is worth noting. As the value of e_1 (and hence D/lK_4) becomes large equation (4.14) tends towards:

$$\tan \psi = \frac{\sinh 2kl - \sin 2kl}{\sinh 2kl + \sin 2kl}$$

i.e. there is a 'saturation' in the input surface phase lag.

4.4 The Output Condition

Suppose now that the input surface is at equilibrium and that the output surface rate processes are finite as are the output concentrations. The steady-state flux equations (3.1) become:

$$J = K'_2 \theta'^2 - K'_1 p' = K'_4 C' - K'_3 \theta' = \frac{-D(C' - C)}{l}$$

and $$C = \frac{K_{sm}\sqrt{p}}{l}$$

Thus:

$$J = \frac{-DC'}{l} + J_{CLAS}$$

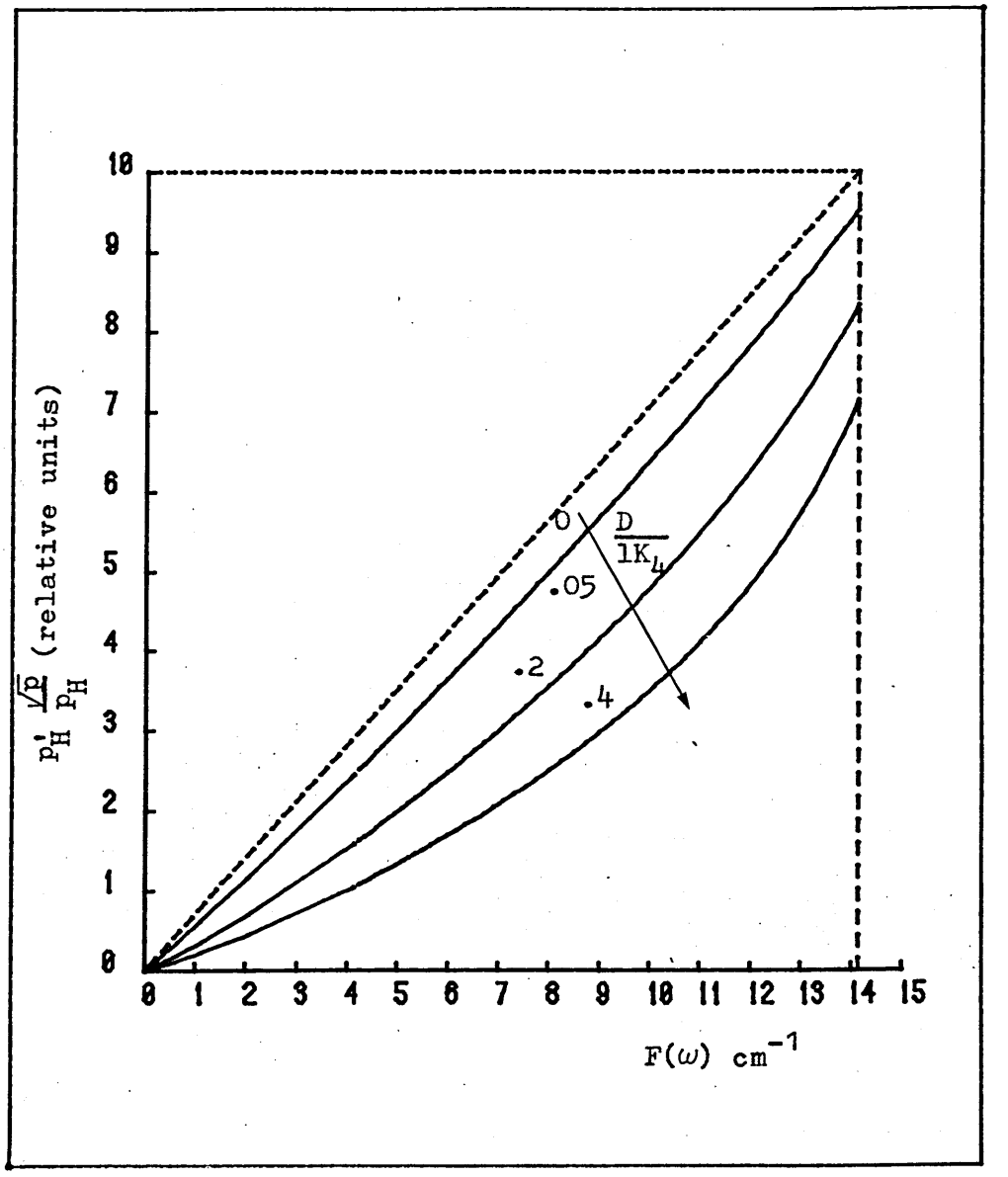

Figure 4.6 The effect of the input parameter $D/1K_4$ on the output pressure amplitude

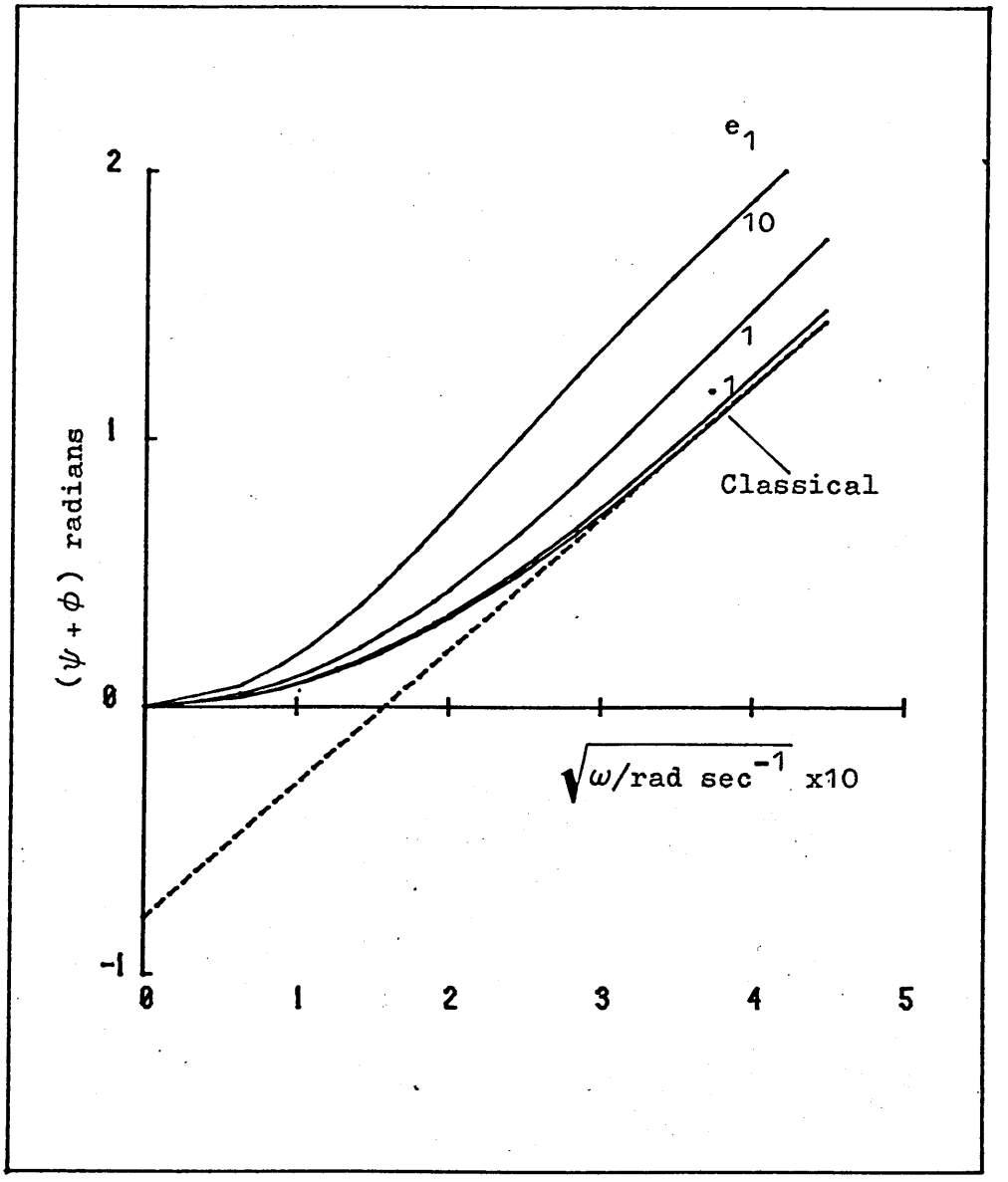

Figure 4.7 Effect of the input parameter $e_1 = \frac{D}{lK_4}$ (kl) on the diffusion phase lag

Again, using the identities for J_{CLAS} and K_{sm} the equation corresponding to equation (4.7) for the steady-state flux, J, in terms of the classical steady-state flux, J_{CLAS} is:

$$J\left[1 + \frac{D}{lK_4'}\right] = J_{CLAS}\left[1 - \sqrt{\frac{J}{K_1'p} - \frac{p'}{p}}\right]$$

For small values of p'/p this becomes:

$$J = J_{CLAS}\left[\frac{1 - \sqrt{J/K_1'p}}{D/lK_4' + 1}\right] \qquad (4.15)$$

Again, two limiting cases present themselves according to whether $J/K_1'p$ is small or D/lK_4' is small.

Case (i) $D/lK_4' \ll 1$ gives:

$$J = J_{CLAS}\,(1 - \sqrt{J/K_1'p}) \qquad (4.16)$$

This case is the output analogue to equation (4.8) where the surface x = 1 produces insignificant delay and the surface $x = 1^+$ produces all the modification. The indicator of this delay is a little more difficult to interpret than in the corresponding input case and is given by the ratio of the flux, J, to the back-flux from the output gas which would occur were the output pressure equal to the input pressure, $K_1'p$.

The oscillatory solutions are now obtained from the bulk modifications (3.19) and (3.20) and also the output surface modifications (3.17) and (3.18). For the bulk diffusion modification it is useful to write the term x_1/x_o in terms of $J/K_1'p$. Using the values in Section 3.8:

$$\frac{x_1}{x_o} = \frac{(\beta K_a' + K_1'K_3'\frac{ART}{V})\frac{D^{\frac{1}{2}}}{2}}{2\,K_2'K_4'\,\theta'}$$

if $1/K_4' \longrightarrow 0$:

$$\frac{\sqrt{2}}{D^{\frac{1}{2}}} \frac{x_1}{x_o} = \frac{K_3'}{K_4'} \frac{1}{2K_2'^{\frac{1}{2}}\theta'} \left[1 + \frac{K_1'p'}{J}\right]$$

but $K_2'^{\frac{1}{2}}\theta' = \sqrt{J - K_1'p'}$

and thus, supposing that the re-solution term is small, i.e. $K_1'p' \ll J$:

$$\frac{x_1}{x_o} = \frac{D^{\frac{1}{2}}}{\sqrt{2}} \frac{K_{sm}}{2K_1'^{\frac{1}{2}}} \frac{1}{\sqrt{J}}$$

and, eventually:

$$\frac{x_1}{x_o} = \frac{\sqrt{\frac{J}{K_1'p}}}{1 - \sqrt{J/K_1'p}} \frac{1}{2\sqrt{2D}}$$

The term x_1/x_o allows definition of the bulk diffusion modifications in amplitude and phase, but the parameters C and tan ζ (like part of the input condition) cannot be written in terms of the steady-state flux deviation alone. Summarising from equations (3.17), (3.18), (3.19) and (3.20):

$$C = \left[(\omega/2K_2'\theta')^2 + 1\right]^{-\frac{1}{2}}$$

$$\tan \quad = \omega/2K_2'\theta'$$

and

$$B = \frac{2kD}{\sqrt{\cosh 2kl - \cos 2kl + \frac{2x_1}{x_o}\omega^{\frac{1}{2}}(\sinh 2kl + \sin 2kl) + 2\left[\frac{x_1}{x_o}\right]^2 \omega (\cosh 2kl + \cos 2kl)}}$$

$$\tan\phi = \frac{\tan kl - \tanh kl + \frac{2x_1}{x_o}\omega^{\frac{1}{2}} \tan kl \tanh kl}{\tan kl + \tanh kl + \frac{2x_1}{x_o}\omega^{\frac{1}{2}}}$$

Expanding the bottom line of B in power series of 2kl as before it can be seen that as $\omega \longrightarrow o$:

$$\hat{C} = 1$$

$$\text{and } \hat{B} = \frac{2kD}{2kl\left[1 + \frac{\sqrt{J/K_1'p}}{2(1 - \sqrt{J/K_1'p})}\right]} \qquad (4.17)$$

The variation of the flux (4.16) and the maximum amplitude modification, $\hat{BC}$, with $J/K_1'p$ is shown in Figure 4.8. This plot is the analogue of Figure 4.3 and it can be seen by comparing these two figures that J falls initially much more rapidly with $J/K_1'p$ than it does for the corresponding input condition J/K_1p. This means that, if $K_1 = K_1'$, output effects in the steady-state flux will manifest themselves earlier (with increasing deviation from equilibrium) than will the corresponding input effects for this type of control. Similar remarks apply to the maximum amplitude modification (at $\omega = o$).

The effects of the parameters $J/K_1'p$ and $c = 2K_2'\theta'$ on the output pressure amplitude through the modifications B and C are shown in Figure 4.9. Note that C does not affect the amplitude at $\omega = o$ ($F(\omega) = 14.14$) since $\hat{C} = 1$. Consideration of Figure 4.8 along with Figure 4.9 shows that, although effects are more rapidly felt at the output than at the input the difference between the extrapolated value of the modified output pressure amplitude, $p_H' \sqrt{p}/p_H$ and the measured steady-state level $p'/2\sqrt{p}$ are not as great as in the case for the input (Figures 4.3 and 4.4).

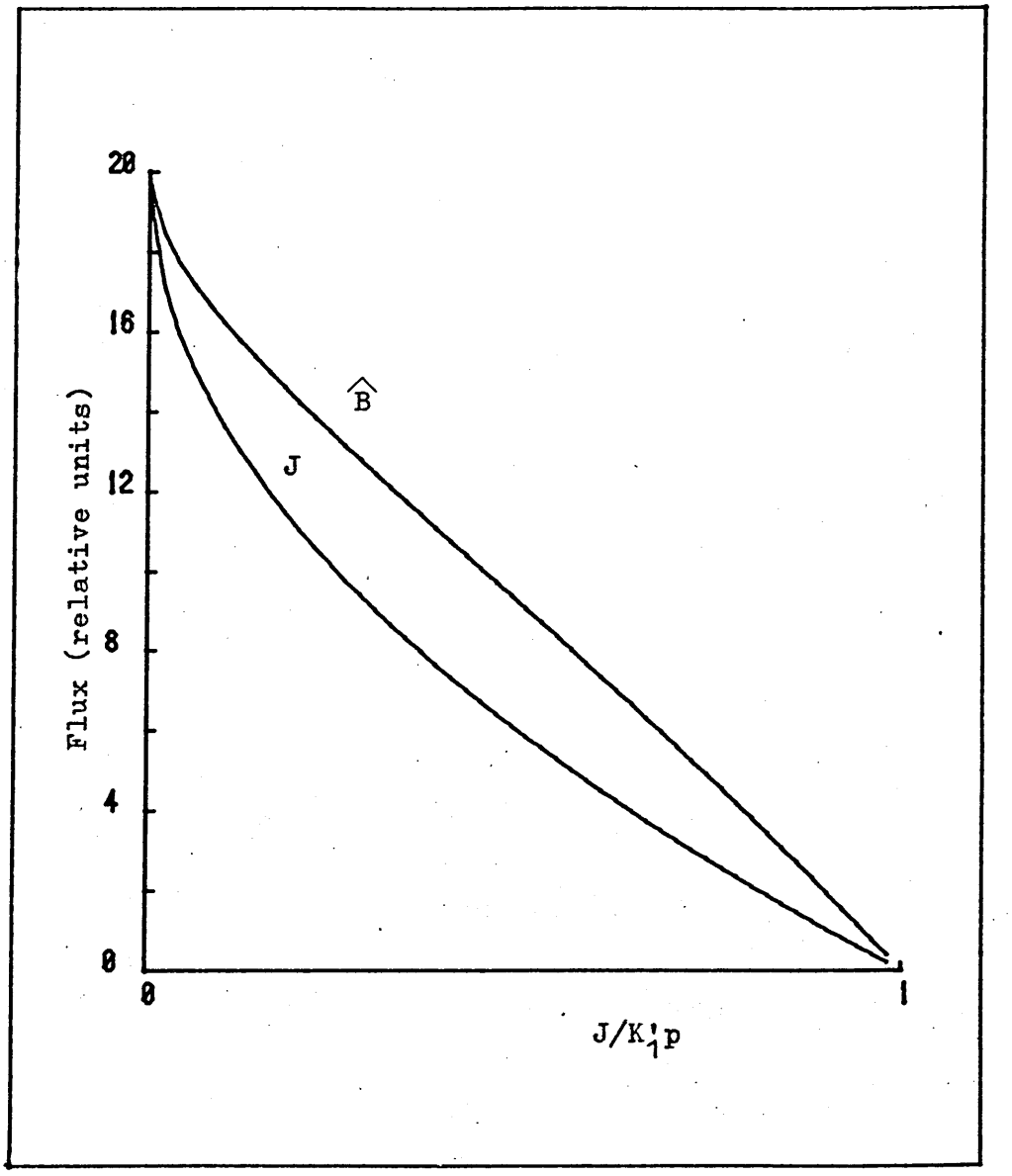

Figure 4.8 The variation of Flux, J, and maximum output pressure amplitude modification, $\hat{B}$, with $J/K_1'p$

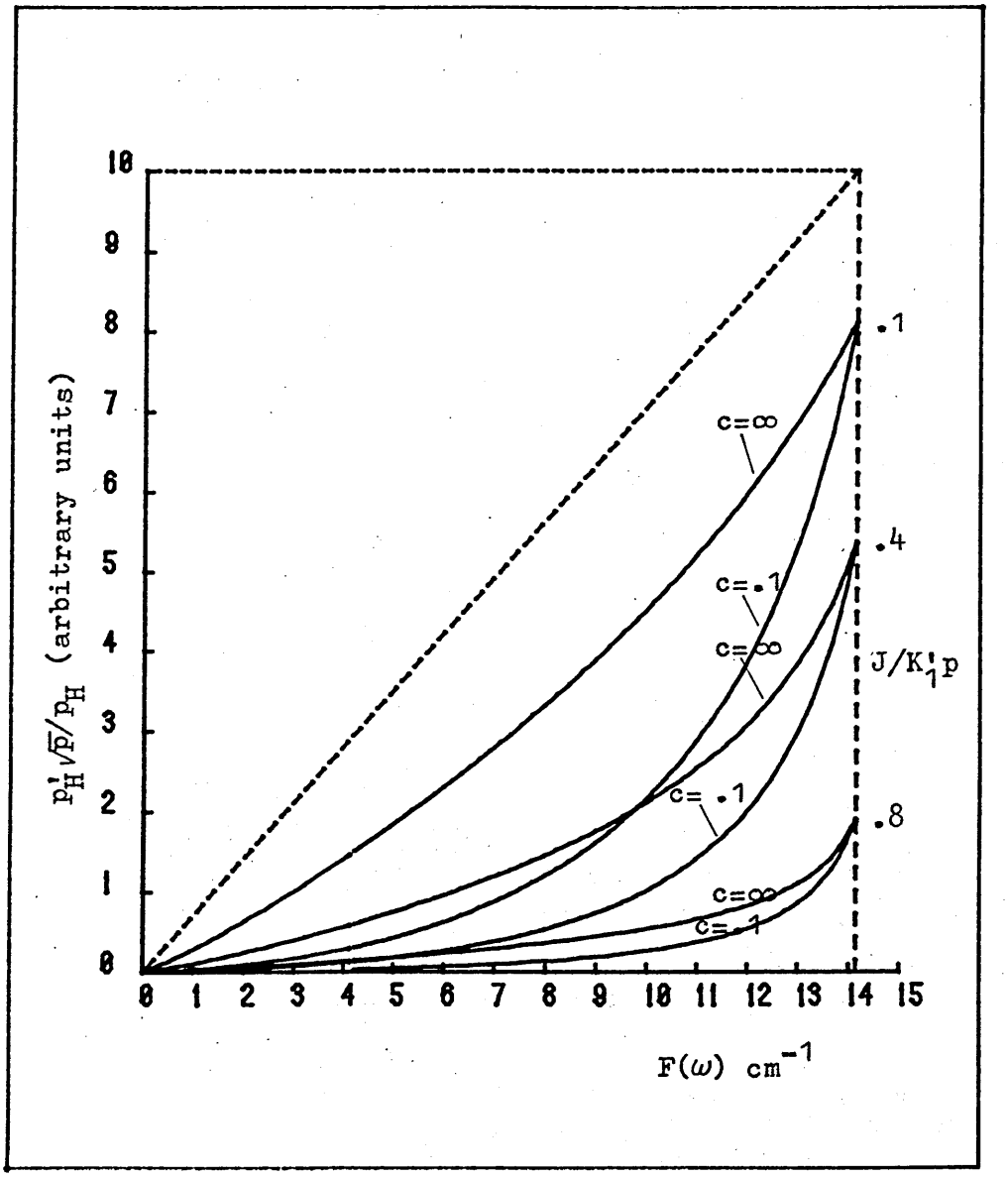

Figure 4.9 Output pressure amplitude modification by the quantities J/K'_1p and $c = 2K'_2\theta'$

Figure 4.10 shows the corresponding phase effects $\phi + \zeta$.

Case (ii) $J/K_1' p \ll 1$ gives:

$$J = J_{CLAS}/(D/lK_4' + 1) \tag{4.18}$$

This is the output analogue of equation (4.12) and is in fact phenomenologically indistinguishable from it. Both effects (input and output) should manifest themselves simultaneously in the steady-state unless the two surfaces are physically different ($K_4' \neq K_4$). The equations for B, C, tan ζ and tan ϕ are the same as for case (i) except that the parametric value of x_1/x_o is changed:

$$\frac{D^{\frac{1}{2}}}{\sqrt{2}} \frac{x_1}{x_o} = \frac{1}{2K_2'\theta'} \left[\frac{K_3'}{K_4'} + \frac{K_1'K_3'}{K_4'} \frac{ART}{V\beta} \right] + \frac{1}{K_4'}$$

which eventually gives, for large K_1' and K_2':

$$\frac{x_1}{x_o} = \frac{D}{lK_4'} \frac{1}{\sqrt{2D}}$$

Thus, as $\omega \rightarrow o$

$$\hat{B} = \frac{D}{l(1+\frac{D}{lK_4'})} \tag{4.19}$$

$$\hat{C} = 1$$

Since the classical value of $\hat{B}$ is D/l (section 4.2) this modification has the same effect at $\omega = o$ as equation (4.13) and thus the output pressure modification is indistinguishable from this unless C is operative. Figure 4.11 shows the amplitudes and Figure 4.12 the phase effects of this modification.

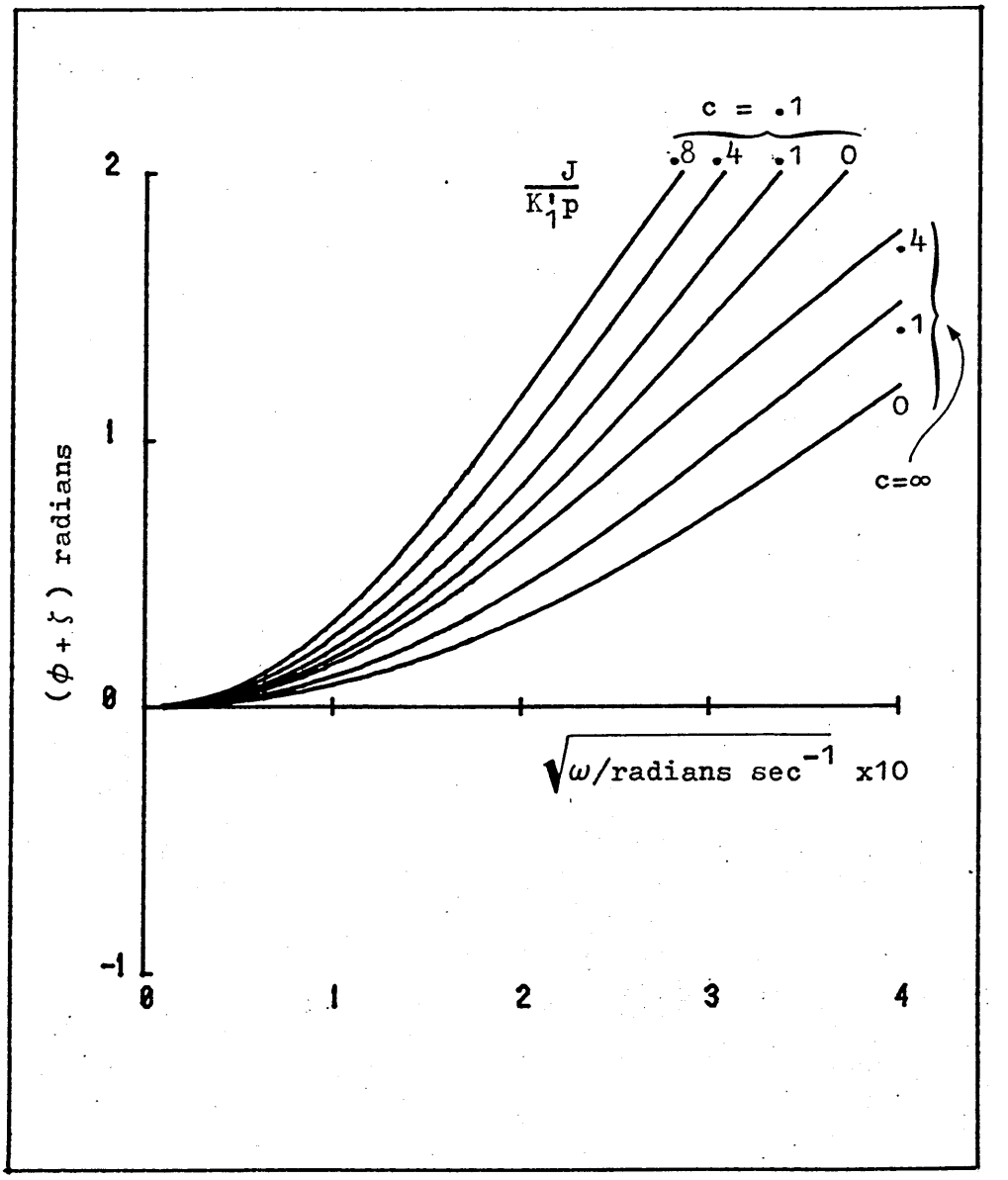

Figure 4.10 Phase effects due to the output parameters $J/K_1'p$ and $c = 2K_2'\theta'$

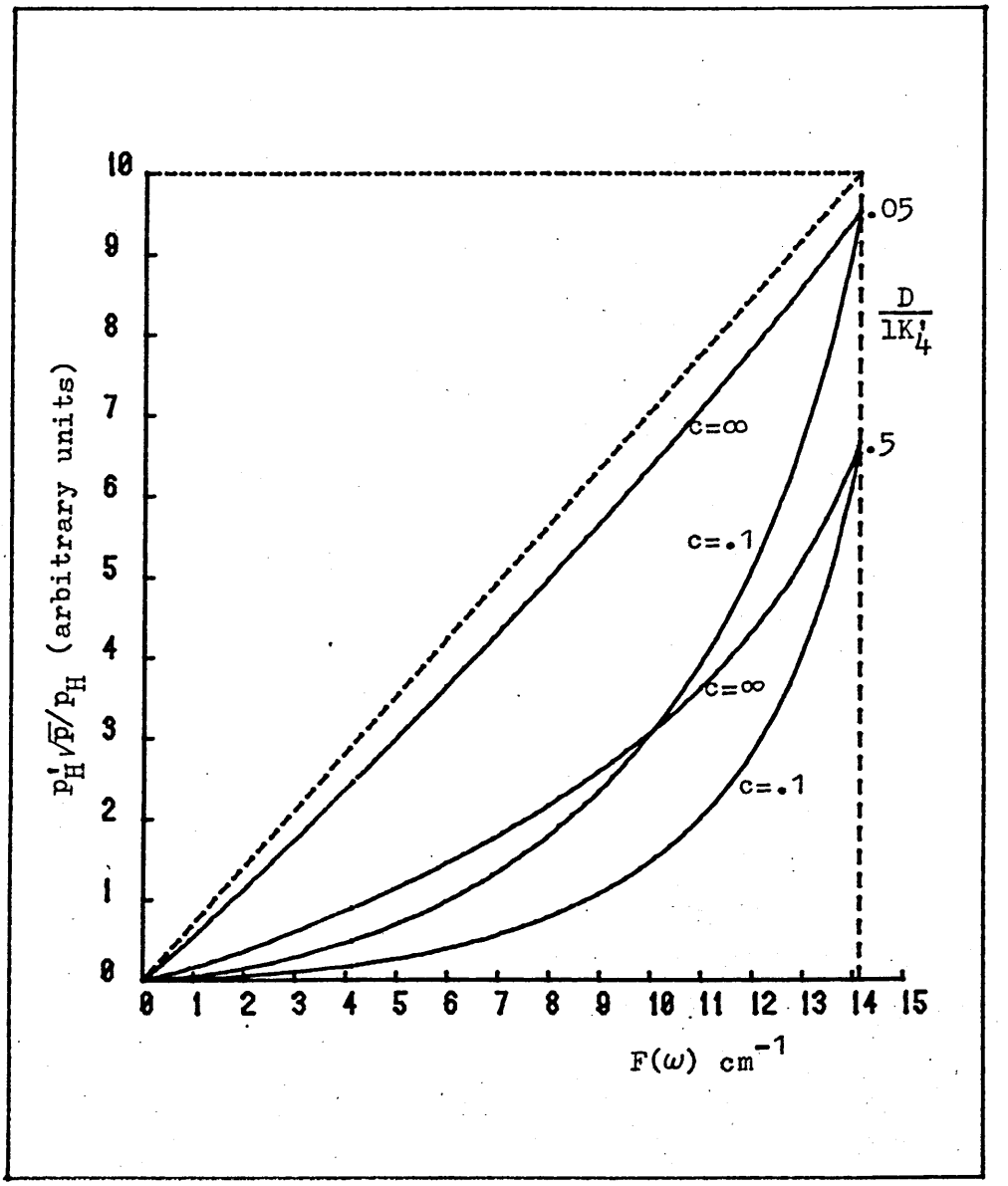

Figure 4.11 The effect of the output parameters $c = 2K'_2\theta'$ and $D/1K'_4$ on the output pressure amplitude

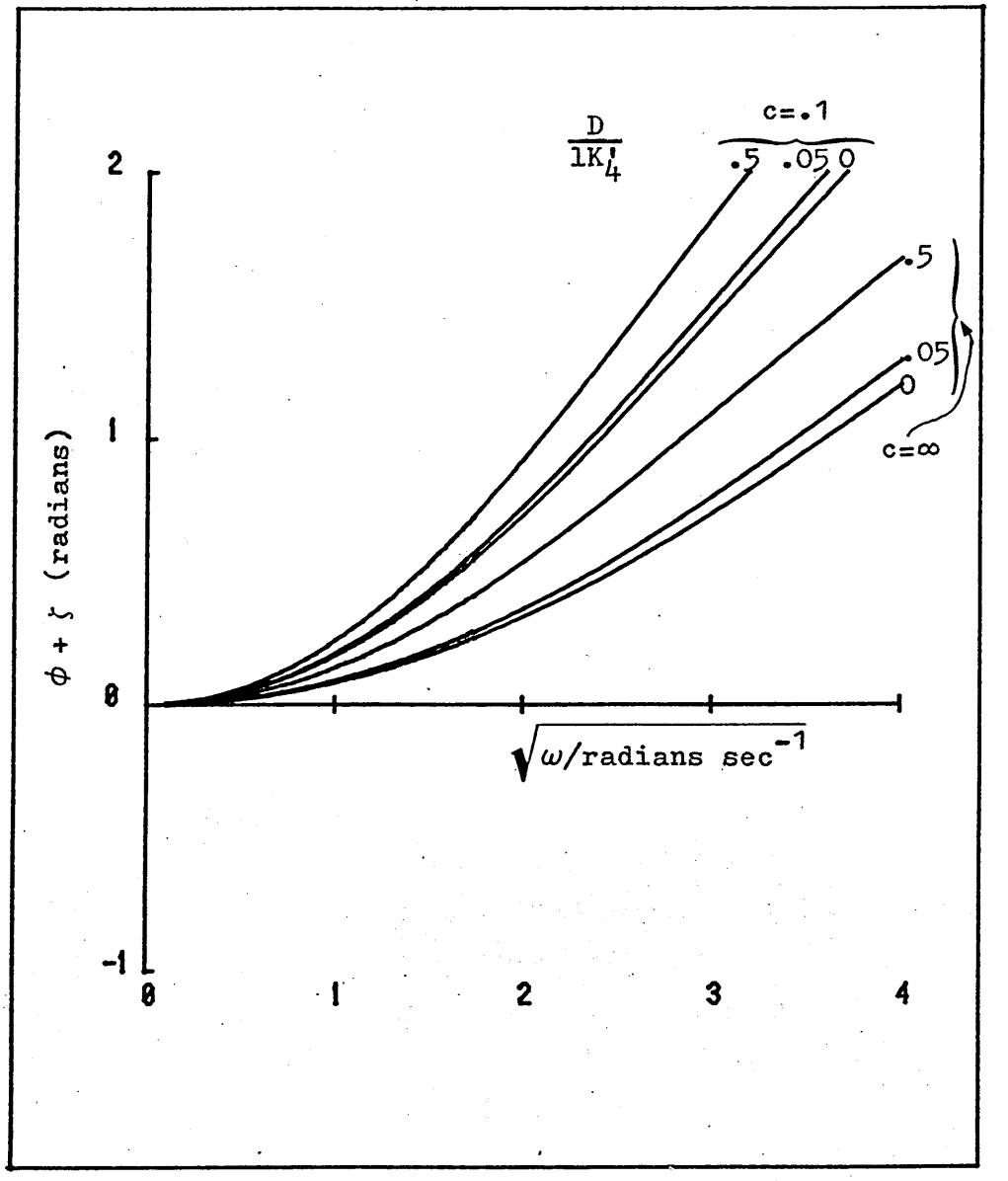

Figure 4.12 The effect of the output parameters $c = 2K'_2\theta'$ and $D/1K'_4$ on the phase.

In both the above cases, D/lK_4' control and $J/K_1'p$ control, there is a 'saturation' in the bulk phase-lag for large x_1/x_o (provided that $\zeta = o$) where the maximum value of ϕ is given by:

$$\hat{\phi} = \arctan (\tan kl \tanh kl) \qquad (4.20)$$

4.5 Oxide-limited Permeation

Another surface condition relevant to this work is that where a permeable oxide exists on one or both of the surfaces. If gas is assumed to pass through the oxide by a solution/diffusion mechanism, the whole problem can be treated as permeation through a composite medium.

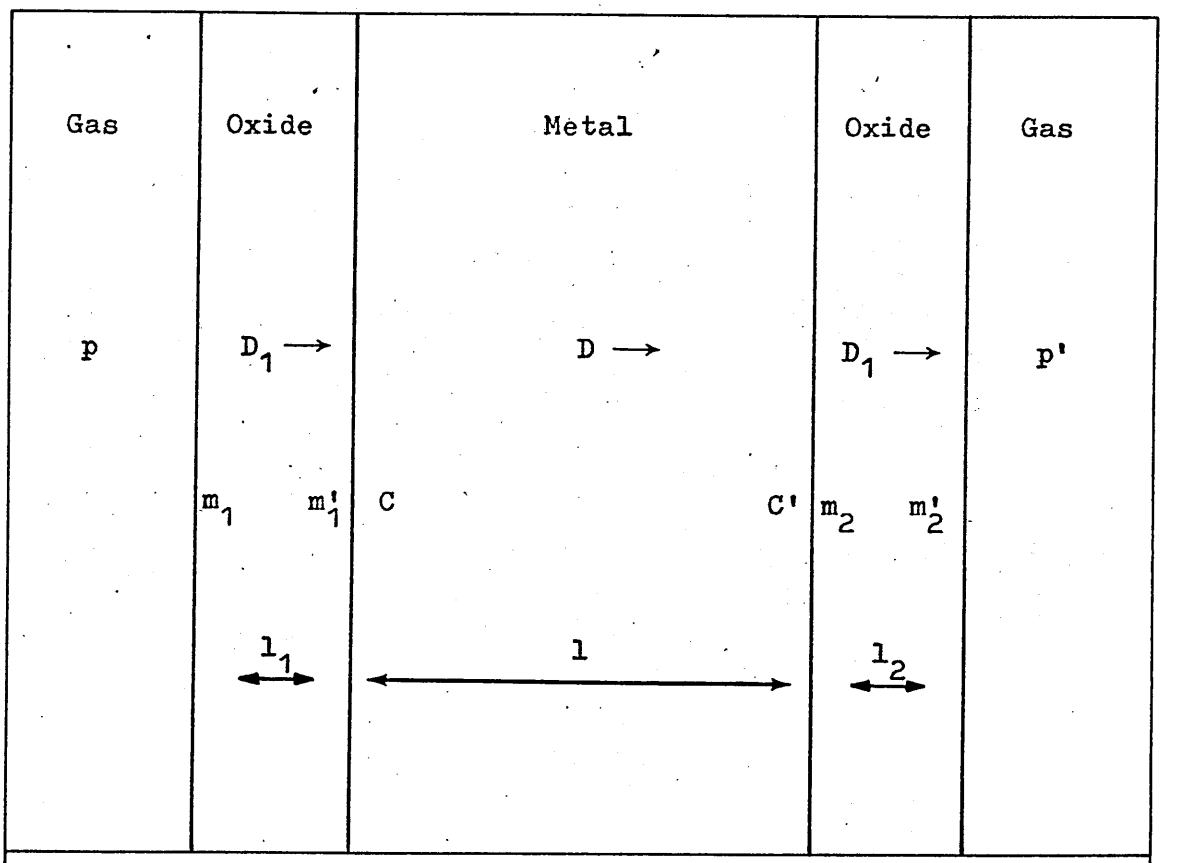

Figure 4.13 Scheme for oxide-limited permeation

If it is further supposed that equilibrium prevails at all the interfaces shown in Figure 4.13 and that the gas dissolves molecularly in the oxide (18) according to the modified Sieverts Law $m = K_{sa}p$, where m is a molecular concentration of hydrogen, then:

$$J = -\frac{D_1}{l_1} m_1' + \frac{D_1}{l_1} K_{sa}p = \frac{D_1}{l_2} m_2 - \frac{D_1}{l_2} K_{sa}p' = \frac{-D(C' - C)}{l}$$

$$\text{and} \quad C = \frac{K_{sm}}{\sqrt{K_{sa}}} m_1'^{\frac{1}{2}} \qquad (4.21)$$

$$C' = \frac{K_{sm}}{\sqrt{K_{sa}}} m_2^{\frac{1}{2}}$$

where l_1, l_2, l are the oxide thicknesses at the input side and output side and the metal thickness respectively.

m_1, m_1', m_2, m_2' are molecular concentrations of gas in the oxide at the input gas/oxide, input oxide/metal, output metal/oxide and output oxide/gas interfaces respectively.

D_1 is the molecular diffusion coefficient of gas in the oxide.

C, C', p, p', D are as before.

These parameters are shown in Figure 4.13.

Writing the corresponding flux equations for J/K_1p control in the model for finite solution processes (i.e. equation (3.1) with the K_3/K_4 surfaces in equilibrium):

$$J = K_1p - K_2\theta^2 = K_2'\theta'^2 - K_1'p' = \frac{-D}{l}(C' - C)$$

$$\text{and} \quad C = \frac{K_3}{K_4}\theta$$

$$C' = \frac{K_3'}{K_4'}\theta'$$

The two situations are exactly analogous where:

$$\left.\begin{aligned} K_1 &\equiv \frac{D_1}{l_1} K_{sa} \\ K_2 &\equiv \frac{D_1}{l_1} \\ K_2' &\equiv \frac{D_1}{l_2} \\ K_1' &\equiv \frac{D_1}{l_2} K_{sa} \end{aligned}\right\} \qquad \begin{aligned} \theta &\equiv m_1'^{\frac{1}{2}} \\ \theta' &\equiv m_2^{\frac{1}{2}} \\ \frac{K_3}{K_4} &= \frac{K_3'}{K_4'} \equiv \frac{K_{sm}}{[K_{sa}]^{\frac{1}{2}}} \\ \frac{K_1^{\frac{1}{2}}}{K_2^{\frac{1}{2}}} \frac{K_3}{K_4} &= \frac{K_1'^{\frac{1}{2}}}{K_2'^{\frac{1}{2}}} \frac{K_3'}{K_4'} \equiv K_{sa} \end{aligned} \qquad (4.22)$$

Unfortunately unless $l_2 = l_1$ there is no reason to suppose that $K_n = K_n'$ as is possible in the case of surface control.

All the results of the surface effects can therefore be written by analogy for oxide-limited permeation.

4.6 Summary

The classical equations show that, in the limit of input surface equilibrium and output surface equilibrium with $C' \longrightarrow o$, the measured variables in the experiment p', p_H', ϕ yield two quantities: the diffusion coefficient, D, and the equilibrium solubility as defined by Sieverts Law $C = K_{sm} \sqrt{p}$.

When the classical conditions apply (i.e. thick specimen, high input pressure, low diffusion coefficient) the process of diffusion in the bulk of the solid is so much slower than the solubilisation processes that the latter have an undetectable effect on the experiment. That the processes are undetectable does not mean, however, that they do not occur nor that the surfaces are indeed in equilibrium.

Under classical conditions measurements derived from

the macroscopic flow of gas through a specimen allow evaluation of the product DK_{sm}: measurements derived from the time taken for gas to traverse a specimen allow evaluation of D alone. Both types of measurement are normally made in experiments where the diffusion coefficient and the solubility are required. If only the permeability (DK_{sm}) is wanted then time-dependent experiments are not necessary.

In the present work, the phase-lag is a function only of the diffusivity and the steady-state is a function only of the permeability. The amplitude is a function of permeability but also depends on the diffusion coefficient in a very specific way through the function $F(\omega)$. The amplitude can therefore be used as a check for internal consistency between the phase (diffusion coefficient) and steady-state (permeability) measurements.

The phase-lags and amplitudes must also bear a specific relationship to the angular frequency of modulation, ω, and failure to do so will be indicative of the extent to which the classical approximation applies.

Checks which can be applied to the steady-state are limited to temperature consistency (Arrhenius behaviour), consistency with thickness (inverse thickness relationship) and consistency with input pressure ('$p^{\frac{1}{2}}$ law'). Failure in any of these instances is failure of the Richardson equation and is indicative of non-classical permeation.

When the time taken for the solubilisation process to occur becomes comparable with the traverse time, the frequency response will become increasingly dominated by solubilisation parameters. The amplitude plots vs. $F(\omega)$ will deviate from the classical straight line and the limiting value as $\omega \rightarrow o$ may become

inconsistent. Phase curves will lie above the classical line and will no longer necessarily extrapolate through $-\pi/4$ on the $\omega = 0$ axis. Inversion of the curvature of the phase plots may also occur.

In the foregoing analysis an attempt has been made to typify the sort of deviations one might expect from classical behaviour for certain limiting cases of the surface processes. It has been found necessary to separate the effects of the input and output processes in order that each may be examined more clearly. A further subdivision has been made into two types of surface control which may be exercised at each of the input and output surfaces; a J/K_1p type of control at the gas-solid interfaces and a D/lK_4 type of control at the bulk-surface interfaces. The four cases are summarised in Figure 4.14 in terms of the steady-state flux equations which describe them. The accompanying graphs are schematic chemical potential diagrams, a discontinuity in chemical potential being indicative that holdup is occurring at a particular interface.

Combination of the four effects shown in Figure 4.14 gives the steady-state flux with all four mechanisms operative.

$$J = \frac{J_{CLAS}}{1 + \frac{D}{lK_4'} + \frac{D}{lK_4}} \left[\sqrt{1 - \frac{J}{K_1 p}} - \sqrt{\frac{J}{K_1' p}}\right]$$

The oscillatory solutions for each of these four cases were also discussed in this Chapter in comparison to the classical oscillatory solution. The character of these solutions could again be separated into J/K_1p and D/lK_4 types but some additional 'secondary' effects were also apparent.

It was also pointed out that the case of oxide-limited

permeation could, with certain assumptions about the nature of the oxide holdup, be treated as a finite surface rate process without D/lK_4 control, i.e.:

$$J = J_{CLAS}\left[\sqrt{1 - J/K_1 p} - \sqrt{J/K_1' p}\right]$$

where the parameters K_1 and K_1' have an entirely different meaning and are related to the molecular solubility of gas in the oxide layer, its molecular diffusion coefficient in the layer and the oxide layer thickness.

Figure 4.14 Schematic description of the four possible areas of surface control

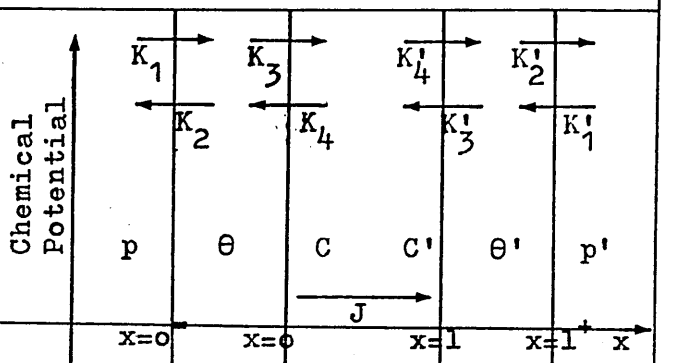

Case a) There is a chemical potential drop at the surface x = o caused by failure of the gas-solid interface to reach equilibrium. The steady-state flux in this case is given by:

$$J = J_{CLAS}\sqrt{1 - J/K_1 p}$$

Case b) There is a chemical potential drop at the surface $x = o^+$ caused by gas not being supplied to the bulk solution rapidly enough to replenish that which is moving down the chemical potential gradient towards the output surface. The steady-state flux is given by:

$$J = J_{CLAS}/(1 + D/lK_4)$$

Case c) Equilibrium is maintained at the input surface but gas is not being removed rapidly enough from solution at x = 1 resulting in a reduction in the concentration gradient in the solid and thus a reduction in the steady-state flux which is given by:

$$J = J_{CLAS}(1 + D/lK'_4)$$

Case d)/

Case d) Equilibrium prevails at the input surface but gas cannot evaporate rapidly enough from the output gas-solid interface. The steady-state flux is given by:

$$J = J_{CLAS}(1 - \sqrt{J/K_1' p})$$

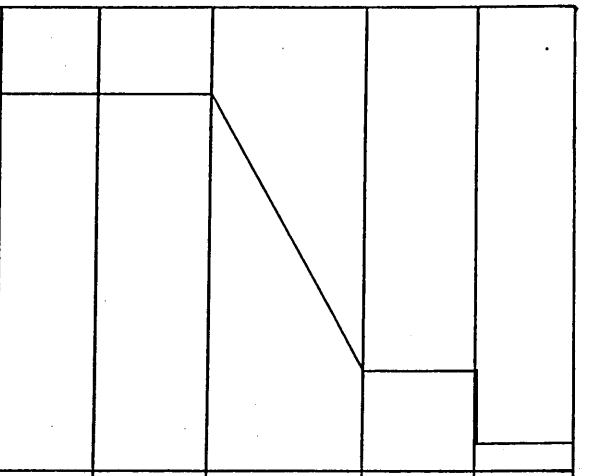

Case e) The only chemical potential gradient is in the bulk of the solid and equilibrium prevails at both surfaces. The output surface concentration is close to zero. The classical steady-state flux is given by:

$$J_{CLAS} = DK_{sm}\sqrt{p}/l$$

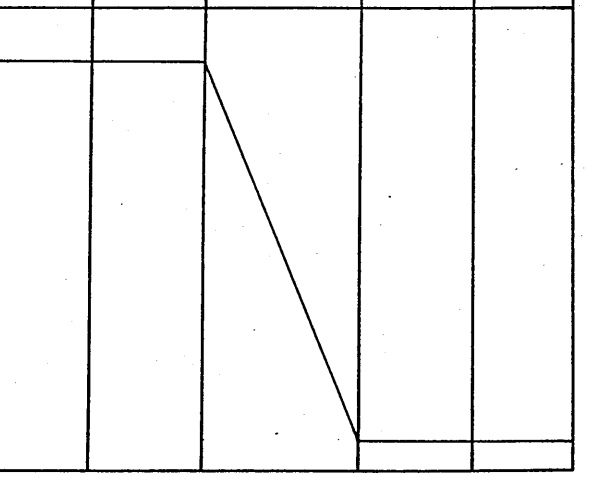

CHAPTER 5

RESULTS

5. Results

This chapter presents an evaluation of the parameters describing the permeation rates in nickel, molybdenum and M316 stainless steel. It details the handling of the raw data: phase lags, amplitude attenuations and steady-state pressure ratios across the specimen and shows how the individual parameters are evaluated. Discussion of these parameters and their comparison with data from the literature is deferred to the next Chapter.

5.1 Nickel

Nickel was chosen as a specimen material in order to provide a proof of the experimental technique since Nickel diffusion coefficients and solubilities are perhaps the best known in the literature. Nickel also has the advantage of showing a large solubility for hydrogen making measurement of the output pressure parameters relatively simple. The temperature range investigated for this material was 620 - 976 K.

The experiment was carried out first with a .6 torr input pressure, where results were analysable in terms of the classical equations. To investigate the pressure effect another frequency run was made at an input pressure of .02 torr at alternate temperatures. At the other alternate temperatures not covered by the .02 torr input pressure a frequency was picked on the basis of the .6 torr results which gave an appreciable phase lag and, running at constant frequency meaaurements were made as a function of input pressure. The discussion is, therefore, separated into two parts: high input pressure (0.6 torr) and low input pressure (0.02 torr).

5.1.1 High input pressure

The 0.6 torr results could be analysed over the full range of frequency and temperature in terms of the classical equations (4.4), (4.5) and (4.6).

A typical run at 0.6 torr input pressure consisted of around eight frequencies at each temperature and at each frequency the values of p_t and p'_t (total input and output pressures, i.e. steady-state and harmonic parts) were measured as a function of time. The results were then reduced by Fourier analysis and signal averaging to yield an amplitude, phase and steady-state level for each of the input and output waves characteristic of each frequency The steady-state level throughout any set of frequencies (i.e. at any given temperature) was found never to vary by more than 2%. The output steady-state level was averaged over all the frequencies and divided by the square root of the input steady-state level averaged in a similar way.

As noted in Section 4.2 equation (4.5), the input and output mean values (p and p') are related to the permeability, P_m, by:

$$\frac{p'}{\sqrt{p}} = \frac{K'}{l} P_M$$

where $\frac{K'}{l}$ is constant with temperature for a given specimen, so that a plot of $\ln \frac{p'}{\sqrt{p}}$ vs. $\frac{1}{T}$ is sufficient to indicate whether or not the permeability behaves in the manner prescribed by the Arrhenius equation. Figure 5.1.1 shows such a plot which was fitted by linear regression analysis the result being shown as a full line. Inclusion of the factor $\frac{K'}{l}$ and transforming the

regression coefficients and standard errors* gives, for the time-independent indication of the permeability:

$$P_{M,s} = 4.32 \times 10^{-8} \exp\left[-\frac{12533}{R\,T}\right] \frac{\text{mole } H_2}{\text{cm sec}\sqrt{\text{torr}}} \qquad (5.1.1)$$

where the standard error on the pre-exponential factor (P_o) is $7 \times 10^{-9} \frac{\text{moles } H_2}{\text{cm sec}\sqrt{\text{torr}}}$ and on the activation energy is 276 calories/mole H_2. The activation energy is given in calories/mole H_2.

The phase lag between the input and output waves was then calculated and plotted against the square root of frequency. Two typical phase plots are shown in Figure 5.1.2. These data were at least squares fit to the classical phase lag given by equation (4.5) by the matrix correlation technique outlined in A.4.

The values of diffusion coefficient so obtained were drawn on an Arrhenius plot and fit by linear regression analysis in the same way as for the permeabilities to give:

$$D = 6.16 \times 10^{-3} \exp\left[-\frac{9523}{R\,T}\right] \text{cm}^2/\text{sec} \qquad (5.1.2)$$

---

*The standard errors in the linear regression coefficients can be written in two alternative ways:

$$\ln x = \frac{A \pm dA}{T} + \ln B \pm d\ln B$$

$$\text{i.e. } x = (B \pm dB) \exp \frac{(A \pm dA)}{T}$$

$$\text{where } dB = B\,d\ln B \qquad \text{——(a)}$$

or

$$\ln x = \frac{A \pm dA}{T} + \ln B \pm \varepsilon$$

$$\text{i.e. } x = Be^{\pm\varepsilon} \exp \frac{A \pm dA}{T}$$

$$\text{i.e. } \left.\begin{aligned} dB^+ &= Be^{\varepsilon} - B \\ dB^- &= Be^{-\varepsilon} - B \end{aligned}\right\} \quad \bar{dB} = \frac{|dB^+| + |dB^-|}{2} \qquad \text{——(b)}$$

Both equations (a) and (b) give similar results even up to fairly large values of $\varepsilon (\sim 5)$ but the form (a) has the advantage that the error is quoted in a symmetric form. The form (b) suggests that errors are more likely in the positive than in the negative direction.

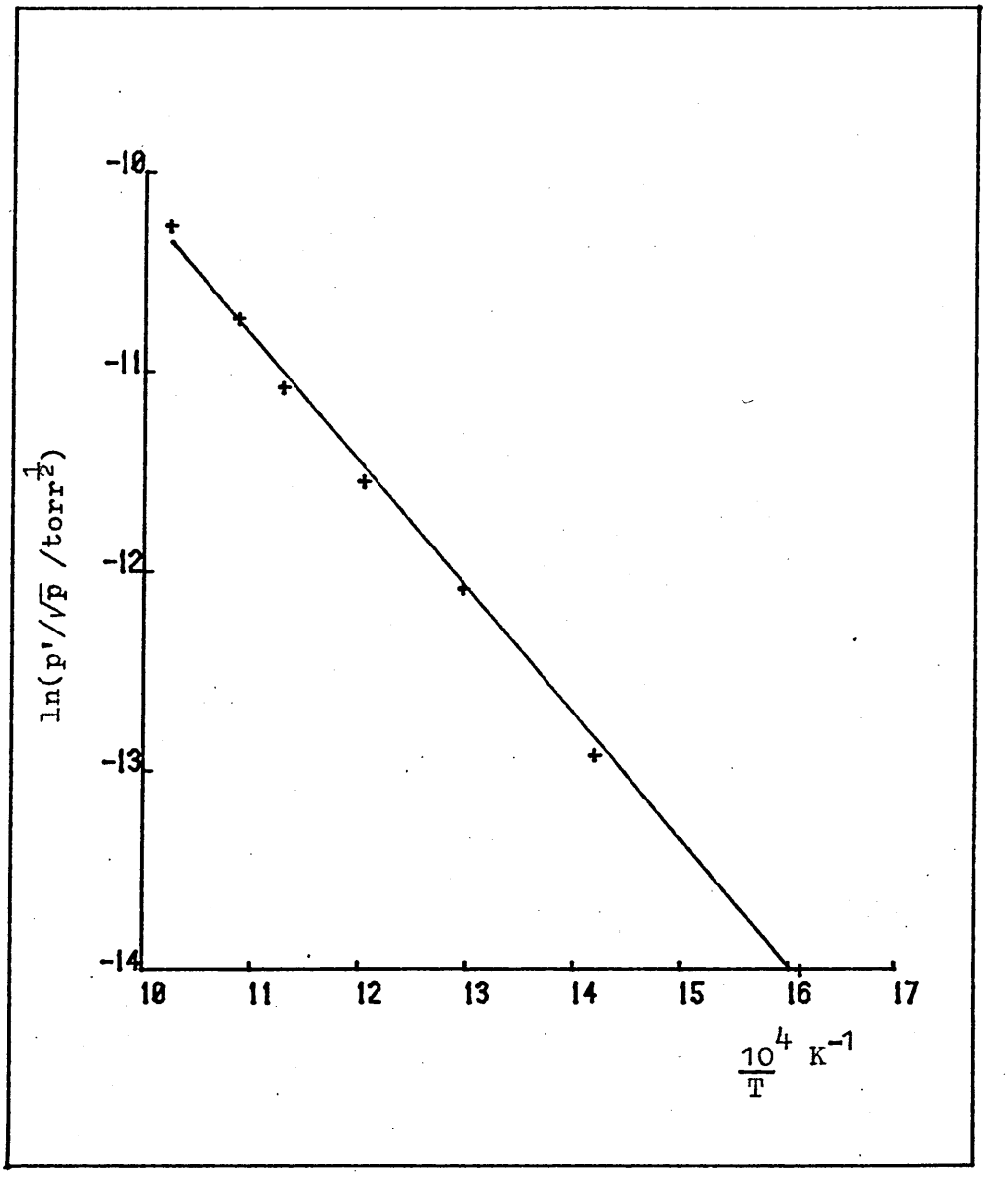

Figure 5.1.1 Steady-state indication of the permeability in 0.5 mm Nickel

Where the standard error on the pre-exponential factor, D_o, was 5×10^{-4} cm^2/sec and that on the activation energy was 123 calories/mole H_2. The activation energy is given in calories/mole H_2.

The individual diffusion coefficient values were used to calculate the function $F(\omega)$ from equation (4.5) for each frequency and the normalised output amplitudes $\frac{p'_H\sqrt{p}}{p_H}$ were plotted against this function in the manner described in Section 4.2. These plots are seen to extrapolate between $\frac{p'}{2\sqrt{p}}$ and zero (Figure 5.1.3). The intercepts with the axis $F(\omega) = \frac{1}{\sqrt{2}l}$ ($\omega = o$) are the time-dependent indications of the permeability. These values of $\frac{p'_H\sqrt{p}}{p_H}$ should again show Arrhenius behaviour with temperature (Section 4.2) and the log-reciprocal plot is shown in Figure 5.1.4.. These data were again fit by linear regression analysis to give, for the time-dependent indication of the permeability:

$$P_{M,t} = 3.41 \times 10^{-8} \exp\left[-\frac{12118}{R\,T}\right] \frac{\text{mole } H_2}{\text{cm sec } \sqrt{\text{torr}}} \qquad (5.1.3)$$

where the standard errors on Po and the activation energy are 5×10^{-9} mole H_2/cm sec $\sqrt{\text{torr}}$ and 258 calories/mole H_2 respectively.

Table 5.1.1 shows the measured values of diffusion coefficient, D, time-independent permeability, $P_{M,s}$ and time-dependent permeability, $P_{M,t}$, at the measurement temperatures, T. The values calculated from equations (5.1.2), (5.1.1) and (5.1.3) respectively are also shown.

5.1.2 Low pressure

The experiments carried out using a 0.02 torr input pressure showed deviations from the classical behaviour observed for the .6 torr experiments in the phase-lag plots only. The phase-lag vs. square root frequency plots lay consistently above

Table 5.1.1 Classical Permeation and Diffusion Data for .5 mm Ni Measured with .6 torr Input Pressure

$D(cm^2/sec)$		$P_{M,s}$ $\frac{\text{mole } H_2}{\text{cm s } \sqrt{\text{torr}}}$		$P_{M,t}$ $\frac{\text{mole } H_2}{\text{cm s } \sqrt{\text{torr}}}$		T(K)
Measured	Calculated	Measured	Calculated	Measured	Calculated	
4.50×10^{-5}	4.54×10^{-5}	7.37×10^{-11}	6.75×10^{-11}	7.32×10^{-11}	6.62×10^{-11}	976
3.32×10^{-5}	3.34×10^{-5}	4.64×10^{-11}	4.51×10^{-11}	4.51×10^{-11}	4.49×10^{-11}	919
2.73×10^{-5}	2.74×10^{-5}	3.28×10^{-11}	3.47×10^{-11}	3.29×10^{-11}	3.48×10^{-11}	885
1.96×10^{-5}	1.91×10^{-5}	2.05×10^{-11}	2.16×10^{-11}	2.13×10^{-11}	2.21×10^{-11}	830
1.27×10^{-5}	1.23×10^{-5}	1.20×10^{-11}	1.21×10^{-11}	1.17×10^{-11}	1.26×10^{-11}	771
6.44×10^{-6}	6.80×10^{-6}	5.19×10^{-12}	5.55×10^{-12}	6.01×10^{-12}	5.92×10^{-12}	704
2.75×10^{-6}	2.70×10^{-6}	1.77×10^{-12}	1.65×10^{-12}	1.91×10^{-12}	1.83×10^{-12}	620

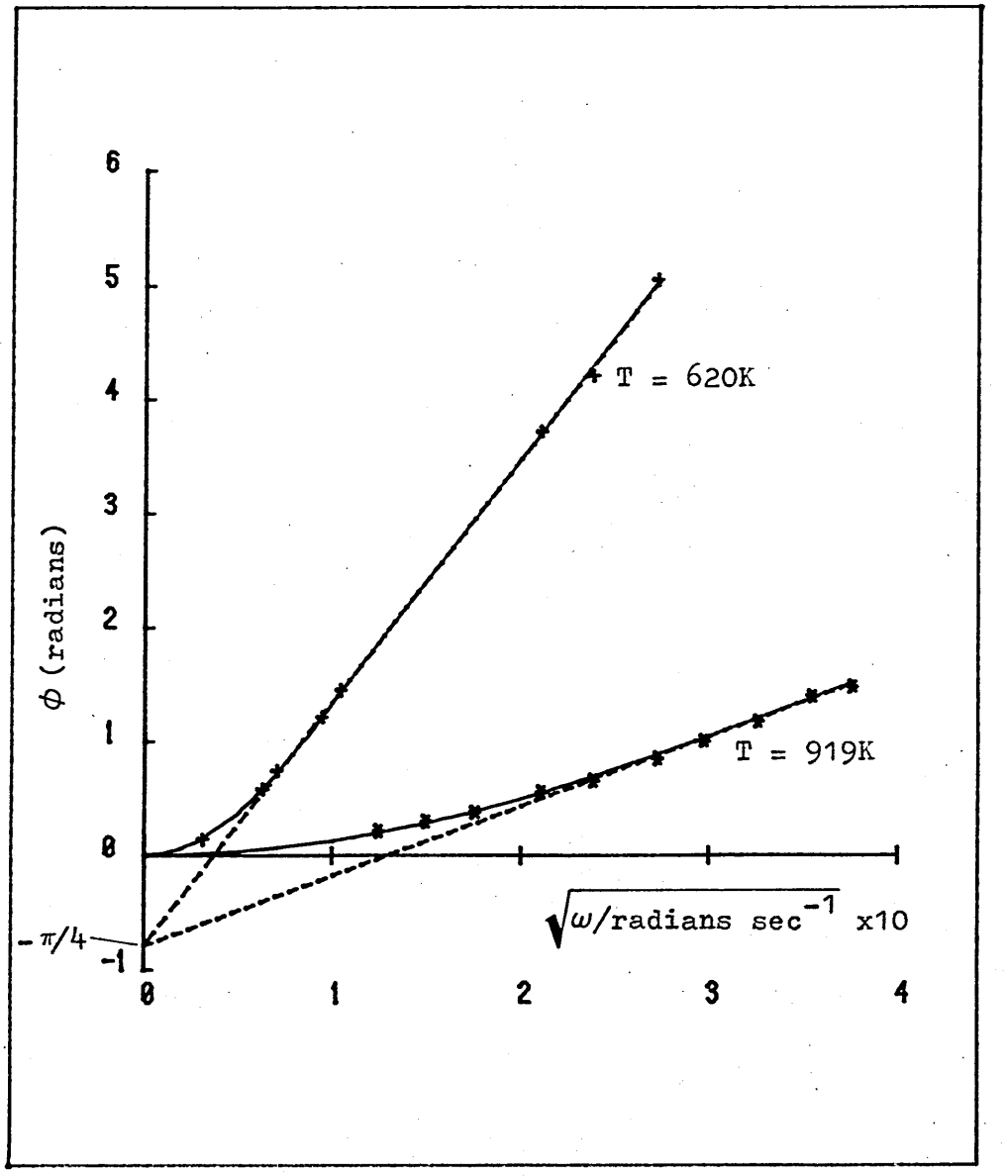

Figure 5.1.2 Typical frequency response curves for phase-lags across a 0.5 mm Ni specimen with input pressure of .6 torr

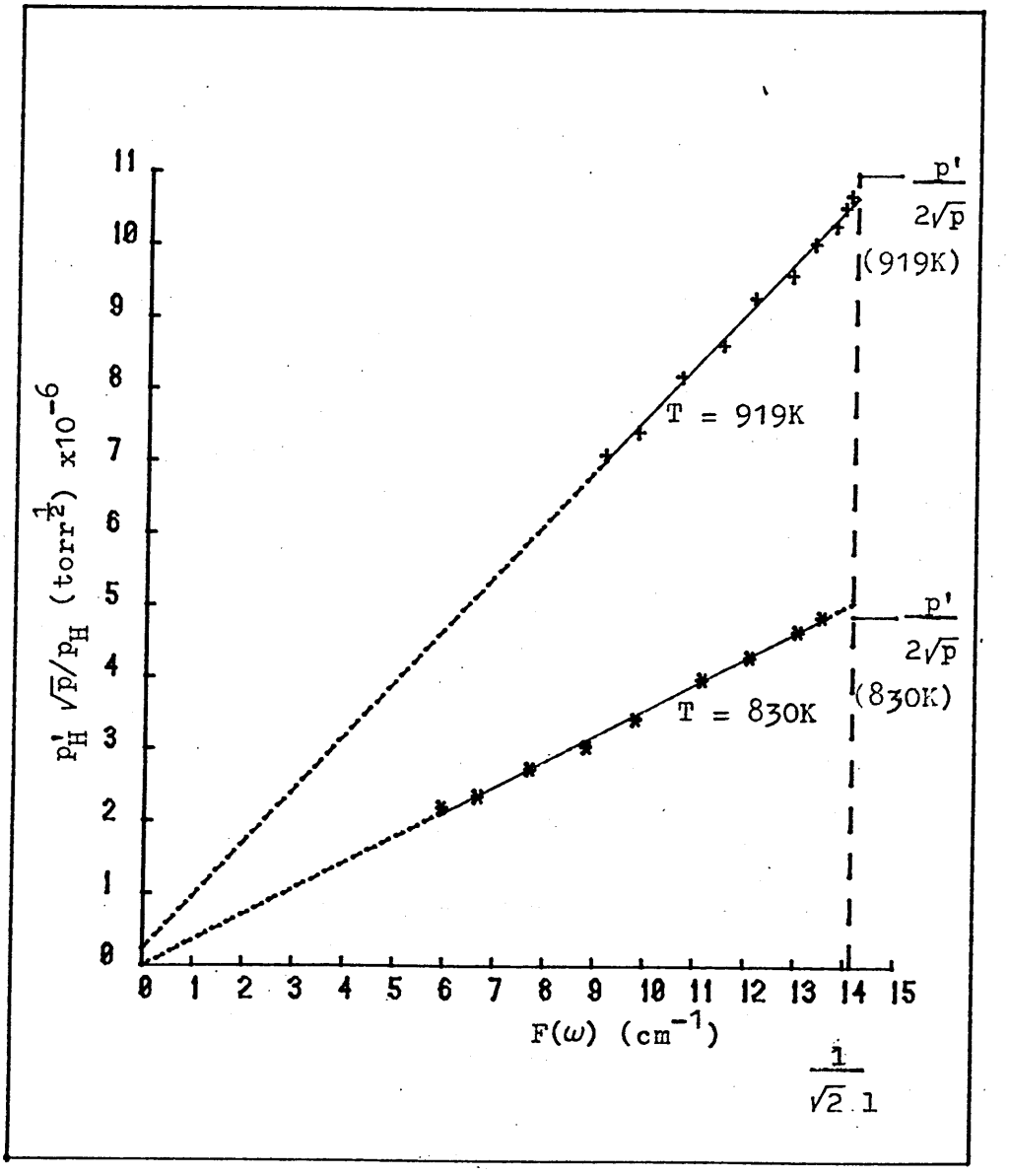

Figure 5.1.3 Typical amplitude plots for .5 mm Nickel specimen with .6 torr input pressure

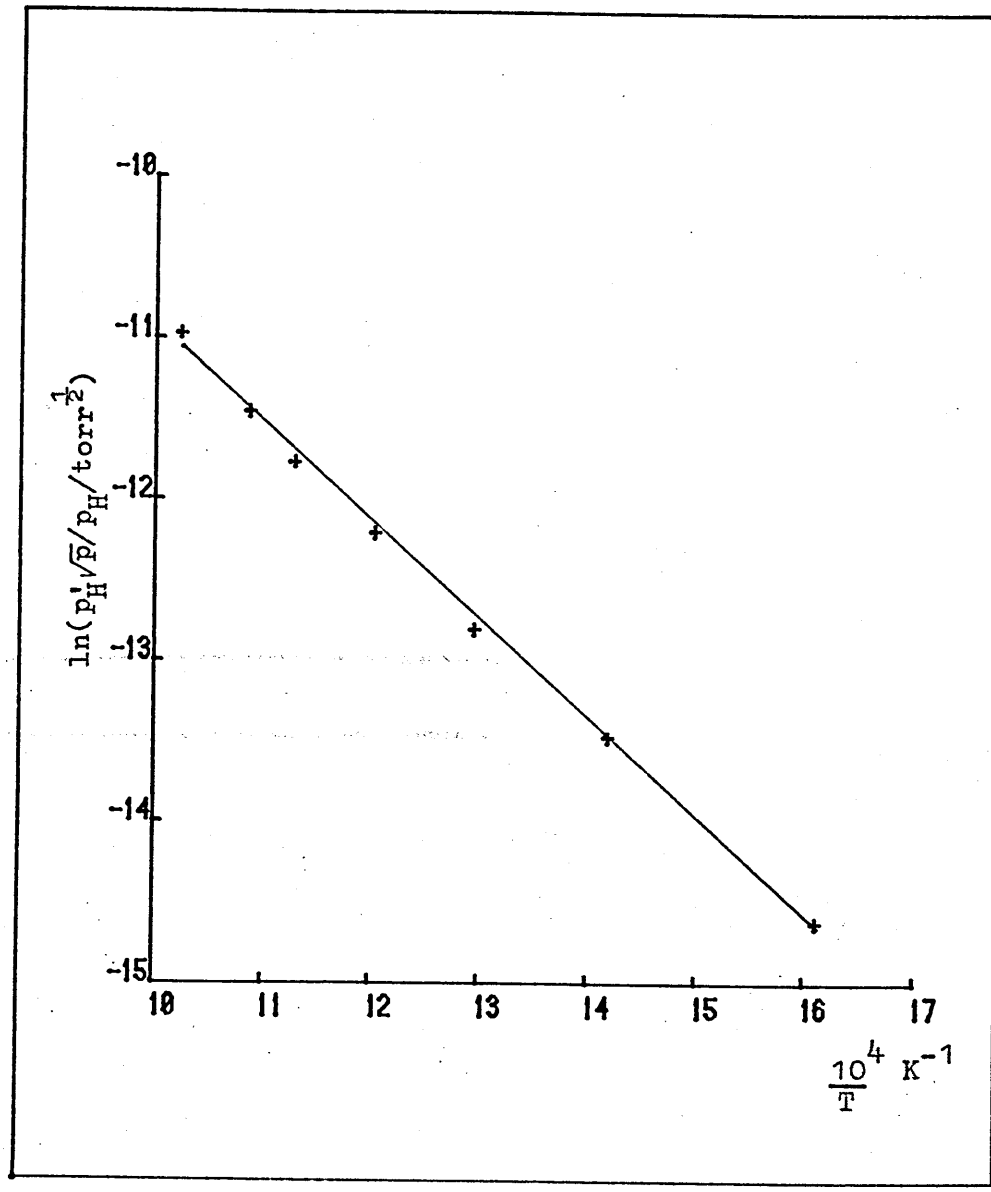

Figure 5.1.4 Time-dependent indication of the permeability in .5 mm nickel with an input pressure of .6 torr

the curves obtained at .6 torr for the same temperature (Figure 5.1.7) but amplitudes showed no significant deviations from the classical straight line.

The variable pressure results showed phase lags which decreased with increasing pressure at constant frequency but had a tendency to flatten at pressures approaching .6 torr (Figure 5.1.8). No effect was observable in the amplitudes once these had been corrected for input amplitude.

The variations of D.C. flux with pressure followed the classical $\sqrt{p}$ relationship and $p'/\sqrt{p}$ was never altered by changes in p at constant temperature (Figures 5.1.5 and 5.1.6).

From these observations the $\frac{J}{K_1 p}$ type of control can be discarded as this would necessarily lead to an aberration of the steady-state plots both vs. pressure and vs. temperature.

A $\frac{D}{lK_4}$ type of control would give an apparently classical p' vs. $\sqrt{p}$, plot but the apparent permeability obtained from such a plot would be low and curved in the Arrhenius plot for both the .6 and the .02 torr results. This is not observed.

This leaves trapping and 'secondary' surface effects as possible explanations. The attitude of this investigator towards trapping is that, unless considerable evidence of the effect can be seen, characterised by 'peaking' in the phase plots (see A.3) then there is no reason to be involved in the added complications that such an effect necessarily produces. No strong evidence of such peaking was seen in this or any of the materials investigated and therefore trapping is not proposed as an explanation of any of the effects observed.

The secondary effects, which affect phase and amplitude plots without influencing the D.C. results, are obtained by assuming

that $\frac{J}{K_1 p}$ and $\frac{D}{lK_4}$ are small enough to be undetectable.

The secondary effect which occurs in the input phase lag, ψ, can be immediately discarded since it involves the constant $\frac{e_1}{e_2} = \frac{D^{\frac{1}{2}} K_{sm}}{\sqrt{2}} \sqrt{\frac{K_1}{K_2}}$ which is not pressure dependent (see Section 4.3).

This leaves the secondary effect on the output phase and amplitude given by equations (3.17) and (3.18).

$$\tan \zeta = \frac{\omega}{2K_2' \theta'}$$

$$C = \frac{1}{\sqrt{\left[\frac{\omega}{2K_2'\theta'}\right]^2 + 1}}$$

The term $\frac{\omega}{2K_2'\theta'}$ should become less significant as either K_2' or θ' increases and θ' will increase with increasing pressure at constant K_2' (i.e. constant temperature).

This analysis can be split into two categories: .02 torr input pressure with variable frequency; constant frequency with variable input pressure. Since the investigation was exploratory, intermediate temperatures were used.

As mentioned previously, no non-classical amplitude or steady-state effects were apparent within the pressure range investigated. As an example Figure 5.1.5 shows the variation of steady-state output pressure with steady-state input pressure at one temperature, and its best fit regression line which extrapolates very close to zero. Figure 5.1.6 shows $p'/\sqrt{p}$ at .02 torr compared with the best fit line for the same quantity obtained from the .6 torr results.

An example of the effect of low pressure on phase-lag is shown in Figure 5.1.7 along with the corresponding curve for .6 torr input pressure. The calculated curve for .02 torr was

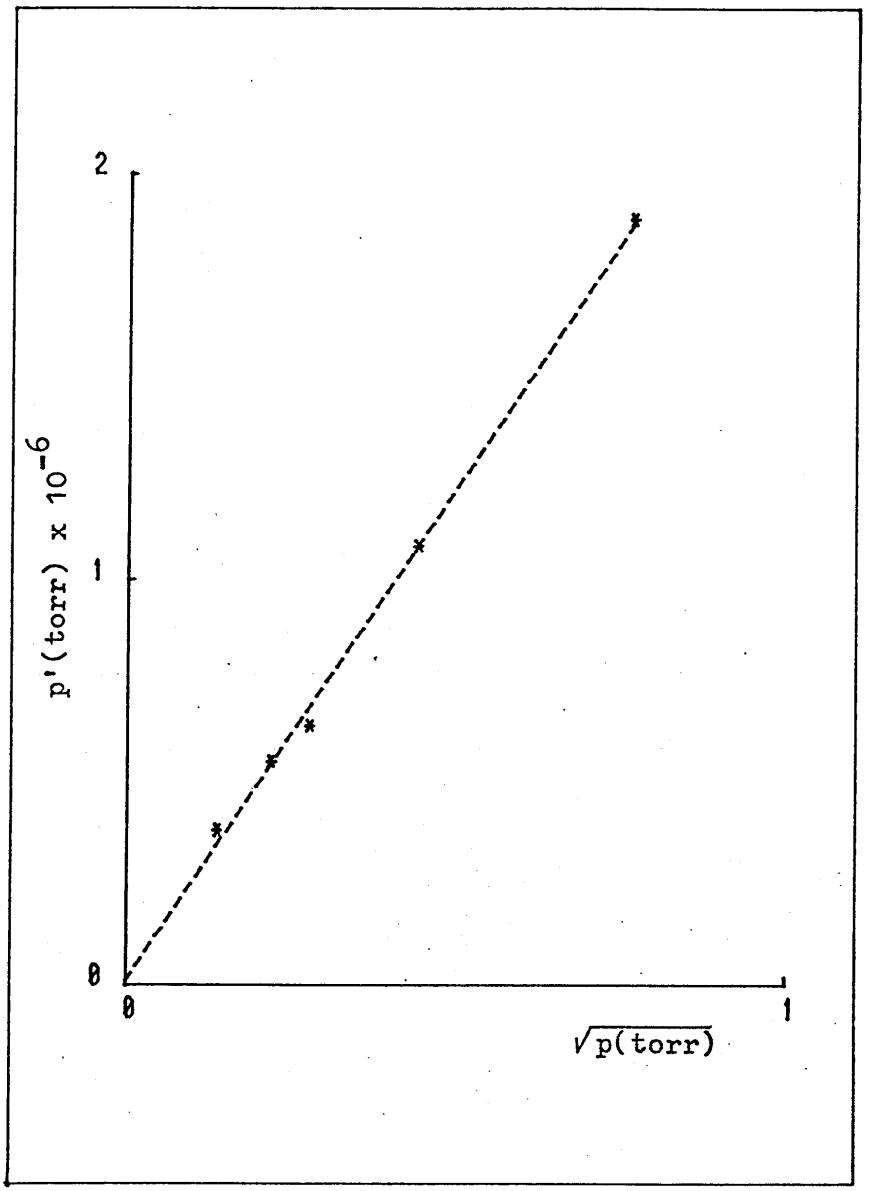

Figure 5.1.5 Steady-state output pressure, p', vs. square root of steady-state input pressure, $\sqrt{p}$ at 704K in .5 mm Ni

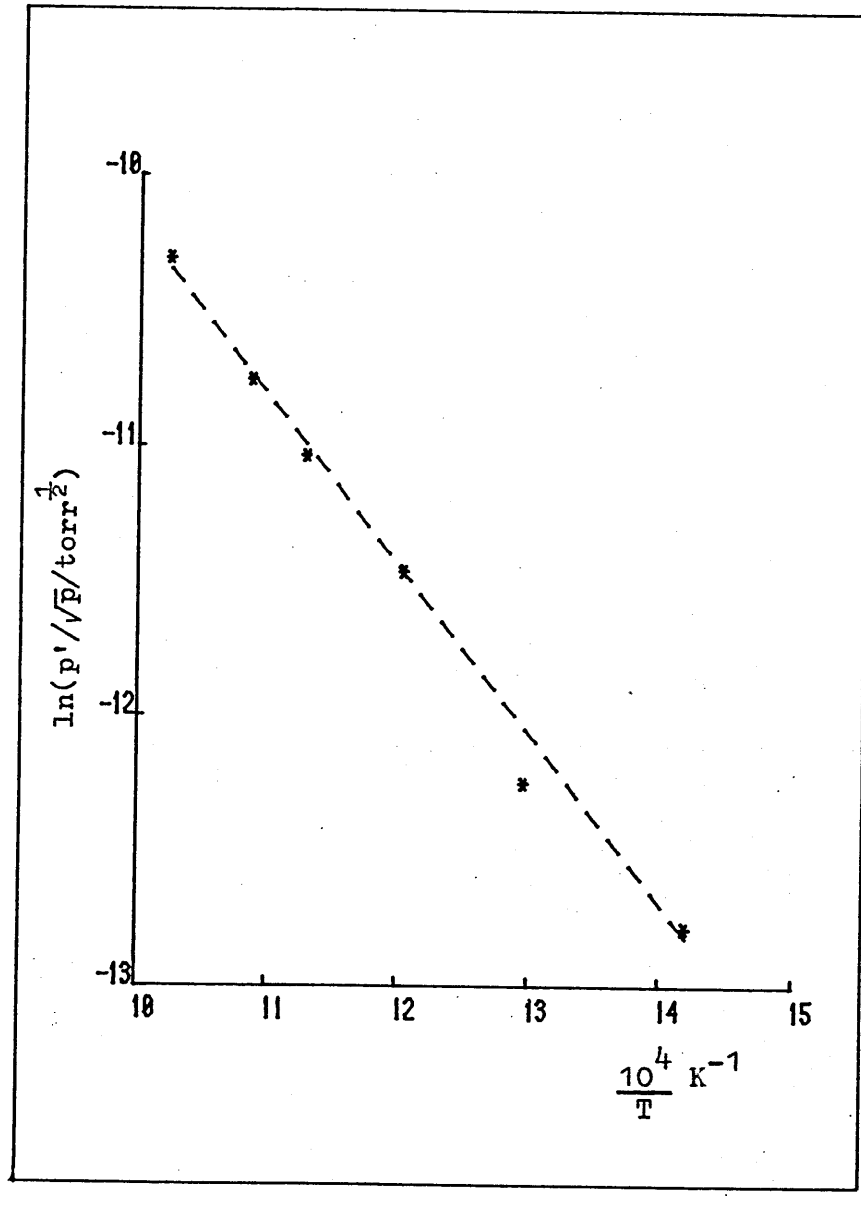

Figure 5.1.6 The steady-state indication of the permeability $\frac{p'}{\sqrt{p}}$ for an input pressure of .02 torr compared with the regression line for the corresponding quantity for an input pressure of .6 torr:0.5 mm Nickel specimen

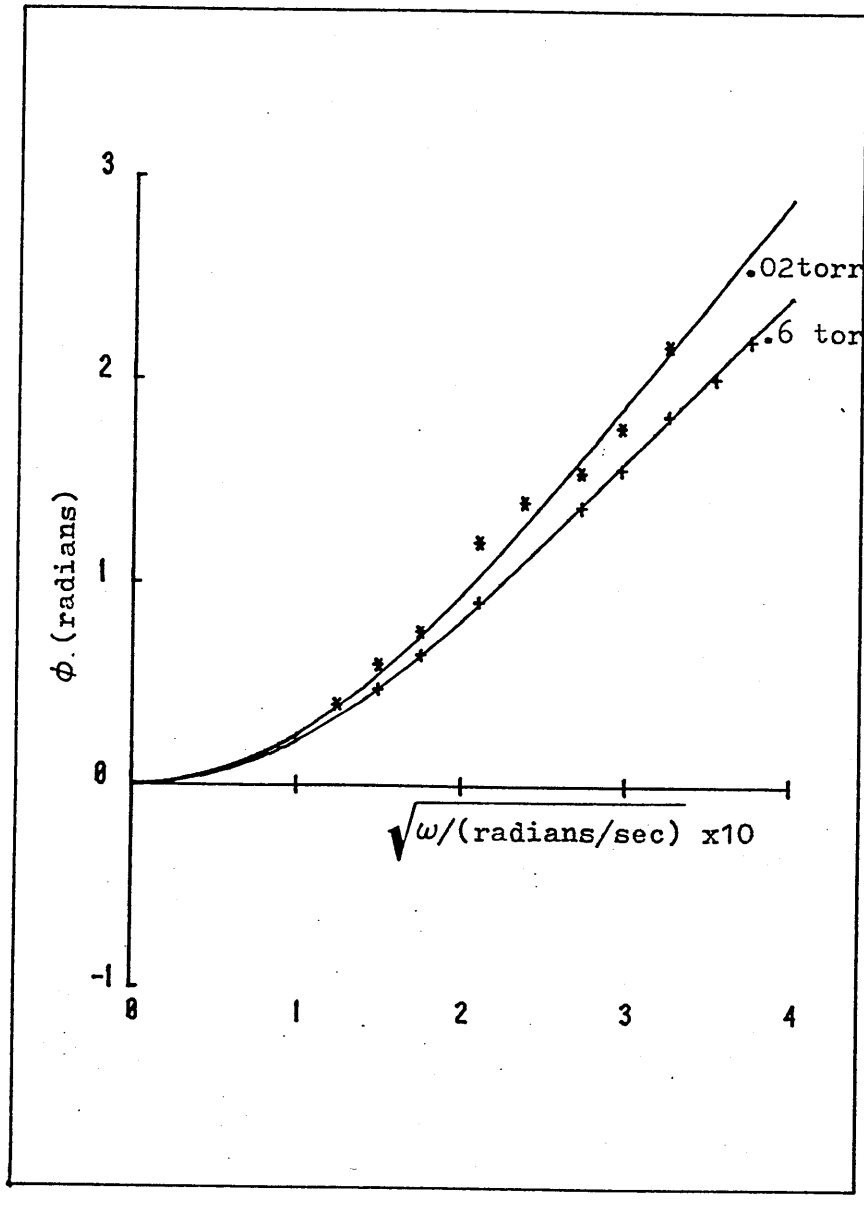

Figure 5.1.7 Frequency response of the phase lag at 830K for .02 torr and .6 torr input pressure

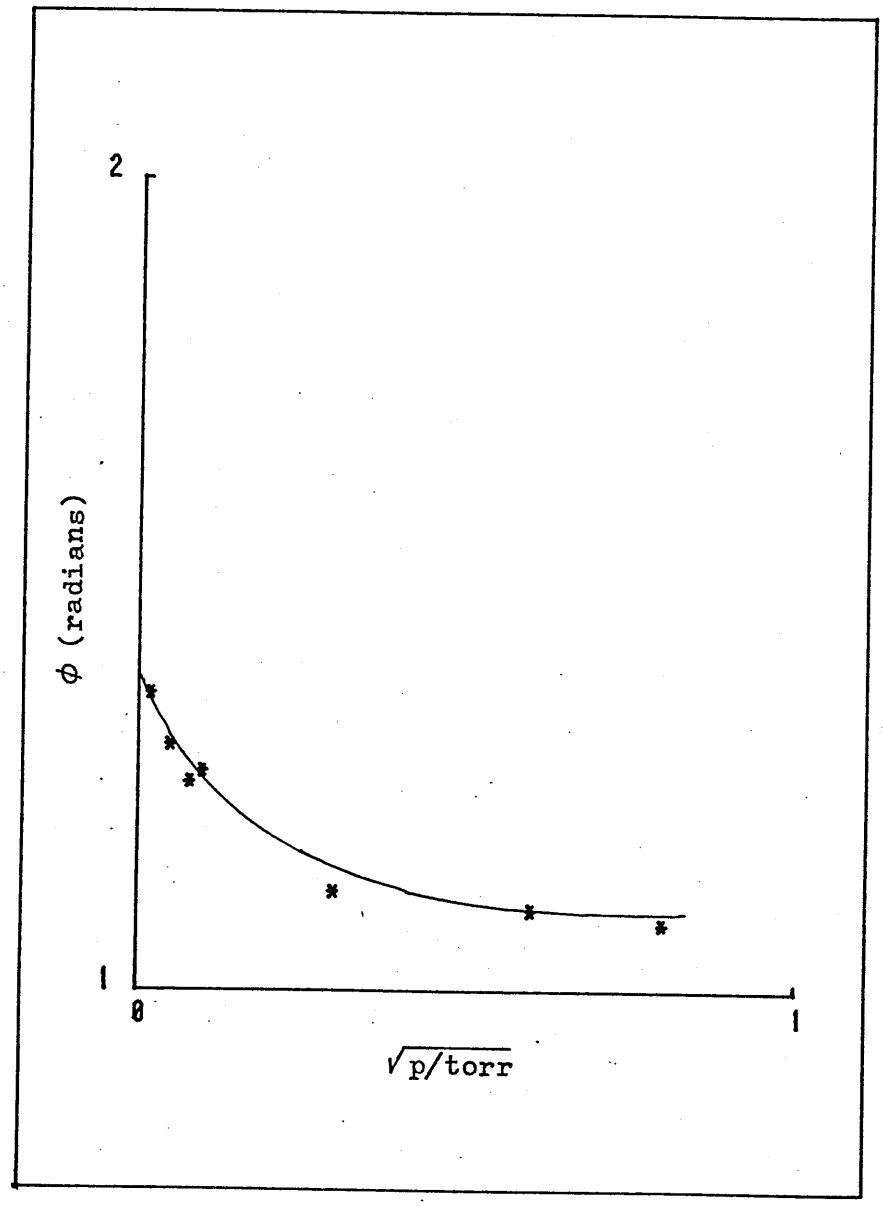

Figure 5.1.8 Effect of input pressure on the phase lag at a frequency of .1257 radians/sec and T = 976K

obtained by assuming the diffusion coefficient in the .6 torr analysis and best fitting for $\frac{1}{2K_2'\theta'}$ in the phase-lag: $\tan \zeta = \frac{\omega}{2K_2'\theta'}$.

The remaining curves for the effect of input pressure on phase are in the form of ϕ vs. pressure curves at constant frequency. One example of such a cruve is shown in Figure 5.1.8.

Using the values at .6 torr for comparison the following values for $\frac{1}{2K_2'\theta'}$ were obtained:

Table 5.1.2

From ϕ vs. frequency		From ϕ at constant frequency	
T(^{o}K)	$\frac{1}{2K_2'\theta'}$,(sec)	T(^{o}K)	$\frac{1}{2K_2'\theta'}$,(sec)
919	2.37	976	2.32
830	3.23	885	2.96
704	3.66	771	5.35

There seems to be some inconsistency at the low temperature end. It seems more likely that the value of 5.35 sec for $\frac{1}{2K_2'\theta'}$, is incorrect since it depends on measurement at only one frequency and since the value at .03 torr input pressure for the same quantity was 2.9 sec.

5.1.3 Summary

The phase, amplitude and steady-state data for the .5 mm Nickel specimen with 0.6 torr input pressure were analysable consistently in terms of the classical equations yielding values for both the permeability and diffusion coefficient.

At reduced input pressure (.02 torr) deviations were observed in the frequency response of the phase-lag but not in

the amplitude or steady-state data. The deviations in the phase could be explained in terms of the time taken for atomic recombination on the output surface and the absence of this effect in the amplitude can be seen by putting the largest measured values of $\frac{1}{2K_2'\theta'}$ along with the largest frequency (0.14 radians/sec) into the amplitude correction factor.

$$C = \frac{1}{\sqrt{\left[\frac{\omega}{2K_2'\theta'}\right]^2 + 1}} = .89 \text{ for } \frac{1}{2K_2'\theta'} = 3.66 \text{ sec.}$$

This means that the maximum deviation one might expect to see even at the highest frequencies and temperatures would be 10%.

5.2 Molybdenum

Two molybdenum specimens of thicknesses .5 and .25 mm were examined over the temperature range 1070 - 667 K. Molybdenum was far more difficult to examine experimentally than Nickel because the solubility/diffusion coefficient ratio was such that phase-lags were very small in the range where the output signal was substantial thus shortening the temperature range where reasonable sensitivity could be achieved.

Input pressure was not used as an experimental variable, apart from a few measurements which confirmed that little or no pressure effect was discernible, and all runs were carried out at 1 torr input pressure, a level required to ensure a strong output signal over the widest possible temperature range.

5.2.1 Steady-state results

Figure 5.2.1 shows the values of $\frac{p'}{\sqrt{p}}$ (output pressure/square root input pressure) as a function of temperature. The

results for the thicker specimen have been doubled so that both sets are directly comparable for an apparent thickness of .025 cm.

If the steady-state results behaved classically the lines would coincide.

The dotted line was drawn through the low temperature points for each specimen where behaviour could definitely be identified as classical from the amplitude and phase plots. The line was obtained by linear regression analysis of the four points involved to give, for the steady-state indication of the permeability

$$P_M = 1.31 \times 10^{-7} \exp\left[\frac{-21333 \text{ cal/mole}}{R.T}\right] \text{ moles } H_2/\text{cm sec}\sqrt{\text{torr}} \quad (5.2.1)$$

Table 5.2.1 shows the measured and calculated values for the steady-state indication of the permeability for these four points.

Table 5.2.1

Permeability (moles H_2/cm sec$\sqrt{\text{torr}}$)		T°K
Measured	Calculated	
5.48×10^{-13}	5.48×10^{-13}	867
2.86×10^{-13}	2.87×10^{-13}	824
4.00×10^{-14}	3.94×10^{-14}	715
1.32×10^{-14}	1.34×10^{-14}	667

In view of the deviations from this assumed classical behaviour at higher temperatures, analysis, with concomitant choice of surface model was first concentrated in the steady-state measurements. The absence of a pressure effect in molybdenum immediately suggests a $\frac{D}{1K_4}$ type of control in the flux equation:

$$J = J_{CLAS} \frac{\left[\sqrt{1 - \frac{J}{K_1 p}} - \sqrt{\frac{J}{K_1' p}}\right]}{\left[1 + \frac{D}{lK_4} + \frac{D}{lK_4'}\right]}$$

The extent of the deviation required to bring the remaining points in Figure 5.2.1 up to the line chosen as the classical line was calculated from the flux equation for each of the cases for $\frac{D}{lK_4}$ control and $\frac{J}{K_1 p}$ control. At any temperature one might expect half the value of either of these corrections for the .5 mm specimen since each contains a thickness-dependent term.

e.g. for $\frac{D}{lK_4}$ control: $l_1 = .025$ cm; $l_2 = .05$ cm

for .25 mm: $J = \frac{J_{CLAS}}{1 + \frac{2D}{l_1 K_4}}$

for .5 mm: $\frac{l_2}{l_1} J = \frac{\frac{l_2}{l_1} J_{CLAS}}{1 + \frac{2D}{l_2 K_4}}$

} assuming that $K_4 = K_4'$

Similar conditions hold for $\frac{J}{K_1 p}$ control since the values of J on the right hand side of the flux equation are not multiplied by $\frac{l_2}{l_1}$.

From this analysis it was again found that the $\frac{J}{K_1 p}$ type of explanation was inappropriate since it suggested temperature variations for the parameter K_1 which would be far from monotonic with temperature.

On this basis, and that regarding the absence of pressure effect, $\frac{D}{lK_4}$ control was chosen as the model to attempt to describe this behaviour, and values of $\frac{2D}{lK_4}$ were calculated to give zero deviation from the classical line.

The values of $\frac{D}{lK_4}$ obtained in this way are shown in

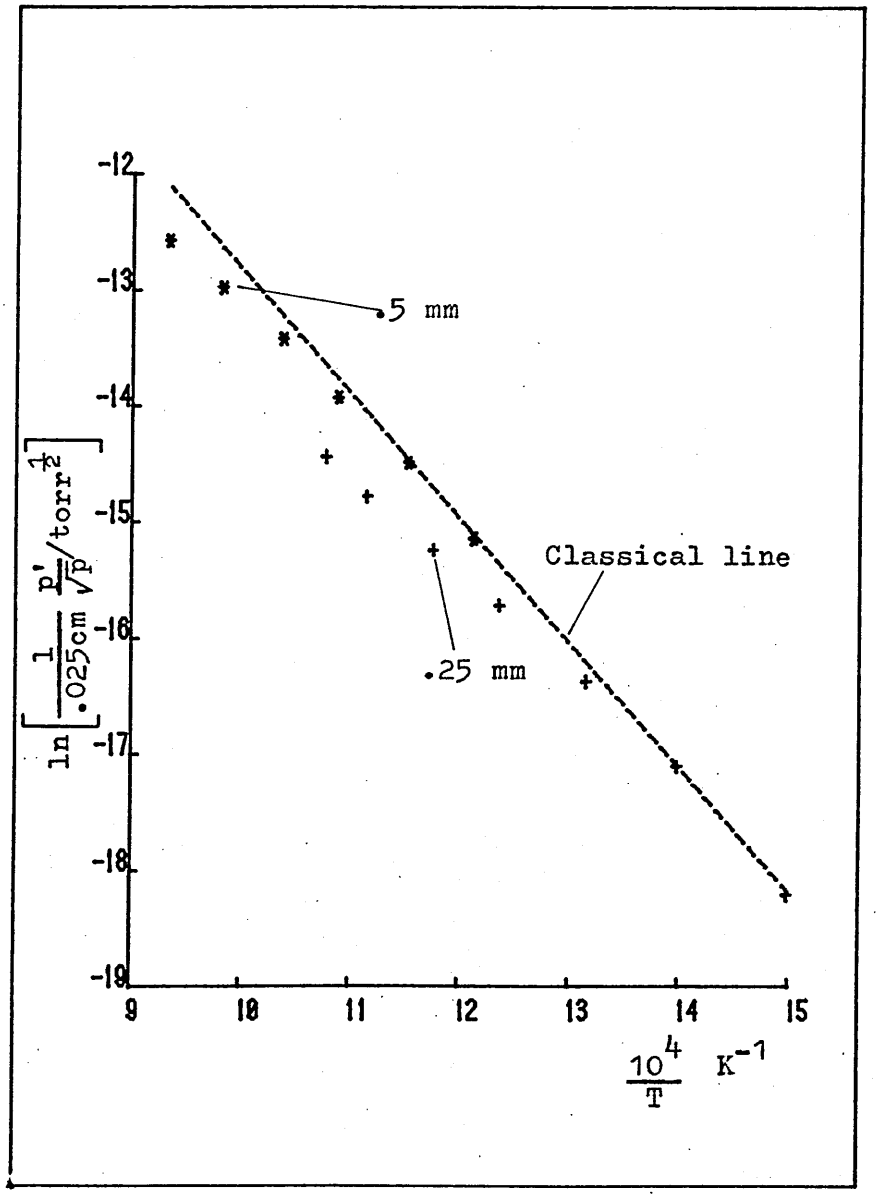

Figure 5.2.1 Corrected values of the steady-state output pressures for .25 mm and .5 mm Molybdenum $\frac{1}{.25\text{mm}}\frac{p'}{\sqrt{p}}$

Table 5.2.2.

Table 5.2.2

.5 mm Specimen		.25 Specimen	
$\frac{1}{T} \times 10^{-4}$	$a = \frac{D}{lK_4}$	$\frac{1}{T} \times 10^{-4}$	$a = \frac{D}{lK_4}$
12.1359	(2.7×10^{-3})	14.9925	(4.9×10^{-3})
11.5340	(0)	13.9860	(0)
10.8932	6.832×10^{-2}	13.1666	.0710
10.3842	9.304×10^{-2}	12.3762	.1902
9.8328	.1859	11.7647	.3254
9.3414	.2785	11.1607	.5002

5.2.2 Phases

Figures 5.2.2 and 5.2.3 show phase plots from the .5 mm and .25 mm specimens respectively. If no cognisance is taken of the $\frac{D}{lK_4}$ correction suggested in Section 5.2.1 and the curves are analysed in terms of classical behaviour, then Figure 5.2.4 results for the diffusion coefficients obtained in this way. It is noticeable that the higher temperature results in both cases do not reach high enough phase lags to produce the linear region which is so useful in determining the behaviour of the system. This means that, although there is no direct evidence of non-classical phase behaviour in this system, neither is there any evidence of classical behaviour at higher temperatures.

If the corrections suggested by the D.C. levels are now applied to the phase plots (neglecting 'secondary' effects at

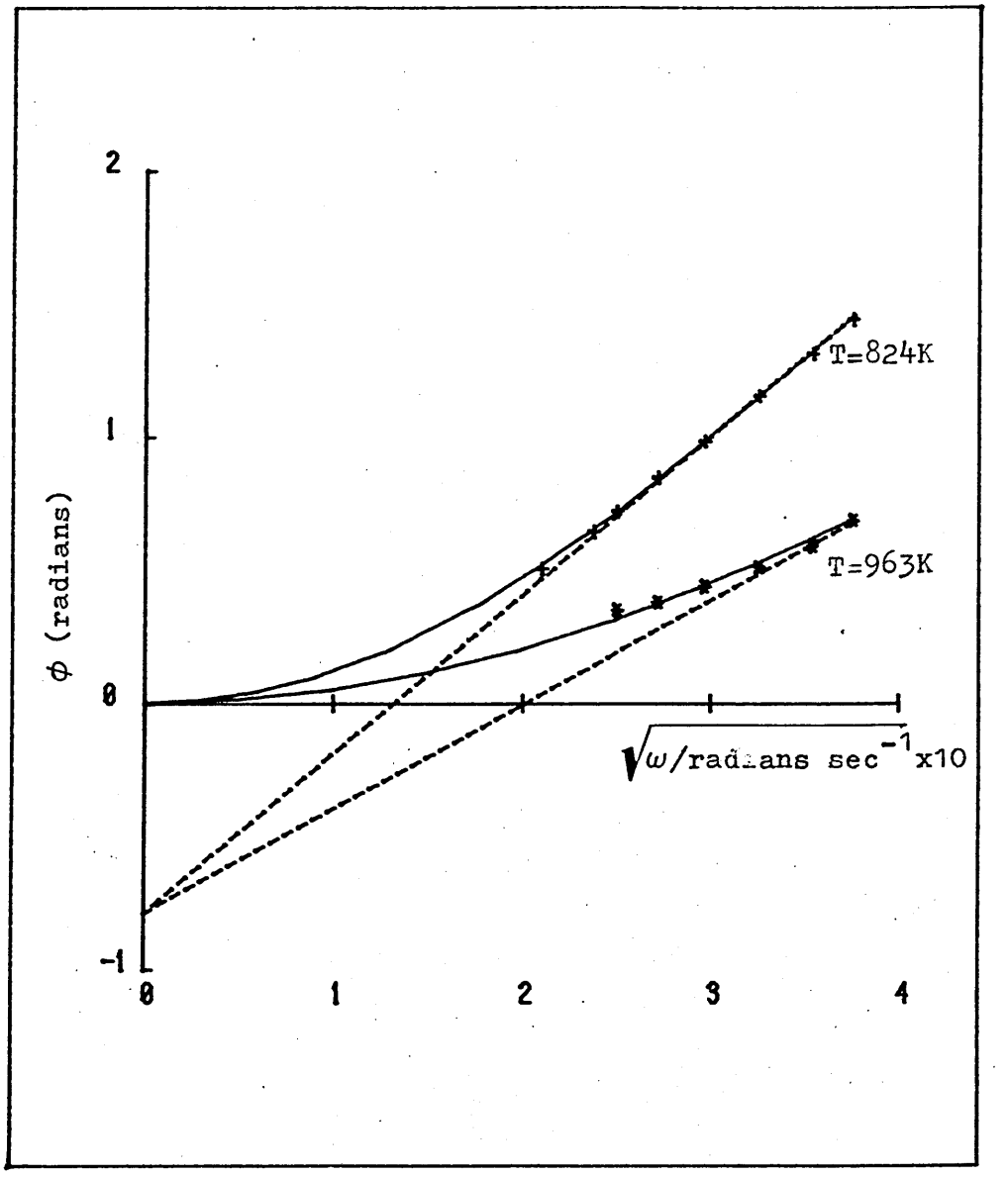

Figure 5.2.2 Typical phase plots for the 0.5 mm Mo specimen with best fit classical curves

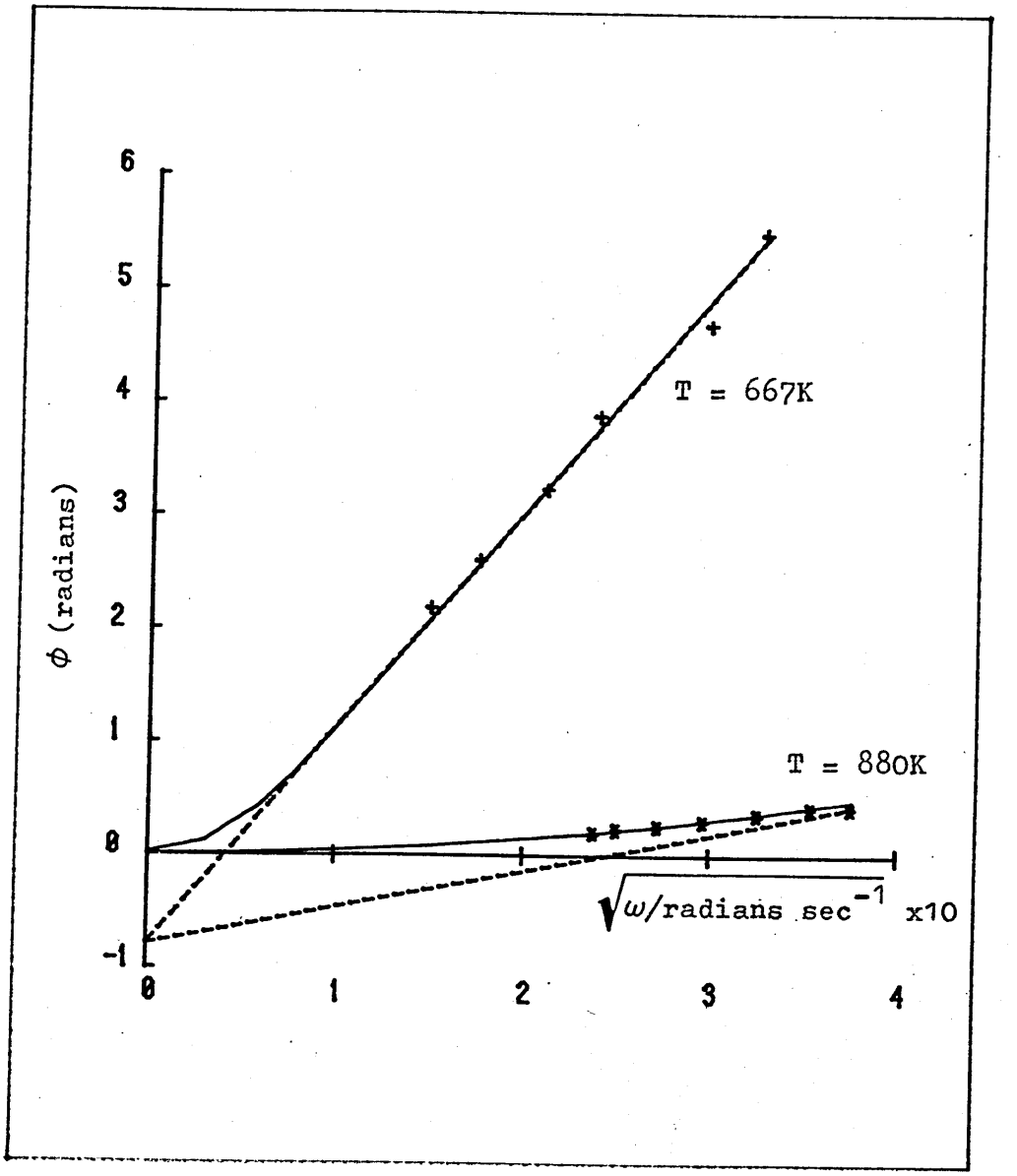

Figure 5.2.3 Typical phase plots for the 0.25 mm Mo specimen with best fit classical curves

the input and output surfaces) the following equations result

$$\phi' = \phi + \psi$$

$$\tan \phi = \frac{\tan kl - \tanh kl + 2akl \tan kl \tanh kl}{\tan kl + \tanh kl + 2akl}$$

$$\tan \psi = \frac{akl \dfrac{\sinh 2kl - \sin 2kl}{\cosh 2kl - \cos 2kl}}{1 + akl \dfrac{\sinh 2kl + \sin 2kl}{\cosh 2kl - \cos 2kl}}$$

where a is the correction term = $\frac{D}{lK_4}$

Note that the $\frac{2D}{lK_4}$ correction in the steady-state equation is divided into one $\frac{D}{lK_4}$ for each of the output ($\tan \phi$) and input ($\tan \psi$) corrections.

The curves in which this correction was significant (higher temperatures) were re-fit using the values in Table 5.2.2. There was no increase in the residual sum of squares for the fit and the resulting modified diffusion coefficients are shown in Figure 5.2.5.

It can be seen that the deviations suggested by the curvature of the original Arrhenius plot (Figure 5.2.4) have been reduced somewhat but that the .25 and .5 mm sets still do not match exactly. This would tend to suggest that slightly more correction ought to be applied to the lower temperature .5 mm results or that slightly less ought to be applied to the .25 mm results.

In either event the high temperature phase plots are not sufficiently sensitive (low phase lags) to undertake any more delicate operations.

Of course, it can further be argued that this slight mis-match may be due to secondary phase effects or that a mixture of $\frac{D}{lK_4}$ control and $\frac{J}{K_1 p}$ control ought to have been considered but, again, these treatments would require a parametric level in the analysis equations which far outweighs the accuracy of the data

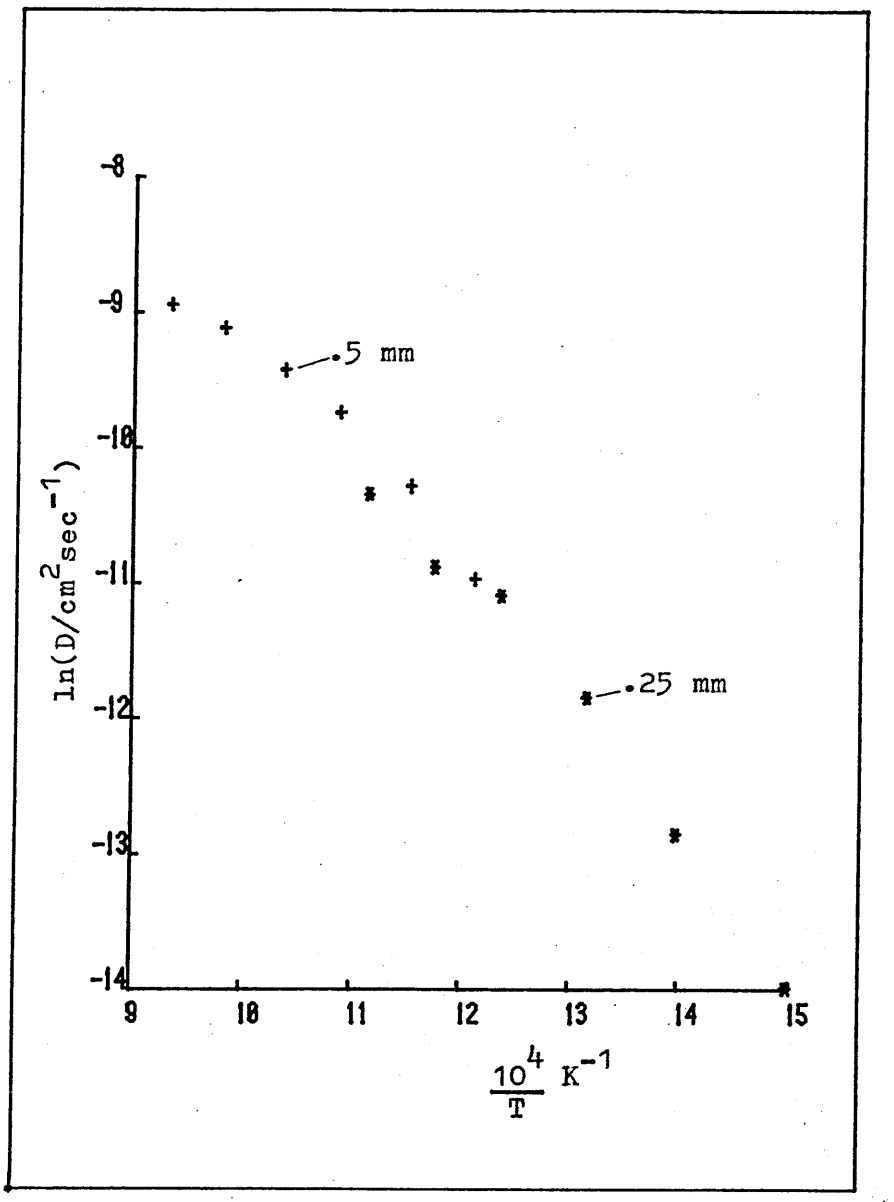

Figure 5.2.4 Diffusion coefficients for Mo suggested by the classical analysis

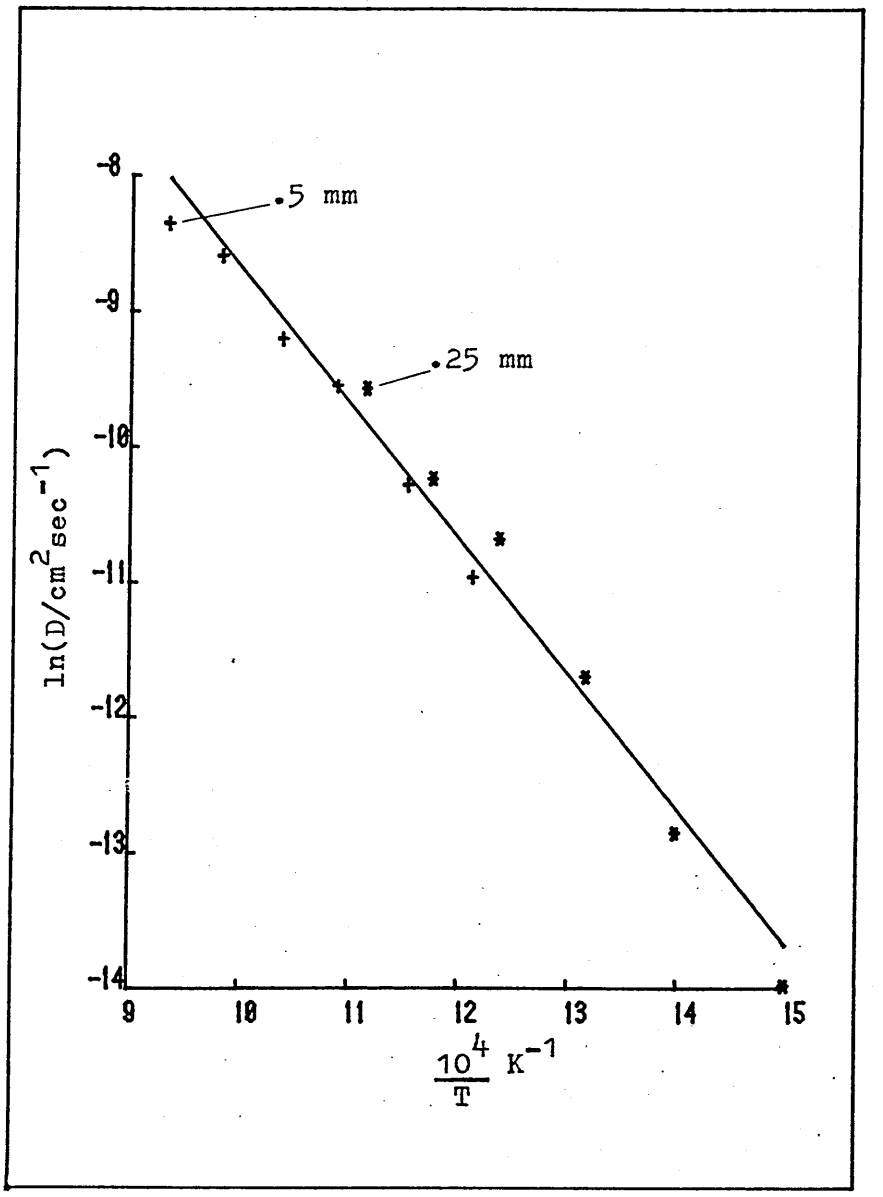

Figure 5.2.5 Molybdenum diffusion coefficients corrected for $\frac{D}{lK_4}$ control at input and output surfaces

in this region.

The best fit least-squares regression line through the diffusion coefficients of Figure 5.2.5 gave:

$$D = 3.76 \exp\left[\frac{-19888 \text{ cals/mole}}{R\,T}\right] \text{cm}^2/\text{sec} \qquad (5.2.2)$$

with a standard error on D_o of $1.9 \text{cm}^2/\text{sec}$ and a standard error of 430 cals/mole on the activation energy.

It should be noted that, if the regression had been concentrated on the uncorrected (low temperature) values in this diffusion coefficient curve that the activation energy would be somewhat larger and the standard errors considerably less.

Table 5.2.3 shows the uncorrected, corrected and calculated diffusion coefficients for hydrogen in molybdenum.

Table 5.2.3

Diffusion coefficient (cm^2/sec)				
Uncorrected	Corrected	Calculated	T($^\circ$K)	
1.33×10^{-4}	2.38×10^{-4}	3.27×10^{-4}	1070.5	.5 mm specimen
1.11×10^{-4}	1.88×10^{-4}	2.00×10^{-4}	1017	
8.18×10^{-5}	1.02×10^{-4}	1.15×10^{-4}	963	
5.97×10^{-5}	7.21×10^{-5}	6.92×10^{-5}	918	
3.48×10^{-5}	3.48×10^{-5}	3.64×10^{-5}	867	
1.75×10^{-5}	1.75×10^{-5}	1.99×10^{-5}	824	
3.26×10^{-5}	7.08×10^{-5}	5.29×10^{-5}	896	.25 mm specimen
1.91×10^{-5}	3.63×10^{-5}	2.89×10^{-5}	850	
1.55×10^{-5}	2.33×10^{-5}	1.57×10^{-5}	808	
7.27×10^{-6}	8.41×10^{-6}	7.11×10^{-6}	759.5	
2.66×10^{-6}	2.66×10^{-6}	3.13×10^{-6}	715	
8.54×10^{-7}	8.60×10^{-7}	1.14×10^{-6}	667	

5.2.3 Amplitudes

Figure 5.2.6 shows amplitude plot in the low temperature (classical) region for the .5 mm specimen. As can be seen, apart from the small but consistent downward deviation there is no reason to suppose that this run showed any departure from classical behaviour.

The deviations suggested by the steady-state results were applied to the non-classical amplitude plots by evaluating the amplitudes (again assuming no 'secondary' effects) which one would expect were the model to hold.

Applying the arguments of Sections 4.3 and 4.4 for case (ii) ($\frac{D}{lK_4}$ control).

$$A = 1\Big/\sqrt{1 + 2akl\left[\frac{\sinh 2kl+\sin 2kl}{\cosh 2kl-\cos 2kl}\right] + 2(akl)^2\left[\frac{\cosh 2kl+\cos 2kl}{\cosh 2kl-\cos 2kl}\right]}$$

$$B = \frac{2kD/\sqrt{\cosh 2kl-\cos 2kl}}{\sqrt{1 + 2akl\left[\frac{\sinh 2kl+\sin 2kl}{\cosh 2kl-\cos 2kl}\right] + 2(akl)^2\left[\frac{\cosh 2kl+\cos 2kl}{\cosh 2kl-\cos 2kl}\right]}}$$

where $a = D/lK_4 = D/lK_4'$

Noting that $A_{CLAS} = 1$ and $B_{CLAS} = 2kD/\sqrt{\cosh 2kl-\cos 2kl}$ the correction factor for amplitudes becomes:

$$\frac{(AB)}{AB}_{CLAS} = 1 + a(2kl)\ \frac{\sinh 2kl+\sin 2kl}{\cosh 2kl-\cos 2kl} + a^2(2kl)^2\ \frac{\cosh 2kl+\cos 2kl}{2(\cosh 2kl-\cos 2kl)}$$

No significantly deviant behaviour was seen in the .5 mm specimen until the diffusion coefficient was so high that the amplitude plot essentially consisted of the extrapolated value at $F(\omega) = \frac{1}{\sqrt{2}\,1}$ but application of the correction factor produced values of $\frac{p_H'\sqrt{p}}{p_H}$ very close to $\frac{p'_{CLAS}}{2\sqrt{p}}$. This is not surprising since the

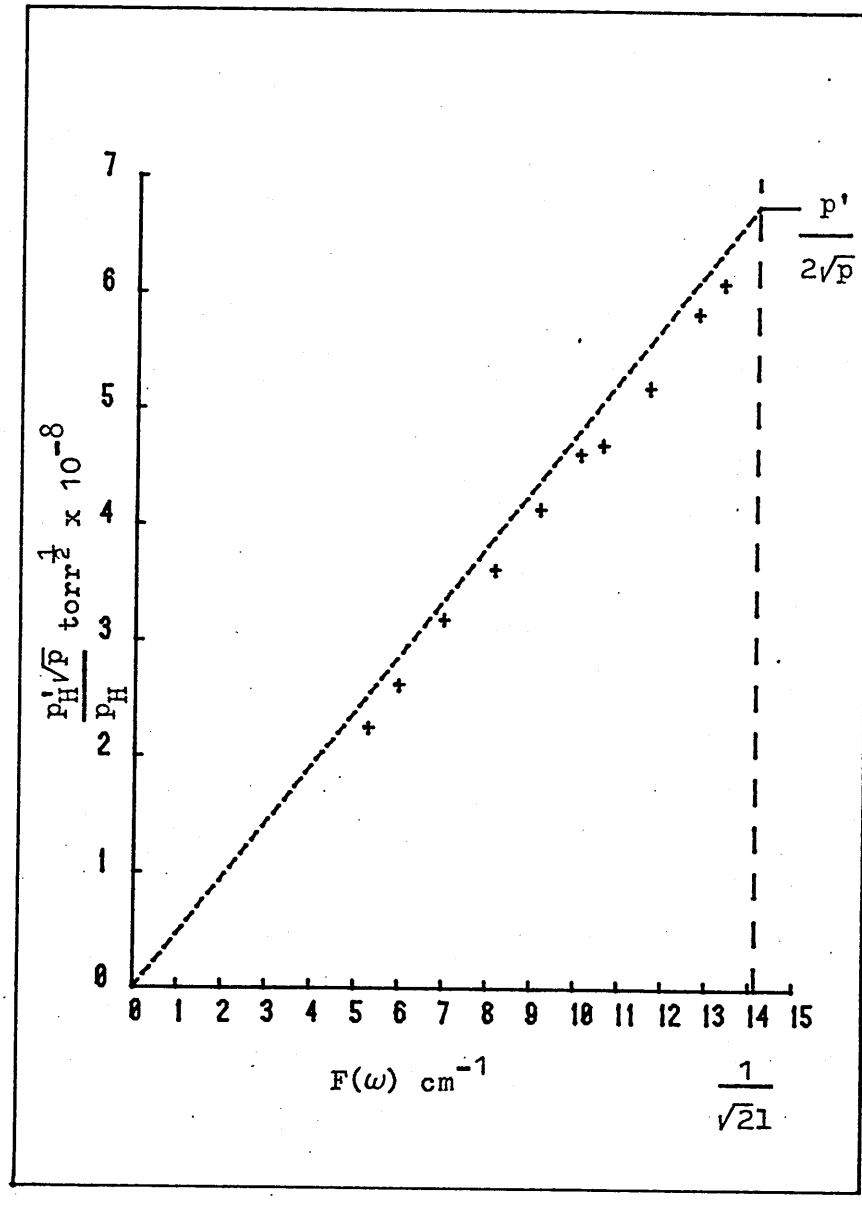

Figure 5.2.6 Amplitude plot for .5 mm Mo specimen at T = 824K

uncorrected values of amplitude were very close to $p'/2\sqrt{p}$ for the uncorrected steady-state fluxes.

The amplitude correction does not consist entirely of multiplying a value of $\frac{p'_H\sqrt{p}}{p_H}$ by the correction factor since the values of $F(\omega)$ have to be re-calculated for the corrected value of D obtained from the phase analysis. An example of this process for the .25 mm specimen at T = 850°K is shown in Figure 5.2.7 and the problem of closure of the plot is highlighted here. The lower set of points are the uncorrected values and although these are very close to the ω = o axis they clearly do not extrapolate through zero at $F(\omega)$ = o. Figure 5.2.8 shows a corresponding plot for T = 667°K. The scatter is fairly large here because at these low temperatures amplitudes are rather small, especially at high frequencies.

5.2.5 Summary

The most strikingly inconsistent behaviour observed in molybdenum was indicated by the $\frac{p'}{\sqrt{p}}$ curves where fluxes tended to be low in the .25 mm specimen. The amplitude plots reflected that inconsistency although in the higher temperature cases the plots were so closed up toward the $\omega \rightarrow$ o end of the $F(\omega)$ spectrum (due to the size of D) that analysis was rendered very difficult. This was particularly so in the case of the .5 mm specimen where it was not actually possible to draw a meaningful amplitude plot at the higher temperatures. However, it was clear that the deviation from classical behaviour increased with increasing temperature and this occurred at lower temperatures in the .25 mm specimen than in the .5 mm specimen.

A similar situation held for the phase plots which appeared to behave (for both specimens) classically at low temperatures with the high temperature behaviour being rather inconclusive.

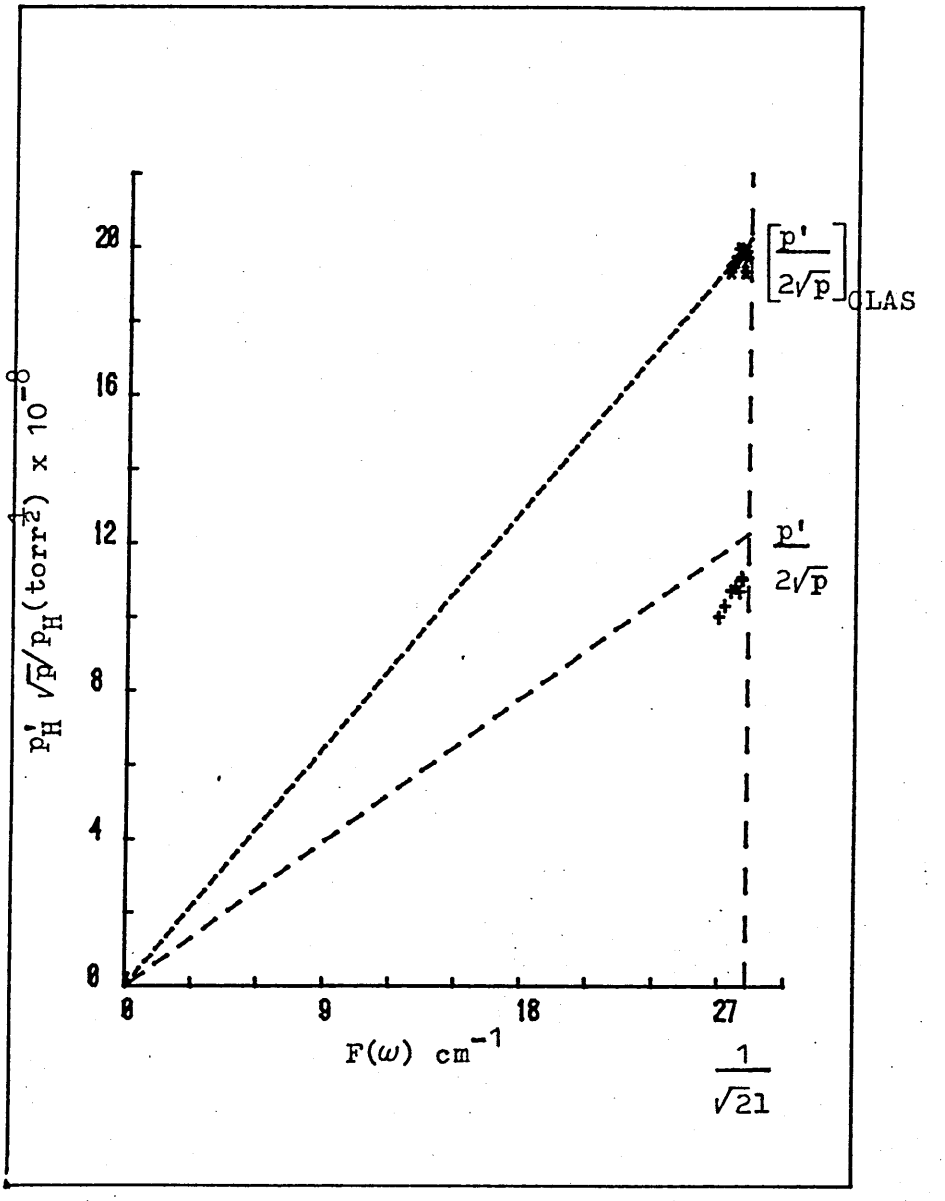

Figure 5.2.7 Amplitude plot for .25 mm Mo specimen at T = 850 K

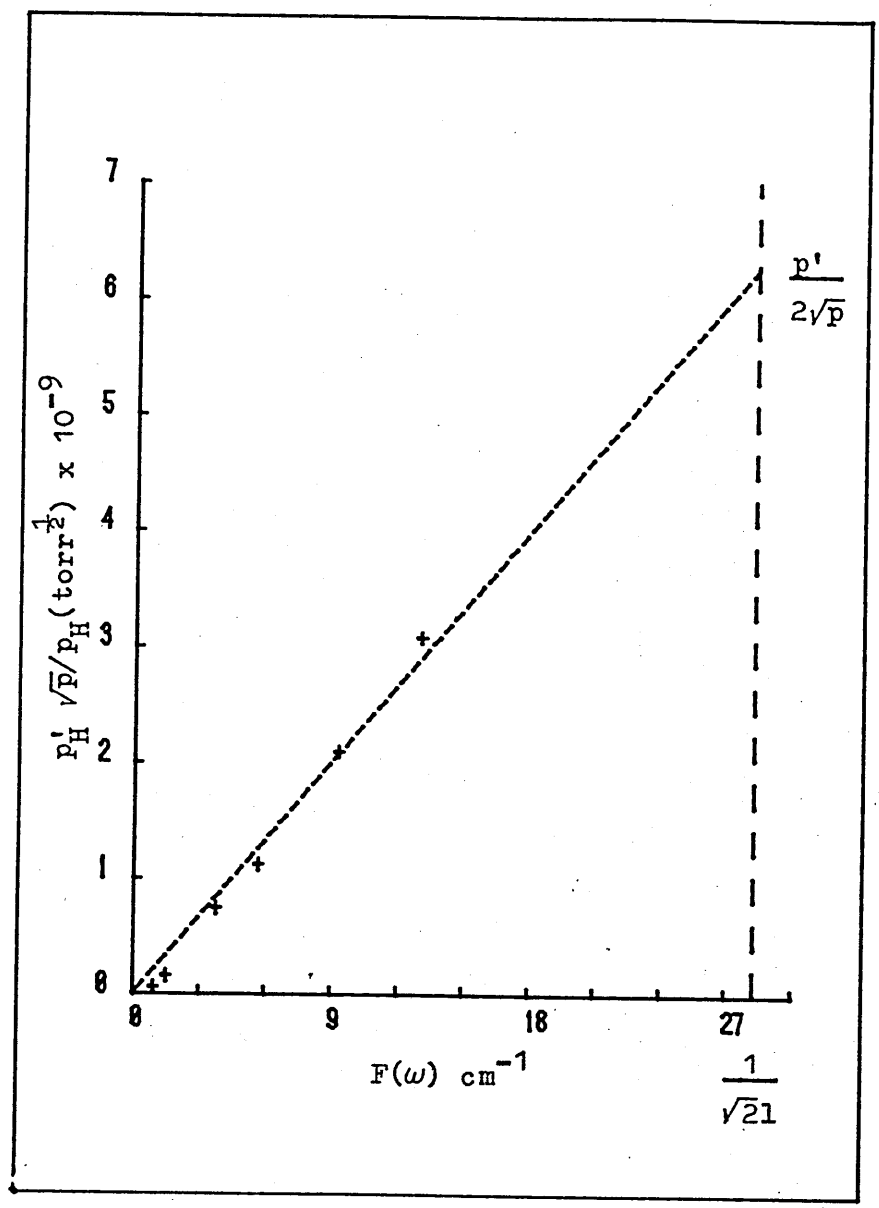

Figure 5.2.8 Amplitude plot for .25 mm Mo at T = 667K

This was because the maximum obtainable phase-lag (by limitation of the modulator) was so small as to prevent the phase vs. $\sqrt{\omega}$ curve reaching the linear region which can be used to characterise its behaviour.

In view of this situation it was considered prudent to treat the low temperature results for both thicknesses with more weight than those at higher temperatures. By doing this it was possible to evaluate, with a reasonable degree of certainty, the classical permeation parameters D, K_{sm} from which deviations for the higher temperature results could be elucidated.

5.3 M316 Stainless Steel

Two stainless steel specimens of thicknesses .25 mm and .1 mm were examined over the temperature range 950 - 555 K. The .25 mm specimen was run throughout its temperature range with an input pressure of 1 torr. An input pressure of .03 torr was used for the .1 mm specimen at higher temperatures but it was found necessary to increase this pressure (to a maximum of .07 torr) in order to produce a reasonable signal at lower temperatures.

In view of the highly deviant behaviour of the results for this material it was decided to first concentrate analysis on the phase plots since literature diffusion coefficients for hydrogen through stainless steel are generally in somewhat closer agreement than the permeabilities.

5.3.1 Phases

The model used here to describe the deviations from classical behaviour is that outlined in Section 4.5 for oxide-limited permeation. Since the solutions are exactly the same as for $\frac{J}{K_1 p}$

control in both the input and output cases the terminology used for finite surface reaction rates has also been used here on the understanding that equations (4.22) hold for the transformation. Figure 5.3.1 shows a typical departure from classical phase-lag behaviour in stainless steel. The principal, and consistent feature of these departures is that the curvature of phase-lag vs. square root of frequency is inverted relative to the classical case, i.e. as ω increases the slope decreases in a way similar to that calculated, for example, for heavy input control (Figure 4.5)

To avoid fitting the phase curves with three unknown parameters it was decided that the limiting cases of surface (oxide) control would first be investigated with a view to putting limits on the diffusion coefficient.

For this purpose, as suggested by the phase plots, a maximum value for phase lags due to the oxide is not sought but rather a maximum inversion of the curvature of these plots. Inversion of curvature is achieved by adding a correction to the phase lag which increases less rapidly with frequency than does the 'classical' phase lag. Hence low order ($<\omega^1$) corrections are of interest.

Corrections only taken to the order $\omega^{\frac{1}{2}}$ have the interesting property that they 'saturate' at high values of the correction factor $\frac{e_1}{e_o}$ or $\frac{x_1}{x_o}$ (see for example equation (4.20)).

For instance, when $\frac{e_1}{e_o}$ is very large and $e_2\omega \ll e_1\omega^{\frac{1}{2}}$ the phase lag due to the input surface becomes:

$$\tan \psi = \frac{\sinh 2kl - \sin 2kl}{\sinh 2kl + \sin 2kl}$$

and the phase-lag is insensitive to further increases in $\frac{e_1}{e_o}$.

If this saturated value is taken along with the classical value for tan ϕ (no output control) it can be shown that the total

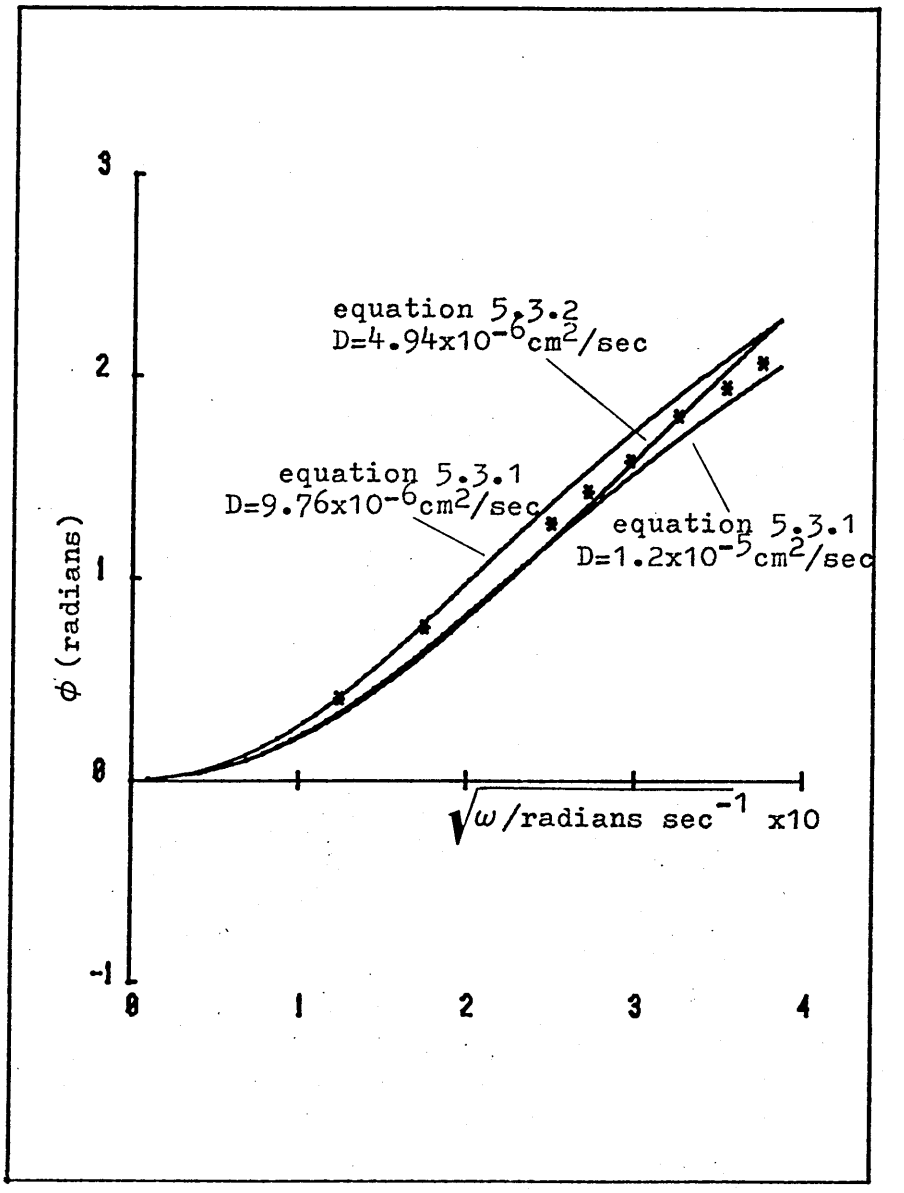

Figure 5.3.1 Non-classical behaviour in .25 mm stainless steel specimen at 950°K

phase lag

$$\tan\phi' = \tan(\phi+\psi) = \tan kl \tanh kl$$

On the other hand if $\tan\psi$ is supposed zero (no input control) and $\tan\phi$ for output control to the $\omega^{\frac{1}{2}}$ approximation is taken:

$$\tan\phi = \frac{\tan kl - \tanh kl + 2\frac{x_1}{x_o}[\tan kl \tanh kl]\sqrt{\omega}}{\tan kl + \tanh kl + 2\frac{x_1}{x_o}\sqrt{\omega}}$$

Again, for large $\frac{x_1}{x_o}$ this curve becomes:

$$\tan\phi = \tan kl \tanh kl \qquad (5.3.1)$$

Thus, the curve (5.3.1) represents the largest amount of inversion of curvature which can be obtained in the phase plots with single surface control.

The phase curves were therefore fitted to both the function (5.3.1) and the classical function:

$$\tan\phi = \frac{\tan kl - \tanh kl}{\tan kl + \tanh kl} \qquad (5.3.2)$$

in order to obtain limiting values for the diffusion coefficients for the case of a single (unspecified) surface control. The results of this analysis are shown for the .25 mm specimen in Figure 5.3.2 and Figure 5.3.1 illustrates the predicted curves for the best fit 'classical' and two different diffusion coefficients for equation (5.3.1).

The upper set of points in Figure 5.3.2 are from the fit to equation (5.3.1) and the lower set from the classical fit. The residual sum of squares values were always lower for the curve

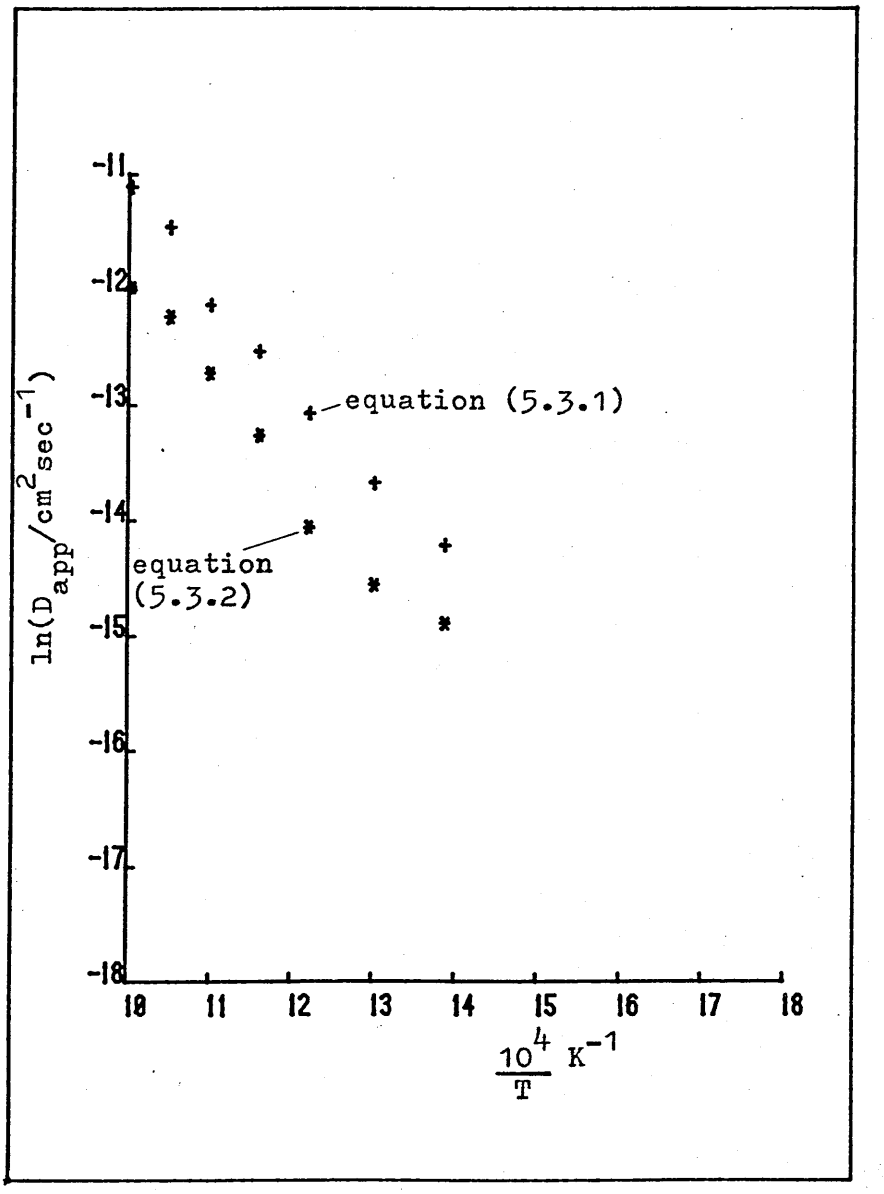

Figure 5.3.2 Apparent diffusion coefficients from the classical (equation (5.3.2)) and surface saturated (equation (5.3.1)) analyses of the phase lag data in .25 mm stainless steel

(5.3.1) but the fit was better from the classical curve at higher temperatures than it was at lower temperatures.

If this model is to be correct then the same values should be obtainable for the .1 mm specimen by the same means. Figure 5.3.3 shows the diffusion coefficients obtained from the 0.1 mm specimen in the same way as for the .25 mm specimen and it is obvious (both from the residual sum of squares values obtained in fitting the phase plots and also from a comparison with Figure 5.3.2) that the inversion of curvature obtained by a single surface oxide control is insufficient to explain the .1 mm phase plots. The sharp change of gradient in Figure 5.3.2 occurs at the point where the input pressure was increased indicating that the phase lags are sensitive to input pressure.

The only way to invert the curvature further is to introduce a second controlling surface. This can be done by assuming 'saturation' at one of the surfaces and adding the second controlling surface to a curve of the form of equation (5.3.1). This can be done in two ways according to whether the input or output surface is assumed to be at saturation.

The full expression for the bulk diffusion modification is:

$$\tan\phi = \frac{\gamma(\tan kl - \tanh kl) - (\alpha+\beta) + (\alpha-\beta)\tan kl \tanh kl}{\gamma(\tan kl + \tanh kl) + (\alpha-\beta) + (\alpha+\beta)\tan kl \tanh kl}$$

where the limit equation (5.3.1) corresponds to large values of $(\alpha-\beta)$ and negligible $(\alpha+\beta)$ and γ. Thus $\delta \simeq \epsilon, \beta \simeq -\alpha, \gamma \simeq 0$ (see equation (3.14). Applying these conditions to the full expression for $\tan\phi$ allows a re-grouping of terms and, again neglecting the terms higher than $\omega^{\frac{1}{2}}$:

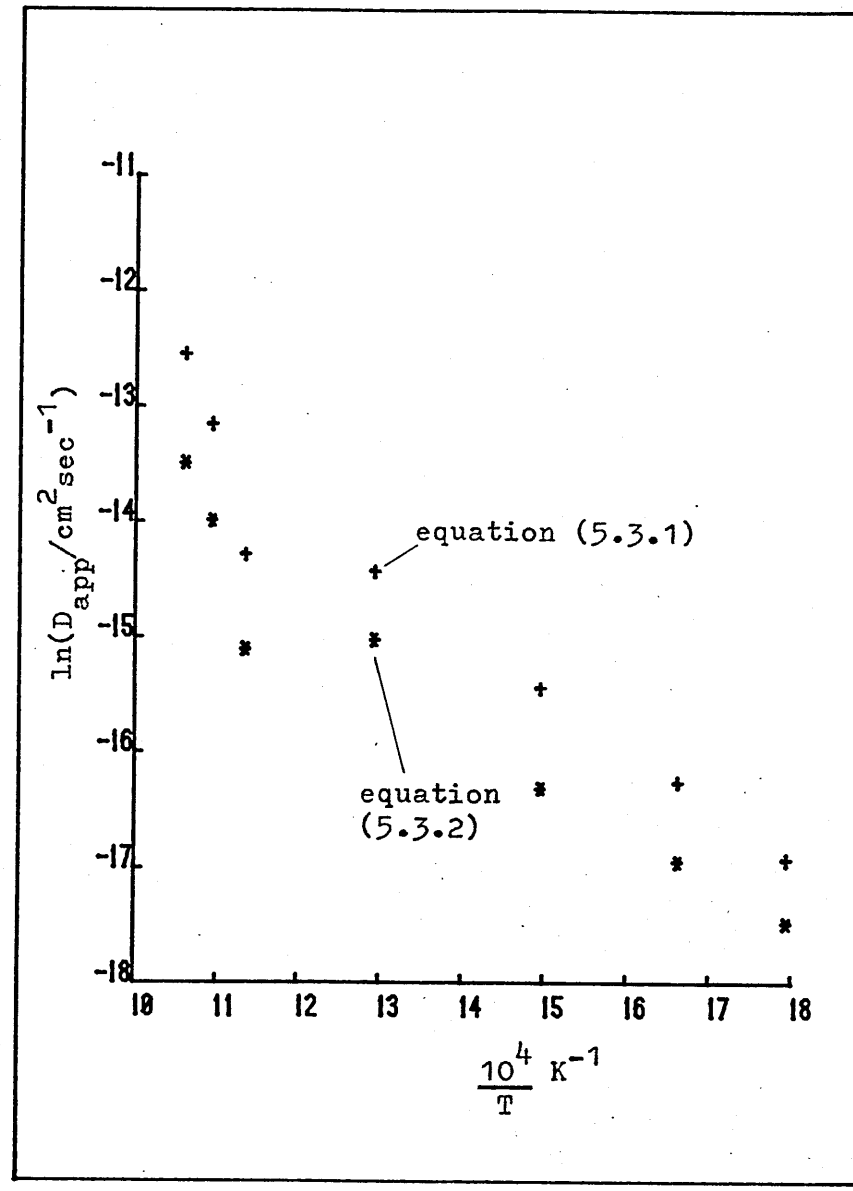

Figure 5.3.3 Apparent diffusion coefficients from the classical (equation (5.3.2)) and surface saturated (equation (5.3.1)) analyses of the phase lag data in .1 mm stainless steel

$$\tan \psi = \frac{\frac{e_1}{e_o}\omega^{\frac{1}{2}} \frac{\sinh 2kl+\sin 2kl}{\cosh 2kl+\cos 2kl}}{1+\frac{e_1}{e_o}\omega^{\frac{1}{2}} \frac{\sinh 2kl-\sin 2kl}{\cosh 2kl+\cos 2kl}} \qquad (5.3.3)$$

Thus using:

$$\tan \phi' = \tan (\phi + \psi)$$

with $\tan \phi = \tan kl \tanh kl$ corresponds to output saturation with additional input effect. This proposition leads to values for the diffusion coefficients in the .1 mm specimen which are very similar to those obtained in the previous analysis for the .25 mm specimen with a greatly reduced residual sum of squares in the phase fits, whereas no noticeable improvement is seen in the fits for the .25 mm specimen phase plots and indeed these tend to converge on a value of $\frac{e_1}{e_o} \rightarrow o$.

The corresponding equation for input saturation and partial output control

i.e. $$\tan \psi = \frac{\sinh 2kl-\sin 2kl}{\cosh 2kl+\cos 2kl}$$

and $$\tan \phi = \frac{\tan kl-\tanh kl+2\frac{x_1}{x_o}[\tan kl \tanh kl]\sqrt{\omega}}{\tan kl+\tanh kl+2\frac{x_1}{x_o}\sqrt{\omega}}$$

do not converge well on the phase-lag data for either specimen.

Superior fits to those obtained from equation (5.2.1) were only found at two temperatures (the two highest) for the .25 mm specimen. These improved fits were obtained by considering intermediate cases between equation (5.3.1) and classical using the partial output surface control equation

$$\tan \phi = \frac{\tan kl-\tanh kl+2\frac{x_1}{x_o}[\tan kl \tanh kl]\sqrt{\omega}}{\tan kl+\tanh kl+2\frac{x_1}{x_o}\sqrt{\omega}} \qquad (5.3.4)$$

Table 5.3.1 Summary of the Analysis of the Phase Data in M316 Stainless Steel

	T(^{o}K)	Input pressure (p) (torr)	Apparent Diffusion Coefficient (cm^2/sec)			
			Equation (5.3.2)	Equation (5.3.1)	Equation (5.3.4)	Equation (5.3.3)
.25 mm specimen	720	1	3.45×10^{-7}	6.83×10^{-7}		
	768	1	4.83×10^{-7}	1.16×10^{-6}		
	818	1	7.93×10^{-7}	2.13×10^{-6}		
	861	1	1.77×10^{-6}	3.65×10^{-6}		
	908	1	3.02×10^{-6}	5.48×10^{-6}		
	950	1	4.94×10^{-6}	1.07×10^{-5}	9.54×10^{-6} (.1579)	
	995	1	6.39×10^{-6}	1.52×10^{-5}	1.33×10^{-5} (.1443)	
.1 mm specimen	557	.1	2.61×10^{-8}	4.50×10^{-8}		8.17×10^{-8} (.6202)
	601	.07	4.44×10^{-8}	8.79×10^{-8}		1.07×10^{-7} (.9268)
	668	.05	8.35×10^{-8}	1.98×10^{-7}		2.64×10^{-7} (.8521)
	773	.05	3.03×10^{-7}	5.45×10^{-7}		1.17×10^{-6} (.5314)
	819	.03	could not be fit	could not be fit		3.54×10^{-6} (.2807)
	880	.03	2.78×10^{-7}	6.29×10^{-7}		3.74×10^{-6} (.3445)
	913	.03	8.51×10^{-7}	1.93×10^{-6}		6.12×10^{-6} (.4030)
	942	.03	1.39×10^{-6}	3.56×10^{-6}		8.90×10^{-6} (.5979)

Table (5.3.1) shows the results of these analyses, the 'best' values of diffusion coefficient being those further to the right of the Table. The columns were left blank when no improvement or a deterioration was observed in the residual sum of squares for the correlation as the complexity of the model was increased.

The numbers in brackets after each final diffusion coefficient indicate the apparent ratio of $\frac{J}{J_{CLAS}}$ (obtained from $\frac{e_1}{e_o}$ or $\frac{x_1}{x_o}$) for the type of control assumed. Note that only the two top temperatures for the .25 mm specimen give values for this ratio, the failure in the rest of the cases being due to saturation. The $(J/J_{CLAS})^{app}$ values for the .1 mm specimen do not take the flux value to the classical flux but merely to the value corresponding to output saturation in the phase.

The diffusion coefficients which represent the best fit from the phase analysis are shown in Figure 5.3.4 and good consistency (Arrhenius behaviour) is obtained down to about 650°K. The results below this temperature may not be accurate enough for a two parameter analysis since there is some increase in the scatter on the phase plots at these temperatures. This inconsistency is also reflected in the loss of the trend in $(J/J_{CLAS})^{app}$ at these lower temperatures.

5.3.2 Steady-state results

The values of $\frac{p'}{\sqrt{p}}$ are shown in Figure 5.3.5. The most obvious point about this plot is that this ratio for the thin specimen is less than that for the thick one, whereas in fact it should be 2.5 times as much were both systems classical. This is hardly surprising since for a non-classical situation as is obviously the case here from the phase plots one would expect a failure of both the classical thickness and pressure relations to give:

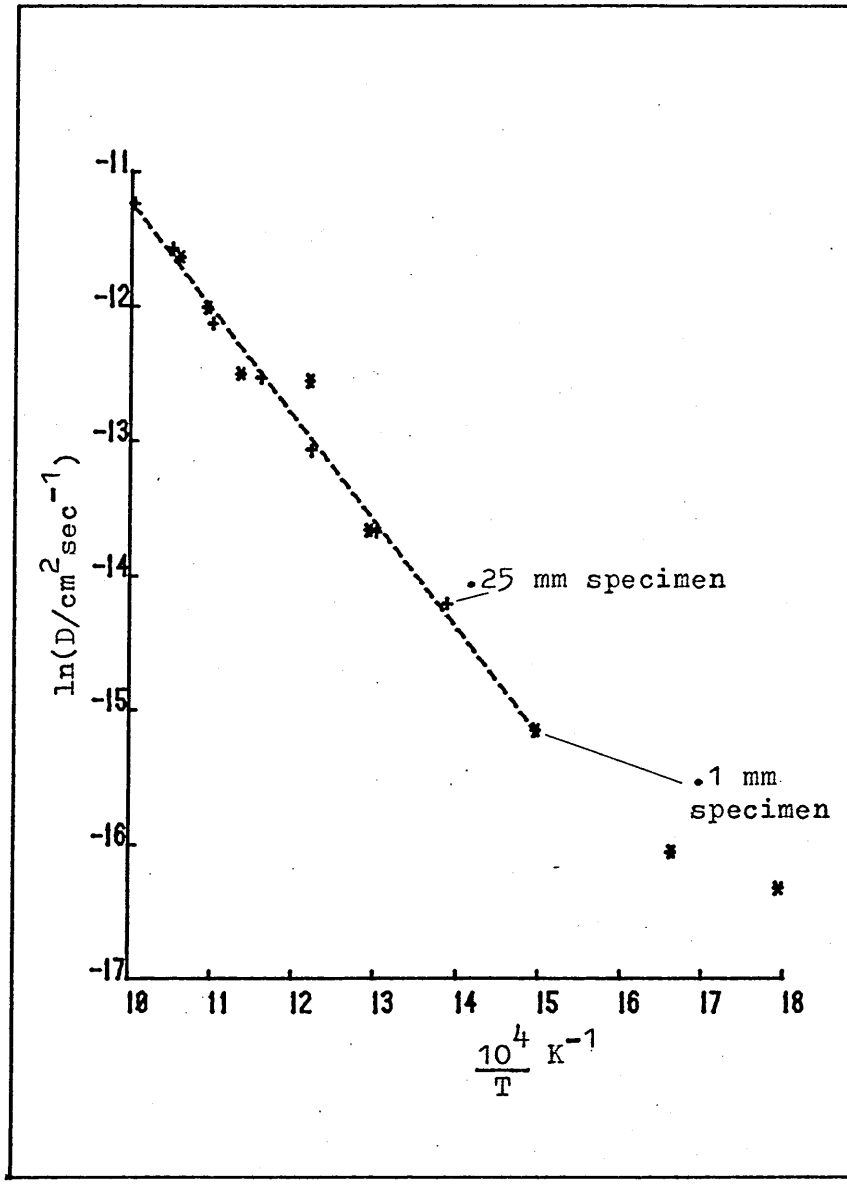

Figure 5.3.4 Final corrected best D's for .1 mm and .25 mm specimens

$$J = J_{CLAS}\left[\sqrt{1 - \frac{J}{K_1 p}} - \sqrt{\frac{J}{K_1' p}}\right]$$

Figure 5.3.5 also shows the result of applying the apparent value of $\frac{J}{J_{CLAS}}$ deduced from the phase analysis. It should again be stressed that this apparent value is only intended to correct for non-classical behaviour at the input surface, bringing flux values up to that level expected for output surface saturation. Since the phase analysis indicates output saturation for the .25 mm specimen, application of $(\frac{J}{J_{CLAS}})^{app}$ to the .1 mm specimen should cause these two lines to coincide. A certain improvement is observed, but it is important to be clear that the separation into input and output control (as was sufficient for the phase analysis) when both surfaces may be causing substantial holdup is entirely artificial particularly when the saturation effects (which imply that $\frac{J}{K_1 p} \rightarrow 1$ and hence $J \rightarrow o$) occur.

To investigate the extent of this non-classical behaviour the plot in Figure 5.3.6 was drawn where the $\frac{p'}{p}$ values for both specimens are shown. The values for the .1 mm specimen have also been multiplied by $\frac{.1 \text{ mm}}{.25 \text{ mm}}$ to allow for the classical thickness relation. These results now lie remarkably close to each other. This is rather surprising since one would expect <u>either</u> a failure of the $\frac{l_2}{l_1}$ relation <u>or</u> the $\sqrt{p}$ relation and a transfer from $J \propto \sqrt{p}$ to $J \propto p$ must imply a loss of sensitivity to thickness. Thus, as was proposed for the phase plots some type of intermediate control could be operative.

It can be seen from Chapter 4, Figures 4.3 and 4.8 that for a $\frac{J}{K_1 p}$ type of control, when $\frac{J}{K_1 p} = \frac{J}{K_1' p}$, output effects are seen before input effects but when $\frac{J}{K_1 p}$ becomes appreciable mixed control takes over. The $\frac{J}{J_{CLAS}}$ values indicated by the phase plots

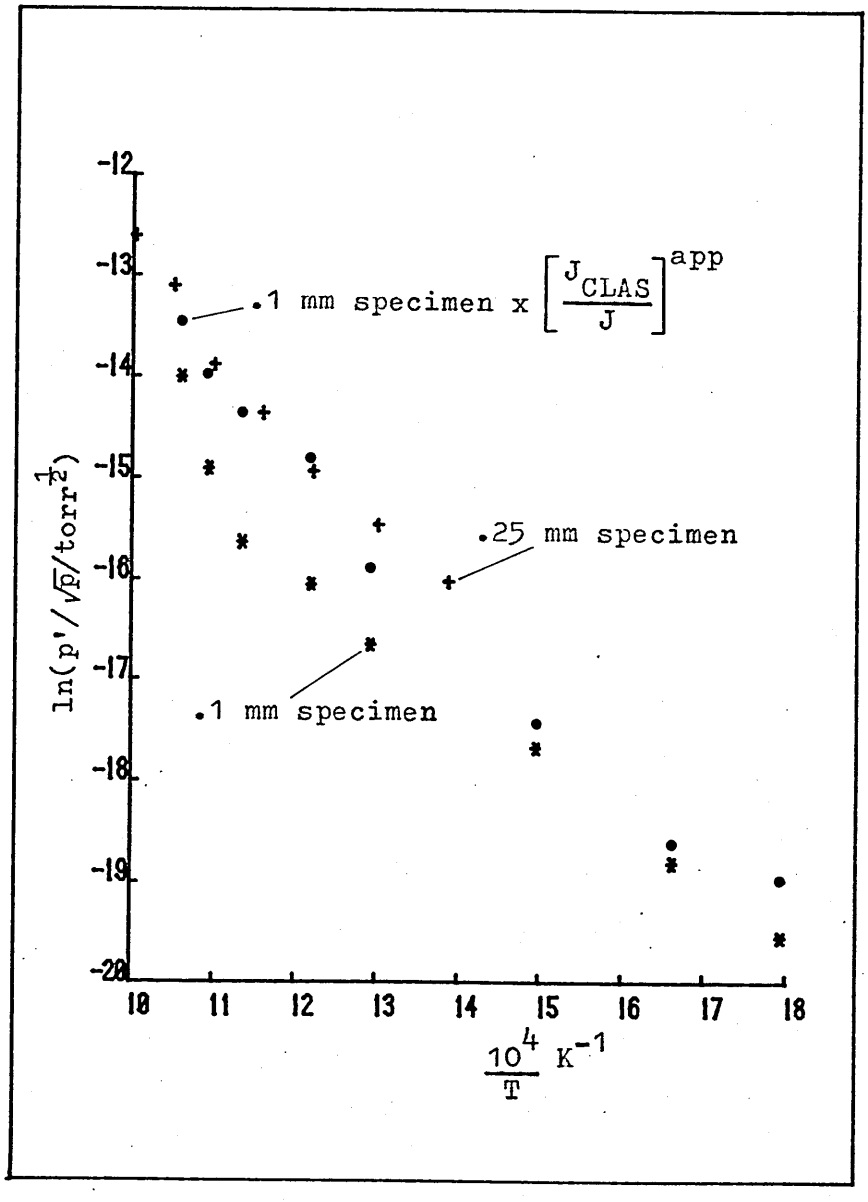

Figure 5.3.5 Steady-state levels for .25 mm and .1 mm stainless steel specimens corrected for $\sqrt{p}$ (input pressure)

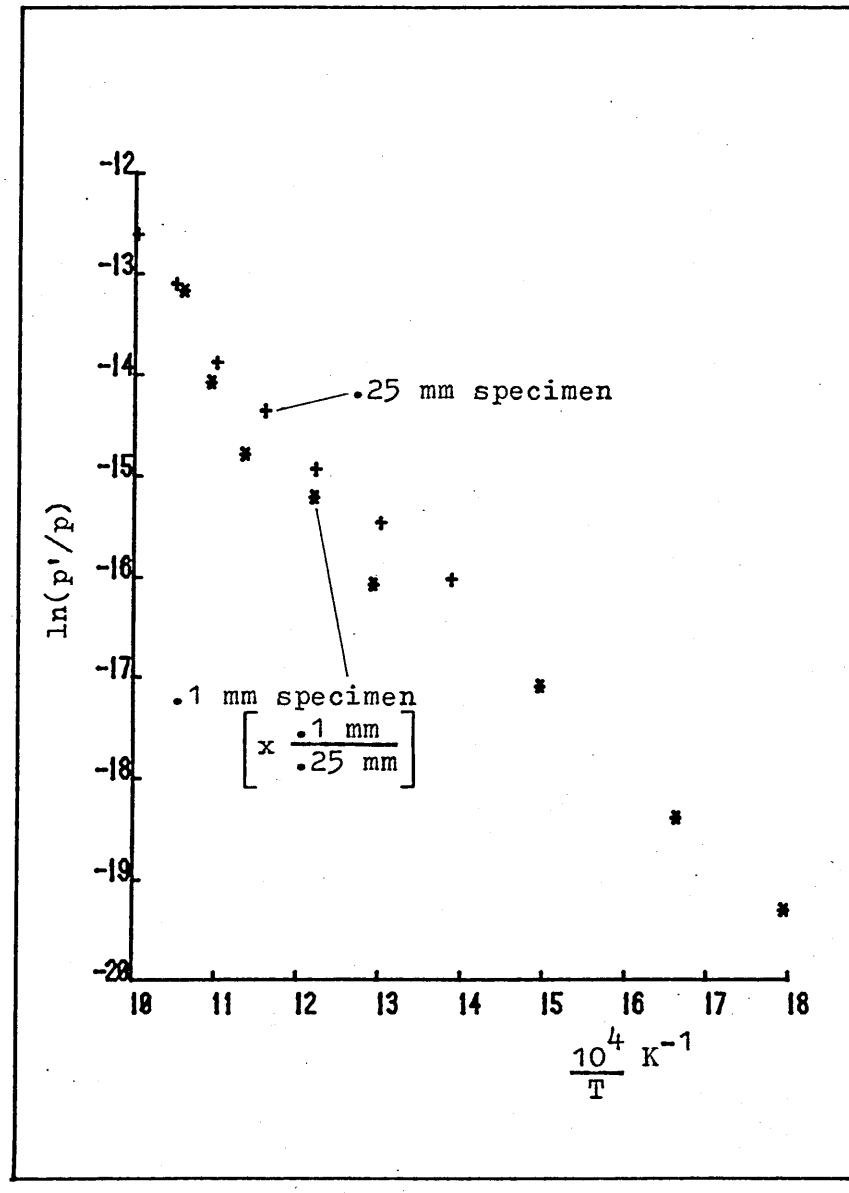

Figure 5.3.6 Steady-state levels from both stainless steel specimens corrected for input pressure and for thickness

suggest values of $\frac{J}{K_1 p}$ where both input and output control are operative.

When steady-state levels and amplitudes are considered, effects such as 'saturation' at either of the surfaces with the consequent implication that J = o are no longer meaningful. The limiting case for heavily oxide-limited permeation in the steady-state is given by $\frac{J}{J_{CLAS}} \rightarrow o$.

$$\text{i.e.} \quad J = \frac{K_1 K_1'}{K_1' + K_1} P \qquad (5.3.5)$$

and J becomes proportional to p for severe attenuation of the steady-state flux. This limit can only be supposed to have been reached if the $\frac{p'}{\sqrt{p}}$ graphs coincide for both specimens, unless the oxide thicknesses are different on each specimen in approximately the ratio 2.5:1 (see foregoing on thickness relation) the thicker oxide being on the .25 mm specimen. This would be consistent with observation since the roughly linear region at low temperature for both specimens has virtually the same slope (Figure 5.3.6).

The steady-state pressure data relevant to Figures 5.3.5 and 5.3.6 are summarised in Table 5.3.2.

5.3.3 Amplitudes

According to the results from the phase plots two of the amplitudes from the 0.25 mm specimen should be analysable in in terms of the $\frac{x_1}{x_o}$ model (i.e. partial control at the output surface).

These (.25 mm) amplitude plots show that control is certainly of $\frac{J}{K_1 p}$ type since the extrapolated value of the amplitude (as $\omega \rightarrow o$) lies between $\frac{p'}{\sqrt{p}}$ and $\frac{p'}{2\sqrt{p}}$ (Section 4.3). Extrapolation is, however, a little dubious because of the uncertainty in D and because of the steepness of the curve. The type of control, whether

input, output or mixed is also uncertain since both would give such an effect but it can be seen from Chapter 4 that amplitudes stay towards the classical extrapolated value for much longer in the case of input control than in the case of output control.

If the two highest temperature output amplitude plots are considered to be of pure output control the following linearisation procedure can be followed. In the model used to interpret the phase plots for these two temperatures, the attenuation in amplitude due to the bulk of the solid:

$$B = \frac{2kD/(\cosh 2kl-\cos 2kl)^{\frac{1}{2}}}{\sqrt{1 + \frac{2x_1}{x_o}\omega^{\frac{1}{2}}\left(\frac{\sinh 2kl+\sin 2kl}{\cosh 2kl-\cos 2kl}\right) + 2\left(\frac{x_1}{x_o}\right)^2\omega\left(\frac{\cosh 2kl+\cos 2kl}{\cosh 2kl-\cos 2kl}\right)}}$$

i.e.

$$B=B_{CLAS}\left\{1+2\frac{x_1}{x_o}\omega^{\frac{1}{2}}\left[\frac{\sinh 2kl+\sin 2kl}{\cosh 2kl-\cos 2kl}\right]+2\left(\frac{x_1}{x_o}\right)^2\omega\left(\frac{\cosh 2kl+\cos 2kl}{\cosh 2kl-\cos 2kl}\right)\right\}^{\frac{1}{2}}$$

If a straight line is drawn through the amplitude closest to $\omega = o$ and through o at $F(\omega) = o$, the value of $\frac{x_1}{x_o}$ for the remaining values of amplitude can be calculated from their deviations from this line. These values of $\frac{x_1}{x_o}$ can be averaged and then applied to the $\omega \rightarrow o$ amplitude to raise it up. A new straight line through o at $F(\omega) = o$ is now drawn and the process repeated until there is no further change. The 995K amplitudes give $\frac{x_1}{x_o} = 12.76$; i.e. $J/J_{CLAS} = .159$ (.144) and the 950K amplitudes give $\frac{x_1}{x_o} = 11.78$; i.e. $J/J_{CLAS} = .195$ (.158). The consistency here between the amplitude and phase (bracketed) results for J/J_{CLAS} led to the attempt to apply this technique to lower temperatures but this did not work perhaps partly due to uncertainties in D and partly due to loss of applicability, where the input surface control can no longer be ignored.

The same procedure was tried for mixed control in order

Table 5.3.2 Steady-state Pressure Data for M316 Stainless Steel

	$T^{\circ}K$	Input pressure, p (torr)	Output pressure, p' (torr)	$\frac{p'}{\sqrt{p}}$ $(\sqrt{torr})$	$\frac{p'}{\sqrt{p}} \times \left(\frac{J^{CLAS}}{J}\right)^{app}$ $(\sqrt{torr})$	$\frac{p'}{p}\left(\times \frac{1}{.25\ mm}\right)$
.25 mm specimen	995	1	3.43×10^{-6}			
	950	1	2.08×10^{-6}			
	908	1	9.48×10^{-7}			
	861	1	5.87×10^{-7}			
	818	1	3.29×10^{-7}			
	768	1	1.95×10^{-7}			
	720	1	1.12×10^{-7}			
.1 mm specimen	942	.03	1.45×10^{-7}	8.42×10^{-7}	1.41×10^{-6}	1.95×10^{-6}
	913	.03	5.90×10^{-8}	3.39×10^{-7}	8.40×10^{-7}	7.78×10^{-7}
	880	.03	2.84×10^{-8}	1.65×10^{-7}	4.80×10^{-7}	3.82×10^{-7}
	819	.03	1.87×10^{-8}	1.08×10^{-7}	3.85×10^{-7}	2.50×10^{-7}
	773	.05	1.34×10^{-8}	5.97×10^{-8}	1.13×10^{-7}	1.06×10^{-7}
	668	.05	4.78×10^{-9}	2.15×10^{-8}	2.51×10^{-8}	3.85×10^{-8}
	601	.07	1.82×10^{-9}	6.91×10^{-9}	7.49×10^{-9}	1.05×10^{-8}
	557	.1	1.04×10^{-9}	3.31×10^{-9}	5.33×10^{-9}	4.19×10^{-9}

to attempt to widen the range of applicability of this technique. To avoid introducing a further variable it was supposed that $\frac{J}{K_1 p} = \frac{J}{K_1' p}$ so that:

$$\frac{x_1}{x_o} = \frac{\frac{J}{K_1 p}}{\left[\frac{J}{K_1 p}\right]^{\frac{1}{2}} \left[1-\frac{J}{K_1 p}\right]^{\frac{1}{2}} - \frac{J}{K_1 p}} \qquad \frac{1}{2\sqrt{2D}}$$

and

$$\frac{e_1}{e_o} = \frac{\frac{J}{K_1 p}}{1-\frac{J}{K_1 p} - \left[\frac{J}{K_1 p}\right]^{\frac{1}{2}} \left[1-\frac{J}{K_1 p}\right]^{\frac{1}{2}}} \qquad \frac{1}{2\sqrt{2D}}$$

and applying these to the attenuation factors A and B, values of $\frac{J}{K_1 p}$ could be obtained for the 995K and 950K amplitudes in the .25 mm specimen. Unfortunately, the range of applicability was not extended, the linearisation procedure tending to seek the maximum value of 0.5 for $\frac{J}{K_1 p}$. Figures 5.3.7 and 5.3.8 illustrate this procedure for the successful cases. The values of $\frac{J}{J_{CLAS}}$ obtained from these three procedures (output control with phases, output control with amplitudes, output and input control with amplitudes) are shown in Table 5.3.3.

Table 5.3.3

T(°K)	Ratio of measured to predicted classical flux in .25 mm stainless steel J/J_{CLAS}		
	Phases (output control)	Amplitudes (output control)	Amplitudes (mixed control)
995	.144	.159	.212
950	.158	.195	.226

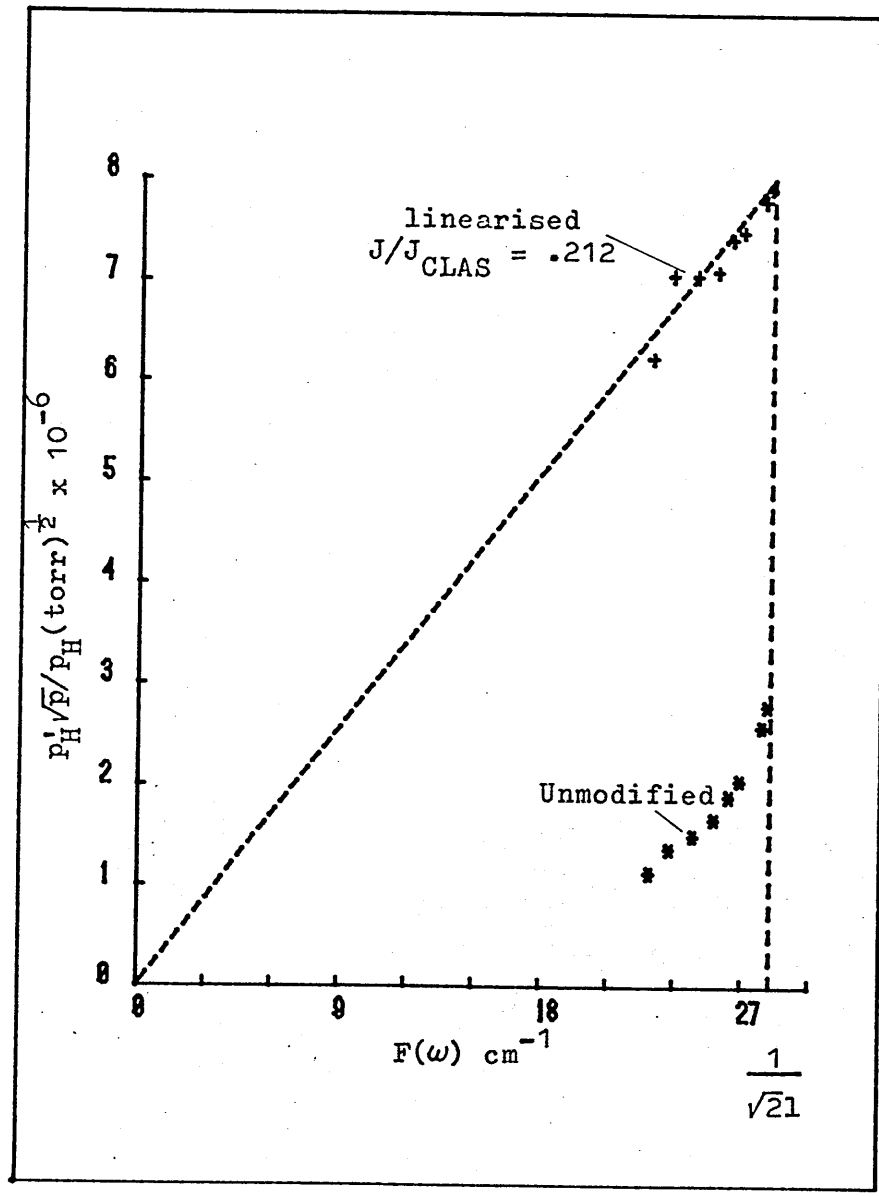

Figure 5.3.7 Linearisation of the output pressure amplitude in .25 mm stainless steel at 995K using mixed input and output control

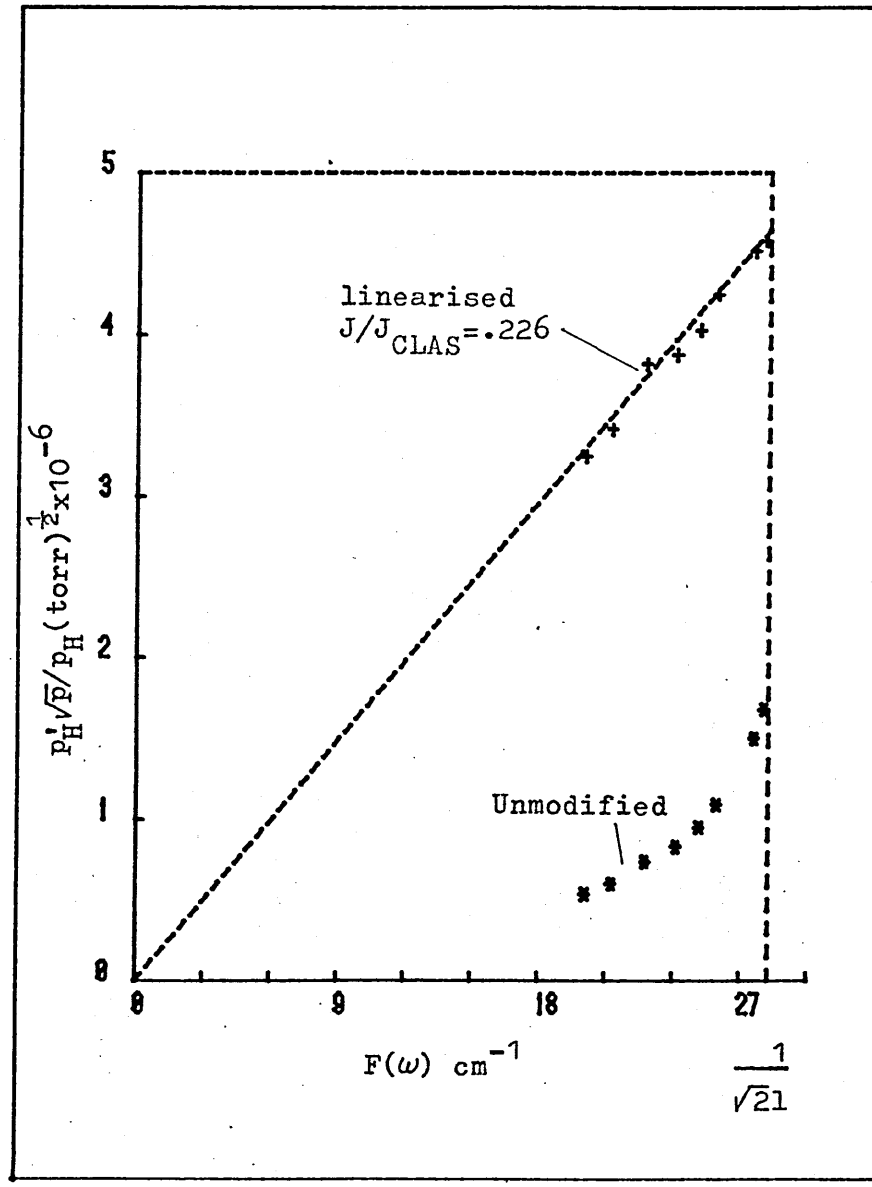

Figure 5.3.8 Linearisation of the output pressure amplitude in .25 mm stainless steel at 950K using mixed input and output control

The .1 mm amplitudes were not tractable using this technique and it appears that there is agreement between the phase and amplitude results to the extent that when saturation occurs the amplitude decrease with increasing frequency is so severe as to render treatment by linearisation very difficult. There is also the possibility that some type of rate-controlling mechanism not covered by the model (perhaps penetration along defects in the oxide layer) becomes operative.

5.3.4 Summary

Stainless steel was more difficult to analyse than either molybdenum or nickel, since there was in this case no direct indication of either the diffusivity or the permeability and it was only possible to obtain these parameters (and then, only in particular cases) by assuming an oxide-limited model for the permeatio process.

The model supposed here was the one outlined in Section 4 where hydrogen is assumed to dissolve molecularly in an oxide layer with close to equilibrium conditions applying at all the interfaces so that the problem could be treated as diffusion through a composite medium.

Unfortunately, it appears that both surfaces were oxidised and rate-controlling but a certain amount of information could be gleaned from the results assuming only one surface to control.

Values were obtained for the diffusion coefficient in all cases although the lower temperature results for the .1 mm specimen were less certain.

The permeability was obtained only for the two highest temperature runs in the .25 mm specimen but a measure of the oxide

permeability/thickness ratio could be deduced from the remaining results and this will be discussed in Chapter 6.

5.4 General Summary

This Chapter has been concerned with the analysis of the experimental results by the methods presented in Chapter 4. Diffusion phase boundary processes have been deduced assuming the model for phase boundary control proposed in Chapter 3.

Chapter 6 will go on to compare these measured parameters with available literature data and the technique will be discussed critically with a view to improvements which could be made to yield further information about permeation processes.

CHAPTER 6

DISCUSSION

6.1 Introduction

This chapter is mainly concerned with the comparison of measured data with that measured by other techniques available in the literature. This comparison is confined to diffusion coefficients, permeabilities and solubilities. Solubility is derived from the diffusivity and permeability by the relation $K_{sm} = P_M/D$. Care has been taken where possible to involve solubilities which have been derived using techniques other than permeation (normally equilibration experiments). Every effort has been made to include as many authors as possible and, more importantly, to include the results of as many measurement techniques as possible. However, where a great deal of data exist (particularly true for nickel and stainless steel) representative results have been chosen for clarity.

The values of the non-classical permeation parameters derived in Chapter 5 are discussed in terms of their implications on the permeation process and with a view to improving the technique to allow more accurate determination of both their magnitude and their role.

6.2 Nickel

The permeability of hydrogen through nickel has been thoroughly investigated by many authors. The data show a high degree of consistency.

It is not intended here to present an exhaustive survey as this would involve the work of at least 50 investigators. Instead, the results of two reviews which supply 'best fit' summaries of the available data have been used. Use has been made of some

individual work in order to illustrate the effect of technique and to indicate the degree of scatter of the data.

Figure 6.2.1 shows the diffusion coefficients from a variety of investigations(31-36) including those obtained by the classical analysis from the 0.6 torr phase plots and their best fit regression line equation (5.1.2). The best fit lines from Vogel and Alefeld's(36) very comprehensive review are also shown in this plot and the discontinuity at the Curie Temperature (T = 638K) is based on the evidence of one author(37) who discovered a small change in diffusion coefficient at this temperature. Neither this work nor the work of Robertson(11) (who was actually looking for a grain-boundary effect) suggest any change in the diffusion coefficient at the Curie Temperature. The best fit line of Robertson's review is not shown on this plot since it is hardly distinguishable from the line of Vogel and Alefeld nor indeed from the regression line for the present work.

Louthan et al.(38) have made the point that measurements of D based on evolution rates tend to be larger than those based on permeation rate of rise. This is confirmed by the data shown in Figure 6.2.1 where the measurements of Katz et al.(31), Dus and Smialowski(33) and Eichenauer et al.(34) are based on measurements of evolution rates. The measurements of Ebisuzaki et al.(35) are based on permeation rise time. In order to test this hypothesis further Table 6.2.1 was constructed from the compilation of Robertson(11), where the temperatures for evaluation of the diffusion coefficients have been chosen to include the ranges of as many investigators as possible.

To avoid repetition of the referencing and since the data are not to be used separately the order of Robertson's original

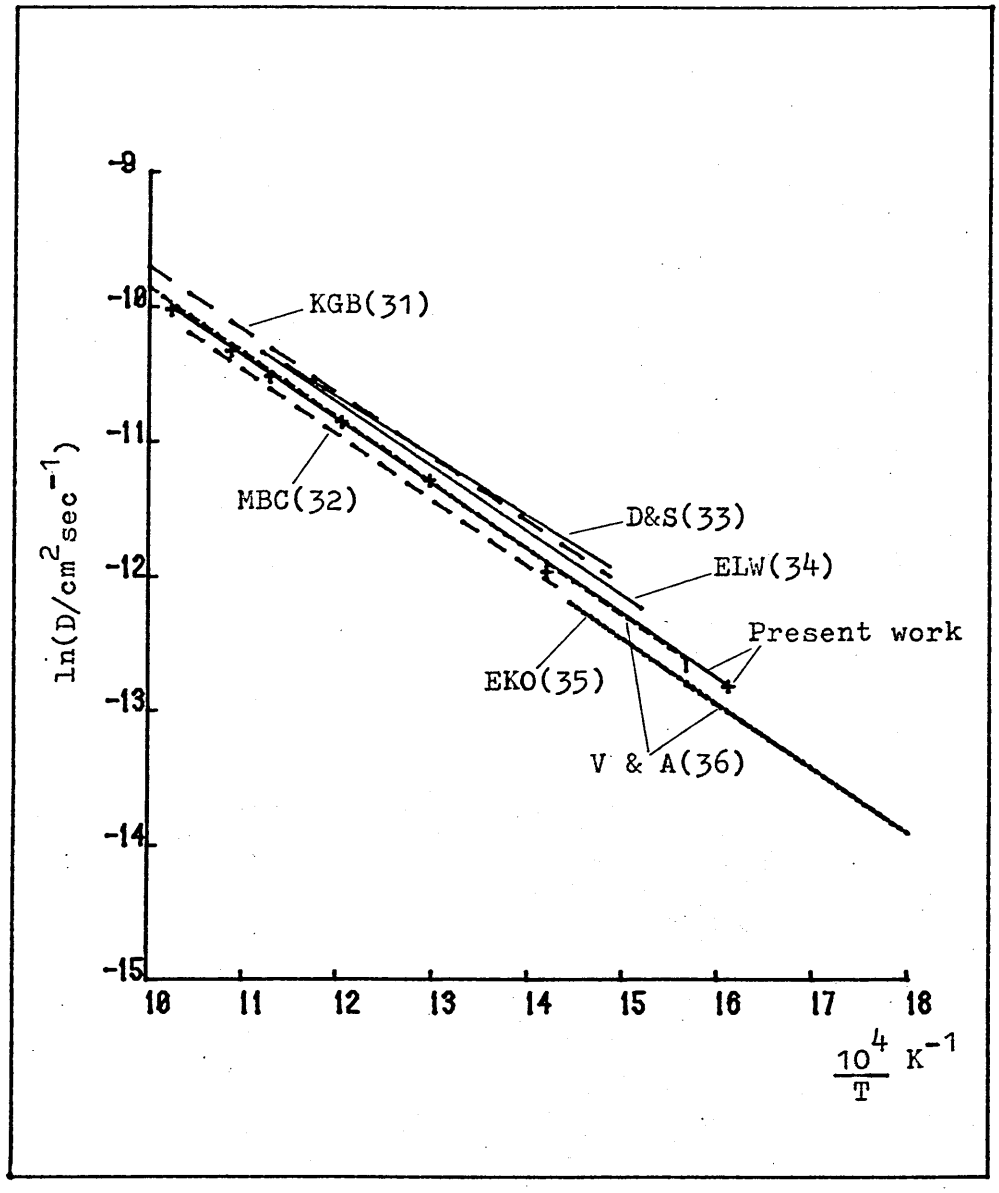

Figure 6.2.1 Diffusion Coefficients for Hydrogen in Nickel

Table 6.2.1 The effect of experimental technique on the diffusion coefficient of hydrogen in nickel

Technique	D(573K) $cm^2/sec \times 10^{-6}$	D(673K) $cm^2/sec \times 10^{-6}$	D(773K) $cm^2/sec \times 10^{-6}$
Evolution	(.96)	(2.99)	(6.93)
Evolution	(2.36)	7.25	16.65
Evolution	(1.29)	4.70	12.22
Evolution	1.48	5.53	(14.72)
Evolution	(2.62)	7.85	17.70
Evolution	(2.18)	(6.97)	(16.52)
Evolution	(1.69)	5.80	14.44
Permeation	1.07	3.79	(9.65)
Evolution	(2.13)	6.62	15.35
Permeation	(.28)	(.71)	(1.43)
Permeation	1.48	(5.32)	(13.72)
Permeation	1.15	(4.04)	(10.23)
Permeation	(1.69)	5.40	12.78
Evolution	1.03	3.64	9.28
Absorption	2.05	6.59	15.70
Evolution	(5.83)	(15.75)	(32.92)
Evolution	(1.77)	6.06	15.09
Permeation	(1.23)	4.35	11.10
Resistivity	(.48)	(1.81)	(4.81)
Permeation	1.05	3.59	(8.89)
Permeation	(1.44)	4.99	12.52

tabulation has been preserved in Table 6.2.1. The only modification is that the results of this investigation have been added at the bottom. The numbers in brackets are those which have been extrapolated out of their temperature range of applicability and these have not been used in the averaging procedure. Table 6.2.2 shows the means and standard deviations of the diffusion coefficients in Table 6.2.1 at the three temperatures chosen separated into those based on an evolution technique and those based on permeation. The number in brackets after each mean and its associated standard deviation is the number of values from which the mean has been derived.

Table 6.2.2

Temperature (^{o}K)	(D ± standard deviation) x 10^{-6} cm^2/sec (no. of values)	
	Permeation	Evolution
573	1.19 ± .20 (4)	1.25 ± .32 (2)
673	4.42 ± .77 (5)	5.93 ±1.36 (8)
773	12.13 ± .90 (3)	14.39 ±2.84 (7)

These results reinforce the hypothesis of Louthan *et al.* who attribute this systematic difference to trapping of hydrogen atoms in the nickel lattice. Their own results in which first the rate of rise to steady-state is monitored and then gas is removed from the input chamber and the rate of evolution is measured also show the assymetry suggested by Table 6.2.2. The experiment of Louthan *et al.* can be likened to the present

experiment with a very deep modulation and a square waveform. If it is supposed that the permeation process is described by a linear differential equation then superposition allows that the solution can be split into a series in the same way as the input wave can be split into its Fourier components. Since the increase in the input pressure in the rise-time part of the experiment is liable to be more rapid than the decrease (due to pumping) preparatory to the evolution part of the experiment it may well be that the observed assymetry in the output wave is simply a reflection of the assymetry of the input wave. Even if this is not the case there is yet another possible explanation in terms of the effect observed at the output surface in this experiment which has been associated with the quantity $\frac{1}{2K_2'\theta'}$. As θ', the output surface hydrogen atomic density decreases, retardation of gas flow through the specimen will occur and this will lead to a decrease in the apparent diffusion coefficient. If one takes into account that the output surface concentration is not actually zero but a very small finite number one might expect that during the rise-time experiment the output surface concentration and hence θ' will increase so that the effective diffusion coefficient might be expected to increase until steady-state is reached. Precisely this effect is found by Louthan et al. so that their kinetic assymetry may merely be due to the assumption, implicit in their analysis, that the output surface concentration is zero.

If hydrogen motion in nickel were to be sensitive to defects in the nickel lattice (trapping) one might expect that, as in mild steels (see, for example Oriani's(39) analysis of the data of Hill and Johnson(40)) the apparent diffusion coefficient would depend on the mechanical condition of the nickel. Neither

Robertson(11) nor Grimes(41) have observed such an effect.

Robertson(11) has derived a 'best-fit' permeability and has also displayed the envelope of results for some 18 investigations. For this reason it only seems necessary to compare the results of this investigation with the best-fit and envelope derived by Robertson. This is shown in Figure 6.2.2. Although the values obtained in this work (equations (5.1.1) and (5.1.3)) lie above the 'best-fit' they are well within the envelope of results. Incidentally, the envelope derived by Robertson is selective in that it discounts permeabilities which are markedly dissimilar to the norm.

The solubility of hydrogen in nickel can quite simply be obtained from the relationship $P_M = DK_{sm}$. Since two equations have been obtained, (5.1.1) and (5.1.3) for the permeability, two equations result for the solubility according to whether the results are based on amplitude or steady-state measurements. These are shown in Figure 6.2.3.

For comparison with values from the literature a mixture of those obtained independently and those obtained from permeation studies has been used. Louthan *et al*'s (D_2), Ebisuzaki *et al*'s and Eichenauer *et al*'s results (38, 35, 34) were all obtained from permeation studies. Armbruster's(42) measurements were specifically designed for solubility as were the more recent results of Jones and Pehlke(43) and McLellan and Oates(44) which were both made over the same temperature range and are almost coincident.

The 'best value' obtained by Robertson(11) based only on 'direct' solubility measurements is also shown.

The consistency between the measured results from amplitudes and from steady-state measurements is good but the

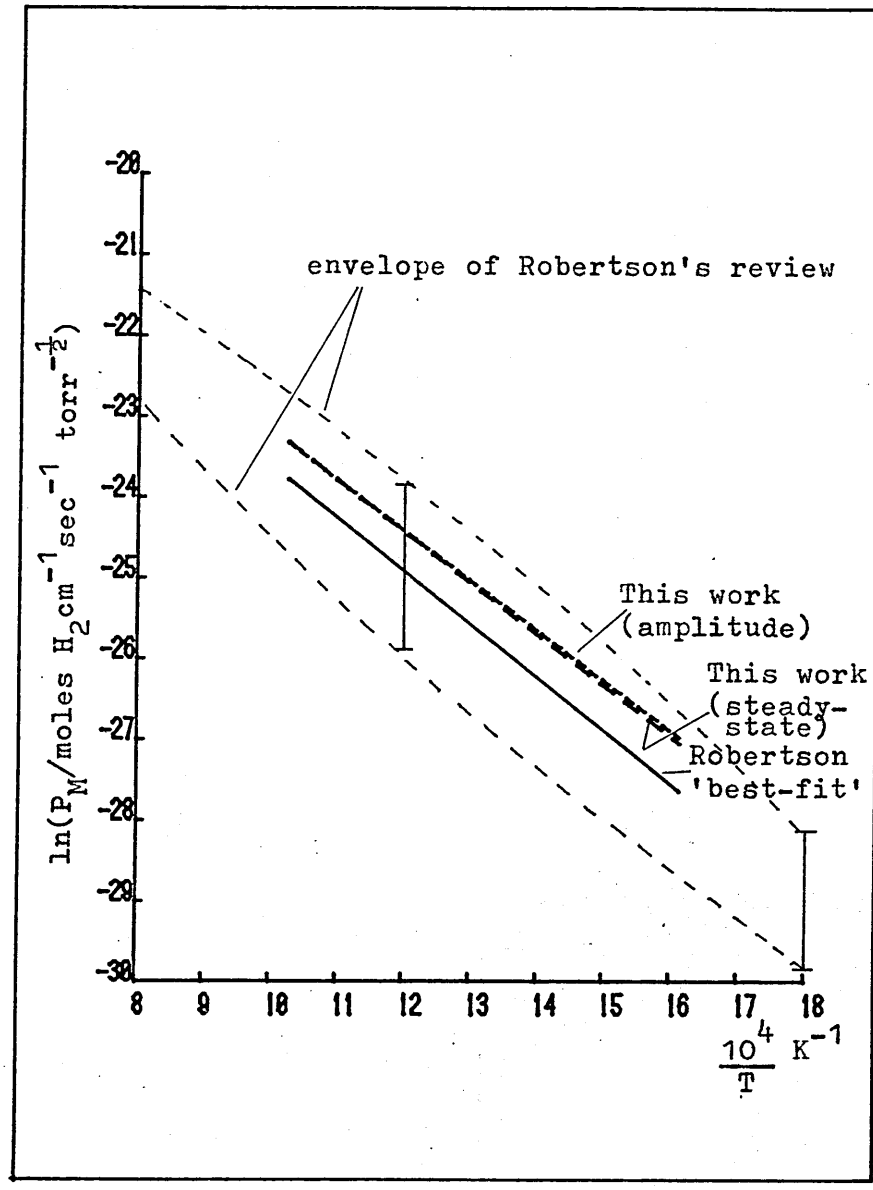

Figure 6.2.2 Comparison of the permeabilities of this investigation with the 'best-fit' and envelope obtained by Robertson(11)

solubility values do seem high compares with Robertson's curve.

Summarising, the values of diffusivity, permeability and solubility are given by:

$$D = 6.16 \times 10^{-3} \exp\left[\frac{-9523}{R\,T}\right] \quad cm^2/sec$$

$$P_{M,s} = 4.32 \times 10^{-8} \exp\left[\frac{-12533}{R\,T}\right] \quad \text{moles } H_2/cm \text{ sec } \sqrt{torr}$$

$$P_{M,t} = 3.41 \times 10^{-8} \exp\left[\frac{-12118}{R\,T}\right] \quad \text{moles } H_2/cm \text{ sec } \sqrt{torr}$$

$$K_{sm,s} = 7.01 \times 10^{-6} \exp\left[\frac{-3010}{R\,T}\right] \quad \text{moles } H_2/cm^3 \sqrt{torr}$$

$$K_{sm,t} = 5.54 \times 10^{-6} \exp\left[\frac{-2595}{R\,T}\right] \quad \text{moles } H_2/cm^3 \sqrt{torr}$$

Little work has been done on low pressure permeation of hydrogen through nickel, the lowest recent investigations being at around 10 torr. All have been steady-state measurements apart from the work of Morrison et al.(32) which used the modulatory technique.

Perhaps the most interesting of these investigations was due to Smithells and Ransley(7) who used their own results along with those of Borelius and Lindblom(45, 46) to demonstrate that the permeation rate of hydrogen through nickel was not described by a classical $\sqrt{p}$ relationship. Instead a modifying factor, $\frac{ap}{1+ap}$, based on the Langmuir Isotherm was applied to account for the low surface coverage (and hence reduction in area used for permeation) at low pressures.

An effect such as that found by Borelius and Lindblom where the J vs. $\sqrt{p}$ curves cross the $\sqrt{p}$ axis at positive values of $\sqrt{p}$ was not observed here but it is possible that reduced pressures below those investigated here could show an effect on the steady-state and amplitude measurements as an extension of the secondary

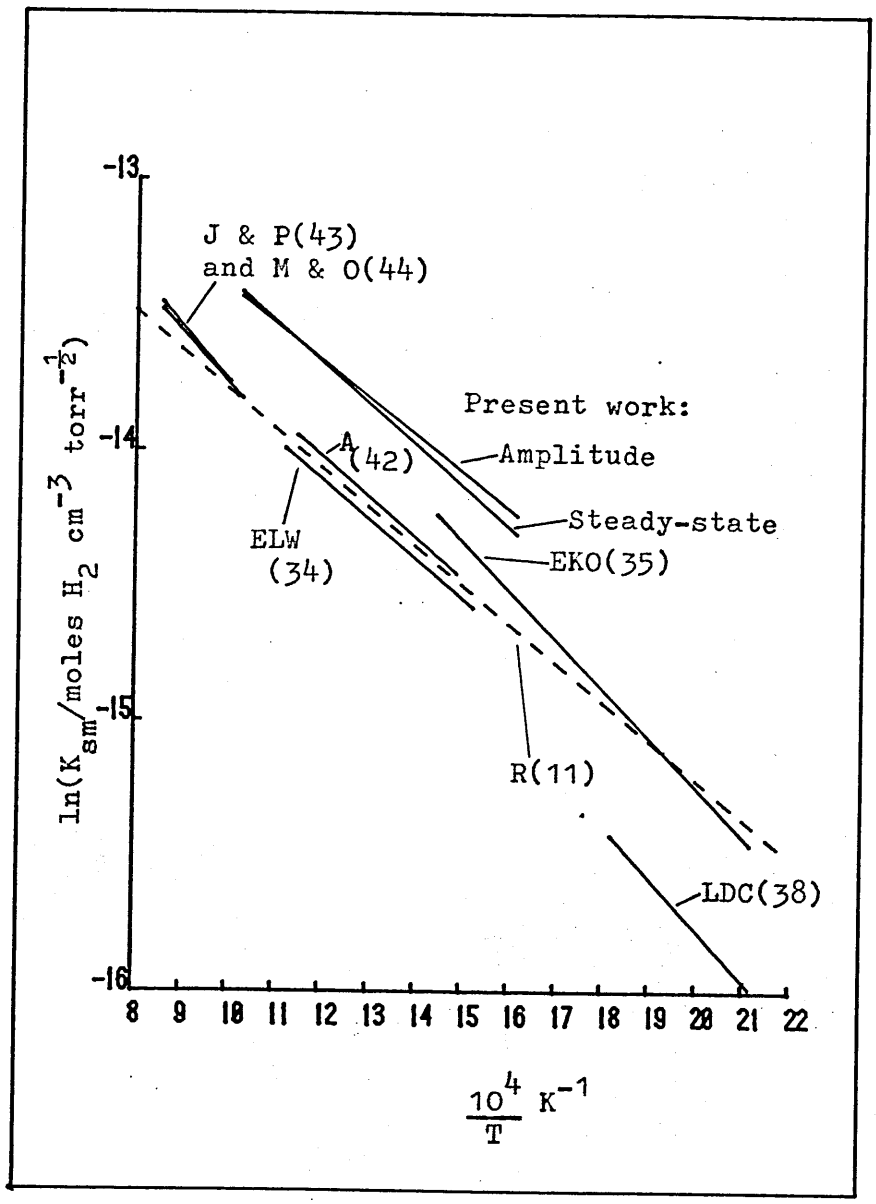

Figure 6.2.3 Solubility of Hydrogen in Ni

effect already seen in the phases.

The product $1/2K_2'\theta'$ calculated from the low pressure phase measurements can be interpreted as the mean time of stay of an atom on the output surface. This quantity should not show a simple temperature dependence at constant input pressure since, as temperature increases, the flux through the specimen increases. Thus, θ' should increase, but K_2' should also increase if it is thermally activated. This would tend to decrease θ'.

As can be seen from the results (Table 5.1.2), $\frac{1}{2K_2'\theta'}$ in fact decreases with increasing temperature. However, this decrease is slow compared with the rate at which the diffusion coefficient increases with temperature so that, although the mean time of stay on the surface is becoming shorter, the rate at which gas is traversing the specimen is getting faster. The net effect of this should be that the phenomenon observed in this system should become more noticeable at higher temperatures.

6.3 Molybdenum

The literature values of the permeation constants for hydrogen in molybdenum are considerably more sparse and divergent than those in nickel. It appears that the permeabilities are rather more consistent than either the diffusivities or solubilities.

The permeability obtained from this investigation, equation (5.2.1) is compared in Figure 6.3.1 with values obtained from the literature.

Due to the limited amount of data available investigations using D_2 gas have also been included in this figure. These permeabilities have not been multiplied by the factor $\sqrt{2}$ normally accepted for D_2/H_2 comparisons but the bar in the bottom left

of the plot shows the value of this factor for convenience of comparison.

The permeabilities seem to be more consistent at lower temperatures and the results of this investigation fall well into this band. The higher temperature values are rather less consistent and the results of this investigation fall somewhat above those of other investigators.

The permeability attributed to Hill(47) was obtained by multiplying his reported solubility and diffusion coefficient. However, Hill's experiment was performed by charging the material at 1280-1700°C and the reperted solubilities really only refer to that temperature range and it may be unjust to this investigator to extrapolate these measurements. The permeability of Guthrie _et al._(48) was measured using 1-2000 torr input pressure of deuterium. These authors also report some preliminary studies with hydrogen and propose a pre-exponential factor $\simeq 1.5$ (approx. $\sqrt{2}$) times that for deuterium although the activation energy is not altered and remains rather low. Huffine and Williams'(49) measurements were made at 810 torr input pressure, but Frauenfelder(50) has investigated a very wide pressure range from 200 torr to 2×10^{-6} torr. This author did find some deviations from classical behaviour at around 2×10^{-2} torr but these effects were supposed to be associated with the extent of pre-dissociation of the gas at the (relatively high) temperatures used.

The solubility of hydrogen in molybdenum is obtained by division of equation (5.2.1) by equation (5.2.2).

$$K_{sm} = 3.64 \times 10^{-8} \exp\left[\frac{-1445}{R\,T}\right] \text{ moles } H_2/cm^3 \sqrt{torr}$$

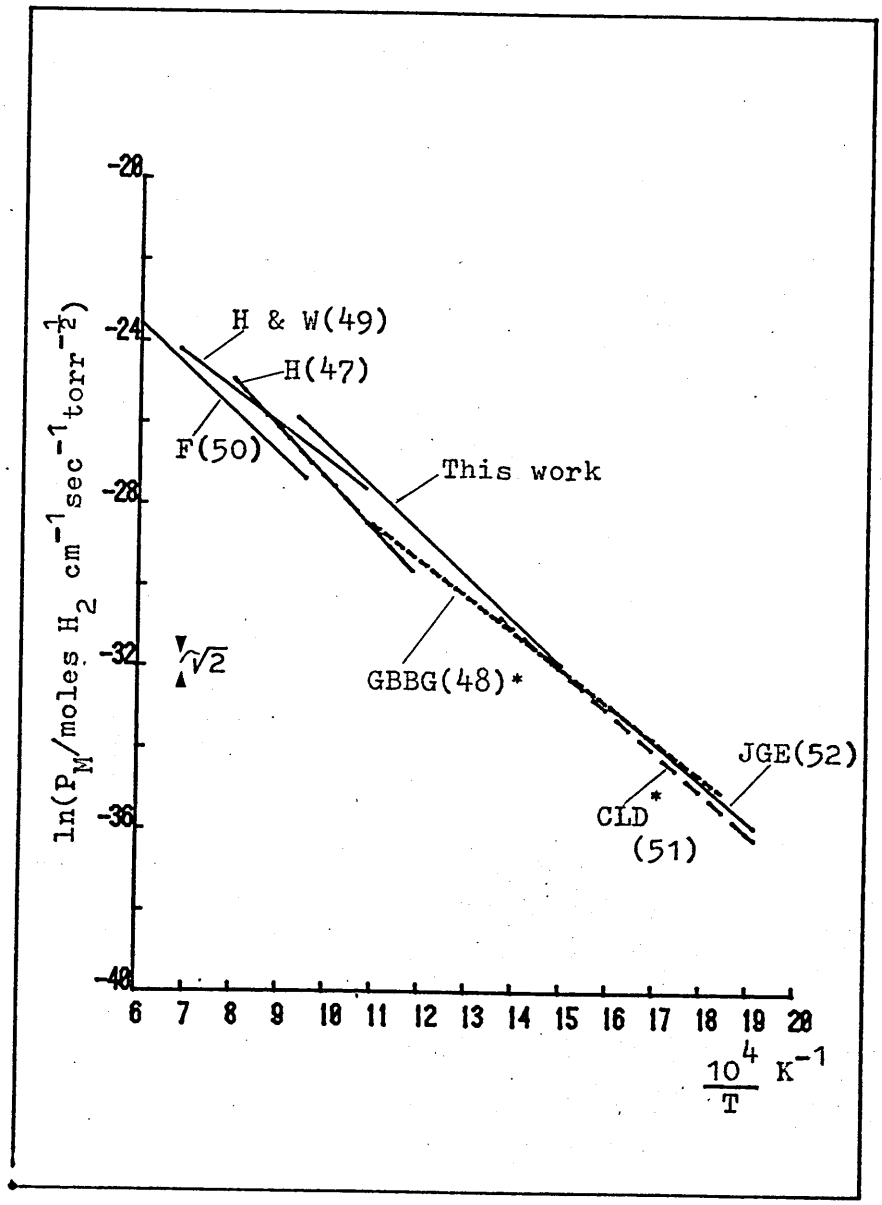

Figure 6.3.1 Permeabilities for hydrogen in molybdenum

(*Experiment carried out using dueterium gas)

This is shown in Figure 6.3.2 along with some data from the literature.

The literature solubilities are rather less tightly bunched than the permeabilities and activation energies vary rather widely even in the same temperature range. The solubility of Hill(47) has been extrapolated from his charging temperature to the temperature at which his diffusivities were measured to attempt to illustrate the effect that this extrapolation has on the permeability plotted in Figure 6.3.1.

Only the data of Oates and McLellan(53) and Sieverts and Bruning(54) were measured directly as opposed to being calculated from permeabilities and diffusivities. Sieverts and Bruning presented their data as individual measurements as opposed to in Arrhenius form, presumably because of the curvature. It is possible though by no means confirmed by the collected data that the solubility of hydrogen in molybdenum actually does show a curvature although one might expect this to be reflected in the permeabilities at higher temperatures. The data of Martin(55), which are not shown here in fact suggest retrograde solubility over part of the temperature range.

The diffusivity, equation (5.2.2), of this study is shown in Figure 6.3.3 along with the literature values.

The results of Jones et al.(43) and of Ryabchikov(56) are shown dotted since they have been extrapolated from outside the temperature range shown. The extrapolated values of Ryabchikov only appear low because the activation energy is rather large and extrapolations from the temperature range shown to the range of these measurements leads to rather less inconsistency.

The experiment of Zakharov et al.(57) is rather different

from normal. Hydrogen was injected into the metal from a glow discharge. The permeation rates were found to be non-linear in the Arrhenius plot and the effective diffusivity showed a 'knee' at around 500°C. These authors interpreted their results in terms of a model whereby diffusion was enhanced by the creation of point defects at the input surface introduced by the glow discharge. These defects were assumed to form complexes with the hydrogen atoms, the migration of the whole complex contributing to the net hydrogen flux through the specimen.

From their results they then calculated a diffusion coefficient for hydrogen and a separate diffusion coefficient for the complexes. Both the diffusion coefficient for complexes and that for hydrogen are shown in Figure 6.3.3. The fact that the diffusion coefficient for complexes is so much higher than that for hydrogen seems rather unlikely, especially when the authors suppose that the defects are self-interstitial molybdenum atoms. A very similar experiment by Faraj(27) under almost identical glow-discharge conditions produced no such effect and in fact led to the evaluation of diffusion coefficients which are remarkably similar to those measured in this investigation.

Since the diffusion activation energy of Hill(47) is around, or perhaps lower than the norm and the permeation activation energy is somewhat higher than the norm this suggests that the solubility activation energy should be somewhat smaller when extrapolated into the temperature range of Figure 6.3.2.

The results of Caskey *et al.*(51) are worthy of some special mention. Their experiment was effectively carried out twice. The first step was to rapidly increase the input pressure to a fixed value and to follow the rate of rise to steady-state.

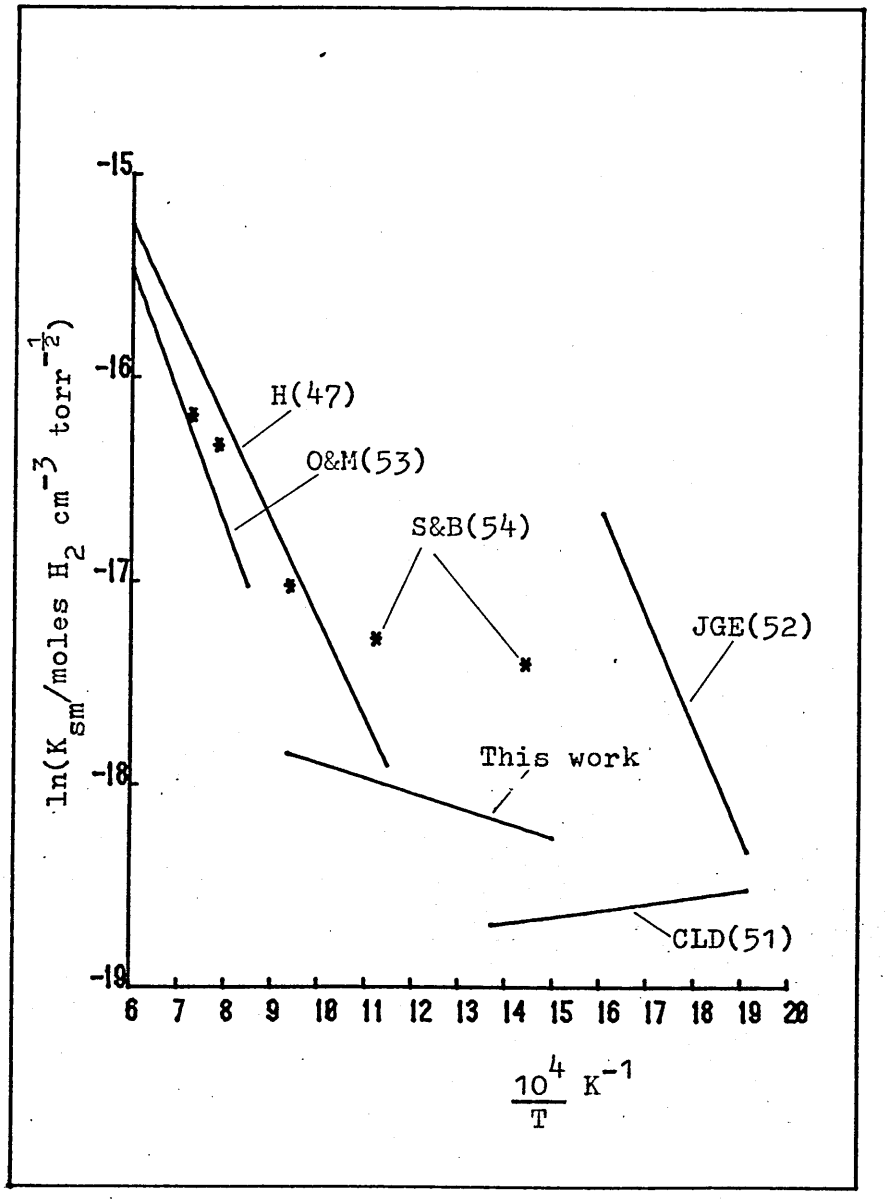

Figure 6.3.2 Solubilities of hydrogen in molybdenum

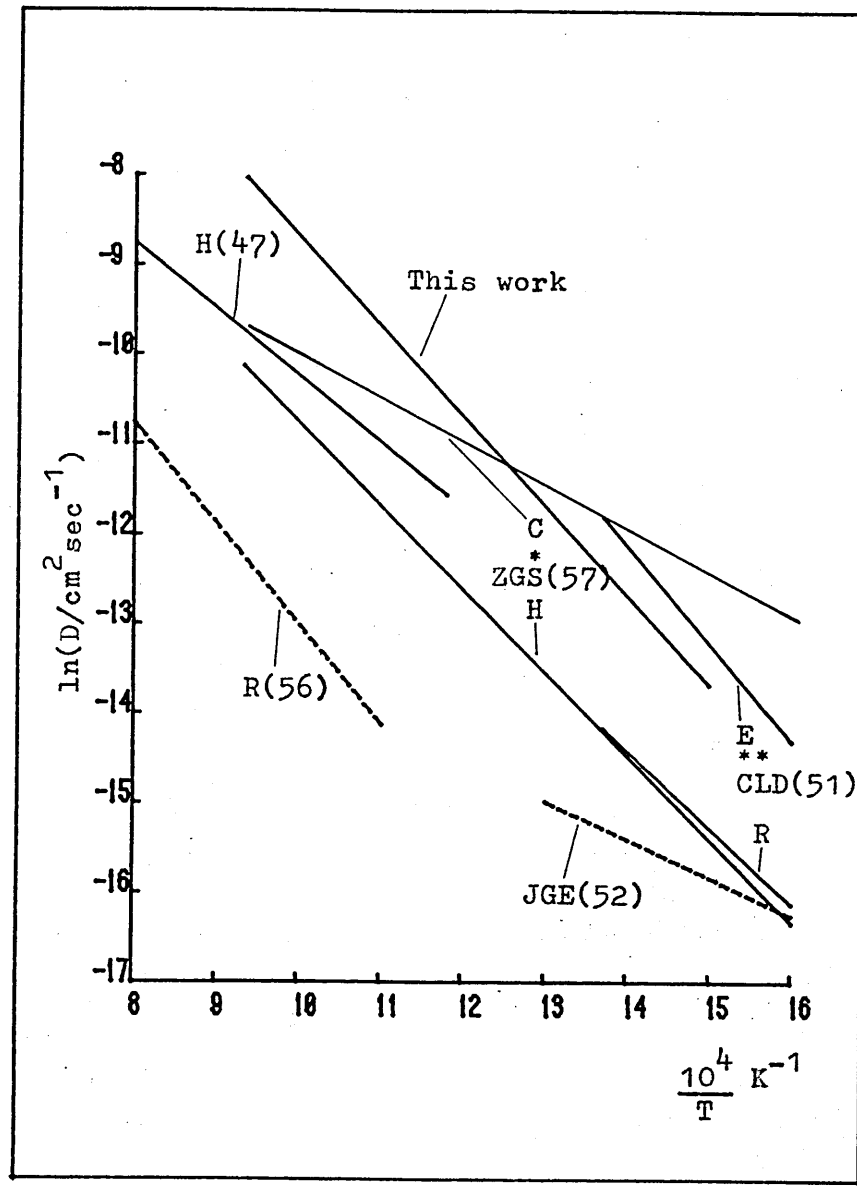

Figure 6.3.3 Diffusivities for hydrogen in molybdenum

(*C and H refer to diffusion coefficients for self-interstitial atom/hydrogen complexes and hydrogen atoms, see text)

(** R and E refer to measurements based on rise-time and evolution rates, see text.)

Gas was then removed from the input side of the specimen and the evolution rate from the specimen was measured. Of course, the steady-state permeability was also measured and is consistent with other investigations. It was found, however, by these authors that the apparent diffusion coefficient was different from rise to steady-state than from decline or evolution rate, the value for evolution rate being larger than that from rise time. These authors propose that such an effect is produced by trapping of hydrogen within the molybdenum but an alternative, equally feasible explanation is also possible in terms of finite surface rate processes. Since the evolution experiment is carried out under conditions where the concentration at the 'output' surface is higher than in the rate-of-rise case, and also since evolution rates are independent of any processes occurring at the input surface one might expect a higher effective diffusivity in this case.

Such large trapping effects (a factor of about 5 in the apparent diffusion coefficients for permeation and evolution) could not fail to be seen in this experiment at low pressures. As already mentioned, no pressure effects were seen in either of the molybdenum specimens. The arguments used by Louthan et al. (38) for nickel with regard to this same effect cannot be used here since the results of both Ryabchikov(56) and Hill(47) were carried out by evolution techniques and both of these sets of data lie below the data of the present investigation. The point made earlier (Section 6.2) about the Caskey/Louthan experiment being effectively a deep modulation can again be considered here and similar remarks apply about the possible assymetry of the input wave.

Summarising, the values of diffusivity, permeability and solubility for hydrogen in molybdenum are given by:

$$D = 3.76 \exp\left[\frac{-19888 \text{ cal/mole}}{R\,T}\right] \text{ cm}^2/\text{sec.}$$

$$P_M = 1.31 \times 10^{-7} \exp\left[\frac{-21333 \text{ cal/mole}}{R\,T}\right] \text{ moles } H_2/\text{cm sec } \sqrt{\text{torr}}$$

$$K_{sm} = 3.64 \times 10^{-8} \exp\left[\frac{-1445 \text{ cal/mole}}{R\,T}\right] \text{ moles } H_2/\text{cm}^3\ \sqrt{\text{torr}}$$

One final, general observation on Figure 6.3.1, 6.3.2 and 6.3.3 is worth noting in the case of molybdenum. It is clear that, when solubilisation becomes a time-dependent process, that time-dependent measurements will fail to separate the diffusivity from the permeability so that the solubility will in some way be involved in the apparent diffusion coefficient. Dividing the permeability by apparent diffusion coefficient will then no longer yield the solubility but some quantity smaller than the solubility, so that compatibility in the permeability but failure of compatibility in the diffusion coefficient and derived solubility is indicative that solubilisation may be a time-dependent process. The lack of any pressure effect in this material and in other studies for molybdenum (apart from the work of Frauenfelder, where the effect is attributable to pre-dissociation of gas, where the part of the solubility associated with splitting of hydrogen molecules is lost before the specimen is encountered) would tend to suggest that the rate-limiting part of the solubilisation process is associated with the value of $\frac{D}{1K_4}$ or $\frac{D}{1K_4'}$.

The values of $\frac{D}{1K_4}$ (assuming $K_4' = K_4$) derived in Section 5.2 have already been presented in Table 5.2.2. If the diffusion

coefficient is removed from these values to obtain the value of K_4 appropriate to each temperature the values in Table 6.3.1 are obtained:

Table 6.3.1

l = .5 mm		l = .25 mm	
T(^{o}K)	K_4 (cm/sec)	T(^{o}K)	K_4 (cm/sec)
824	-	667	-
867	-	715	-
918	2.11×10^{-2}	759.5	4.74×10^{-3}
963	2.19×10^{-2}	808	4.89×10^{-3}
1017	2.03×10^{-2}	850	4.46×10^{-2}
1070.5	1.17×10^{-2}	896	5.66×10^{-3}

It can be seen that in both specimens activation of K_4 is absent to the accuracy of the method of determination. This means that the quantity $\frac{D}{lK_4}$ will become larger the higher the temperature since D is always increasing with temperature. If K_4 is as variable in magnitude as is indicated by the two measurements with nominally identical surfaces then one might expect that measured permeabilities will become more divergent the larger is D, i.e. the higher is the temperature. This is obviously the case from a perusal of Figure 6.3.1.

It is proposed, therefore, that K_4 is a highly surface sensitive parameter with a very low activation energy so that as the diffusion coefficient increases incompatibilities in permeabilities will increase.

The factor of around 4 difference in the value of K_4 between the .5 mm and .25 mm specimens would probably be considerably reduced by choosing the classical line for permeability in Figure 5.2.1 somewhat steeper. This would alter the diffusivities somewhat and make them lie closer to the same straight line. However, it is not thought that the high diffusivity phase curves are accurate enough for a second iteration of this type.

Because the diffusivity needs to be rather large, or rather the mean time of stay in the specimen rather small to measure such surface effects equipment with a higher frequency capability and faster response would probably improve knowledge of permeation of hydrogen in molybdenum.

6.4 M316 Stainless Steel

From the point of view of permeation experiments, stainless steel is a far more complex material than either nickel or molybdenum.

Firstly, it is an alloy with a rather high content of substitutional solutes which will cause distortions of the lattice which are potential trapping sites for a small interstitial like hydrogen. Furthermore, the alloy and impurity content can vary quite considerably even within the specification of a particular steel. Fortunately, stainless steels normally contain only one phase (austenite) and therefore one need not consider the additional complications of a two-phase matrix as is the case for some lower alloy steels. Another property of stainless steels which can influence permeation properties is that from which they derive their name; the formation of a very stable and relatively impermeable iron chromium oxide on surfaces exposed to air for even very short

lengths of time. This oxide is, by its nature, thin since its impermeability disallows further contact of oxygen with the parent metal after the first layers of oxide have formed.

There is a vast amount of literature on the permeation characteristics of hydrogen in stainless steels. Much of this work is concerned with fusion reactor technology and a lot of interest seems to have been shown in Type 304 stainless steel. Rather less work has been done on Type 316 steel(58-61). Of these, two studies (58, 61) have only measured the permeability and one of these has produced rather anomalous results. The remaining two studies have been carried out at very low temperatures with tritium as the diffusant and one of these (59) has been concerned only with grain boundary diffusion which is not considered (59) to have an effect at the temperatures of the present study.

However, a number of authors (e.g. 60, 62) have commented on the apparent lack of an effect of alloy content on the permeation behaviour of stainless steels.

Figure 6.4.1 shows the data points for the diffusion coefficient derived in Section 5.3.1 along with some values from the literature. It can be seen that these values lie reasonably close to those of the literature, but tend to stray below the literature values at lower temperatures.

Figure 6.4.2 shows 'apparent permeabilities' (dotted lines) obtained from Figure 5.3.5. The data points for both the .25 mm and .1 mm specimens were treated as if they were assumed to be classical and 'permeabilities' were obtained in the same way as, for example, nickel. The top pair of solid lines in Figure 6.4.2 represent the result of a review by Le Claire (18) for upper and lower bounds of the permeability of hydrogen through

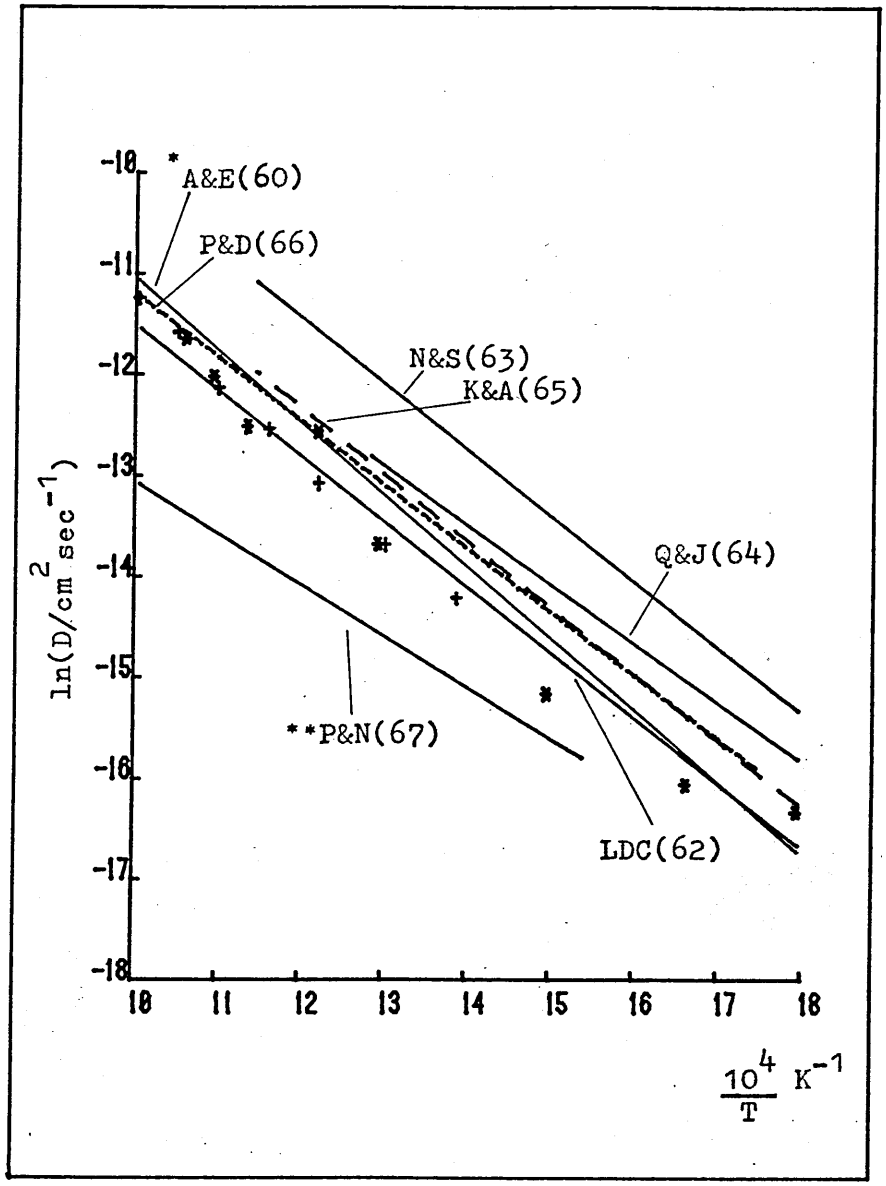

Figure 6.4.1 Some diffusion coefficients for hydrogen in stainless steels along with the data points from this study.

Steel types:

304, 304L : P & N, N & S
310 : Q & J
321 : P & D
309S : K & A
Various : L.D.C.

**Deuterium

*Extrapolated from 222°C ($10^4/T = 20.2K^{-1}$) for tritium in 316 - not corrected for isotopic mass ratio

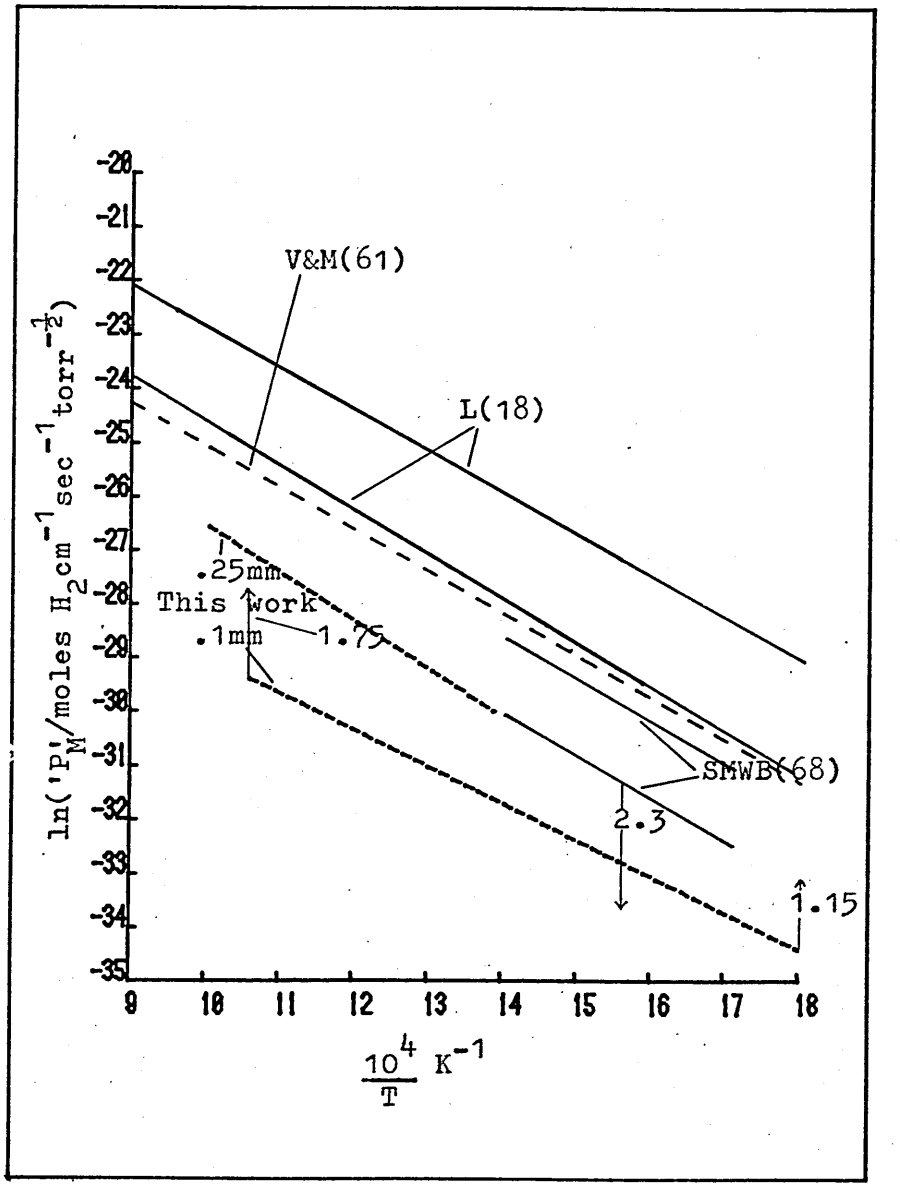

Figure 6.4.2 Permeabilities for hydrogen through stainless steel

stainless steels. It is not surprising that the data from this investigation lie below these bounds taking into account the considerations of Section 5.3. The lower pair of solid lines summarise some work done by Swansiger et al.(68)(SMWB) and the bounds represent various degrees of oxidation of the 309S alloy which these authors used. It must be stressed that these lines are not directly comparable with this work since both sets (SMWB and this work) have been derived on the assumption that the flux through the specimen is proportional to $p^{\frac{1}{2}}$. In the extreme case where the flux is proportional to the first power of input pressure the SMWB curves would be displaced downwards by 2.3 logarithmic units (arrow) and the lower dotted line (.1 mm specimen) would be displaced upwards by 1.75 logarithmic units at the high temperature end and 1.15 logarithmic units at its low temperature end. The .25 mm line would be unaffected.

The two highest temperature permeabilities for the .25 mm specimen were corrected as suggested by the factors derived in Section 5.3 and summarised in Table 5.3.3. The corrected points are shown as bars in Figure 6.4.2, the extension of the bar being indicative of the range of J/J_{CLAS} of Table 5.3.3. These corrections bring these two data points very close to the diffusion-controlled region defined by the bounds of Le Claire.

If the lower temperature portion of the permeation curves in this work is to be oxide-controlled to the extent that J is proportional to p, ie. equation (5.3.5) holds:

$$J = \frac{K_1 K_1'}{K_1' + K_1} \; p$$

Then, in principle, the activation energy for diffusion of hydrogen

through the oxide layer can be obtained.

This activation energy, obtained by two separate linear regressions at the low temperature ends of the curves in Figure 5.3.6 is -14817 cal/mole for the .1 mm specimen and -14115 cal/mole for the .25 mm specimen. Rewriting equation (5.3.5) in terms of the oxide permeation parameters, equations (4.22):

$$J = \frac{D_1 K_{sa}}{l_1 + l_2}$$

where D_1 is the molecular diffusion coefficient for hydrogen through the oxide

K_{sa} is the molecular solubility of hydrogen in the oxide

l_1, l_2 are the thicknesses of the oxide at the input and output surfaces.

Thus, the activation energies derived above can be seen as the activation energies for molecular permeability of hydrogen through the oxide. However, these values are remarkably close to the value -15,148 cal/mole for permeation of hydrogen through bulk M316 stainless steel obtained by Van Deventer and Maroni(61). This similarity immediately calls to mind the model of defect-limited permeation described by Strehlow and Savage(26). Here, the flux equation for permeation is likened to Ohm's Law so that a 'permeation resistance' can be defined

$$R = l/DK_{sm}A \qquad (A = \text{cross sectional area of specimen})$$

A result for the electrical analogue for the constriction resistance for a set of circular holes of average radius, a, and average separation, 2b, due to Holm(69) is invoked and the flux can be

written:

$$J = \frac{aDK_{sm}\sqrt{p}}{b^2}$$

This could explain in part the failure of the thickness relation and would also lead to apparent permeabilities with an activation energy similar to that obtained in a non-oxide limited specimen. However, unless permeation through the oxide is also occurring it is difficult to explain either the curvature of the $p'/\sqrt{p}$ plots or the time-dependent results.

6.5 Summary and Suggestions for Future Work

This experiment was designed to identify and, if possible, quantify the parameters governing the permeation of hydrogen through metal discs. It was intended in particular that the areas of phase boundary controlled permeation would be identified and that the diffusion coefficient and permeability would be measured. These aims would appear to have been met in all cases except stainless steel where the permeability was only obtainable at the highest temperatures of investigation.

One clear point that emerges from the work as a whole is that surface-limited behaviour is not necessarily confined to particular areas of temperature or pressure. This means that decreasing the input pressure is not guaranteed to produce surface-limited behaviour (e.g. molybdenum). Likewise, general statements like "surface limited behaviour is likely to occur at high/low temperatures" cannot be made (compare stainless steel and molybdenum). However, it is always the case that one is more likely to detect

phase-boundary processes when the specimen is thin than if it is thick.

A simplified model has been used in this work in order to clarify the surface situation and also so that the operative surface process need not be defined by more than one parameter. However, when the surface process becomes dominant, as in the case of stainless steel, difficulties are encountered which may well be due to such simplifications.

Apart from the oxide-limited behaviour in stainless steel the surface processes seen here have been rapid (characterised by times of around a few seconds) and a great improvement in the accuracy of measurement would be obtained with equipment having a higher time resolution and a shorter control time. In particular, the ability to go to higher modulatory frequencies on the input wave would have been a distinct advantage in the case of molybdenum. The ability to use lower pressures would have accentuated the effect observed in nickel and it would have been interesting if this effect could have carried to its natural conclusion of dominant surface control.

In contrast, the results for stainless steel seem to have shown too much surface control. This problem has been associated with oxide contamination of one or both surfaces of the specimen. Improvements would perhaps best be made by cleaning of the specimen in vacuo perhaps by a plasma discharge.

Further work in this field would best be carried out after a thorough characterisation procedure for the metal surfaces had been developed. In particular, it would be most interesting to see a quantitative repetition of the effects observed by Fast (20,21) on varying surface preparation.

The principal way in which this work differs from other studies in the field is that a method has been devised by which non-classical permeation processes can be immediately detected. This is seen as a major advantage of the modulatory technique.

In addition, the mathematical analysis of Chapters 3 and 4 has shown that a detailed consideration of the ways in which the phase, amplitude and steady-state measurements deviate from their classical values can allow one to distinguish between different types of surface rate-limiting behaviour. This can be done even if the classical permeation parameters (D, K_{sm}, P_m) are not known although the analysis is greatly facilitated if a separate measurement of these parameters can be made.

In the experiment on nickel, the diffusion coefficient and solubility were measured in a region of input pressure where the system could be seen to be behaving classically. Analysis of the behaviour at lower input pressures could then be made with a high degree of confidence.

In molybdenum, the classical region was confined to the lower temperatures of investigation in each specimen so that the classical parameters at other temperatures had to be obtained by interpolation or extrapolation. Furthermore, the existence of departures from classical behaviour in the phase, amplitude and steady-state measurements in the non-classical region required that all these types of measurement had to be considered before a decision could be made on the type of rate-controlling behaviour. Fortunately, the lack of an effect by varying the input pressure limited the number of possible models. However, due to the relatively large diffusion coefficient and relatively low solubility of hydrogen in molybdenum, measurements could not be made over as wide a range

of frequency or input pressure as might have been hoped and the interpretation of the results in molybdenum must be tempered by these observations.

In stainless steel, the non-classical effects were so pronounced as to preclude measurement of the permeability at all but the highest temperatures (steady-state and amplitude results). More success was achieved with the phase results where diffusion coefficients consistent with the literature were obtainable over a large fraction of the temperature range investigated. However, since a fully classical region could not be identified it is not certain whether the observed effects were due to heavily oxide-limited permeation as described by the model outlined in Section 4.5, or due to some other process such as the penetration of hydrogen through defects in the oxide layer as described by Strehlow and Savage (26).

It is hoped that in some future investigation in this field it will prove possible to find an experiment and a material where measurements can be made over the full range from totally surface-limited to totally volume-limited permeation. This would provide a useful test of the applicability of the surface model.

APPENDIX

A.1 The Surface Concentration in Equilibrium with an Oscillatory Gas Pressure

In connection with the classical treatment of this experiment and also for comparison of the non-classical relations with the classical treatment it is of interest to know the surface concentration which is in equilibrium with a modulated pressure.

The solution is found simply by applying Sieverts' Law to a modulated pressure:

i.e. if the pressure is given by:

$$p_t = p + p_H e^{i\omega t}$$

Then the concentration in equilibrium with this pressure is

$$C_t = K_{sm}\sqrt{p + p_H e^{i\omega t}}$$

Expanding the square-root term gives

$$(p + p_H e^{i\omega t})^{\frac{1}{2}} = \sqrt{p}\left[1 + \frac{p_H}{2p} e^{i\omega t} + \frac{p_H^2}{8p^2} e^{2i\omega t} \ldots\right]$$

Harmonics higher than the principal are not considered in this experiment since p_H is small compared with p, and also since higher frequency waves suffer more attenuation by the specimen than do lower frequencies, so that the concentration in equilibrium with a modulated pressure is considered to be given by:

$$C_t = K_{sm}\sqrt{p} + \frac{K_{sm} p_H}{2\sqrt{p}} e^{i\omega t}$$

A.2 General Solution of Fick's Second Law for Harmonic Surface Concentration

In order to produce particular solutions for the output pressure in response to an oscillatory input pressure it is necessary to solve Fick's Second Law:

$$\frac{\partial C}{\partial t} = D \frac{\partial^2 C}{\partial x^2}$$

Since the particular solutions are dependent on the boundary condition chosen these are not discussed here. However, some general aspects of the boundary conditions are chosen in order to make the general solution useful in the developments of Chapter 3.

It is first assumed that the concentration can be written as the product of two functions: one in x only and one in t only:

$$C = T(t).\ \Omega(x)$$

Substituting into Fick's Law:

$$\Omega \frac{dT}{dt} = DT \frac{d^2\Omega}{dx^2}$$

$$\text{i.e} \qquad \frac{1}{T} \frac{dT}{dt} = \frac{D}{\Omega} \frac{d^2\Omega}{dx^2}$$

In order that this equation can hold for all x,t each side must be equal to some constant which is not a function of either x or t

$$\text{i.e.} \qquad \frac{1}{T} \frac{dT}{dt} = \lambda$$

and this has the solution $T = Ae^{\lambda t}$

and $$D\frac{d^2\Omega}{dx^2} - \lambda\Omega = 0$$

and this has the solution

$$\Omega = R \exp(\sqrt{\frac{\lambda}{D}}\, x) + S \exp(-\sqrt{\frac{\lambda}{D}}\, x)$$

Combining these to give $C = \Omega T$

$$C = A_1 \exp(\sqrt{\frac{\lambda}{D}}\, x) \exp(\lambda t) + A_2 \exp(-\sqrt{\frac{\lambda}{D}}\, x) \exp(\lambda t)$$

This solution can be made more specific if discussion is limited to solutions of the form $\underset{\sim}{C} = \underset{\sim}{Z}\, e^{i\omega t}$. The complex multiplier is required to allow for the fact that there may be a phase shift between the concentration and the input pressure defined in A.1. Equating the time-dependent parts of these two equations (since Z will only be a function of x) leads to:

$$\lambda = i\omega$$

Hence $$\sqrt{\frac{\lambda}{D}} = (1 + i)\sqrt{\frac{\omega}{2D}} = (1 + i)k = \underset{\sim}{a}$$

Furthermore, for ease of manipulation, the concentration will be written in complex form so that

$$\underset{\sim}{C}_{H,x} = \left[\underset{\sim}{A}_1 e^{\underset{\sim}{a}x} + \underset{\sim}{A}_2 e^{-\underset{\sim}{a}x} \right] e^{i\omega t}$$

Since one of the major quantities of interest in Chapter 3 is the flux at x = 1, i.e. $\left(\frac{\partial \underset{\sim}{C}_{H,x}}{\partial x}\right)_{x=1}$ it is worthwhile to rewrite the arbitrary constants $\underset{\sim}{A}_1$ and $\underset{\sim}{A}_2$ so that

$$\underset{\sim}{C}_{H,x} = \left[\underset{\sim}{A}\, e^{\underset{\sim}{a}(x-1)} + \underset{\sim}{B}\, e^{\underset{\sim}{a}(1-x)} \right] e^{i\omega t}$$

in order that the exponential functions of x disappear when x=1.

A.3 Solution of the Diffusion Equation with Trapping for Classical Boundary Conditions

Here, a solution to the diffusion equation of the McNabb-Foster (13) type is supposed to represent reversible trapping within the solid. Traps are assumed to be modelled by the two parameters p, k, where p is the probability that an occupied trap will release its captive within 1 second. The parameters p and k are dependent on the temperature on n or C where n is the fraction of the traps (N/unit volume) which are filled and C is the dissolved atom concentration.

Therefore, the number of atoms released per second in volume $\delta V = pnN\,\delta V$. Also, the number of atoms captured/sec in $\delta V = kCN(1 - n)\,\delta V$

where k is a trapping probability.

From a consideration of the balance of the total hydrogen content and applying Fick's Law, McNabb and Foster obtain the simultaneous differential equations:

$$\frac{\delta C}{\delta t} + N \frac{\delta n}{\delta t} = \text{div (D grad C)}$$

$$\text{and} \quad \frac{\delta n}{\delta t} = kC(1 - n) - pn$$

Solution of the above equations is probably not possible analytically but if the approximation is made that n,C are small so that the cross-term Cn in the second equation can be neglected then:

$$\frac{\delta n}{\delta t} = kC - pn \qquad (A.1)$$

$$\text{and} \quad \frac{\partial C}{\partial t} + N \frac{\partial n}{\partial t} = D \frac{\partial^2 C}{\partial x^2} \qquad \text{(A.2)}$$

(in one dimension)

If N is assumed not to be dependent on x,t the variable n can be eliminated from the above pair of equations to yield:

$$-D \frac{\partial^3 C}{\partial t \partial x^2} + \frac{\partial^2 C}{\partial t^2} - pD \frac{\partial^2 C}{\partial x^2} + (p + kN) \frac{\partial C}{\partial t} = 0 \qquad \text{(A.3)}$$

If a solution of the form:

$$C = f(x) + F(x)e^{i\omega t}$$

is assumed for equation (A.3) then two ordinary differential equations for F(x) and f(x) can be obtained:

$$\frac{\partial^2 f}{\partial x^2} = 0 \qquad \text{(A.4)}$$

and

$$D(p + i\omega) F'' + (\omega^2 - (p + kN)i\omega)F = 0 \qquad \text{(A.5)}$$

Equation (A.4) is unaltered from that which would be obtained from Fick's Law indicating that the effects of trapping will not be apparent in a non-time-dependent experiment. The solution for the phase and amplitude of the oscillatory part show a distinct resemblance to those for Fick's Law in the classical case where, for simplicity, input surface equilibrium and very small output surface concentration are assumed.

Solving A.5 for the boundary conditions given in Section 3.5, the phase-lag and amplitude modifications can be seen to be given by:

$$\tan \varphi_T = \frac{u \tan vl - v \tanh ul}{v \tan vl + u \tanh ul} \qquad \text{(A.6)}$$

$$B_T = \frac{D\sqrt{u^2 + v^2}}{\sqrt{\sinh^2 ul + \sin^2 vl}} \qquad (A.7)$$

These equations are comparable with equations (3.9) and (3.10)

and $$\hat{u} = B \cos\left[\tfrac{1}{2}\tan^{-1}\frac{b}{a}\right]$$

$$v = B \sin\left[\tfrac{1}{2}\tan^{-1}\frac{b}{a}\right]$$

$$B = \frac{\{a^2 + b^2\}^{1/4}}{D(p^2 + \omega^2)}$$

$$a = kN\omega^2$$

$$b = \omega^3 + p(p + kN)\omega$$

If there is no trapping, i.e. p,k = 0 then a = 0 and $b = \omega^3$ and equations (A.6) and (A.7) reduce to (3.10) and (3.9) for the corresponding case with Fick's Law governing mass transport in the solid.

Figure A.1 shows some of the features that equation (A.6) lends to the phase-lag versus square-root frequency plots for the 'standard' D and l used in Chapter 4. These curves show one very disturbing feature of this trapping model. It appears that it is possible, and indeed likely, using this model that the slope of the φ vs. $\sqrt{\omega}$ curve can become <u>smaller</u> than the classical curve with the same phase lag. This means that the trapping curve will ultimately cross the classical curve.

This would suggest that the propogation time (φ/ω) for the pressure wave through the solid can be smaller for a trapped than for an untrapped solid. This does not occur in the surface holdup model where the phase lag is always greater for material with additional holdups.

A.4 Matrix correlation technique for phase plots

Even at the simplest (classical) level the function (equation (3.10))

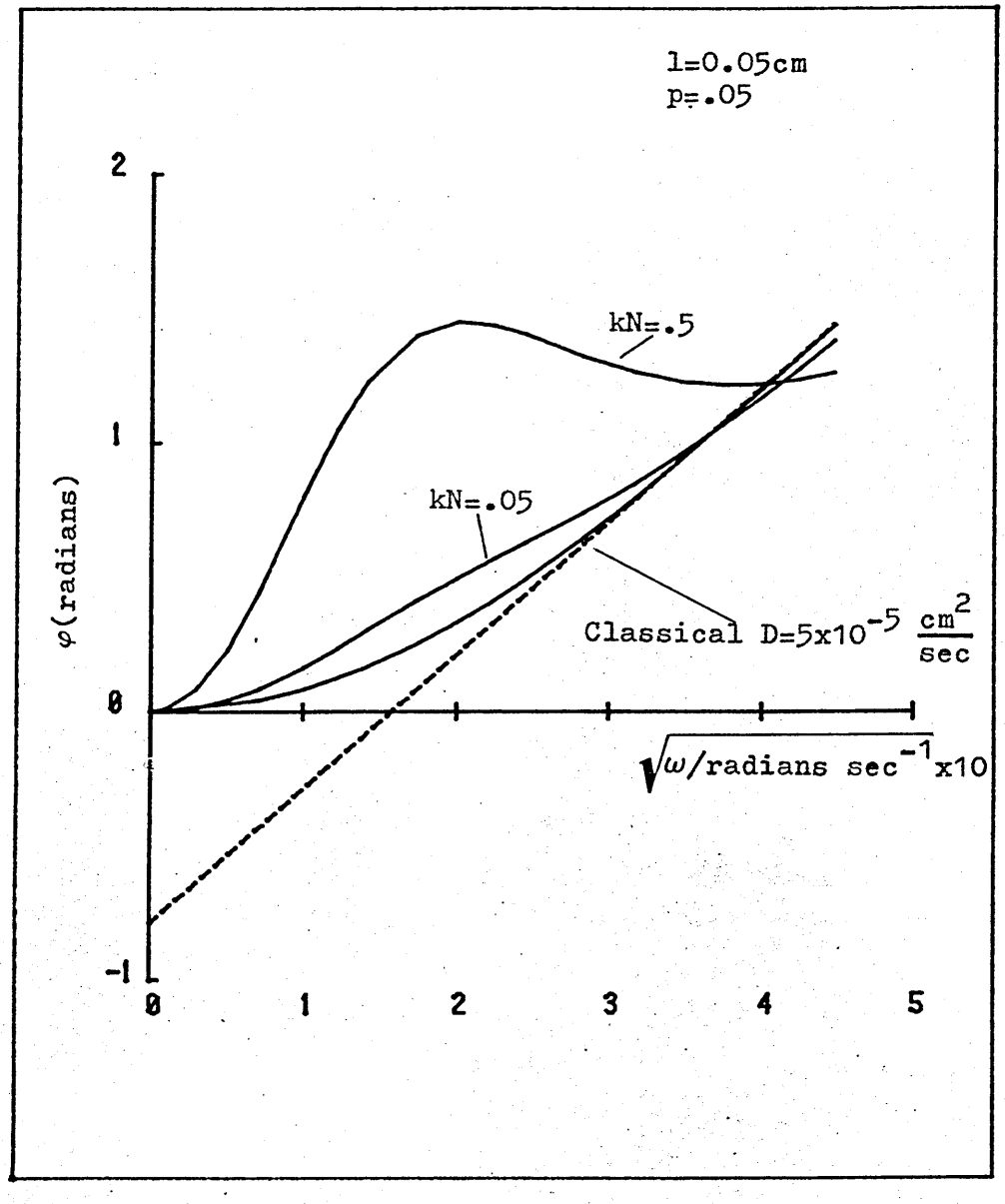

Figure A.1 The effect of trapping on the classical phase plot

which defines the phase-lag in terms of the diffusion coefficient is rather complicated to solve for the diffusion coefficient. It has been found useful to fit these curves to the kinetic parameters D, K_1, K_2 etc. by a least squares technique in order that full use of all the information can be made.

The method is based on an analogue with linear regression where one has a set of x_i, y_i to which a fit to an equation of the form $y = ax + b$ is proposed.

The resulting set of simultaneous equations can be written:

$$\begin{bmatrix} \uparrow \\ y_i \\ \downarrow \end{bmatrix} = \begin{bmatrix} \uparrow & \uparrow \\ x_i & 1 \\ \downarrow & \downarrow \end{bmatrix} \begin{bmatrix} a \\ b \end{bmatrix}$$

i.e. $Y = J \quad P$

Hence $\tilde{J}\,Y = \tilde{J}JP$

so that $P = (\tilde{J}J)^{-1}\tilde{J}Y$

Thus, the parameter matrix $P \equiv \begin{bmatrix} a \\ b \end{bmatrix}$ can be found and this form is very useful for computers which are capable of performing matrix arithmetic.

A variance-covariance matrix can be defined to obtain the standard error on the parameters a,b such that

$$\sigma_A^2 = (\tilde{J}J)^{-1}_{11} \quad \sigma_y^2$$

$$\sigma_B^2 = (\tilde{J}J)^{-1}_{22} \quad \sigma_y^2$$

where σ_A and σ_B are the standard errors on a and b and σ_y^2 is the residual sum of squares:

$$\sigma_y^2 = \sum (y^{obs} - y^{calc})^2 \Big/ N'$$

where N' is the number of degrees of freedom in the system. The variance-covariance matrix $(\tilde{J}J)^{-1}$ is given by

$$(\tilde{J}J)^{-1} = \begin{bmatrix} \frac{N}{|\tilde{J}J|} & -\frac{\sum x_i}{|\tilde{J}J|} \\ -\frac{\sum x_i}{|\tilde{J}J|} & \frac{\sum x_i^2}{|\tilde{J}J|} \end{bmatrix} \quad ; \quad |\tilde{J}J| = N\sum x_i^2 - (\sum x_i)^2$$

N = number of observations

In practice the standard errors for the parameters σ_A and σ_B have only been evaluated for the linear regressions in this work (e.g. diffusion coefficient vs. temperature). For testing different forms of equation for φ vs. ω, the residual sum of squares has been used as an indicator of goodness of fit.

The method just outlined can be extended to cases where the proposed relationship between the variables is not linear. For example, at a given value of frequency the phase lag through the specimen can be written as a function of the diffusion coefficient, D and a series of rate parameters say k, l, m, n, etc.

i.e. $\varphi = f(D,k,l \ldots.)$

This function can be expanded in a Taylor series about the value of the function corresponding to a first estimate of the parameters D_o, k_o, etc. The 'correct' values of the parameters are D, k, etc. Thus:

$$\varphi = \varphi_o + \left[\frac{\partial f}{\partial D}\right]_o (D-D_o) + \left[\frac{\partial f}{\partial k}\right]_o (k-k_o) + \ldots..$$

(where the subscripts 'o' denote evaluation at $D=D_o$, $k=k_o$, etc.)

If the quantity $y = \varphi^{OBS} - \varphi$ is now defined then:

$$y = \varphi^{OBS} - \varphi_o - \left[\frac{\partial f}{\partial D}\right]_o (D-D_o) - \left[\frac{\partial f}{\partial k}\right]_o (k-k_o) + \cdots\cdots$$

The values of the parameters for a given value of frequency are therefore given by $y = 0$, i.e:

$$\varphi_o - \varphi^{OBS} = -\left[\frac{\partial f}{\partial D}\right]_o (D-D_o) - \left[\frac{\partial f}{\partial k}\right]_o (k-k_o) - \cdots\cdots$$

For a set of frequencies the set of simultaneous equations for evaluation of $(D-D_o)$ and $(k-k_o)$ can be written in a way analogous to the linear regression case, i.e:

$$\Delta Y = J \quad \Delta P$$

i.e.

$$\begin{bmatrix} (\varphi_o^{(1)} - \varphi_{(1)}^{OBS}) \\ \vdots \\ (\varphi_o^{(N)} - \varphi_{(N)}^{OBS}) \end{bmatrix} = \begin{bmatrix} -\left[\frac{\partial f}{\partial D}\right]_o^{(1)} & -\left[\frac{\partial f}{\partial k}\right]_o^{(1)} \cdots\cdots \\ \vdots & \vdots \\ -\left[\frac{\partial f}{\partial D}\right]_o^{(N)} & -\left[\frac{\partial f}{\partial k}\right]_o^{(N)} \cdots\cdots \end{bmatrix} \begin{bmatrix} D - D_o \\ k - k_o \\ \vdots \end{bmatrix}$$

and solving as before

$$\Delta P = (\tilde{J}J)^{-1} \tilde{J} \Delta Y$$

If D_o is considered to be an original estimate of D (the 'best' value of D) this technique can be used to iterate until the ΔP matrix $\rightarrow 0$ so that best values of the parameters D, k, l, etc, are obtained.

i.e. after the first iteration

$\Delta P_1 = D - D_o$ i.e. next estimate $D_1 = D_o + \Delta P_1$

$\Delta P_2 = k - k_o$ i.e. next estimate $k_1 = k_o + \Delta P_2$

after second iteration

$$\Delta P_1 = D - D_1 \qquad \text{i.e. } D_2 = D_1 + \Delta P_1$$

$$\Delta P_2 = k - k_1 \qquad \text{i.e. } k_2 = k_1 + \Delta P_2$$

and this is continued until none of the parameters require any further increase, i.e. $D_z \rightarrow D$; $k_z \rightarrow k$, etc.

The residual sum of squares can also be followed during this process since it is equal to the sum of the squares of the members of the ΔY matrix.

A.5 Derivation of the coefficients x, y, r, s

The purpose of this appendix is merely to show in more detail the origin of the parameters x, y, r, s in Section 3.8 of the main text.

If one takes as a starting point the equation on the bottom of page 68 and substitutes the following values for C'_H and $(\delta C_{H,x}/\delta x)_1$:

$$C'_H = (\underset{\sim}{A} + \underset{\sim}{B})e^{i\omega t}$$

$$\left(\frac{\delta C_H, x}{\delta x}\right)_1 = \underset{\sim}{a}(\underset{\sim}{A} - \underset{\sim}{B})e^{i\omega t}$$

then the following equation results:

$$\left[\frac{d^2}{dt^2} + (2K'_2\theta' + \beta - K'_1\frac{ART}{V})\frac{d}{dt} + 2\beta K'_2\theta'\right]K'_4(\underset{\sim}{A} + \underset{\sim}{B})e^{i\omega t}$$

$$+ \left[\frac{d^2}{dt^2} + (\beta + K'_a - K'_1\frac{ART}{V})\frac{d}{dt} + \beta K'_a - K'_1K'_3\frac{ART}{V}\right]D\underset{\sim}{a}(\underset{\sim}{A} - \underset{\sim}{B})e^{i\omega t} = 0$$

Performing the differentiation operations and collecting terms in $\underset{\sim}{A}$ and $\underset{\sim}{B}$ gives the following relationship:

$$\underset{\sim}{A}\left\{\frac{-D^{\frac{1}{2}}}{\sqrt{2}}\omega^{5/2} - K_4'\omega^2 - (\beta + K_a' - K_1'\frac{ART}{V})\frac{D}{\sqrt{2}}^{1/2}\omega^{3/2}\right.$$

$$+ (\beta K_a' - K_1'K_3'\frac{ART}{V})\frac{D}{\sqrt{2}}^{1/2}\omega^{1/2} + 2\beta K_2'K_4'\theta'$$

$$+ i\left[\frac{-D}{\sqrt{2}}^{1/2}\omega^{5/2} + (\beta + K_a' - K_1'\frac{ART}{V})\frac{D}{\sqrt{2}}^{1/2}\omega^{3/2}\right.$$

$$\left.\left. + K_4'(2K_2'\theta' + \beta - K_1'\frac{ART}{V})\omega + (\beta K_a' - K_1'K_3'\frac{ART}{V})\frac{D}{\sqrt{2}}^{1/2}\omega^{1/2}\right]\right\}$$

$$= \underset{\sim}{B}\left\{\frac{-D}{\sqrt{2}}^{1/2}\omega^{5/2} + K_4'\omega^2 - (\beta + K_a' - K_1'\frac{ART}{V})\frac{D}{\sqrt{2}}^{1/2}\omega^{3/2}\right.$$

$$+ (\beta K_a' - K_1'K_3'\frac{ART}{V})\frac{D}{\sqrt{2}}^{1/2}\omega^{1/2} - 2\beta K_2'K_4'\theta'$$

$$+ i\left[\frac{-D}{\sqrt{2}}^{1/2}\omega^{5/2} + (\beta + K_a' - K_1'\frac{ART}{V})\frac{D}{\sqrt{2}}^{1/2}\omega^{3/2}\right.$$

$$\left.\left. -K_4'(2K_2'\theta' + \beta - K_1'\frac{ART}{V})\omega + (\beta K_a' - K_1'K_3'\frac{ART}{V})\frac{D}{\sqrt{2}}^{1/2}\omega^{1/2}\right]\right\}$$

Comparing this with equation (3.8) shows the origin of the x_n, y_n, r_n, s_n.

REFERENCES

REFERENCES

1. STICKNEY, R.E. The Chemistry of Fusion Technology. Proceedings of American Chemical Society Symposium, Boston; Ed. D. M. Gruen; Plenum, New York, 1972, pp. 241-321.
2. AUSTIN, J. H., ELLEMAN, T. S. and VERGHESE, K. J. Nucl. Mater, 1973, 48, 307.
3. MARTIN, G. and BENOIST, P. Scripta Metall., 1977, 11, 503.
4. AUSTIN, J. H. and ELLEMAN, T. S. J. Nucl. Mater., 1972, 43, 119.
5. SMITH, R. P. Acta Metall., 1953, 1, 578.
6. RICHARDSON, O. Phil. Mag., 1904, 7, 266.
7. SMITHELLS, C. J. and RANSLEY, C. E. Proc. Roy. Soc., 1935, A150, 172.
8. CRANK, J. The Mathematics of Diffusion, Clarendon Press, 1975.
9. CHUNG, G. K. Ph.D. Thesis, University of York, 1974.
10. CASKEY, G. R., LOUTHAN, M. R. and DERRICK, R. G. J. Nucl. Mater., 1975, 55, 279.
11. ROBERTSON, W. M. Z. Metallkde, 1973, 64, 436.
12. CALDER, R. D., ELLEMAN, T. S. and VERGHESE, K. J. Nucl. Mater, 1973, 46, 46
13. McNABB, A. and FOSTER, P. K. Trans. Met. Soc., AIME, 1963, 227, 618.
14. FOSTER, P. K., McNABB, A. and PAYNE, C. M. Trans. Met. Soc. AIME., 1965, 233, 1022.
15. ROBERTSON, W. M. and THOMSON, A. W. Met. Trans., 1980, 11A, 553.

16. ELLERBROCK, H. G., VIBRANS, G. and STUWE, H. P. Acta Metall., 1972, 20, 53.

17. DARKEN, L. S. AIME Technical Publication No. 2311, 1948.

18. Le CLAIRE, A. D. Unpublished work.

19. WANG, J. Proc. Camb. Phil. Soc., 1936, 32, 657.

20. FAST, J. D. Philips Tech. Rev., 1941, 6, 365.

21. FAST, J. D. Philips Tech. Rev., 1942, 7, 74.

22. ASH, R. and BARRER, R. M. Phil. Mag., 1959, 4, 1197.

23. ALI-KHAN, I., DIETZ, K. J., WAELBROECK, F. G., WIENHOLD, P. J. Nucl. Mater., 1978, 76 and 77, 337.

24. SHUPE, D. S. J. Chem. Phys., 1978, 68, 2612.

25. PERKINS, H. K. and NODA, T. J. Nucl. Mater., 1978, 71, 349.

26. STREHLOW, R. A. and SAVAGE, H. C. J. Nucl. Mater., 1974, 53, 323.

27. FARAJ, E. Ph.D. Thesis, The Open University, 1981.

28. SWANSIGER, W. A. and BASTASZ, R. J. Nucl. Mater., 1979, 85 and 86, 335.

29. KUBASCHEWSKI, O. and EVANS, E. L. Metallurgical Thermochemistry, Butterworth-Springer, 1951.

30. ALPERT, D. Handbuck der Physik, Bd. XII, Springer, Berlin, 1955, p.609.

31. KATZ, L., GUINAN, M. and BORG, R. J. Phys. Rev. B., 1971, 4, 33(

32. MORRISON, H. M., BLACKBURN, D. A. and CHUI, K. M. J. Nucl. Mater., 1978, 69 and 70, 578.

33. DUS, R. and SMIALOWSKI, M. Acta Metall., 1967, 15, 1611.

34. EICHENAUER, W., LOSER, W. and WITTE, H. Z. Metallkde., 1965, 56, 287.

35. EBISUZAKI, Y., KASS, W. J., O'KEEFE, M. J. Chem. Phys., 1967, 46, 1378.

36. VOLKL, J. and ALEFELD, G. Diffusion in Solids, Recent Developments. Academic Press, N.Y. 1975. p.231.

37. BELYAKOV, Yu. I. and IONOV, N. I. Sov. Phys. Tech. Phys., 1961, 6, 146.

38. LOUTHAN, M. R. DONOVAN, J. A. and CASKEY, G. R. Acta Metall., 1975, 23, 745.

39. ORIANI, R. A. Acta Metall., 1970, 18, 147.

40. HILL, M. L. and JOHNSON, E. W. Trans. Met. Soc. AIME, 1959, 215, 717.

41. GRIMES, H. H. Acta Metall., 1959, 7, 782.

42. ARMBRUSTER, M. H. J. Am. Chem. Soc., 1943, 65, 1043.

43. JONES, F. G. and PEHLKE, R. D. Met. Trans., 1971, 2, 2655.

44. McLELLAN, R. B. and OATES, W. A. Acta Metall., 1973, 21, 181.

45. BORELIUS, G. and LINDBLOM, S. Ann. Physik., 1927, 82, 201.

46. BORELIUS, G. Ann. Physik., 1927, 83, 121.

47. HILL, M. L. J. Metals., 1960, 12, 725.

48. GUTHRIE, J. W. BEAVIS, L. C., BEGEAL, D. R. and PERKINS, W. G. J. Nucl. Mater., 1974, 53, 313.

49. HUFFINE, C. L. and WILLIAMS, J. M. Corrosion, 1960, 16, 340.

50. FRAUENFELDER, R. J. Chem. Phys., 1968, 48, 3955.

51. CASKEY, G. R., LOUTHAN, M. R. and DERRICK, R. G. J. Nucl. Mater., 1975, 55, 279.

52. JONES, P. M. S., GIBSON, R. and EVANS, J. A. AWRE Report No. O-16/66, 1966.

53. OATES, W. A. and McLELLAN, R. B. Scripta Metall., 1972, 6, 349.

54. SIEVERTS, A. and BRUNING, K. Arch. Eisenh., 1934, 7, 407.

55. MARTIN, E. Arch. Eisenh., 1929, 3, 407, 641.

56. RYABCHIKOV, L. N. Ukr. Fiz. Zh, 1964, 9, 293.

57. ZAKHAROV, A. P., GORODETSKY, A. E. and SHARAPOV, V. M. Z. Phys. Chem., 1979, 117, 245.

58. FLINT, P. S. Knolls Atomic Power Laboratory Report KAPL-659, 1951.

59. CALDER, R. D., ELLEMAN, T. S. and VERGHESE, K. J. Nucl. Mater, 1973, 46, 46.

60. AUSTIN, J. H., ELLEMAN, T. S. J. Nucl. Mater, 1972, 43, 119.

61. Van DEVENTER, E. H. and MARONI, V. A. Trans. Amer. Nucl. Soc., 1978, 28, 199.

62. LOUTHAN, M. R., DONOVAN, J. A., and CASKEY, G. R. Nucl. Tech., 1975, 26, 192.

63. NELSON, H. G. and STEIN, J. E. N.A.S.A. Rep., TND-7265, 1972.

64. QUICK, N. R. and JOHNSON, H. H. Met. Trans., 1979, 10A, 67.

65. KASS, W. J. and ANDRZEJEWSKI, W. J. A.E.C. Rep. SC-DR/72/0136, 1972.

66. PHILLIPS, J. R. and DODGE, B. F. A.I. Chem. Eng. Jl., 1968, 14, 3.

67. PERKINS, H. K. and NODA, T. J. Nucl. Mater., 1978, 71, 349.

68. SWANSIGER, W. A., MUSKET, R. G., WEIRICK, L. J. and BAUER, W. J. Nucl. Mater, 1974, 53, 307.

69. HOLM, R. Electric Contacts Handbook (Springer-Verlag, Berlin, 1958).